PACKING DENSITY AND REACTIVITY OF WASTE QUARRY DUST AS A SUPPLEMENTARY CEMENTITIOUS MATERIAL

Norliza Rima Norbidin

Supervisors: Kypros Pilakoutas and Maurizio Guadagnini

A thesis submitted in partial fulfilment of the requirements for the degree of Doctor of Philosophy

Department of Civil and Structural Engineering

Faculty of Engineering

The University of Sheffield

[January 2024]

Abstract

In response to concerns about global warming, the construction industry is actively seeking to reduce CO2 emissions linked with the production and use of Ordinary Portland Cement (PC). While the use of conventional supplementary cementitious materials (SCMs) can help reduce the amount of PC used in construction, this well-established practice faces challenges due to evolving energy policies and scarcity of materials. This study explores the potential of waste quarry dust as a sustainable alternative, aiming to recycle waste and minimize the environmental impact of construction.

The research focuses on utilizing milled waste quarry dust in cementitious mixtures, exploring its role as a filler or SCM. Investigating particles ranging from 0.24μm to 250μm, the study aims to understand their impact on packing density, formation of cement hydration products, and reactivity in cementitious mixtures.

The research enhances the theoretical 2-parameter packing model, incorporating particle size distribution for more accurate predictions of blended cement density. Findings indicate that milled quarry dust enhances early-stage hydration and contributing to new hydrate development in the cement matrix. The study also explores the absorption characteristics of cement-based composites with quarry dust, revealing a 10% increase in water absorption and a 20% rise in pore phase area fractions, indicative of altered material porosity. Findings also include the predictable nature of capillary absorption across different QD types and the identification of factors such as hydration heat and pore structure influencing absorption rates. Overall, this research provides experimental evidence that supports the use of quarry dust as a viable and sustainable alternative to cement, paving the way for more environmentally friendly construction practices.

Acknowledgement

First and foremost, I wish to express my gratitude to my supervisors, Kypros Pilakoutas and Maurizio Guadagnini for their endless support, guidance, and encouragement throughout the course of this research. Your expertise and insightful feedback have been invaluable to my academic growth and the completion of this thesis.

I would also like to extend my sincere thanks to the CEE group members, for their valuable insights and constructive criticism that greatly contributed to the refinement of this research.

My heartfelt appreciation goes to the lab technician at the 'Heavy Structures Laboratory' especially Kieran Nash, X-ray Laboratory in Material Science Department, and The Geography Department Laboratory (Robert A Ashurst) for their support during data collection.

I am immensely grateful to my family, for their patience, and endless encouragement. Your belief in my abilities and constant support have been my strength throughout this journey.

I would also like to acknowledge the financial support received from the Sabah State Government, which made my research possible.

Finally, I extend my thanks to all those who, directly or indirectly, contributed to the successful completion of my thesis.

Table of Contents

List of Figures

List of Tables

This page is intentionally left blank

Chapter 1: Introduction

1.1 BACKGROUND

Global warming has become a worldwide emergency, and there is a drive with various international agreements and legislations to reduce CO_2 emissions, with advanced economies aiming for zero emissions by 2050 [1]. The production of Portland cement releases 8–9% of global CO_2 emissions and uses 12–15% of the total energy consumed by industry [2]. Cement is the cheapest and most widely available binder for construction, and currently only a few alternatives are used as substitute binder materials.

To address the concerns of global warming and environmental issues, the construction industry is increasingly focusing on more cost-effective, sustainable, and durable concrete. Direct solutions like Carbon capture and storage (CCS) for reducing cement manufacturing emissions are currently prohibitively expensive [2]. Indirect strategies, such as the use of supplementary cementitious materials (SCM), have played a vital role in enhancing concrete sustainability over the last 30 years. However, changes in power generation and the shift away from coal as an energy source have led to shortages in the supply of widely used SCMs like fly ash [3].

This scarcity has prompted industry and academia to explore alternative materials. When available, natural pozzolans like zeolites, pumice, and clays are pulverized to the right particle size and used as partial cement replacements, proving to enhance concrete performance [4]. With conventional high-quality SCMs becoming less available [5], there is a current shift towards other substitutes, known as filler materials, such as limestone. The use of inert fillers can reduce cement content to meet economic, technical, and environmental requirements [6]. Although increasing fineness through grinding or reducing the water/cement ratio can partially compensate for cement dilution, the grinding process adds costs and requires energy. Alternative fine materials found in nature, or derived from waste products, could offer more economical and environmentally friendly solutions.

Emerging SCMs can replace conventional SCMs, but their poor reactivity due to stable crystallinity makes them unsuitable for direct substitution. Among different treatment options, particle size reduction efficiently increases reactivity; This reduction also improves packing density, potentially lowering the water-cement (w/c) ratio by minimizing void spaces. Smaller particles create a more uniform and thin water film around them, which reduces internal friction and enhances flowability (Hunger & Brouwers, 2009; Wong & Kwan, 2005). Polycarboxylate superplasticizers further aid by dispersing these particles effectively, ensuring the mix remains workable with less water (Khayat, 1999; Feng & Wang, 2018)

Among the various fine fillers considered for such applications, quarry dust and waste materials from tile and polished stone manufacture have gained attention. These wastes are reported at about 1 tonne of stone powder for every 50 tonnes of manufactured aggregate in Brazil. In Greece alone, 10 million tonnes of waste dust are produced annually, with most countries inevitably facing similar situations [5]. Quarry dust is by far the material available in the largest quantities, and it is currently landfilled. Due to its fineness and propensity to disperse easily, quarry dust is an environmental pollutant. Quarry dust is also found on crushed aggregates and, as a result, such aggregates are often considered unsuitable for use in concrete. Using QDs as a cement replacement presents a complex issue with both potential benefits and drawbacks. On the one hand, quarry dust can become an environmental pollutant if not managed properly, contributing to air pollution, water contamination, and land degradation. However, its use in concrete can also provide significant environmental benefits by aiding in waste management, reducing the carbon footprint of cement production, and conserving natural resources like limestone.

From a technical perspective, quarry dust can enhance concrete properties such as compressive strength and durability when used in appropriate proportions (Dehwah, 2012; Raman et al., 2011). By partially replacing cement with QD, the overall cement content in the mix is reduced. This not only lowers production costs but also mitigates the heat of hydration, decreasing the risk of thermal cracking in large concrete pours.

Currently, there is little knowledge on the effects of fine quarry dust as a material to replace cement in concrete. The influence of particle size on the performance of quarry

dust used as a filler has not been comprehensively characterized, especially for its contribution to packing density and reactivity. Therefore, the main question is: "How can we effectively and efficiently utilise waste quarry dust, and does increasing the packing density and its reactivity enhance its potential use as a sustainable construction material?"

1.2 AIMS

This work aims at increasing knowledge on the suitability and effect of milled waste quarry dust (QD) in cementitious mixtures when used as a filler or supplementary cementitious material (SCM). In the context of this work, QD particles have grain sizes ranging from 0.24 μm to 250 μm, similar to cementitious materials. These particles may be inert and increase the packing density of QDs in cementitious materials, and contribute to the formation of cement hydration products, resulting in higher strength and durability.

The hypothesis of this work is that significant amounts of ordinary Portland cement (PC) can be replaced by a controlled, maximised packing density of QDs without adversely compromising mechanical properties or durability.

1.3 SCOPE OF STUDY

The scope of this work includes assessing and optimizing the packing density of microfines of various particle size distributions (PSD) and identifying their reactivity in cementitious mixtures. Furthermore, the effect of introducing QDs on mechanical characteristics and durability will be evaluated.

1.4 OBJECTIVES OF STUDY

Following a literature review on particle packing, cement hydration and reactivity, mechanical strength, and durability of cementitious materials, the main objectives of this study are to:

1. Evaluate the performance of existing particle packing models for different blends of milled QD and PC.

2. Develop an enhanced packing model capable to account for the actual PSD of the QD and provide more reliable estimates of packing density.
3. Assess the hydration kinetics of milled QDs and determine the role of milling in cementitious mixes.
4. Evaluate the impact of QD addition on the durability parameters of cementitious materials.
5. Make recommendations for QD processing and usage in cementitious mixtures to meet target performance requirements.

1.5 RESEARCH SIGNIFICANCE

The research contributes through:

1. A more accurate and generalised packing model that accommodates powders with a broad PSD through the introduction of suitable parameters, such as the coefficient of uniformity (Cu) and the coefficient of curvature (Cc).
2. A better understanding of how to increase or maximise the utilisation of waste QDs in cementitious mixes.
3. Increased knowledge that should facilitate the use of waste QDs in the concrete industry as a cost-effective and sustainable alternative material to commercially available SCMs.

1.6 THESIS LAYOUT

This thesis is structured into five mains chapters. It begins with an introductory chapter (**Chapter 1**), followed by three chapters written in the form of paper publication-style chapters, and a concluding section. It also includes four appendices detailing the methods used and the full experimental results of the tests conducted.

Chapter 2 addresses objectives 1 and 2 and examines the influence of particle size distribution on packing density of blended cement and QD. This study initially evaluates the well-known 2-parameter model that includes particle interaction for predicting packing density of microfines. The performance of the model is tested against the results obtained from experimental tests on blended mixtures containing milled

quarry powders and cement in different proportions. It is found that the 2-parameter model generally underestimates the packing density of microfines and modifications to the model are proposed to increase its accuracy.

Chapter 3 addresses objectives 3 and 5 and investigates the influence of fineness of quarry dust on the hydration kinetics in cementitious mixes. Recognizing the need for more eco-friendly cement options, this study explores the use of QDs as an alternative source of SCMs. The key aspect of the study is understanding how particle fineness affects cementitious performance. A novel area of investigation in this study is the impact of particles size on the hydration development of PC-QDs mixes under controlled packing conditions. This involves experiments that explore how different particle sizes of QDs from different sources affect cement hydration kinetics, and elemental composition.

Chapter 4 addresses objectives 4 and 5 and examines the effect of QD on the durability of blended mixtures. This section discusses how the incorporation of QDs alters the pore phases and elemental composition of hydrated cement and investigates how this affects durability parameters such as water absorption, capillarity, and shrinkage behaviour.

Chapter 5 presents a summary of the key findings from each chapter and offers recommendations for future works.

This page is intentionally left blank

Chapter 2:Influence of particle size distribution on packing density of blended cement with quarry fines having

H I G H L I G H TS

- Utilizing waste quarry fines enhances the packing density in cement-based composite.
- No evident correlation between size ratio, *s* and packing density in microfine.
- A novel analytical particle packing model introduced, incorporating actual PSD, C_u and C_c.
- Experimental validation confirms the accuracy of the proposed packing density predictions.

A B S T R A C T

Keywords: Packing models, Packing density, Waste quarry fines, Particle size distribution, Coefficient of uniformity, Coefficient of curvature

The use of quarry dust and other microfines can result in denser and more environmentally friendly concretes. However, proportioning particle size distribution (PSD) in microfines is not easy to control, especially particles that are finer than 75 microns, due to cost, complexity, and availability of micro sieves. Microfines analysed by particle laser diffraction show very high standard deviation, which makes the mean diameter size useless in discrete particle packing models. This paper addresses this issue of PSD in particle packing model, by analysing blends of cement and quarry dusts in various quantities to assess packing density. It then develops an analytical particle packing model by using the actual particle size distribution (PSD) a coefficient of uniformity (C_u) and a coefficient of curvature (C_s). The predicted packing density is in

good agreement with the experimental results. Best results are obtained for particle distributions that are not too similar. This work will lead to the optimal use of cement replacements and, hence, better performing, and cheaper concretes.

2.1 INTRODUCTION AND BACKGROUND

Large amounts of waste dusts generated by quarries are available worldwide. Quarry dusts (QD) if not managed properly can cause serious threats to air, land and water if dumped in open landfills. Finding ways of maximizing the use of QD is important to help improve the environment by reducing waste and carbon dioxide emissions by cement replacement. QD can replace cement to create eco-efficient concrete. Fine filler materials are known to improve the packing characteristics of cementitious mixes and can also be reactive [20,21]. To use QD as a supplementary cementitious material (SCMs) and/ or filler it is important to be able to identify and modify its characteristics so as to achieve optimum packing density.

The use of reactive SCMs such as fly ash and slag to replace cement in concrete is a well-established technique for 'green concrete'. However, considering the limited availability of such materials in many regions and their green credentials under question [1], it is worth considering other non- reactive natural resources/waste as cement replacement.

To maximise microfines utilization, it is essential to enhance the packing density of the resultant powder. Despite numerous packing density studies focusing on granular materials, limited information exists on microfine/ powder (particles smaller than 75 microns) packing density. The few studies that involve powders (see **Table 2.1**), use the same approaches as developed for coarse aggregate discrete packing density, by adopting the mean diameter size to characterize the particle size distribution (PSD). Given the very high deviation in PSD such an approach was found by the authors to be inappropriate. Hence, it is important to find a particle packing model that can predict the packing density of microfines so that such materials can make a bigger contribution to greener concrete.

This study initially evaluates the well-known 2-parameter model (with particle interaction) in predicting the packing density of microfines, from 0.24 μm to 250 μm representing cementitious materials, by comparing its predictions with experimentally results. Milled quarry powders and cement are used in different proportions in the experiments. It will be seen that in general the 2-Parameter model under-estimated the

prediction of packing density. Errors in the two-parameter model are identified and a new model is proposed for microfines.

Table 2.1: Reported studies on particle packing models with microfines in the literature.

Model	Material	Particle size	Reference
de Larrard's [2] and Yu's [3]	Rock and cement	75μm -1.8mm	Kwan et al., 2009 [4]
de Larrard's [2] and Yu's [3], and Kwan's [5],[6]	Sand, polyethylene, and glass	75μm -20mm	Chan et al., 2014 [7]
de Larrard's [2] and Yu's [3], and Kwan's [5],[6]	Alumina powder	2 μm, 10 μm, 70 μm	Du et al., 2022 [8]

2.2 BACKGROUND OF PARTICLE PACKING THEORIES AND MODELS

Several theoretical packing theories were developed over the years aiming to enhance particle packing of a solid skeleton. Their classification and evolution over the years (since 1907) are summarized diagrammatically in **Figure.2.1**.

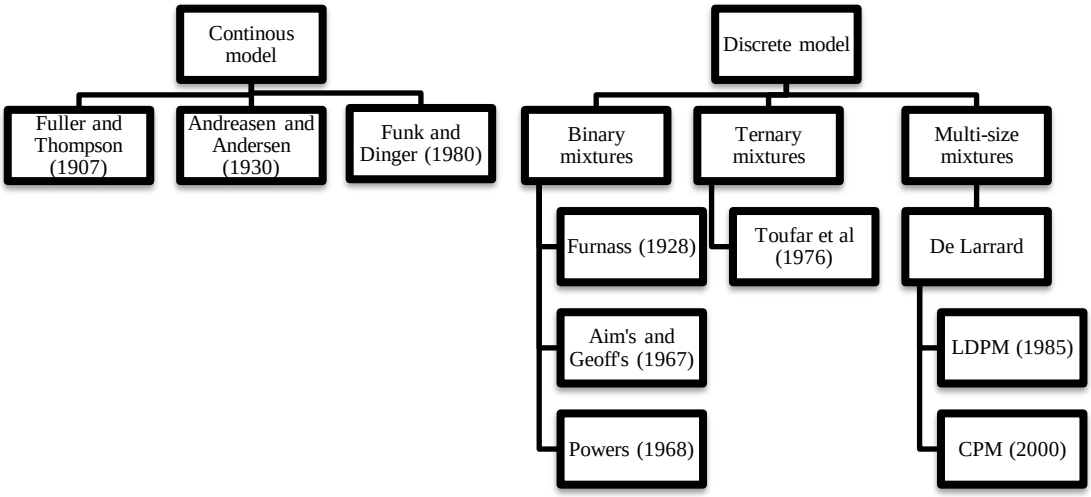

Figure 2.1: Evolution and classification of particle packing models

In general, theoretical packing models are divided into continuous and discrete models. In conventional concrete formulation methods, granular mixtures are determined empirically, often from particle curves (ideal distribution curves), as in works by Fuller & Thompson, d' Andreasen & Andersen and Dreux. However, these methods do not predict the packing density and may require experimental iterations for the optimization of the granular mix [9]. These methods are generally used to achieve a targeted PSD and usually aim for an ideal PSD to achieve good packing [10].

The discrete models are preferred by researchers as they can provide an understanding of the effect of various particles on the densification of the mixtures. An early discrete model, introduced by Furnass [11] in 1928, was developed for binary mixes without consideration of particle interaction. Powers [12] in 1967 introduced the "loosening effect" while Aim and Goff [5] and Toufar et al. [13] the "wall effect". Modern packing models such as by Stovall et al. [14] and the compressive packing model (CPM) [2] consider both loosening and wall effects in their models.

The 2-Parameter packing models based on the particle interaction of the loosening effect and wall effect and are generally associated with the discrete models. in **Figure 2.1**, the model developed by De Larrard, particularly his LPDM (Linear Density Packing

Model) and CPM (Compressible Packing Model), are modern packing models that consider both the loosening and wall effects, making the representative of the 2-prameter model approach.

In the 2-parameter model, the packing density is a function of mean particle size and volumetric fraction of constituent materials. The following equations (2.1), (2.2) and (2.3) identify the basic parameters and concepts involved in packing density predictions.

When coarse particles are dominant

$$\frac{1}{\phi_2 *} = \frac{r_2}{\phi_2} + a.\frac{r_1}{\phi_1} \qquad \textbf{Equation (2.1)}$$

Where r_1 and r_2 are the volumetric fraction of size class 1 (fine particles) and size class 2 (coarse particles), ϕ_1 and ϕ_2 are the initial packing densities of class 1 and class 2 respectively and a is the "loosening effect" parameter (see equation 2.4).

When fine particles are dominant:

$$\frac{1}{\phi_1 *} = \frac{r_1}{\phi_1} + r_2 + b.(1-\phi_2).\frac{r_2}{\phi_2} \qquad \textbf{Equation (2.2)}$$

Where b is the wall effect parameter (see equation 2.5).

For a binary mixture, the packing density is the smallest of $\phi_1 *$ and $\phi_2 *$.

Packing Density, $\phi = \min(\phi_1 *, \phi_2 *)$ **Equation (2.3)**

The particle interactions that describe the loosening and wall effects are expressed as a function of the size ratio (*s*). Where s is the size ratio of the mean diameter of fine to coarse particles.

Loosening effect:

$$a = 1-(1-s)^{3.3} - 2.8s(1-s)^{2.7} \qquad \textbf{Equation (2.4)}$$

Wall effect:

$$b = 1-(1-s)^{2.0} - 0.4s(1-s)^{3.7} \qquad \textbf{Equation (2.5)}$$

The loosening effect (represented by a in equation 2.4) occur when coarse particles are dominant. Small particles filling the gap between larger particles cannot be fully packed leading to the separation of the larger particles that would otherwise pack more

compactly (see **Figure 2.2a** and **b**). The wall effect (represents by *b* in equation 2.5) occurs when fine particles are dominant. It develops when large particles cause interstice in the grain mixture leaving spaces with ow particle packing (see **Figure 2.3a**)

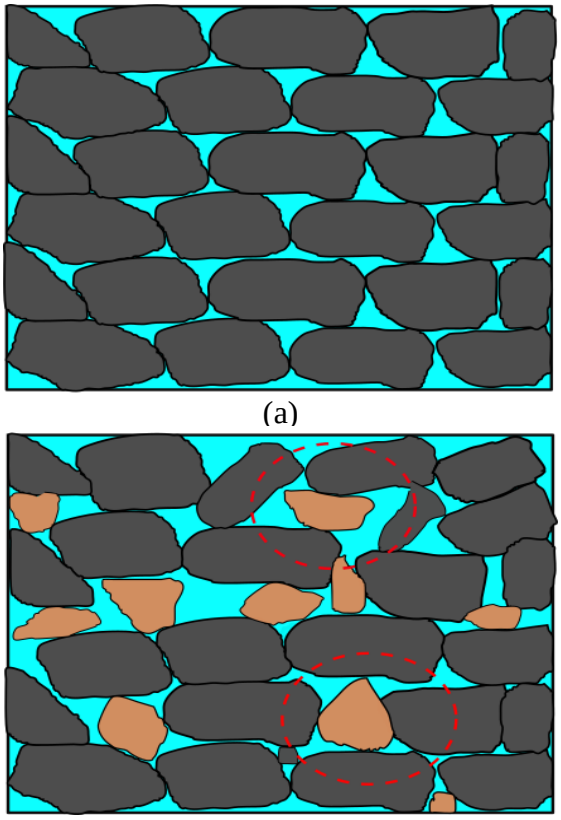

(a)

(b)

Figure 2.2:(a) Monodisperse of single particles and (b) Loosening effect)

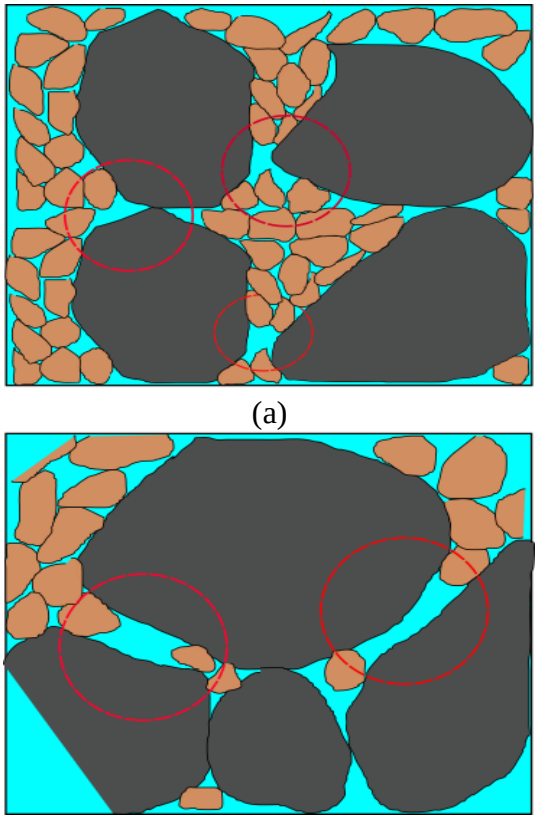

(a)

(b)

Figure 2.3:(a) Wall effect and (b) Wedging effect)

Researchers [6],[7] found discrepancies between the 2-parameter model and experimentally measured packing densities. To improve predictions, Kwan et. al [5] proposed a third particle interaction called the 'wedging effect' (see **Figure 2.3b**). They described the wedging effect as a phenomenon found in coarse and fine particle dominance when fine particles become trapped in narrow gaps between coarse particles. While Roquier [13] proposed a fourth particle interaction called the 'critical cavity size', which indicates the boundary condition that specifies the capacity of smaller particles to enter into gaps or 'cavities' generated between bigger particles (see **Figure 2.4** and **2.5**). The critical cavity size denoted as x_0, is a key parameter in the 4-parameter compressible packing model that indicates the size ratio below which a fine particle can fit into the voids created by larger particles without disturbing their arrangement. For spherical particles, x_0 is typically around 0.2, based on the theoretical size of tetrahedral cavities. This parameter helps define the loosening effect, where adding smaller particles disrupts the packing structure of larger particles. The value of x_0 varies depending on the shape and roughness of the particles, being lower for more angular particles. Roquier used mathematical formulae derived from completely spherical particle packing conditions to modify the equations for the loosening and wall effect interaction.

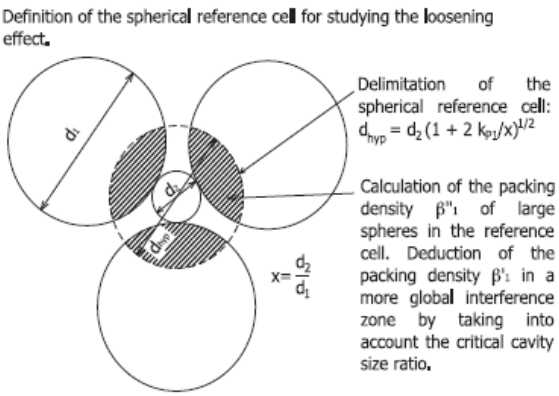

Figure 2.4: Definition of the spherical reference cell for loosening effect by [15]

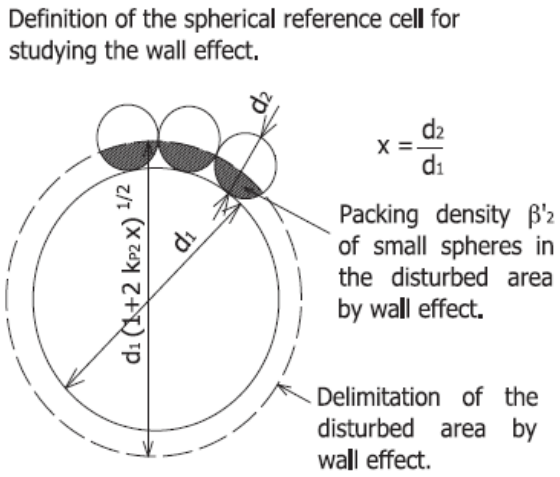

Figure 2.5: Definition of the spherical reference for wall effect by [15]

Particle interactions used in the 2-, 3- and 4-parameter models are heavily dependent on the size ratio [16], [17]. These models are developed for materials sieved or proportioned into narrow sub classes (of adjacent sieve apertures) and provide very good predictions for materials of diameter sizes greater than 75 μm. However, it is not established if they are suitable for cementitious materials, such as microfines, that normally have a wider particle size distribution (PSD). Obtaining narrow distributions in industrial-scale production for powders is complex and expensive, hence, proportioning microfines is currently a challenge [18].

In conclusion, very few studies evaluated the accuracy of the theoretical packing models with experimental data for microfines [8]. This study aims to assess the suitability of the 2-parameter model in predicting the packing density of microfines, as this model represents the fundamental principles of packing theory. For this purpose, the packing density of three different mean sizes of QD's, from three different sources, mixed with standard PC CEM I, are determined experimentally. Comparisons are then made with the predictions of the 2-parameter model and improvements to the model are proposed.

2.3 EXPERIMENTAL DETERMINATION OF PACKING DENSITY

This section describes the material used and the experimental procedure for the determination of packing density. The purpose of the testing was to measure and compare experimental to model-predicted results at different PSD conditions.

CEM I 52.5 (obtained from Hanson Cement), which complies with all the requirements of BS EN 197-1 and BS EN 197-2, was used in the experiments.

Three different QD sources were collected in the form of sludge from Papar and Tawau, Malaysia, and Tarmac, the United Kingdom. The QDs were reported by the quarries to be sandstone, diorite, and granite, and these are designated as S, D, and G for Papar, Tawau, and Tarmac, respectively.

The QDs were oven dried at 105 °C until reaching a constant weight and passed through a 75μm sieve before being milled. Following trials of various durations, the milling times of 60s and 200s were selected. Beyond 200s, no further particle size reduction was observed, and at 60s, the mean diameter would roughly reduce to half.

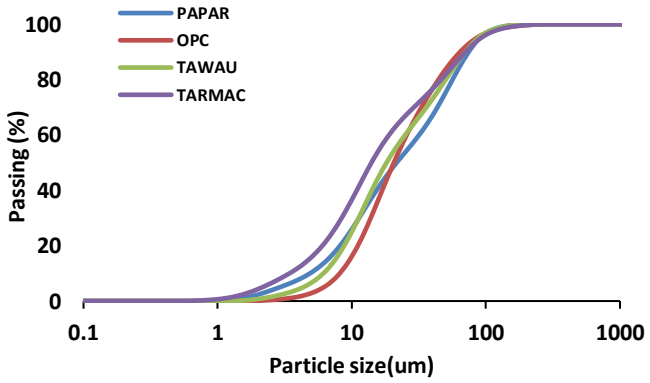

(a) Particles not milled

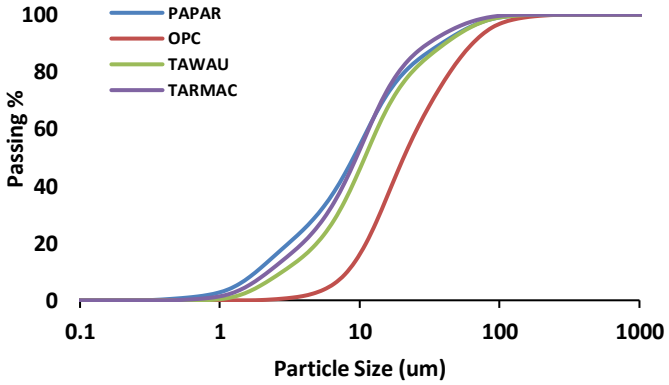

(b) Particles milled at 60s

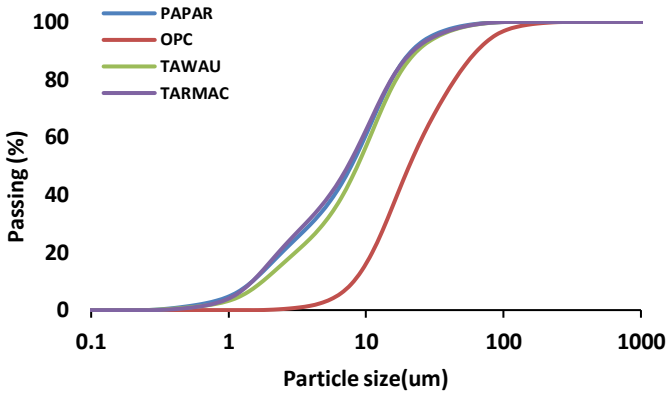

(c) Particles milled at 200s

Figure 2.6: Particle size distribution of microfine used in this study.

The PSD for CEM I and nine different QDs were determined using laser diffraction scattering equipment, (LA 950). **Table 2.2** and **Figure 2.6** show the PSD results, and the physical characteristics of each material. The material chemical oxides were evaluated using x-ray fluorescence (XRF) using 'PANalytical Zetium,' and the oxides and loss on ignition (LOI) are shown in **Table 2.3**. A third generation of polycarboxylate-based superplasticizer (SP) was added at 1.5 percent of the cementitious total mass to all mixes with a constant water to binder (w/b) ratio of 0.3.

Table 2.2: Physical properties of cementitious powder

Properties	CEM I (52N/mm²)	PAPAR S0	S60	S200	TAWAU D0	D60	D200	TARMAC G0	G60	G200
Mean Dia. (μm)	30.32	32.62	15.52	10.42	29.92	17.34	11.54	27.38	14.07	10.45
SD*	28.84	29.66	19.90	10.79	28.51	9.81	11.66	32.04	15.68	11.40
SG	3.14		2.30			2.30			2.10	
Initial PD	0.55		0.52			0.52			0.52	

*Standard deviation

Table 2.3: Chemical oxides composition of cement and QDs powders in %

Component	CaO	SiO_2	Al_2O_3	MgO	K_2O	Fe_2O_3	TiO_2	Na_2O	MnO	SO_3	P_2O_6	LOI
CEM I	65.0	20.0	6.0	2.0	0.5	3.0	0.2	0.5	0.1	1.5	0.1	1.0
Granite (G)	3.14	56.81	13.60	3.07	3.69	3.13	0.74	2.83	0.09	0.05	0.18	12.25
Sandstone (S)	1.48	50.17	8.80	1.02	1.73	2.88	0.38	1.29	0.05	0.63	0.05	31.20
Diorite (D)	5.85	60.43	16.30	2.81	2.61	5.65	0.58	2.85	0.10	0.06	0.14	1.97

The initial packing density of each QDs and the packing density of binary mixtures were calculated using the wet packing density method given in Eqs. 2.6 and 2.7, developed by Wong and Kwan [15]. This method involves experimental measurements and the use of equations to estimate the packing density of the mixtures.

Experimentally measured values:

1. Mass of the paste (M):

After thorough mixing, the mass of the paste, consisting of water, cementitious materials (CEM I), and quarry dust (QD), was measured. The paste was placed in a cylindrical mould, and its total mass was recorded. This measured mass is essential for determining the solid concentration within the mix.

This experimental value served as the basis for the subsequent calculation of the packing density.

2. Calculation of packing density:

The packing density (ϕ) was calculated using the following equations:

Solid volume calculation:

The solid volume (V_s) of the materials within the paste, was determined using the mass of the paste and the specific gravity (S.G) of the constituent materials. The solid volume was calculated using:

$$V_s = \frac{M}{\rho_w U_w + \rho_\alpha R_\alpha + \rho_\beta R_\beta} \qquad \textbf{Equation (2.6)}$$

V_s is the solid volume, M is the mass, ρ_w, ρ_α and ρ_β is the specific gravity (S.G) for water, CEM I, and quarry fines, respectively. While U_w is the w/b ratio, and R_α, R_β are the volumetric fractions of CEM I and QDs, respectively.

Solid Concentration (Packing Density) calculation:

The packing density (ϕ) was then calculated as the ratio of the solid volume (V_s)to the total volume of the cylindrical mould (V) using Equation:

$$\phi = \frac{V_s}{V} \qquad \textbf{Equation (2.7)}$$

This ratio represents the solid concentration of the mixture, indicating the proportion of the total volume that is occupied by solid materials. It provides a quantitative measure of how closely the materials (CEM I and quarry dust) are packed within the paste.

The packing density (ϕ) was identified as the maximum solid concentration achieved during the experiment. This value represents the point at which the particles in the paste are most tightly packed, with minimal void space between them. A total of 45 binary mixes were assessed for their packing densities, and the volume replacement varied from 0% to 50% in 10% increment.

The **Table 2.4** below provides the formulation details for the cementitious mixes, including the amounts of superplasticizer and water. The water-to-binder ratio (W/B) is fixed at 0.3, and the superplasticizer dosage is set at 1.5% of the total binder content. These parameters are held constant across all mixes to ensure consistency in comparing the effects of different Quarry Dust particle sizes, with a consistent 40% replacement of PC. The QDs used in this study are denoted as S, D, and G, representing sandstone, diorite, and granite, respectively. The numbers following these letters (e.g., S60, D200) indicate the duration of milling in minutes. This approach allows for the accurate assessment of particle size influence without the variability introduced by changes in water or admixture content.

Mix Proportions:

Table 2.4: Formulation details of cementitious mixes

Mix	Portland Cement (PC) (kg/m3)	Quarry Dust (QDs) (Kg/m3)	W/B Ratio (Kg/m3)	Superplasticizer (Kg/m3)
PC	1000.0	0	300	15
PC+S0	523.5	476.5	300	15
PC+S60	523.5	476.5	300	15
PC+S200	523.5	476.5	300	15
PC+D0	523.5	476.5	300	15
PC+D60	523.5	476.5	300	15
PC+D200	523.5	476.5	300	15
PC+G0	500.8	499.2	300	15
PC+G60	500.8	499.2	300	15
PC+G200	500.8	499.2	300	15

2.4 RESULTS AND DISCUSSION

2.4.1 EVALUATION OF THE 2-PARAMTER MODEL FOR BINARY MIXTURES.

To evaluate the predictive capabilities of the 2-parameter model, it is crucial to assess two critical criteria often employed in such studies by [4] and [7]. These criteria include (i) the deviation at the maximum packing density (also known as the ideal packing density) and (ii) the deviation at each fraction of the model-predicted packing density compared to the experimentally observed packing density. The evaluation of these criteria provides valuable insights into the model's ability to offer suggestion for appropriate mixing proportions and packing densities.

Based on the results presented in **Figure 2.10**, **2.11**, and **2.12**, as well as **Table 2.5**, **2.6**, and **2.7**, it can be observed that increasing the QDs fraction initially leads to an improvement in the packing density, which then reaches a maximum, and subsequently begins to decline. This pattern is consistent with previously investigated packing

models, and both the 2-parameter model predictions and the experimental results support this trend.

However, a distinct trend is observed in the 2-parameter model's prediction for QDs with PSDs similar to that of CEM I. Rather than a parabolic plot, the model exhibits a flat trend, implying that adding QDs to the mixture no longer enhances packing density. This is in contrast to experimental data, which do not support this tendency. A possible explanation to such trend is that the 2-parameter packing model uses the mean diameter instead of an actual PSD.

If the PSD of QD is similar to CEM I, the model would predict little to no improvement in packing density, as it essentially equates adding QD to adding more CEM I. However, this assumption overlooks the broader PSD of QD, which typically has a higher standard deviation, indicating a more varied range of particle sizes. This broader distribution includes both large and small particles that can fit into the voids between the existing cement particles, leading to better packing efficiency. Consequently, while the 2-parameter model's reliance on mean diameter suggests minimal improvement, the actual PSD of QD contributes to a higher packing density than predicted.

Thus, the experimental results suggest that the enhanced packing density observed in mixtures with QD can be attributed to the broader PSD of QD, which is not fully captured by the 2-parameter packing model. This highlights the need to consider the complete PSD, rather than relying solely on mean diameter, when assessing packing density improvements in cementitious materials.

The 2-parameter model, while effective for predicting the behaviour of particles larger than 75 μm, falls short when applied to mixture containing QDs or powder materials. The model consistently underestimated experimental results, with mean absolute percentage errors ranging from 6.2-10.9%. This lack of accuracy highlights the need for improvements to the model's parameters to accurately predict packing behaviour in these mixtures. Considering the amount of QDs needed to achieve maximum packing density, both model-predicted and experimentally measured values were found to be mutually achievable at a volumetric fraction of 40 percent QDs.

To explore the impact of size ratio on the packing density of binary mixtures, all combinations with size ratios of roughly 0.9, 0.5 and 0.3 were plotted. Specifically, **Figure 2.7a** depicts a representative result of PC-D0, PC-D60 and PC-D200 mixtures, where the ratio of mean diameter particle size of the finer particles to the coarse particles is used as the size ratio, denoted as *s*.

Previous studies have reported a sensitivity of size ratio, s, to packing density, where decreasing s leads to an increase in packing density, as shown in **Figure 2.7b** (Kwan et al., [16]). However, our observations reveal no clear trend of sensitivity of QDs or powder to size ratio, as seen in **Figure 2.7a**. This finding suggests that the particle interactions of the loosening effect and wall effect, which are functions of size ratios, cannot be incorporated into predictions of packing density of PC-QDs or powder materials.

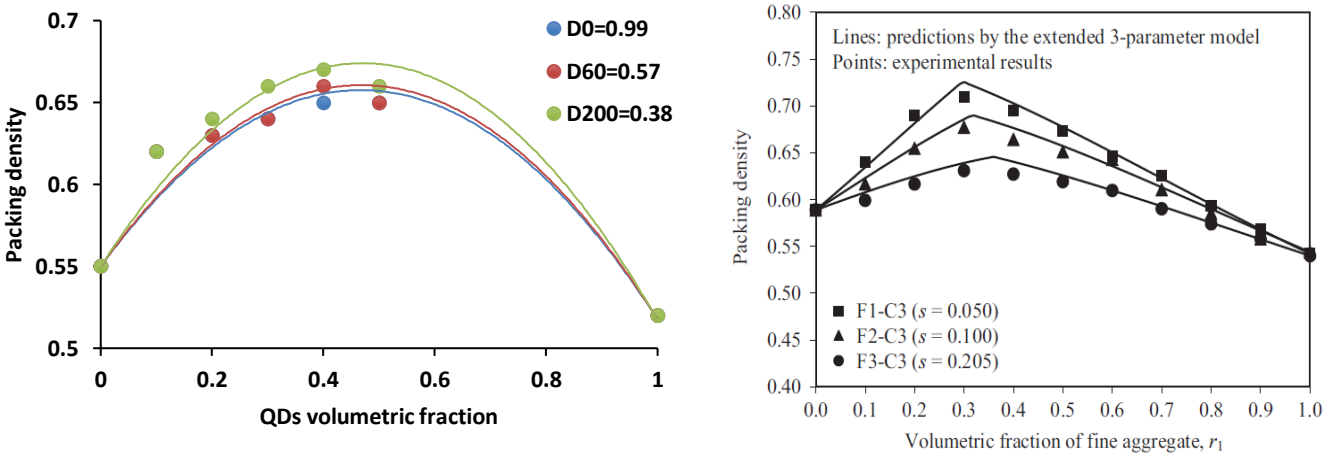

(a) (b)

Figure 2.7: (a) Normal trends of packing density for blended binder observed in this study (b) sensitivity of size ratio to packing density from previous studies [19]

2.4.2 EFFECT OF PACKING DENSITY ON THE COEFFICIENTS OF UNIFORMITY (C_U) AND CURVATURE (C_C)

There are two critical concerns with the mean diameter employed in the 2-parameter packing model in predicting the packing density for powder material: i). The PSD's high SD (see **Table 2.2**), which renders questionable adoption of the mean

diameter size that represents the whole sample size; ii) the packing density, which is insensitive to changes in size ratio, s. Because continuous distributions are widely encountered in materials with naturally occurrences and waste from quarry products, we argue that a particle packing theory that represents the packing of actual distributions should be based on continuous distributions.

Hence, we suggest the actual PSD should be incorporated into the model by adopting a parameter that could describe, characterize, and capture the changes in PSD through the introduction of the coefficient of uniformity (C_u) and the coefficient of curvature (C_c).

The Coefficient of Uniformity (Cu) and Coefficient of Curvature (Cc) are widely recognized parameters used to describe the gradation of soil particles. These coefficients play an essential role in understanding the distribution of particle sizes within a soil sample, which significantly affects the soil's compaction behaviour, permeability, and suitability for engineering purposes [22,23]

The Cu provides a measure of the range of particle sizes in a soil sample. It is calculated as the ratio of the diameter corresponding to 60% passing (D60) to the diameter corresponding to 10% passing (D10), as outlined in Equation 2.8:

$$C_u = \frac{D_{60}}{D_{10}} \qquad \textbf{Equation (2.8)}$$

A higher Cu suggests a wider distribution of particle sizes, which typically indicates well-graded soil, leading to better compaction and increased strength. Conversely, a low Cu indicates uniform soil with a narrow range of particle sizes, which may result in reduced shear strength and stability [2, 3]. This parameter is especially useful in classifying soils based on their gradation, as defined in ASTM D2487 [4]

By incorporating C_u we can account for the spread of range of particles sizes in the PSD

The Cc represents the shape of the particle size distribution curve, particularly in the middle range of particles, and is expressed by Equation 2.9:

$$C_c = \frac{(D_{30})^2}{(D_{60}.D_{10})} \qquad \textbf{Equation (2.9)}$$

A Cc value typically between 1 and 3 is indicative of well-graded soils [1, 5]. Soils with Cc values outside this range may exhibit poor gradation (either gap-graded or poorly graded), which can negatively impact compaction and load-bearing properties [6, 7].

To better comprehend the relationship between packing density and this parameter, a number of plots have been made. **Figure 2.8** shows the correlation between α_n C_u, α_n C_c and packing density of mixed binders (PC and Papar QD). A parabolic relationship was discovered between the investigated parameters to packing density.

The first plot shows the packing density plotted against Cu for three (3) different samples (S0, S60, S200). S0 refers to quarry dust that was not milled, serving as the baseline material with its original particle size distribution. S60 denotes quarry dust milled for 60 seconds, resulting in a reduction in particle size compared to the unmilled sample. Finally, S200 corresponds to quarry dust milled for 200 seconds, achieving the finest particle size distribution among the three categories. The second plot shows the packing density plotted against Cc for the same three (3) samples. Each sample's data points are fitted with a polynomial curve.

The polynomial relationship indicates that the impact of Cu and Cc on packing density is not simply proportional. Instead, it follows a curve where packing density initially increases with Cu, reaches a peak, and then decreases. This behavior reflects an optimal range of particle sizes (indicated by Cu) and an optimal grading curve (Cc) that maximizes packing density, while very high Cu values may lead to poor packing due to excessive fines.

The parameter α_n is an adjustment parameter used in the model to account for the combined influence of the coefficient of uniformity (Cu) and curvature (Cc) on packing density. It is not a separate parameter for Cu and Cc but rather a unified term reflecting the shared effects of particle size distribution (PSD). The PSD descriptors Cu and Cc are both derived from the same PSD data points (D10, D30, and D60), allowing α_n to integrate their combined influence on packing density in a consistent way. The value of α_n is calculated based on the quarry dust volumetric fraction (fvf)

$$a_n = 0.09 + (n-1)0.09 ,$$

$$n = \frac{fvf}{0.1}$$

ensuring that α_n varies appropriately for different material compositions. The fitting process involved collecting experimental packing density data points for various combinations of Cu, Cc, ϕ1, ϕ2,r1, r2, and fvf, and then using least squares regression to determine and calibrate α_n by minimizing the error between model predictions and experimental data.

The mixture containing 100% QDs had the highest $\alpha_n C_u$ and $\alpha_n C_c$ values of 6.56 and 1.17, respectively, which resulted in a lower packing density. The highest packing density was observed when the $\alpha_n C_u$ was valued at 2.60–3.30 and the $\alpha_n C_c$ was between 0.58–0.7. Therefore, we suggest the existence of an optimum $\alpha_n C_u$ and $\alpha_n C_c$ value to achieve a maximum packing density for cementitious material. This can be due to the fact that at this value, there is a wider spread of PSD and a higher maximum content of fine particles that can ideally fit into available voids between larger particles, which results in an increase in packing density. A further increase in the $\alpha_n C_u$ and $\alpha_n C_c$ values will not always increase the packing. This decrease in packing density can be attributed to an imbalance in the void volume created by coarser particles, resulting in an excess of finer particles that can fill in voids between larger and medium particles.

Coarser particles create significant void space due to their larger size, disrupting the close packing of smaller particles. These larger voids result in an imbalance, as smaller particles may not sufficiently fill these spaces, leading to decreased overall packing density. Studies using the discrete element method (DEM) have shown that larger particles create substantial voids that smaller particles cannot fill effectively, leading to reduced packing density (Liu and Zeng, 2023).

Fine particles can fill the voids created by larger particles, initially improving packing density. However, if the distribution of particle sizes is too wide (high Cu), it can lead to inefficiencies. The finer particles may not completely fill all voids, resulting in reduced packing density. Research indicates that an optimal distribution of fine and coarse particles can enhance packing density, but excessive variation (high Cu) causes

inefficiencies as fine particles cannot fill the larger voids created by coarse particles effectively (Gan, Yu, and Zhou, 2016; Alizadeh et al., 2014).

The additional volume of QDs changes the PSD of PC and increases the packing density until it reaches a maximum point. This effect can be explained by the filling of voids between the larger PC particles with smaller quarry dust particles, resulting in a broader and more efficient particle size distribution (PSD), which enhances solid skeleton packing. As the amount of QDs increases beyond the optimum point, the PSD becomes imbalanced due to an excess of fine particles relative to the larger ones. This leads to a "void to fill" mismatch, disrupting the optimized packing structure and reducing the overall packing density.

At this stage, the smaller QDs dominate, and the contribution from the larger PC particles diminishes. This shift causes a perturbation in the PSD, reducing the packing efficiency as the distribution of fine and coarse particles is no longer balanced. The underlying phenomenon parallels the particle interaction seen in the two-parameter model, where the inclusion of foreign material (like QDs) alters the overall PSD of the mixture, leading to variations in packing efficiency.

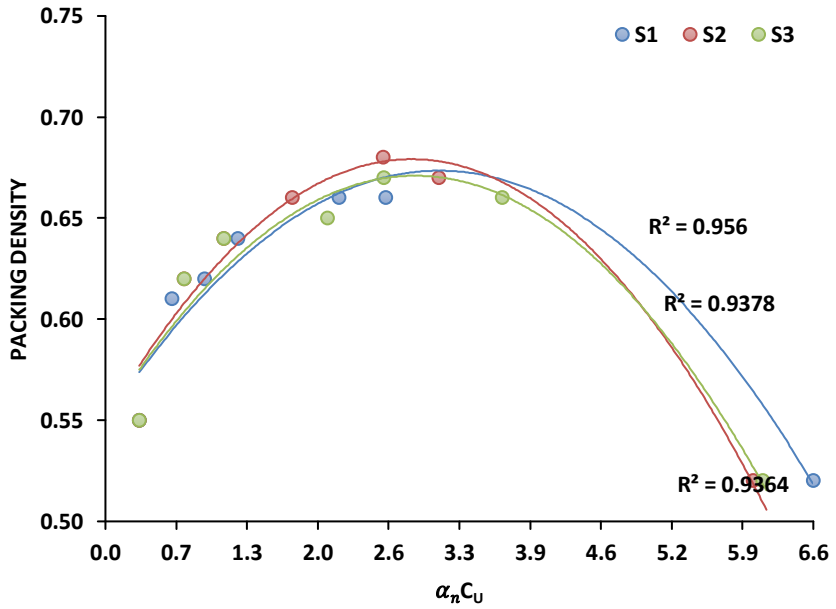

(a)

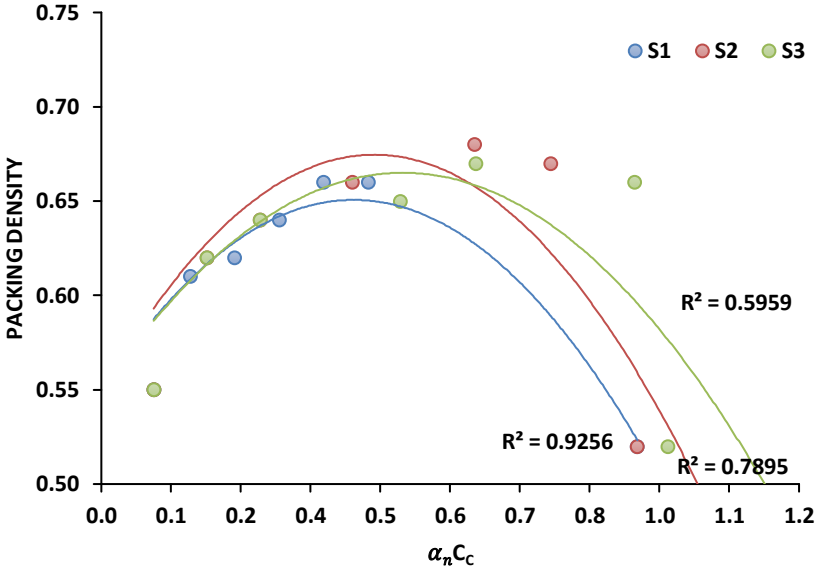

(b)

Figure 2.8: Effect of α_n Cu (a) and α_n Cc (b) of blended cements on packing density of binders (PC + Papar QD)

2.4.3 PROPOSED MODEL WITH THE INCORPORATION OF PARTICLE SIZE DISTRIBUTION (PSD)

Instead of using the mean diameter as in the current model, an actual PSD is needed to predict the packing densities of PC-QDs or any powder material more accurately. Our strategy is to incorporate PSD by introducing the C_u and C_c that could describe PSD changes. From the results in **Figure 2.10**, **2.11**, and **2.12**, it is evident that the maximum volumetric fractions are not affected by the introduction of C_u and C_c into the model, where the maximum packing appears at the same point in the 2-parameter model. While incorporating this effect, this condition must be met.

To provide context, the original 2-parameter model accounts for packing density using the effects of loosening and wall interactions between fine and coarse particles: Loosening Effect: Fine particles disrupt the packing of coarse particles when they are not small enough to fit into the voids between coarse particles, reducing packing density.

Wall Effect: Coarse particles act as "walls," disrupting the packing of fine particles, increasing void space.

These effects are represented mathematically as:

$$\frac{1}{\phi_2 *} = \frac{r_2}{\phi_2} + a.\frac{r_1}{\phi_1} \quad \text{(for coarse-dominant System)}$$

$$\frac{1}{\phi_1 *} = \frac{r_1}{\phi_1} + r_2 + b.(1-\phi_2).\frac{r_2}{\phi_2} \quad \text{(for fine-dominant system)}$$

Where:

ϕ1∗, ϕ2∗: Effective packing densities for fine and coarse particles.

ϕ1, , ϕ2: Intrinsic packing densities of fine and coarse particles.

r1, r2: Volumetric fractions of fine and coarse particles (r1+r2 =1).

a, b: Loosening and wall effect parameters, which depend on the size ratio of particles.

While this model captures particle interactions, it does not account for the effects of particle size distribution (PSD) on packing density, limiting its predictive accuracy. To address this limitation, the coefficients of uniformity and curvature were introduced to capture PSD effects on packing density.

Empirical observations showed that Cu and Cc significantly influence packing density. Scaling terms like $0.05 \cdot Cu \cdot Cc^{0.7}$ and $0.15 \cdot Cu \cdot Cc^{-0.50}$ were introduced to represent these effects.

The coefficients Cu and Cc replace the traditional loosening and wall effects, making the model more sensitive to PSD variations

When coarse particles are dominant, the change in PSD is influenced by the amount of QDs introduced into the mixtures. On the other hand, after it reaches its maximum packing density, the fine particles become dominant, and the disturbance of the PSD is due to the coarse particles. Therefore, the equation can be written as follows:

Coarse dominant,

When coarse particles dominate the mixture, larger particles disrupt the packing arrangement of the fine particles. The equation accounts for this by adjusting the packing density of coarse particles through the term $0.15C_uC_c^{-0.5}$, which captures the effect of the PSD on this disturbance. This adjustment reflects how the distribution of

coarse particles limits the efficiency of fine particles in filling the voids, leading to the overall packing behaviour being controlled by the coarse particles.

$$\frac{1}{\phi_2 *} = \frac{r_2}{\phi_2} + a_n(0.15Cu.Cc^{-0.5})\frac{r_1}{\phi_1}$$ **Equation (2.10)**

Fine Dominant

In contrast, when fine particles dominate, the packing behaviour shifts to how well these smaller particles can fill the voids left by the larger particles. The equation reflects this through the term $0.05C_uC_c^{-0.70}$, which accounts for how the PSD of fine particles contributes to filling these gaps.

$$\frac{1}{\phi_1 *} = \frac{r_1}{\phi_1} + r_2 + a_n(0.05Cu.Cc^{0.7})(1-\phi_2)(\frac{r_2}{\phi_2})$$ **Equation (2.11)**

Where:

The coefficient α_n empirically derived from experimental data of PC-QD mixtures with varying volumetric fractions. It ensures the model accurately reflects PSD's influence on packing density.

$$a_n = 0.09 + (n-1)0.09$$ **Equation (2.12)**

Where n is the QDs volumetric fraction (fvf) to 0.1.

$$n = \frac{fvf}{0.1}$$ **Equation (2.13)**

Hence, the packing density of the binary mix, ϕ;

Packing Density, $\phi = \min(\phi_1 *, \phi_2 *)$ **Equation (2.14)**

It can be concluded that with some modification to the 2-parameter model, it can increase the ability to predict packing density of PC-QDs mixtures. This modified model would give an accurate tool for predicting packing density of cementitious materials. Hence, any PSD not conforming to the recommended gradation would be able to be used without the need to alter the natural PSD of powder just to conform to the recommended gradation to obtain a good packing.

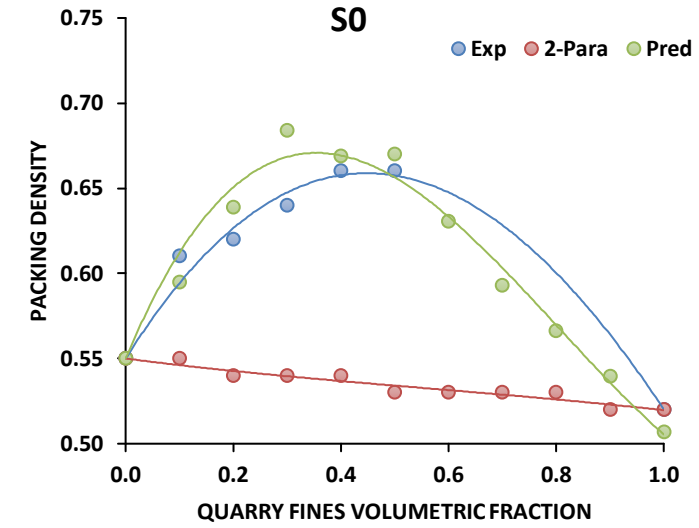

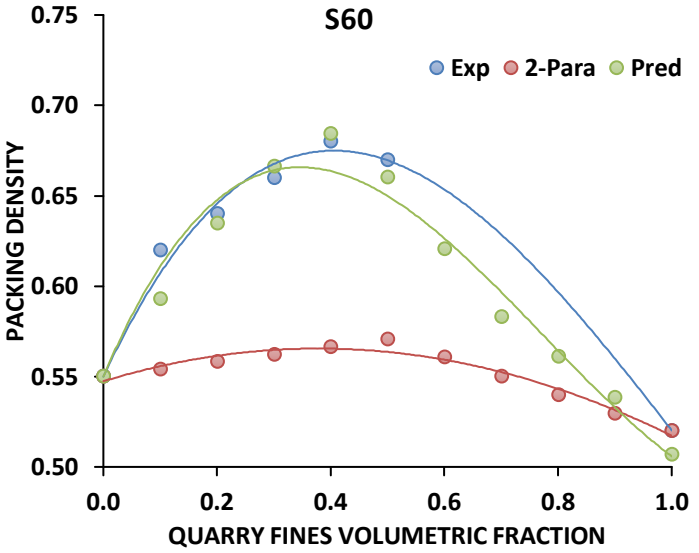

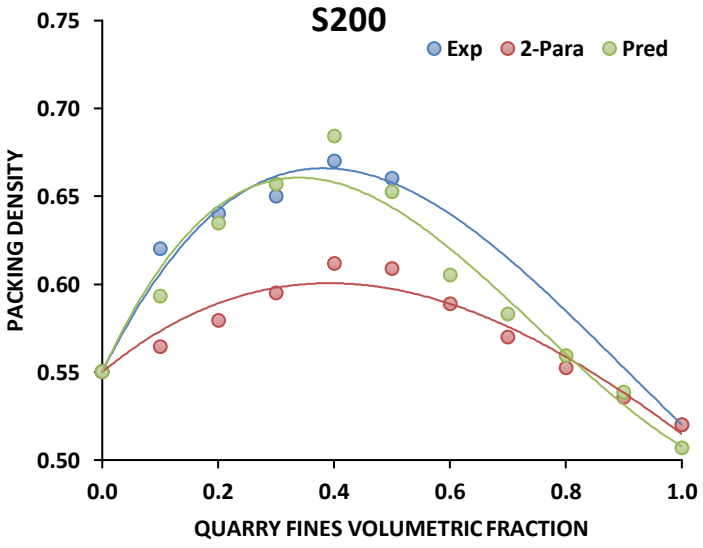

Figure 2.9: Plots of the experimental results, 2-parameter model, and prediction by the enhanced model for S

Table 2.5: Recorded error for Sandstone

a	EXP	2-PARA	ERROR (%)	PRED	ERROR (%)
S0	0.55	0.55	0.0	0.55	0.0
	0.61	0.55	9.8	0.59	2.5
	0.62	0.54	12.9	0.64	3.0
	0.64	0.54	15.6	0.68	6.8
	0.66	0.54	18.2	0.67	1.3
	0.66	0.53	19.7	0.67	1.5
		0.53		0.63	
		0.53		0.59	
		0.53		0.57	
		0.52		0.54	
	0.52	0.52	0.0	0.51	2.5
	Mean Abs Err		10.9		2.54

b	EXP	2-PARA	ERROR (%)	PRED	ERROR (%)
S60	0.55	0.55	0.0	0.55	0.0
	0.62	0.55	10.64	0.59	4.34
	0.64	0.56	12.79	0.63	0.83
	0.66	0.56	14.81	0.67	0.94
	0.68	0.57	16.69	0.68	0.62
	0.67	0.57	14.81	0.66	1.43
		0.56		0.62	
		0.55		0.58	
		0.54		0.56	
		0.53		0.54	
	0.52	0.52	0.0	0.51	2.52
	Mean Abs Err		9.96		1.52

c	EXP	2-PARA	ERROR (%)	PRED	ERROR (%)
S200	0.55	0.55	0.0	0.55	0.0
	0.62	0.56	8.99	0.59	4.34
	0.64	0.58	9.49	0.63	0.83
	0.65	0.60	8.45	0.66	1.06
	0.67	0.61	8.69	0.68	2.12
	0.66	0.61	7.75	0.65	1.12
		0.59		0.61	
		0.57		0.58	
		0.55		0.56	
		0.54		0.54	
	0.52	0.52	0.0	0.51	2.52
	Mean Abs Err		6.20		1.71

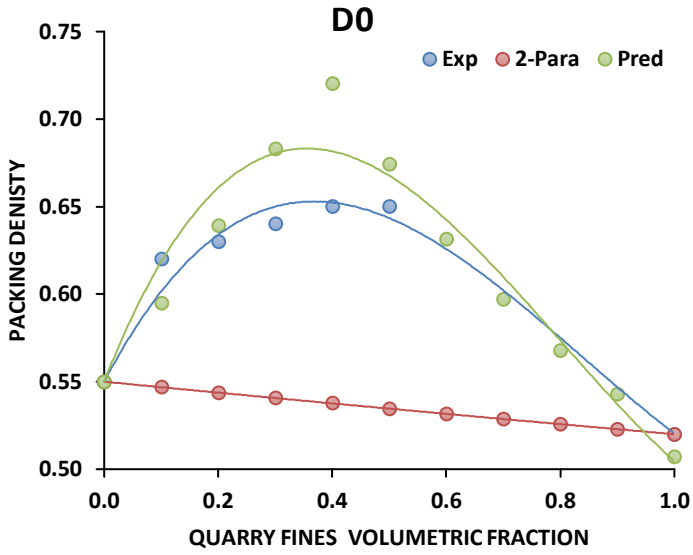

Table 2.6: Recorded error for Diorite

a	EXP	2-PARA	ERROR (%)	PRED	ERROR (%)
D0	0.55	0.55	0.0	0.55	0.0
	0.62	0.55	11.80	0.59	4.08
	0.63	0.54	13.69	0.64	1.42
	0.64	0.54	15.52	0.68	6.72
	0.65	0.54	17.29	0.72	10.81
	0.65	0.53	17.76	0.67	3.72
		0.53		0.63	
		0.53		0.60	
		0.53		0.57	
		0.52		0.54	
	0.52	0.52	0.0	0.51	2.52
	Mean Abs Err		10.87		4.18

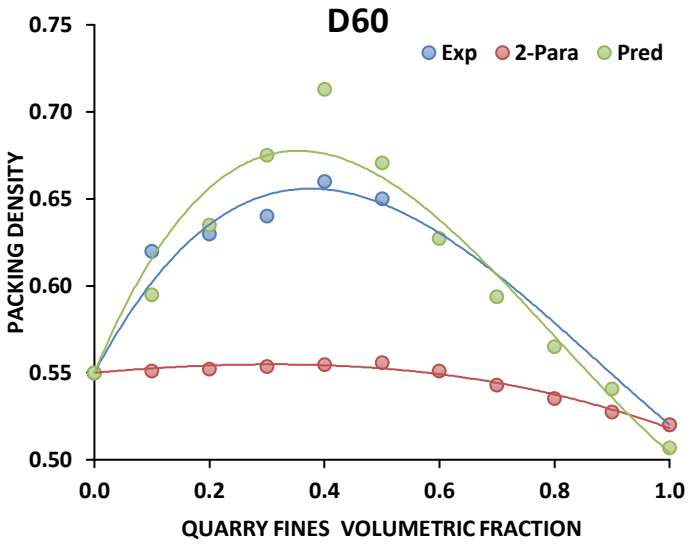

b	EXP	2-PARA	ERROR (%)	PRED	ERROR (%)
D60	0.55	0.55	0.0	0.55	0.0
	0.62	0.55	11.10	0.59	4.08
	0.63	0.55	12.32	0.63	0.78
	0.64	0.55	13.51	0.67	5.46
	0.66	0.55	15.94	0.71	8.05
	0.65	0.56	14.47	0.67	3.21
		0.55		0.63	
		0.54		0.59	
		0.54		0.57	
		0.53		0.54	
	0.52	0.52	0.0	0.51	2.52
	Mean Abs Err		9.62		3.44

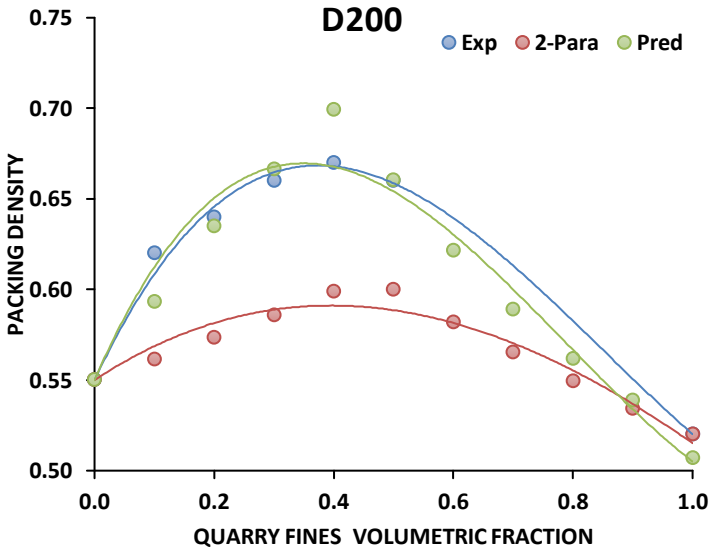

c	EXP	2-PARA	ERROR (%)	PRED	ERROR (%)
D200	0.55	0.55	0.0	0.55	0.0
	0.62	0.56	9.44	0.59	4.31
	0.64	0.57	10.40	0.63	0.80
	0.66	0.59	11.23	0.67	0.99
	0.67	0.60	10.61	0.70	4.37
	0.66	0.60	9.10	0.66	0.06
		0.58		0.62	
		0.57		0.59	
		0.55		0.56	
		0.53		0.54	
	0.52	0.52	0.0	0.51	2.52
	Mean Abs Err		7.25		1.87

Figure 2.10: Plots of the experimental results, 2-parameter model, and prediction by the enhanced model for D

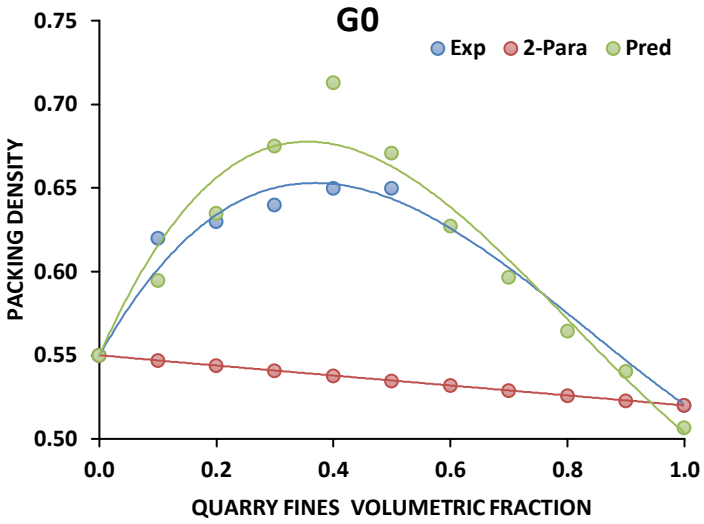

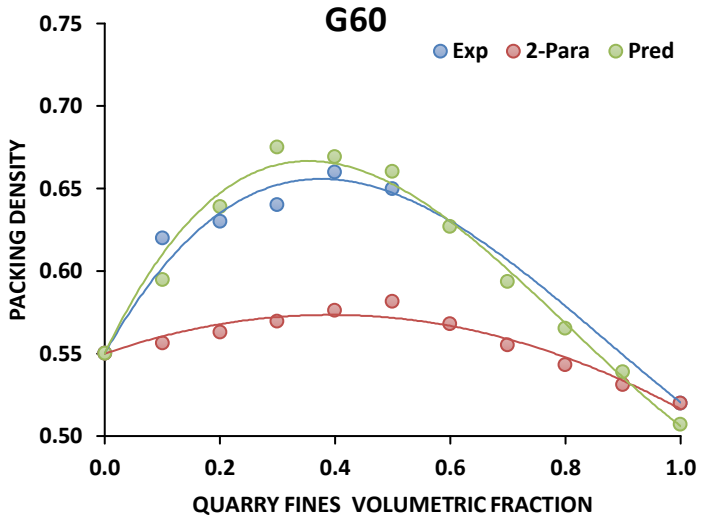

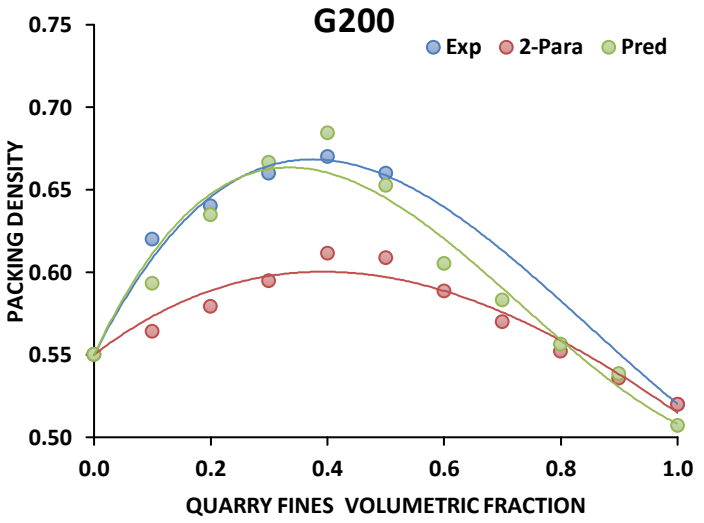

Figure 2.11:Plots of the experimental results, 2-parameter model, and prediction by the enhanced model for G

Table 2.7: Recorded error for Granite

a	EXP	2-PARA	ERROR (%)	PRED	ERROR (%)
G0	0.55	0.55	0.0	0.55	0.0
	0.62	0.55	11.79	0.59	4.08
	0.63	0.54	13.67	0.63	0.78
	0.64	0.54	15.50	0.68	5.47
	0.65	0.54	17.26	0.71	9.72
	0.65	0.53	17.71	0.67	3.20
		0.53		0.63	
		0.53		0.60	
		0.53		0.56	
		0.52		0.54	
	0.52	0.52	0.0	0.51	2.52
	Mean Abs Err		10.85		3.68

b	EXP	2-PARA	ERROR (%)	PRED	ERROR (%)
G60	0.55	0.55	0.0	0.55	0.0
	0.62	0.56	10.27	0.59	4.08
	0.63	0.56	10.67	0.64	1.42
	0.64	0.57	11.03	0.67	5.46
	0.66	0.58	12.69	0.67	1.39
	0.65	0.58	10.54	0.66	1.61
		0.57		0.63	
		0.56		0.59	
		0.54		0.57	
		0.53		0.54	
	0.52	0.52	0.0	0.51	2.52
	Mean Abs Err		7.88		2.36

c	EXP	2-PARA	ERROR (%)	PRED	ERROR (%)
G200	0.55	0.55	0.0	0.55	0.0
	0.62	0.56	9.01	0.59	4.31
	0.64	0.58	9.52	0.63	0.80
	0.66	0.59	9.88	0.67	0.99
	0.67	0.61	8.74	0.68	2.14
	0.66	0.61	7.79	0.65	1.12
		0.59		0.61	
		0.57		0.58	
		0.55		0.56	
		0.54		0.54	
	0.52	0.52	0.0	0.51	2.52
	Mean Abs Err		6.42		1.70

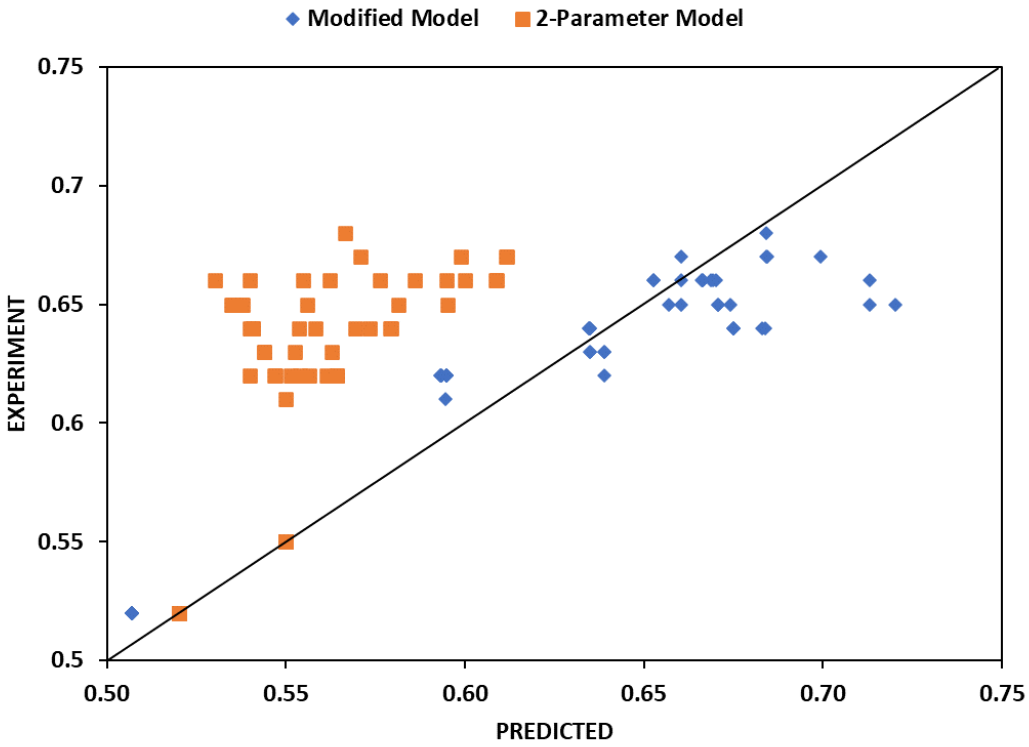

Figure 2.12:Validations on the theoretical prediction by the modified model and the 2-Parameter model

2.4.4 VALIDATION OF PROPOSED MODIFIED MODEL

In **Figure 2.13**, it can be seen that, in general, the data points lie very closely to the equality line. This implies the modified model predictions agree very closely with the experimental results. However, it can be seen that while most data points lie near the line, some other points lie slightly above and more to below the line. In general, the theoretical prediction and experimental results have a very good agreement of a R^2 of 0.91.

The theoretical predictions of the 2-parameter model are also plotted in **Figure 2.13**. It can be seen that most of the data points lie above the equality line. This implies that the 2-parameter model has an overall trend of underestimating the packing density. A very low agreement of $R^2 = 0.43$ between the experimental and model predictions was found to be very low.

2.5 CONCLUSION

Interest in enhancing particle packing in cementitious materials stems from efforts to reduce the content of Portland cement, reduce water demand, and maximise the usage of waste QDs. Hence, it decreases the cost and environmental impact as well as improving the material performance.

This work evaluated the conventional 2-parameter model, which was found to underestimate the packing density for microfines particles (finer than 75 microns), leading to unacceptable discrepancies between predicted and measured packing densities. It is postulated herein that such discrepancies may be attributed to the actual PSD, which has not been accounted for in the discrete packing model.

A series of packing density versus $\alpha_n C_u$ and $\alpha_n C_c$ were plotted to understand its relationship, and it indicate that the packing density has similar relationship of packing density to the volumetric fraction. Hence, it can be concluded that the packing density is a function of the PSD and amounts of particles present in mixtures (volumetric fractions). Increasing the QDs volumetric fraction would increases the $\alpha_n C_u$ and $\alpha_n C_c$ as well.

Some modifications have been made where the actual PSD is added by the introduction of C_u and C_c into the model. Because the size ratio is insensitive to packing density and has a significant high standard deviation of the PSD, particle interaction is excluded from the model, which can be considered not viable. With the modification, the theoretical predictions by the enhanced model have been compared to the experimental results, and they show a very good agreement, with absolute mean errors reduced by a range of 1.52% to 4.18%. The results of the modified 2-parameter packing model should allow improved prediction of the packing densities of many commonly encountered microfines in cementitious particle systems. For future studies, it is recommended to use the C_u and C_c for aggregates with particles larger than 75 microns.

This page is intentionally left blank

Chapter 3:Influence of fineness of quarry dust on hydration kinetics in cementitious mixes

H I G H L I G H TS

- No direct relationship of quarry dust fineness on increasing hydration kinetics.
- CASH, AFm phases monosulfate and monocarbonate were formed in PC-QDs hydrated cement-based composite,
- Increased in strength due to milling are attributed to the physical (filler), surface chemical (nucleation) effects.

A B S T R A C T

Keywords: Waste quarry dust, Milling, Controlled packing, Hydration kinetics

Reducing emissions associated with cement consumption, conserving resources, and reusing waste are vital objectives for the construction industry. This study explores the feasibility of employing quarry dust derived from sandstone, diorite, and granite as supplementary cementitious materials. This paper delves into the detailed examination of the effectiveness of milling in reducing particle size to enhance hydration kinetics. The quarry dust serves as a replacement for Ordinary Portland Cement (PC) within a controlled compaction scenario at a replacement volume of 40%. Dust particles passing through the 75-micron sieve undergo pre-treatment via milling for durations of 0, 60, and 200 seconds. Raw materials are subjected to examination using x-ray fluorescence (XRF), x-ray diffraction (XRD), and particle size distribution (PSD). Meanwhile, cement-based composites are evaluated using heat of hydration (HoH), cube compressive strength, and SEM-EDX. Despite the milling process aimed at reducing particle sizes, we found no clear directly proportional relationship between particle size and the enhancement of hydration kinetics. The most significant improvements were noted at the 60s milling, where the mean particle size (D_{50}) was approximately 10 μm.

Observations included the formation of CASH and AFm phases. However, milling beyond 60s to finer sizes (200s) did not yield proportional improvements and in some cases led to decrease in hydration kinetics, indicating a saturation point beyond which further size reduction becomes ineffective. Further investigation is needed to clarify the mechanisms behind this behaviour and to determine the optimal milling parameters for enhancing hydration kinetics. Overall, it is concluded that quarry dust milled for 60 seconds to achieve a D_{50} of 10 μm offers the most favourable results in hydrated cement-based composites. This research should lead to more sustainable concrete mixes.

3.1 INTRODUCTION AND BACKGROUND

Concrete remains an indispensable construction material in the industrialized world, with Ordinary Portland Cement (PC) serving as its predominant binder. However, PC production carries a substantial environmental burden, emitting approximately one tonne of CO2 for each tonne of cement produced and contributing to 5-7 percent of global CO2 emissions [1], [2]. This makes PC a significant driver of climate change. Consequently, there is a pressing need to develop more sustainable cements that consume less energy and produce fewer CO2 emissions, ultimately fostering greater environmental sustainability. The construction industry also consumes vast amounts of materials, including aggregates, and generates considerable waste. Aggregate quarries, particularly during crushing and washing operations, can produce up to 10% waste dust by volume [3], which, due to its fine nature, poses disposal and environmental challenges.

The incorporation of supplementary cementitious materials (SCMs) in concrete is an established approach to reducing carbon dioxide emissions in concrete construction. It is evident that the utilization of up to 70% mineral additives in cementitious materials can yield more durable, cost-efficient, and eco-friendly concrete by curtailing CO2 emissions and repurposing industrial waste [3]. However, conventional SCMs like slag and fly ash (FA) are in limited supply and anticipated to become scarcer in the future [4], [5]. Consequently, alternative sources of SCMs, such as quarry dust (QDs), are gaining prominence due to their natural abundance, accessibility, and cost-effectiveness [6], [7].

The use of quarry waste in cement-based products has been extensively researched in recent years. Ramos et al [2] produced concrete with a w/b ratio of 0.50 by using a fine (d_{50} of 13μm) and a very fine marble sludge (d_{50} of 3.5μm) at cement replacement levels of 10%. The addition of fine waste had no significant effect on the strength and durability of concrete; however, very fine waste enhanced its resistance to alkali-silica reaction by up to 38% and resistance to chloride penetration by 70% when compared to reference mixes.

Medina et al. [4] explored the use of granitic quarry dust as a cement replacement (10% and 20%) and reported strength improvements and pozzolanic activity based on

both mechanical testing and microstructural analyses. While these findings suggest the potential for pozzolanic reactivity, it is important to recognize that strength development alone cannot be taken as conclusive evidence of pozzolanic activity. Strength improvement could result from other mechanisms, such as improved particle packing or filler effects, and these factors must be considered and ruled out before attributing the observed behaviour to pozzolanic reactions. However, to confirm the presence of a pozzolanic reaction, it is necessary to look beyond mechanical and microstructural analysis alone. The pozzolanic reaction is a chemical process where pozzolanic materials react with calcium hydroxide (CH) in the presence of water to form secondary cementitious compounds, such as calcium silicate hydrate (CSH) and calcium aluminate silicate hydrate (CASH). This reaction results in CH consumption and contributes to improved durability and mechanical properties. According to Snellings et al. (2016), the formation of these compounds is a key indicator of pozzolanic activity.

Strength gains alone cannot be used as conclusive proof of a pozzolanic reaction, as they may arise from other factors, such as physical filler effects or hydration acceleration. Direct evidence of CH depletion, new phase formation, and associated microstructural changes is required to confirm the reaction. In Medina et al.'s study [4], while mechanical tests indicated improved strength, it was the microstructural changes, such as the reduction of CH content observed through techniques like X-ray diffraction (XRD) and scanning electron microscopy (SEM), that provided conclusive evidence of pozzolanic activity. These methods enable the visualization of reaction products like CSH, which are essential for confirming the pozzolanic reaction (Seraj et al., 2017; Burris & Juenger, 2016).

The combination of mechanical strength testing, SEM, and XRD, as used in these studies, allows for the monitoring of CH consumption, the identification of new reaction products, and the observation of microstructural changes. Together, these analyses provide the comprehensive evidence necessary to conclude pozzolanic activity in cementitious systems.

Ndahirwa et al [5] explored the use of a calcined sandstone washing mud (d_{50} around 8.0 μm) to replace up to 30% of Portland cement in mortars and they also found this to

have pozzolanic activity. The largest strength enhancement was obtained in samples comprising waste that had been calcined at 850°C for 1 hour, at a 20% replacement level.

However, while the use of quarry dust as a supplementary cementitious material offers several advantages, it is essential to acknowledge its disadvantage.

One notable disadvantage of incorporating quarry dust, particularly with high fines content, is the increased water demand. The fine particles possess a higher specific surface area compared to cement particles, necessitating more water to achieve the desired workability in the concrete mix. This increase in water demand can impact the water/cement ratio, raising concerns about strength and durability.

The high surface area of fine particles increases the amount of water required to wet the particle surfaces adequately. This phenomenon is due to capillary action and surface tension effects, which become significant at smaller particle sizes. A higher surface area-to-volume ratio means that more water is needed to form a lubricating layer around each particle, facilitating flow and reducing friction between particles. However, the fine particles also contribute to improved packing density. Enhanced packing density reduces void spaces within the concrete mix, which can offset the need for additional water. The concept of packing density is important in understanding the behavior of quarry dust in cementitious materials. By achieving high packing density, the amount of cement paste required to fill the voids is minimized, which in turn allows for a lower water-cement ratio. This principle is critical in producing high-performance concrete such as Ultra-High-Performance Concrete (UHPC), where fine materials are used to maximize density and minimize water content (Roussel et al., 2012; Hossain et al., 2022).

Incorporating fine particles into concrete is also known to have a substantial impact on performance. Overall, prior research [6] shows that the addition of fine particles can yield benefits on three distinct levels:

(i) Physically (filler effect): Particles fill intergranular voids between cement particles and thus improve packing density of the concrete.

(ii) Surface chemistry: By acting as nucleation sites, the extra particles enhance hydration and as a result form an essential element of the cement paste.

(iii) Chemically: The particles react directly with a cement ingredient like calcium hydroxide (CH) to create cement gel.

Nucleation sites are points of initiation of cement hydration. They mark the onset of reactions, such as the formation of cement hydrates, and could be enhanced by the presence of quarry dust. Essentially, nucleation directs the beginning of the hydration process and can influence its rate. The mechanism behind the nucleation sites formed by fine particles is depicted in **Figure 3.1**. In cement containing CSH, nuclei are generally believed to form exclusively on cement grain surfaces. However, the inclusion of fine particles, like QDs, expands both the number and surface area of these nucleation sites.

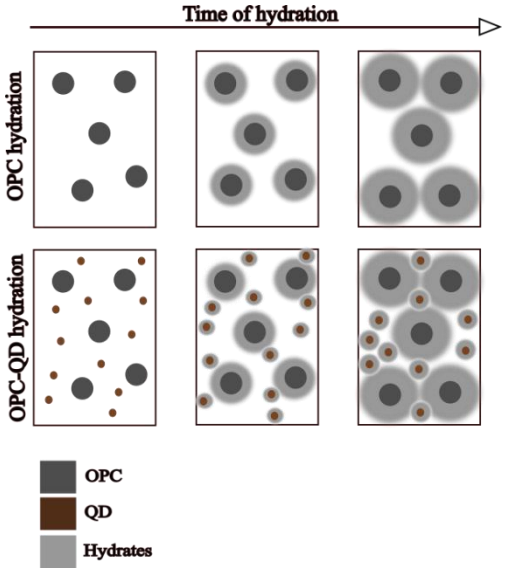

Figure 3.1:Schematic presentation of nucleation sites on the hydration PC and PC-QDs paste.

The reactivity of SCM such as zeolite and fly ash are also known to be enhanced by milling. This process has the potential to decrease crystallinity and increase the amorphous content, thereby enhancing reactivity [2], [5], [7]. In particular, researchers have identified that the de-crystallization of minerals is caused by the structural collapse resulting from the rupture of Si-O-Si and Si-O-Al bonds on the exterior surfaces of minerals [6].

Knop and Peled [8], in their study with limestone materials, demonstrated that limestone with smaller particle sizes had a greater effect on chemical reactivity than

limestone similar sized to PC. This further highlights the potential for particle size reduction to enhance the reactivity of SCMs, including QDs.

Despite extensive research on this topic, little is known about the impact of different particle sizes on QDs reactivity and hydration development in a controlled packing condition, i.e., maximised packing of cement paste with various PSD of waste QDs. Notably, none of the investigations in the literature have examined cementitious systems using milled QDs under controlled packing density. Thus, this study aims to provide a deeper understanding of the effect of milled QDs as SCMs. The primary objective is to create sustainable blended cements by partially replacing cement with different QDs.

The effect of QDs particle size is examined on the following: cement hydration kinetics, compressive strength, and elemental composition. Three different PSD sourced from three different quarry locations are examined using semi-adiabatic.

3.2 MATERIALS AND METHODS

An Ordinary Portland Cement CEM I 52.5 N (obtained from Hanson Cement) complying with the requirements of BS EN 197-1 and BS-EN 197-2 was used in the production of cement pastes. A polycarboxylate ether-based superplasticizer (SP) was added at a dosage of 1.50% by mass of binder (cement + QD) to obtain a homogeneous mixture and avoid agglomeration of the fine particulates.

The three different types of QDs examined in this study were obtained from the three quarries shown in **Figure 3.2** and comprised granite (G), sandstone (S) and diorite (D). The quarry waste was collected in the form of sludge and milled into different particle sizes using a TEMA milling machine.

(a) TARMAC Whitwell Quarry

(b) HAP SENG Tawau Quarry

(c) HAP SENG Papar Quarry

3.2.1 BINARY MIXTURES (PASTE)

A total of nine paste mixtures were obtained by combining PC with 40% by volume of the QDs obtained from the three different sources, each milled to achieve 3 different PSD. As identified in a previous study by the authors (REF), this proportion was used to achieve maximum packing density. The cement and QD powder were dry mixed for 2 minutes prior to adding water and superplasticizer (SP) and further mixed for another 3 minutes. A water to binder (w/b) ratio of 0.3 was used in all mixes. Each mix is labelled according to QD type (D, S, or G) and its corresponding milling period of 0, 60s, or 200s. The amount of Portland cement, QDs, water, and SP were kept constant in all the pastes.

Figure 3.2:Source location of the three QDs used in this study: (a) granite, (b) sandstone and (c) diorite.

Blended cement paste was prepared to evaluate heat of hydration (HoH), while the hydrated cement was used to assess the, compressive strength, and hydrates generated.

The **Table 3.1** below provides the formulation details for the cementitious mixes, including the amounts of superplasticizer and water. The water-to-binder ratio (W/B) is

fixed at 0.3, and the superplasticizer dosage is set at 1.5% of the total binder content. These parameters are held constant across all mixes to ensure consistency in comparing the effects of different Quarry Dust particle sizes, with a consistent 40% replacement of PC. This approach allows for the accurate assessment of particle size influence without the variability introduced by changes in water or admixture content.

Table 3.1: Formulation details of cementitious mixes

Mix	Portland Cement (PC) (kg/m3)	Quarry Dust (QDs) (Kg/m3)	W/B Ratio (Kg/m3)	Superplasticizer (Kg/m3)
PC	1000.0	0	300	15
PC+S0	523.5	476.5	300	15
PC+S60	523.5	476.5	300	15
PC+S200	523.5	476.5	300	15
PC+D0	523.5	476.5	300	15
PC+D60	523.5	476.5	300	15
PC+D200	523.5	476.5	300	15
PC+G0	500.8	499.2	300	15
PC+G60	500.8	499.2	300	15
PC+G200	500.8	499.2	300	15

3.2.2 RHEOLOGICAL EFFECTS OD QUARRY DUST IN CEMENT PATES

Although the primary focus of this study is on mechanical performance and hydration, it is important to discuss the potential effects of QD on the rheological properties of cement paste. Based on existing literature, the incorporation of quarry dust, particularly fine QD particles, can influence the viscosity of the paste. Finer particles have higher specific surface areas, which can increase water demand or require more superplasticizer to maintain workability. Studies by Zhang et al. (2020) have shown that finer supplementary materials can increase the viscosity and reduce the flowability of cement pastes due to this higher water demand.

Conversely, well-graded QD may improve packing density, reducing the overall water demand and enhancing workability. As observed in Ultra-High-Performance Concrete (UHPC), fine materials can fill voids between larger particles, improving the cohesiveness of the mix and reducing particle friction. This effect can lead to better flow characteristics despite a lower water-to-binder ratio (Lee et al., 2018). The fine particle

packing in QD-incorporated mixes potentially improves workability, similar to the behaviour of UHPC systems.

3.2.3 HEAT OF HYDRATION (SEMI-ADIABATIC CALORIMETRY)

Heat of hydration tests were performed on cement paste mixtures cast into an insulated container. Each container was equipped with a thermocouple sensor linked to a data logger to monitor the temperature development inside the container. This method (semi-adiabatic) quantifies the amount of heat generated during cement hydration. Data collection commenced immediately after mixing and sealing the mixture in the container. Temperature was recorded every 10s for a total of 72 hrs (3 days).

3.2.4 COMPRESSIVE STRENGTH

The ability of a binder to react with CH in the presence of water results in the formation of additional cementitious hydrates that contribute to strength development. As a result, the compressive strength can provide an indirect measure of pozzolanic behaviour [11]. Compressive tests were performed on 2cm cube specimens, using a universal testing machine equipped with a 300kN load cell at a rate of 0.5 MPa/s. The average compressive strength is calculated as the mean of three test results.

3.2.5 SCANNING ELECTRON MICROSCOPY (SEM) WITH ELEMENTAL ANALYSIS

SEM-EDX was performed on 7- and 28-day samples to derive the atomic ratio plots of Al/Ca vs Si/Ca and S/Ca vs Al/Ca and identify the formation of hydrates [12]. Changes between 7 and 28 days can help identify the evolution of the hydration phases.

Backscattered electron (BSE) images were analysed in ImageJ [13] using a grey level thresholding method [14] to identify the area fraction of pores, hydrates, and un-hydrated cement [15]. An automated thresholding was applied, using the method of tangent slope (see **Figure 3.3**). The first peak represents the hydrated products, and the portlandite (CH) is clearly identifiable by a small hump in this area. The second peak represents the un-hydrated cement.

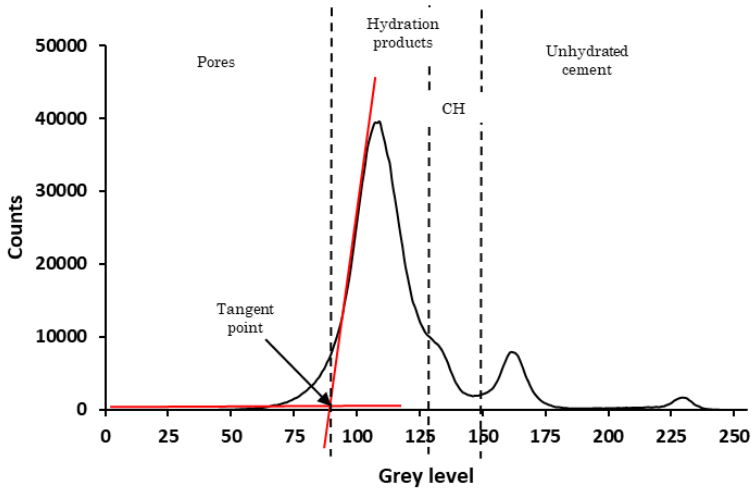

Figure 3.3: Grey level histogram of a typical SEM-BSE image and threshold levels for different phases

3.3 EXPERIMENTAL RESULTS AND DISCUSSION

The SEM images (**Figure 3.4**) of QDs and PC show a predominance of angular to sub-angular particles, indicative of a mechanical fracturing process, such as milling. There

is a notable presence of smaller particles adhering to the surface of larger grains, which is more pronounced on the PC (**Figure 3.4a**).

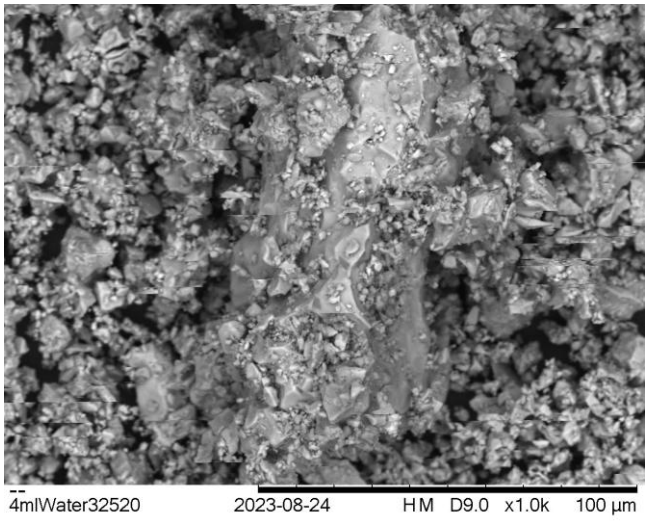

(a) PC passing 75µm

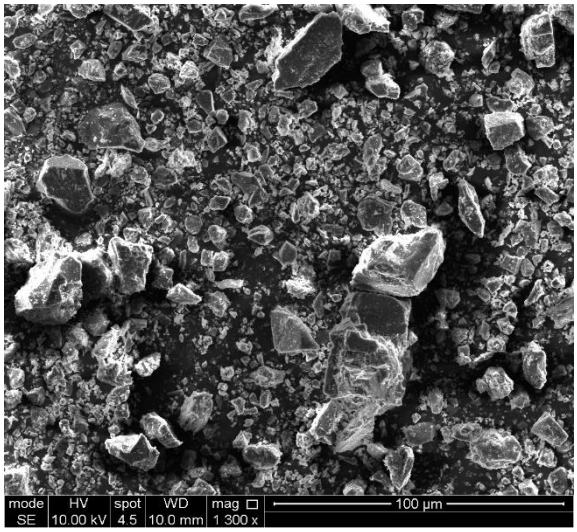

(b) Diorite passing 75µm

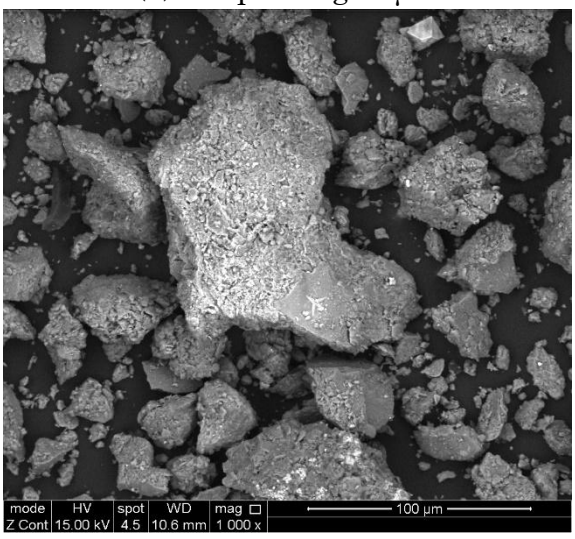

(c) Sandstone passing 75µm

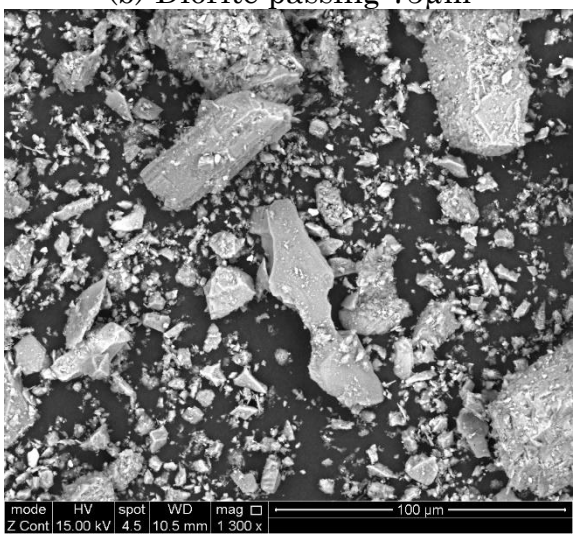

(d) Granite passing 75µm

Figure 3.4: SEM images of (a) PC and (b) diorite, (c) sandstone, (d) granite QDs

The particle size distributions of cement and QDs (**Figure 3.5**) were determined using a laser scattering machine LA-950. **Table 3.2** lists the D_{10}, D_{50}, and D_{90} values of the particle size distributions (PSD), which respectively refer to the particle size below which 10%, 50% and 90% of the particles in a sample lie, along with the D_{mean}, which is calculated by averaging the diameters of particles, weighted by their volume. As expected, a reduction in particle size is observed with increasing milling time, and a

mean particle size (D_{mean}) of approximately 10µm was achieved after milling for 200s. Unmilled QDs (0s) had a D_{mean} of around 30µm, similar to cement. The mechanical treatment reduces the particle sizes to significantly smaller sizes than PC and enhances the QD potential as a filler.

Table 3.2: Particle sizes of PC and QDs at d10, d_{50}, d_{90}, and mean diameter

		PC	Sandstone (S)			Diorite (D)			Granite (G)		
Milling Time (s)		0	0	60	200	0	60	200	0	60	200
Particle sizes (µm)	D_{10}	8.13	4.88	1.82	1.49	6.14	2.80	1.77	3.43	2.22	1.43
	D_{50}	20.60	21.62	9.03	7.80	18.17	10.87	8.65	14.03	9.46	7.38
	D_{90}	64.21	74.41	38.57	21.52	70.17	40.99	23.65	70.59	30.96	22.04
	D_{mean}	30.32	32.62	15.52	10.42	29.92	17.34	11.54	27.38	14.07	10.45

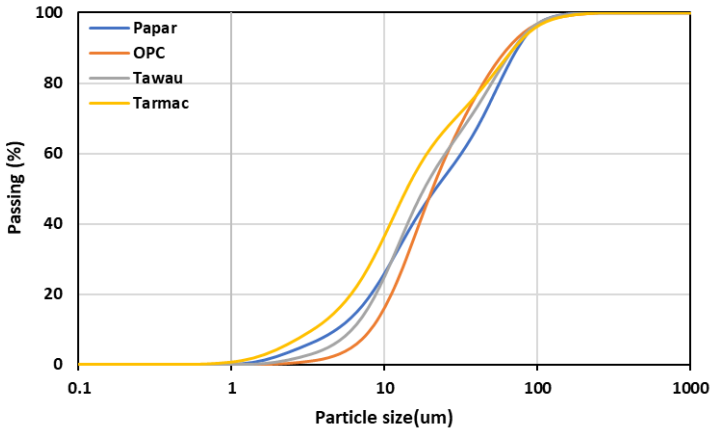

(a) Particles not milled

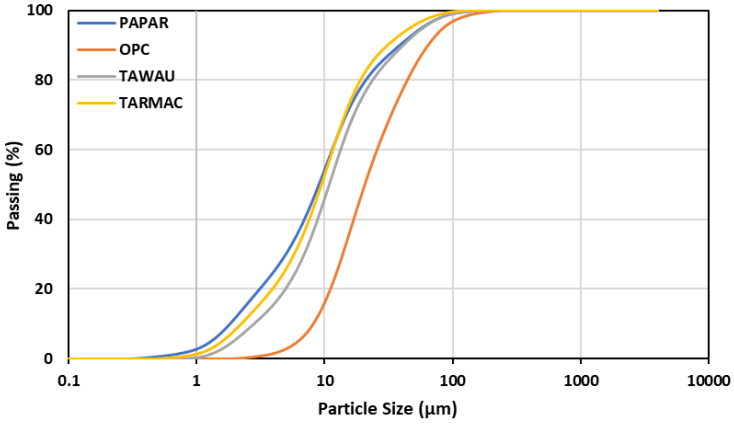

(b) Particles milled at 60s

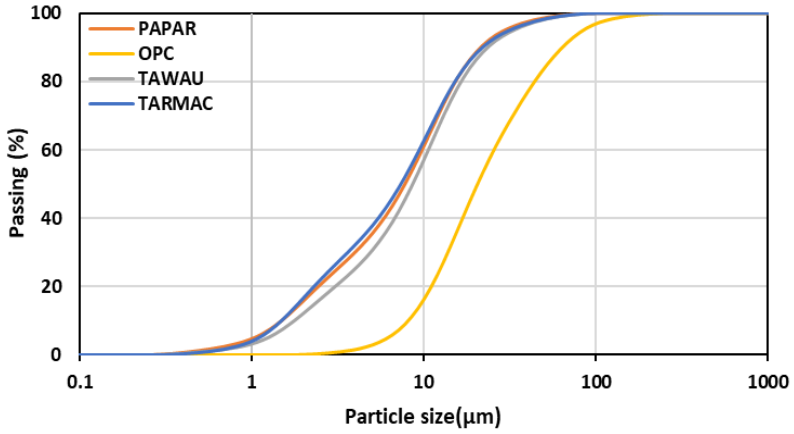

(c) Particles milled at 200s

Figure 3.5: Particle size distribution of PC and QDs for different milling time

3.3.1 PHYSICAL AND CHEMICAL CHARACTERIZATION

The Oxide composition of PC and QDs is presented in **Table 3.3**. The total amount of silicon, aluminium, and iron oxides for granite, and diorite QDs corresponds to 73.5%, and 82.4% respectively, exceeding the requirement of a pozzolanic material prescribed in ASTM C618 (70%). For the sandstone QD, this amount is 61.9%, which is below the requirement.

Table 3.3: Oxide composition of the materials used.

Material	Oxide (wt. %)											
	SiO_2	Al_2O_3	Fe_2O_3	MnO	MgO	CaO	Na_2O	SO_3	K_2O	TiO_2	P_2O_5	LOI
PC	20.0	6.0	3.0	0.1	2.0	65.0	0.5	1.5	0.5	0.2	0.1	1.0
Granite	56.81	13.60	3.13	0.09	3.07	3.14	2.83	0.05	3.69	0.74	0.18	12.25
Sandstone	50.17	8.80	2.88	0.05	1.02	1.48	1.29	0.63	1.73	0.38	0.05	31.20
Diorite	60.43	16.30	5.65	0.10	2.81	5.85	2.85	0.06	2.61	0.58	0.14	1.97

X-ray diffraction (XRD) analysis (conducted using a Siemens D-500 with Cu-Kα radiation) was performed on the QDs samples and the main mineral phases were identified to be quartz (SiO2) and corundum (Al2O3). **Figure 3.6** presents typical XRD patterns for milled QDs. It can be seen that increasing grinding time reduces the diffraction peak intensity of quartz, especially from 75µm to 60s. This indicates that the

crystallinity of quartz declines, which is possibly due to the quartz crystals breaking down into an amorphous state. This was also found in a study [16] on the impact of mechanical grinding on iron ore tailing powder.

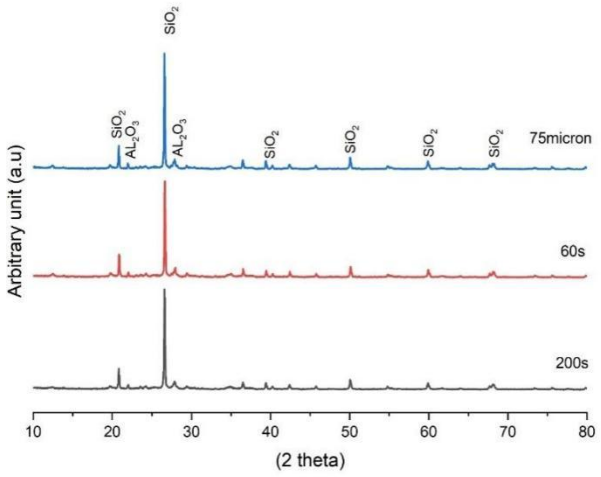

Figure 3.6: XRD patterns for Sandstone QDs with different grinding times.

In the XRD patterns, sharp peaks mean that the quartz and corundum have a regular, repeating atomic structure, which means they are crystalline. This did not change during the milling. An amorphous material would show a broad hump where the atoms are arranged in no specific order.

3.3.2 INFLUENCE OF MILLING ON HYDRATION KINETICS

The paste temperature and cumulative temperature (°C ·hour) of the various PC-QD pastes during hydration are shown in **Figure 3.7a-c**, as recorded through a semi-adiabatic calorimeter. The red dotted lines (PC60%) are determined by scaling down to 60% the PC curve. This is done to represent the expected heat profile when only 60% of PC is present in the paste and the rest of the material is inert. The active components in PC are mainly Belite-C_2S, Alite-C_3S and Aluminate-C_3A. Any surplus temperature in the PC-QDs curves may indicate a contribution from the QDs. **Table 3.4** shows the time and value of the hydration peak and the cumulative temperature hour at 72 hours.

The inherent difference in water-to-cement (w/c) ratios between PC 60% and QD-containing samples significantly impacts the hydration process. Specifically, the water available for hydration in the PC 60% mix is substantially reduced compared to the 100% PC sample, thereby limiting the validity of direct comparisons between the two.

Given this limitation, the data for PC 60% will be used only as a guide to observe trends and the influence of quarry dust (QD) replacement under a constant water-to-binder (w/b) ratio. This ensures that the primary variable under investigation is the replacement of PC with QD while acknowledging the limitations posed by the reduced water content available for PC hydration in the 60% mix. The results will provide insights into the behaviour of QD-containing mixes relative to PC 60% but will not be treated as a direct comparison.

To enable a true direct comparison in future studies, additional data should be collected for a 100% PC sample with a w/c ratio equivalent to that of the QD-containing samples. This would allow the effects of QD replacement to be isolated under comparable hydration conditions, facilitating a more robust analysis. For this study, the PC 60% data serve as a reference to guide the interpretation of trends rather than providing a definitive direct comparison.

The curves representing the QDs milled for 0 and 60 seconds are always above that of PC60%, thus indicating increased hydration activity. QDs milled for 200s in general show a lower trend of hydration kinetics, especially QDs from Tawau and Tarmac. This may indicate a saturation point, where further milling does not benefit the hydration kinetics. This is in line with the hypothesis that, finer materials can enhance the nucleation and hydration reactions up to a certain extent. However, to attribute the increased hydration kinetics to the filler effect it is necessary to examine the final hydrate composition from SEM-EDX.

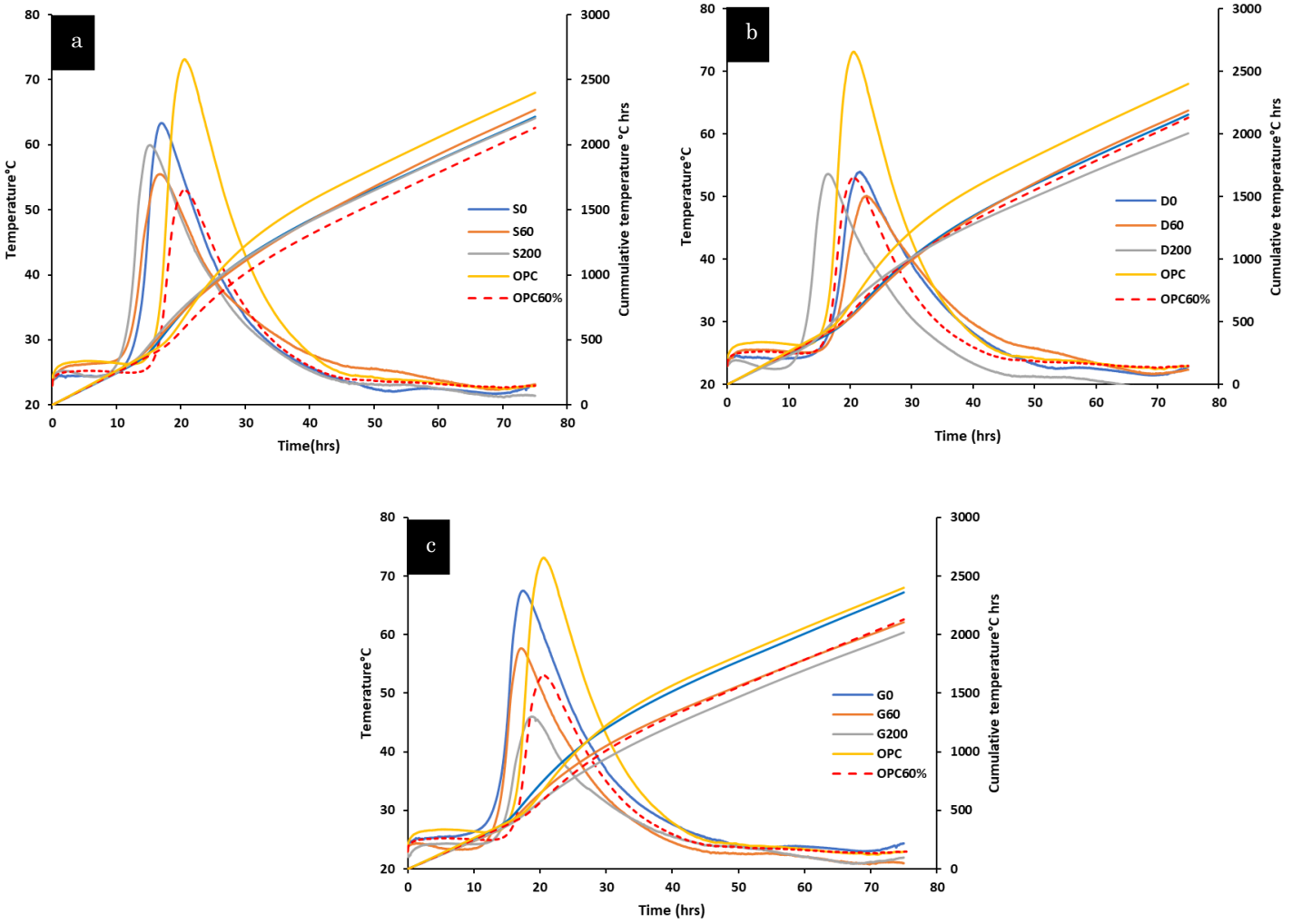

Figure 3.7: Hydration kinetics for (a) Sandstone (b) Diorite and (c) Granite

Table 3.4: Calorimetric parameters for binder hydration.

Cementitious mix	Age of hydration peak		Intensity of hydration peak		Cumulative temperature hour (after 72h)	
	Measured (h)	% of 60% PC	Measured (°C)	% of 60% PC	Measured (°C)	% of 60% PC
PC	20.52		73.12		2404	-
60% PC	20.66	100	52.93	100	2123	100
S0	16.97	82	63.32	120	2214	104
S60	16.68	81	55.41	105	2268	107

S200	15.20	74	59.95	113	2196	103
D0	21.49	104	53.89	102	2154	101
D60	22.70	110	50.11	95	2182	103
D200	16.30	79	53.68	101	2003	94
G0	17.44	84	67.39	127	2364	111
G60	17.13	83	57.53	109	2121	100
G200	18.81	91	45.94	87	2020	95

3.3.3 INFLUENCE OF PARTICLE SIZE ON CUBE COMPRESSIVE STRENGTH.

The average compressive strength at 7 and 28-days, shown in **Table 3.6**, is used to determine how the various PSDs affect strength development in the mixes. It is clear from the strength development beyond 7 days that hydration continues over time. As expected, the PC-QDs mixes have a lower compressive strength at both 7 and 28 days compared to the reference mix. This can be attributed to the dilution effect of the cement matrix formation and reduction in C_3S and C_2S. This is also reported in a another study [18] on iron tailings.

The relative compressive strength per weight of PC (f_c/W_{cement}) is also calculated. This ratio is used as a baseline to enable comparisons with pure PC. At both 7 and 28 days, all QD mixes have greater relative compressive strength per weight of PC compared to the reference mixes. This suggests that the QDs are contributing to the strength development either by the filler effect or the effect of new hydrated components in the cement paste. Though there is a consistent increase in strength at 28 days between mixes with raw QD (0s) and mixes with QD milled for 60s, this is not consistent for mixes with QD milled for 200s. As also discussed in paragraphs 3.2 and 3.3, this shows that there is no direct influence of QD fineness on strength improvement.

Table 3.5: Average compressive strength and relative compressive strength

QDs Source		PAPAR			TAWAU			TARMAC		
Mix	PC (Ref)	PC-S0	PC-S60	PC-S200	PC-D0	PC-D60	PC-D200	PC-G0	PC-G60	PC-G200
					7days age					

Compressive strength, f_c [MPa], (SD)	70.5 (12.2)	46.3 (1.6)	43.8 (12.8)	37.4 (16.9)	46.6 (3.0)	51.3 (3.8)	56.56 (2.7)	59.6 (3.4)	60.3 (2.1)	54.0 (0.4)
	28days age									
	91.2 (9.0)	65.2 (0.5)	68.3 (3.2)	68.7 (3.7)	67.5 (4.1)	74.8 (1.2)	70.6 (3.2)	74.3 (1.8)	67.5 (3.6)	66.5 (3.2)
f_c/W_{cement}	7days age									
	2.8	3.1	2.9	2.5	3.1	3.4	3.5	4.0	4.0	3.6
	28days age									
	3.6	4.3	4.5	4.6	4.5	5.0	4.7	4.9	4.5	4.4
Strength ratio relative to PC (%)	7 days age									
	100	111	104	89	111	121	125	143	143	129
	28 days age									
	100	119	125	128	125	139	131	136	125	122

3.3.4 STRENGTH ACTIVITY INDEX (SAI)

The SAI is a measure commonly used in the field of cement and concrete technology to assess the pozzolanic activity of SCMs. According to ASTM C618 (standard specification for coal fly ash and raw calcined natural pozzolan for use in concrete), the SAI is determined by comparing the 7- or 28-day compressive strength of a blended mixture of cement and the SCMs to that of a control mix with cement alone. The SCM is considered to possess pozzolanic activity if the strength activity index meets or exceeds 75%. The formula for calculating the SAI is as follows:

$$SAI = \left(\frac{A}{B}\right) x100 \qquad \textbf{Equation (3.4)}$$

Where;

A = average compressive strength of the PC-QD cubes in MPa

B = average compressive strength of the control mix mix cubes in MPa

The SAI is commonly used to evaluate the relative strength contribution of SCMs when partially replacing Portland cement (PC) in a mixture. A benchmark of 75% of the control mix's compressive strength at 28 days is typically used to indicate potential

pozzolanic activity. However, it is important to acknowledge that the SAI result alone does not provide definitive evidence of pozzolanic reactivity, especially in cases where low replacement levels of materials that are not truly pozzolanic (such as aggregates) may meet this strength threshold. For example, a non-pozzolanic material used at a low replacement level, such as 1%, could still meet the SAI requirement but would not be classified as pozzolanic.

To fully confirm pozzolanic activity, additional tests, such as X-ray diffraction (XRD), thermogravimetric analysis (TGA), and calcium hydroxide consumption tests, are necessary. These tests help determine whether the material reacts chemically with calcium hydroxide ($Ca(OH)_2$) to form the secondary calcium silicate hydrates (C-S-H), which are indicative of pozzolanic reactions. Therefore, while the SAI provides an initial indication of strength contribution, it should be used in conjunction with other tests to verify the material's pozzolanic properties and ensure that conclusions are based on a comprehensive evaluation.

Table 3.6: Strength activity index and averages per milling period

Strength Activity Index (SAI) %			Average Strength Activity Index (SAI)		
Mix	7-days	28-days	Milling Period (s)	7-days	28-days
S0	66	71			
S60	62	75	0	72.3	75.7
S200	53	75			
D0	66	74			
D60	75	82	60	74.3	77
D200	75	77			
G0	85	82			
G60	86	74	200	68.3	75
G200	77	73			

As shown in **Table 3.7**, in general, the SAI is over 75 percent indicating that most QDs contribute to the compressive strength of the concrete. The average results for each milling period indicate that a milling period of 60 seconds provides the best outcome. This contribution to the strength may be attributed to either better particle packing or better conditions for the development of hydration products.

3.3.5 MICROSTRUCTURE FROM SEM-EDX

To determine if the presence of fine QDs in the mixes affects cement microstructure, backscattered electron (BSE) imaging with energy dispersive X-ray spectroscopy (EDX) was used. 60 spectrums were obtained for each image to determine the atomic ratio of aluminium, calcium, and sulphur.

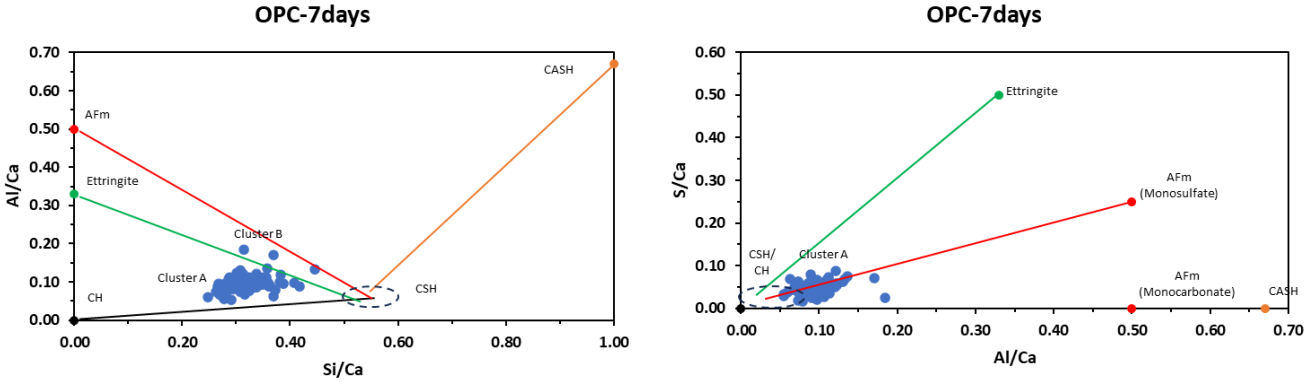

Figure 3.8: Atomic ratio plots for PC at 7-days for (a) Al/Ca vs Si/Ca (b) S/Ca vs Al/Ca

The findings show two major clusters for PC: Cluster A representing the CSH/CH phase; and Cluster B representing the ettringite phase. The observation of a dominant CSH phase, indicated by cluster A (see **Figure 3.10a** and **3.10b**), is consistent with previous research identifying CSH as the predominant binding phase in cement [9], [19]. Its development is often associated with a well-hydrated cement paste in which alite (C3S) and belite (C2S) have interacted with water to form this gel-like phase. In cluster B, there is a small cluster of ettringite phases that may be detected. Ettringite, a sulphate phase, is formed early in the hydration process when the cement's calcium aluminate combines with gypsum.

The presence of ettringite in small clusters is typical for CEM I and is expected as part of the normal hydration process. The ettringite levels observed are within the expected norms for CEM I, which ensures that the material is behaving as anticipated

without the presence of excessive sulphate that could lead to sulphate attack over time. Given that CEM I's composition, including sulphate content, is regulated, the ettringite observed is within permissible levels, confirming that there is no risk of long-term sulphate-related deterioration [20]. This regulated composition helps to control the sulphate content, ensuring that the cement is performing as intended in its hydrated state.

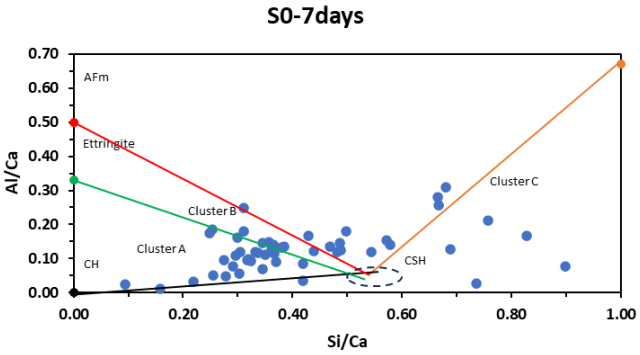

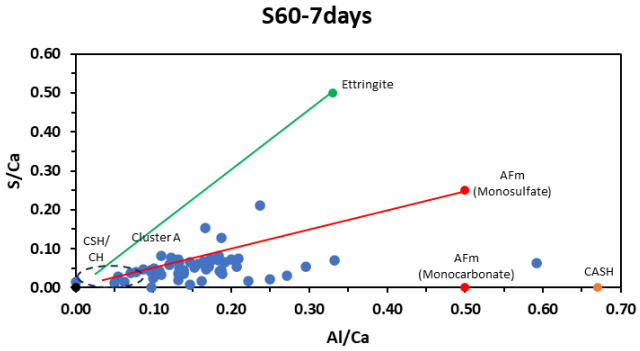

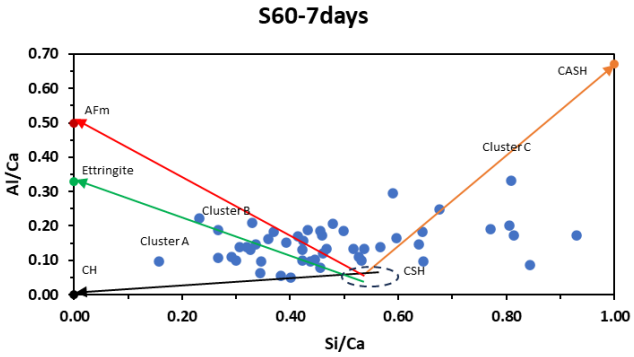

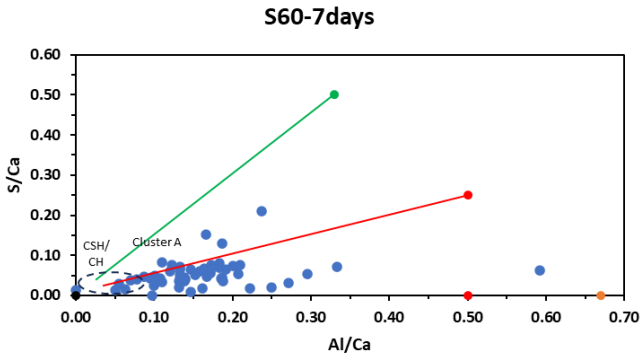

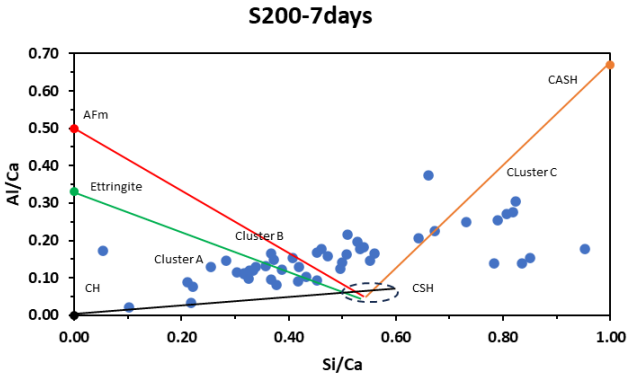

Figure 3.9: Atomic ratio plots for Sandstones at 7-days for Al/Ca vs Si/Ca (a) Un-milled, (b) milled 60s and (c) milled 200s

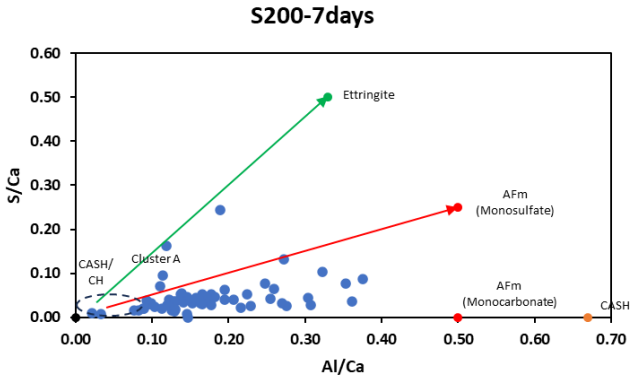

Figure 3.10: Atomic ratio plots for Sandstones at 7-days for S/Ca vs Al/Ca (a) Un-milled, (b) milled 60s and (c) milled 200s

The incorporation of sandstone QDs in mixes shows a different trend compared to the PC with cluster C (see **Figure3.11**) being indicative of CASH phases. This may indicate that the high alumina content [21] of the QDs could aid the formation of the CASH structure. This may impact the binding properties, which can affect porosity, binding capacity, and overall mechanical strength.

A further cluster corresponding to the AFm phases of monosulfate and monocarbonate is also present. Monosulfate is a phase that forms during the hydration of PC, especially in the absence of sufficient sulphate, while monocarbonate is commonly observed when aluminate phases react with carbonate ions. The formation of monocarbonate can indicate effective utilization of the aluminate phase from the QDs, which can be a positive aspect in terms of both strength and durability. This is known to help stabilise the cement structure and minimise porosity [22]. While AFm phases are not primary contributors to the strength of cementitious systems (that role is played by CSH), they still play a role in the microstructural development and overall matrix of the hydrated cement paste.

In this study, the formation of monocarbonate was identified through X-ray diffraction (XRD) complemented by the analysis of atomic ratio plots (S/Ca vs Al/Ca). These plots allowed for a clear comparison between the hydration products in the CEM I system and the QD + CEM I system.

In the CEM I atomic ratio plots, the formation of AFm phases, including monosulfate and monocarbonate, is primarily driven by the reaction of C_3A (tricalcium aluminate) with available sulfates and carbonates. The trends in these plots are consistent with the expected hydration behavior of pure PC, showing typical clusters related to AFm phases but without significant contributions from other alumina sources.

When Quarry Dust (QD) is introduced at 40% replacement of PC, the QD + CEM I atomic ratio plots show a distinct shift. The additional aluminate phase from the QD, particularly from alumina-rich minerals like feldspar, plays a critical role in the formation of monocarbonate. This is especially evident in the milled QD samples, where the finer particles (milled for 60 and 200 seconds) result in a more pronounced formation of monocarbonate.

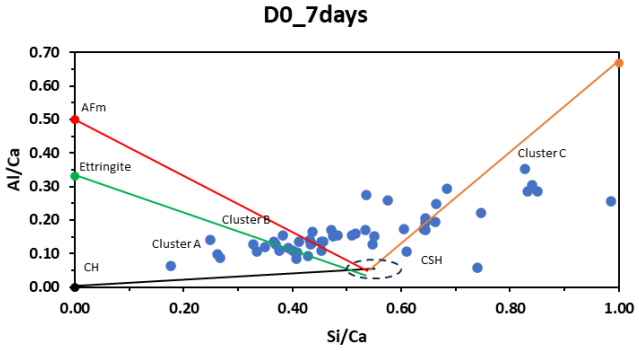

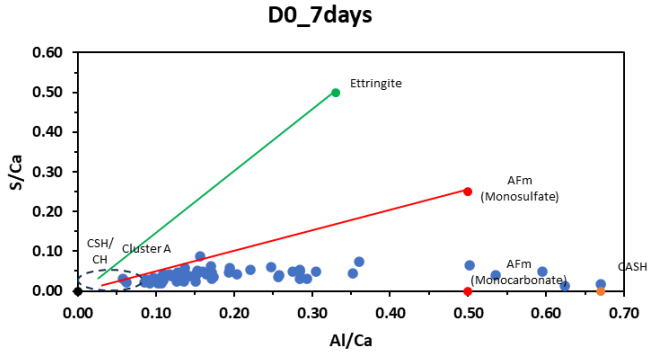

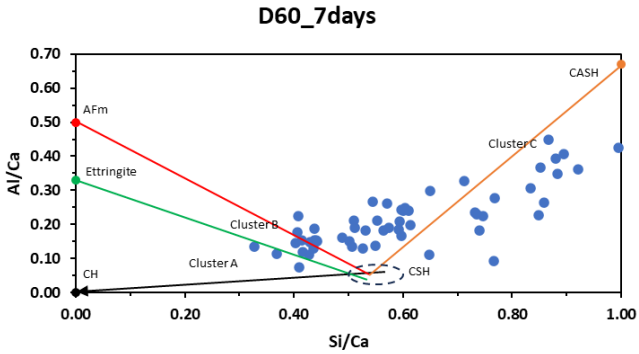

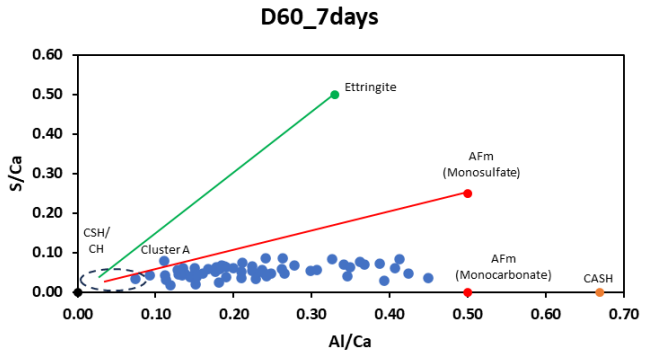

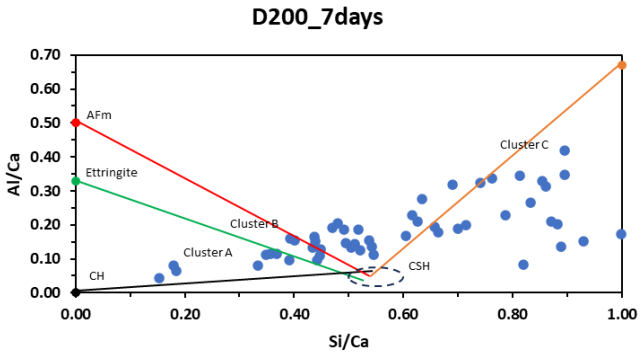

Figure 3.11: Atomic ratio plots for Diorite at 7-days for Al/Ca vs Si/Ca (a) Un-milled, (b) milled 60s and (c) milled 200s

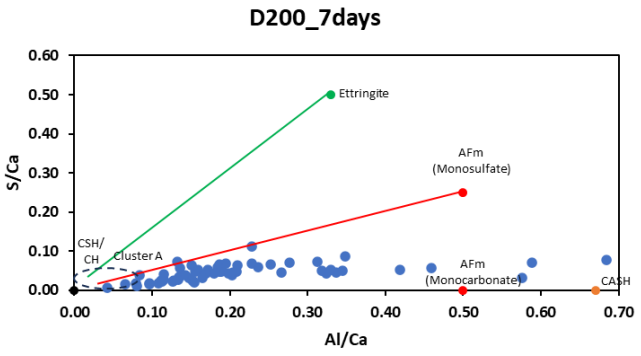

Figure 3.12: Atomic ratio plots for Diorite at 7-days for S/Ca vs Al/Ca (a) Un-milled, (b) milled 60s and (c) milled 200s

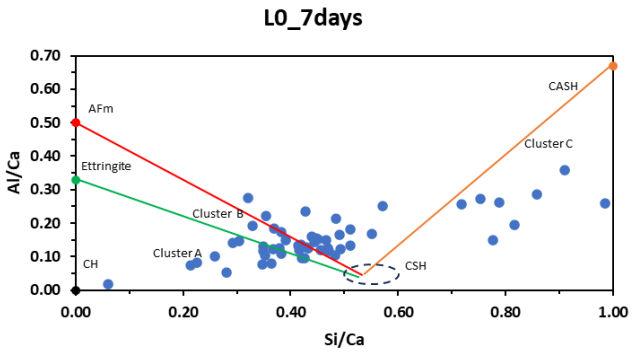

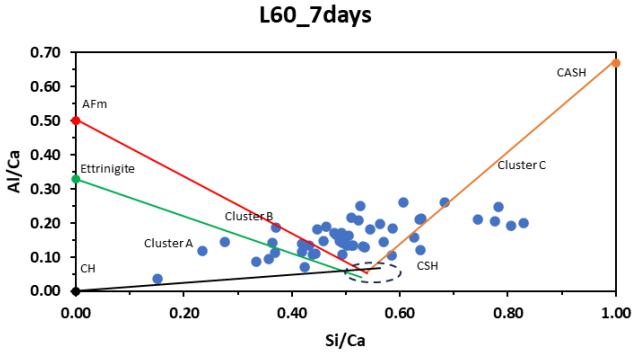

Figure 3.13: Atomic ratio plots for Granite at 7-days for Al/Ca vs Si/Ca (a) Un-milled, (b) milled 60s

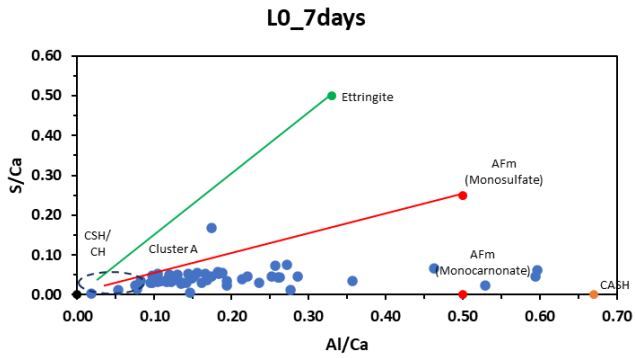

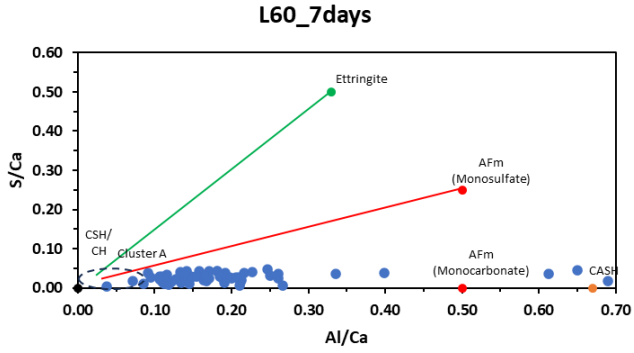

Figure 3.14: Atomic ratio plots for Granite at 7-days for S/Ca vs Al/Ca (a) Un-milled, (b) milled 60s

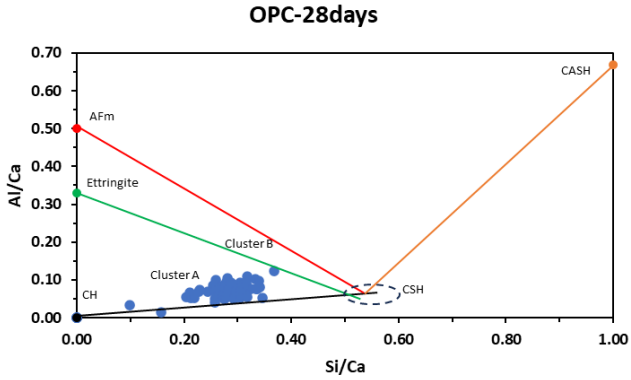

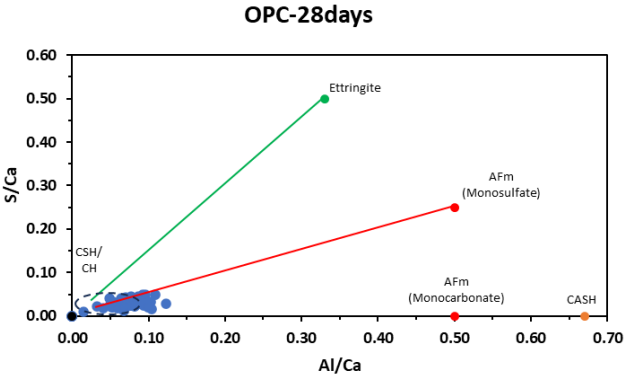

Figure 3.15: Atomic ratio plots for PC at 28-days for (a) Al/Ca vs Si/Ca (b) S/Ca vs Al/Ca

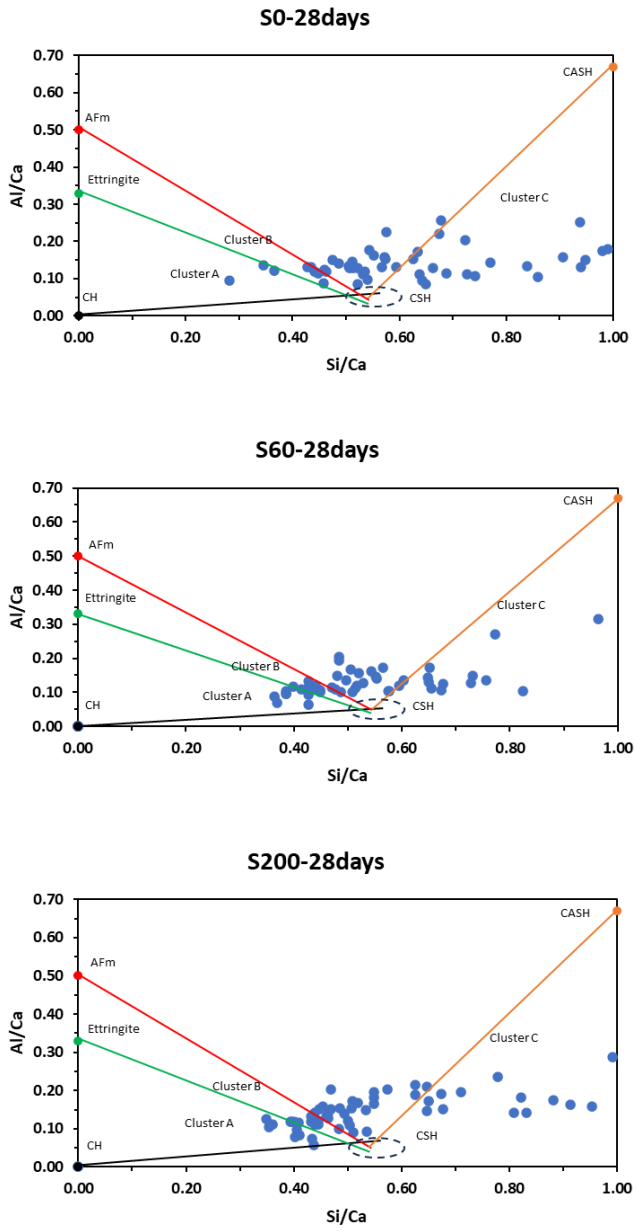

Figure 3.16: Atomic ratio plots for Sandstone at 28-days for Al/Ca vs Si/Ca (a) Un-milled, (b) milled 60s and (c) milled 200s

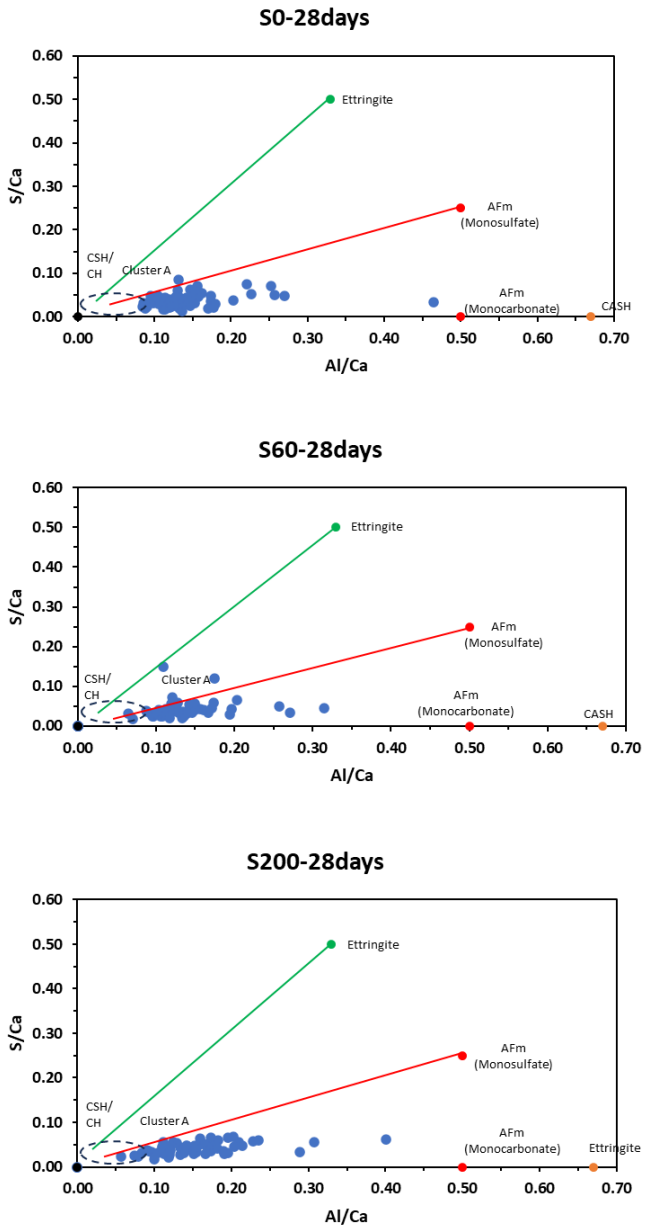

Figure 3.17: Atomic ratio plots for Sandstones at 28-days for S/Ca vs Al/Ca (a) Un-milled, (b) milled 60s and (c) milled 200s

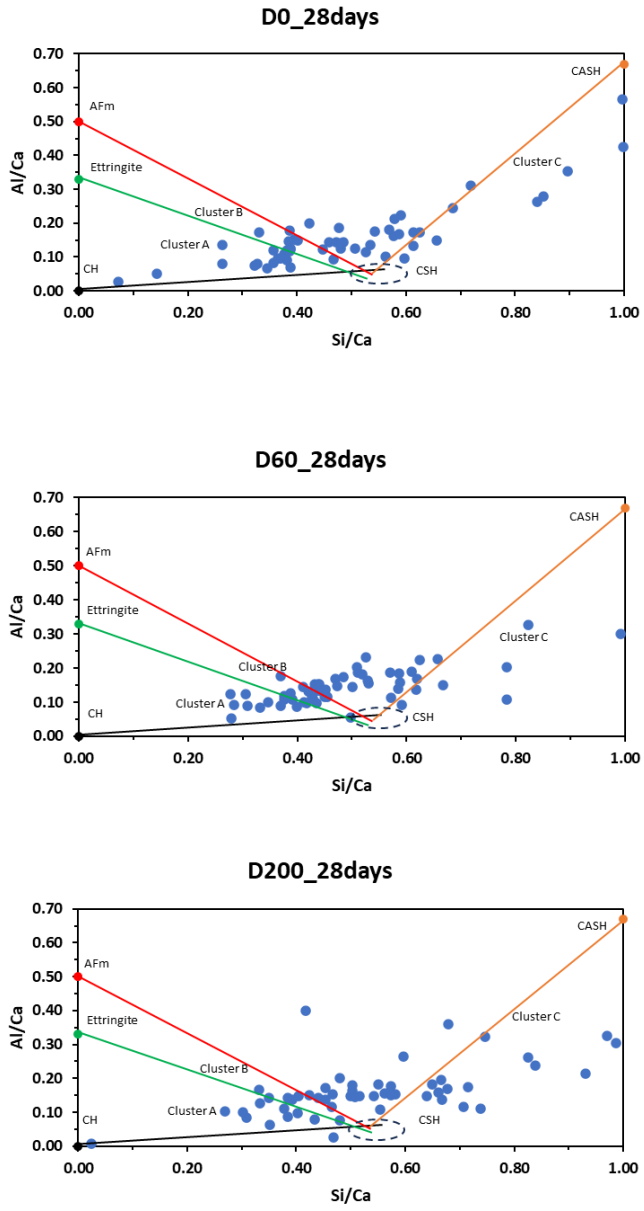

Figure 3.18: Atomic ratio plots for Diorite at 28-days for Al/Ca vs Si/Ca (a) Un-milled, (b) milled 60s and (c) milled 200s

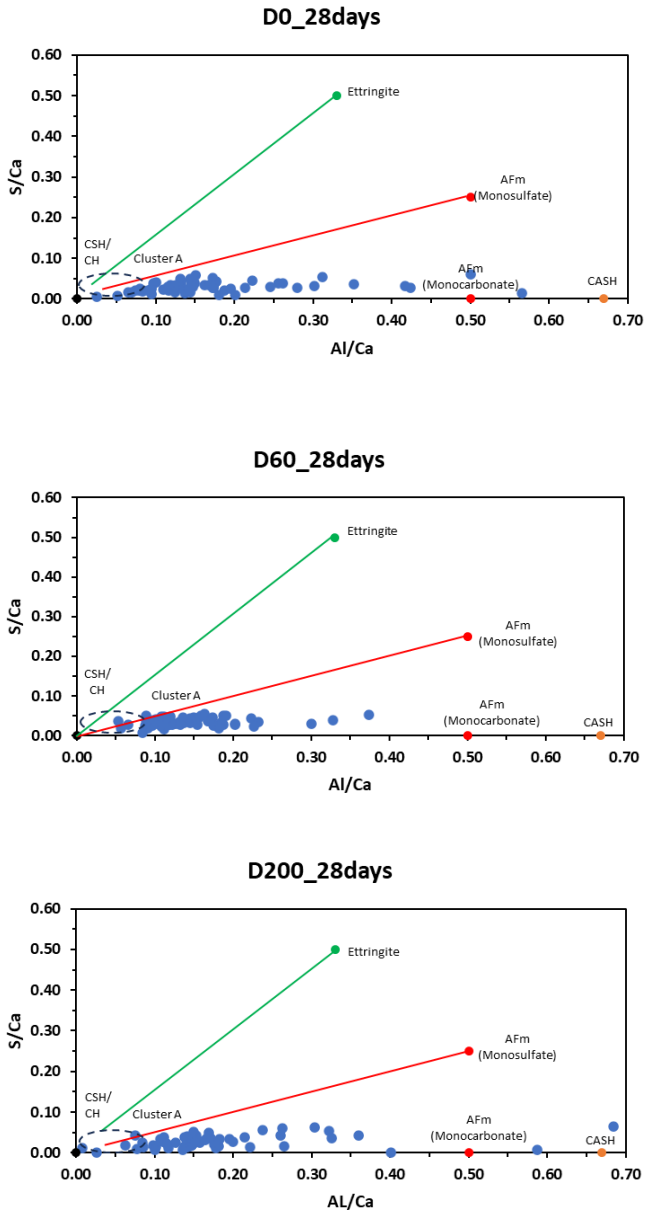

Figure 3.19: Atomic ratio plots for Diorite at 28-days for S/Ca vs Al/Ca (a) Un-milled, (b) milled 60s and (c) milled 200s

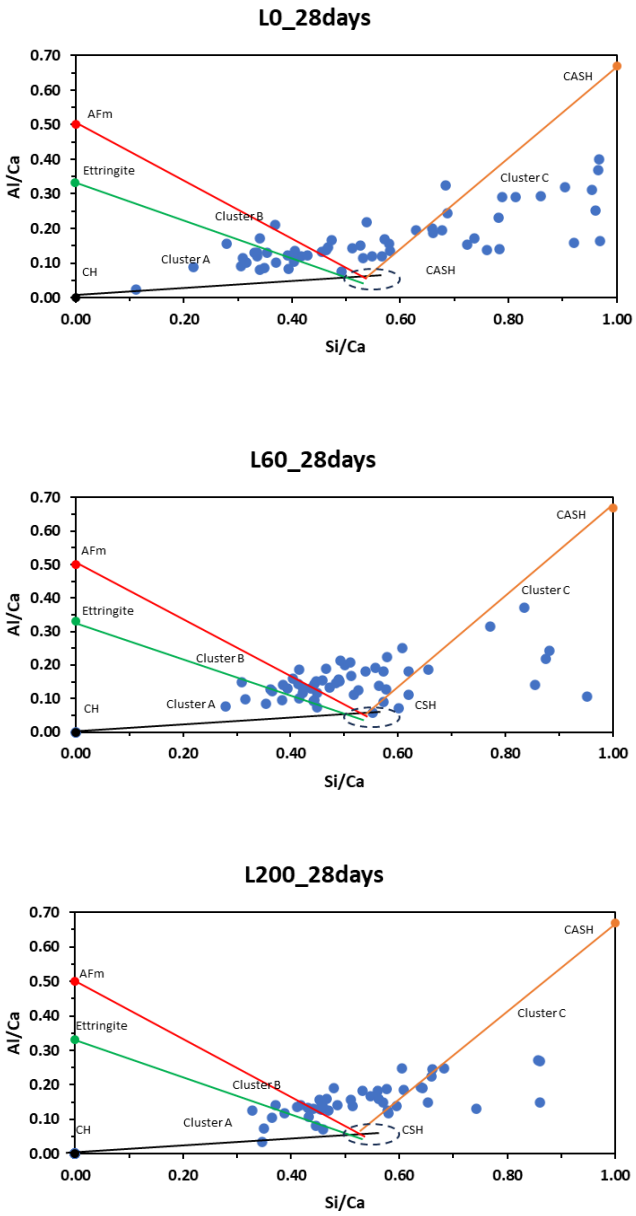

Figure 3.20: Atomic ratio plots for Granite at 28-days for Al/Ca vs Si/Ca (a) Un-milled, (b) milled 60s and (c) milled 200s

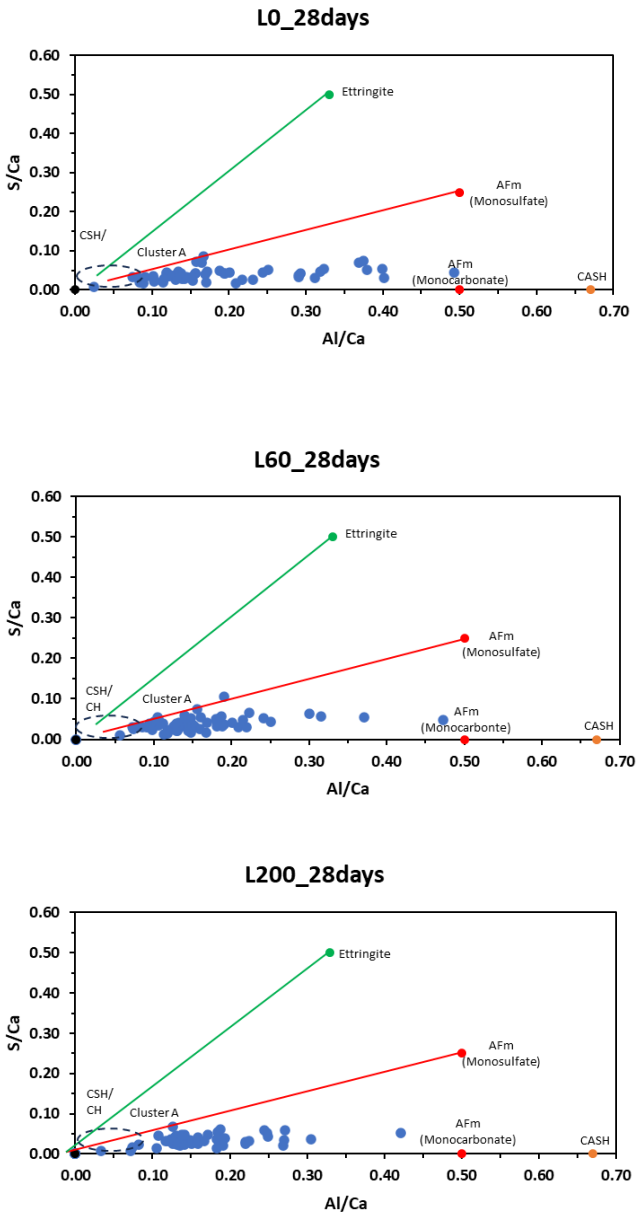

Figure 3.21: Atomic ratio plots for Granite at 28-days for S/Ca vs Al/Ca (a) Un-milled, (b) milled 60s and (c) milled 200s

3.3.6 PHASE AREA FRACTION FROM SEM-BSE IMAGES.

SEM-BSE images of 7 and 28 days were analysed to provide a better understanding on how fineness of QDs affects the hydrates phase.

As can be seen in **Figure 3.24a**, **c** and **e**, at 7 days, S60 had the most substantial improvement in the hydrates phase, with a 15.3% increase over PC. The hydration gains

for D60 and G60, on the other hand, were quite modest. At the same milling time, D60 exhibits the maximum increase of 10.4% in the hydrates phase, whereas G60 shows a smaller improvement of 3.8%. At 28 days age (**Figure 3.24b**, **d** and **f**), D60 shows a notable improvement of 13% in the hydrates phase, while S and G QDs also show improvement, though less compared to D. The highest improvement recorded was 9.4% for S60 followed by G200 which displayed an 84% improvement.

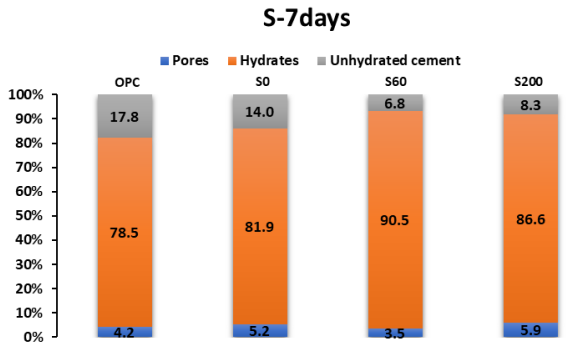

(a): Sandstone at 7 days

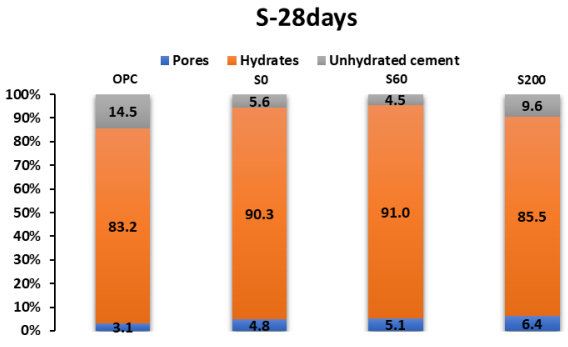

(b): Sandstone at 28 days

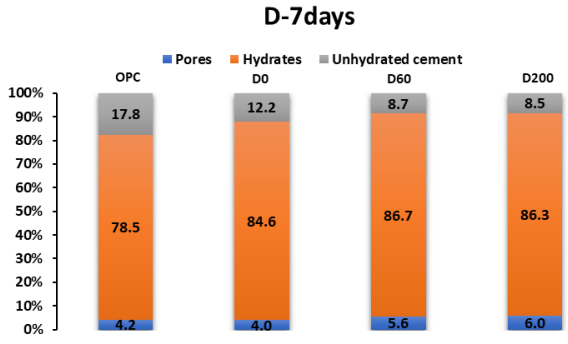

(c): Diorite at 7 days

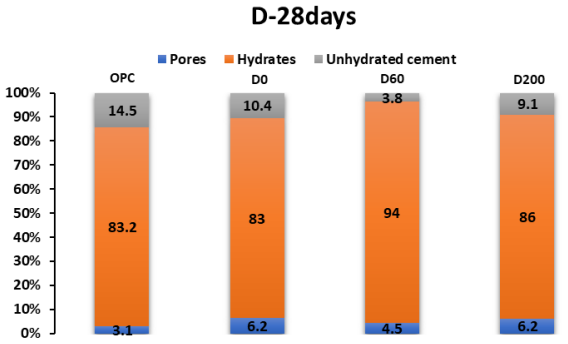

(d): Diorite at 28 days

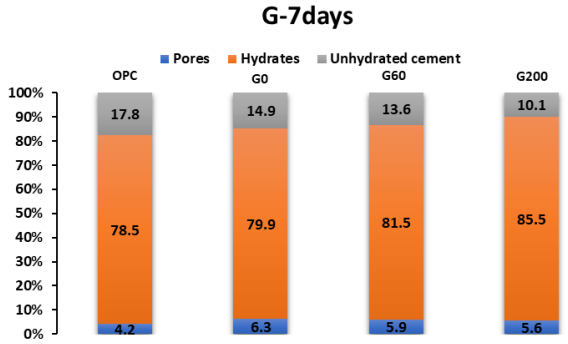

(e): Granite at 7 days

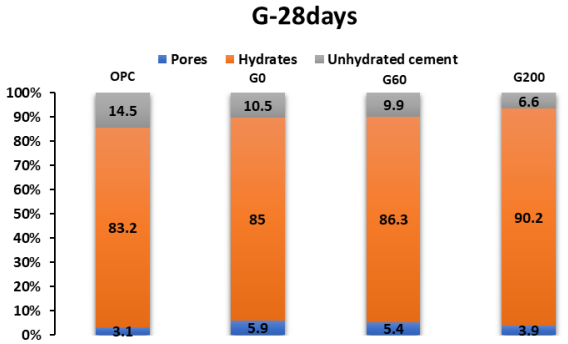

(f): Granite at 28 days

Figure 3.22: The proportion of phases by BSE image analysis approaches.

In our analysis, 60 data points were collected for both the control sample and the sample with added quarry dust in the hydrates phase at 7 and 28 days. The findings indicate that a milling time of 60 seconds generally leads to an improvement in the hydrates phase at both time intervals.

3.4 CONCLUSIONS

This study aimed to ascertain whether pre-milling QDs can enhance the hydration kinetics of cement-based composites. A comprehensive set of tests, including semi-adiabatic calorimetry, cube compressive strength, and scanning electron microscopy were conducted to evaluate the feasibility of using QDs as supplementary cementitious materials (SCMs) in cement. Based on the experimental results, the following conclusions can be drawn:

1. The semi-adiabatic calorimetry results indicate that the milling process influences the hydration kinetics of PC-QD pastes. While QD0 and QD60 show enhanced hydration compared to PC, QD200 shows a reduction in hydration kinetics, suggesting the possibility of reaching a saturation point due to excessive fineness or reduced reactivity at this particle size.
2. PC-QD mixes exhibit lower overall compressive strength compared to the PC reference due to the dilution effect of replacing PC with QDs. However, these mixes demonstrate a higher relative compressive strength per cement weight. The filler effect of QD at optimal fineness improves the microstructural density, but beyond a certain fineness (QD200), the compressive strength does not improve significantly.
3. The strength activity index of most PC-QD mixes surpasses the 75% minimum threshold for pozzolanic materials as defined by relevant standards. Notably, QD60 shows the highest activity index, suggesting its optimal balance of filler effect and pozzolanic potential.
4. QDs influence the matrix microstructure, as revealed by SEM images, which show the formation of new hydration products such as CASH and AFm phases (monosulfate and monocarbonate). The formation of these phases is likely linked to the alumina content in QDs, effectively utilizing the aluminate phases present in the system. These additional hydrates, observed across all QD types, contribute to improved microstructural development.

From the above findings, it can be concluded that Quarry Dust can be effectively used as a supplementary cementitious material (SCM), particularly when milled for 60 seconds to achieve a D50 of 10 μm. This specific fineness offers the most beneficial

balance between the filler effect in cement-based composites. These findings highlight a sustainable method to utilize quarry waste, providing both economic and environmental advantages.

This page is intentionally left blank

Chapter 4: Absorption characteristics and drying shrinkage of cement-based composites incorporating QDs

HIGHLIGHTS

- Quarry Dust (QD) from Sandstone, Granite, and Diorite increases water absorption, both by immersion and capillary action, in cement-based composites.
- Water absorption by immersion is influenced by the peak heat of hydration (HoH), the volume of permeable voids, and the compressive strength of the composite.
- Water absorption by capillarity is influenced by CH, area fraction of voids, and cumulative temperature of the HoH
- A prediction equation is proposed to estimate water absorption by immersion and capillarity for PC-QDs cement-based composites.

ABSTRACT

Keywords: Waste quarry dust, Packing density, Drying shrinkage, Water absorption, Durability

Ordinary Portland cement (PC) is the primary binder in concrete mixes, but its adverse environmental impact, in particular high CO_2 emissions, has led to the exploration of alternative binder options. Quarry dust (QD), a waste from the crushing process of rocks, offers a potential partial replacement for PC. Previous studies suggested that replacing PC with QD can lead to changes in hydrate composition that can affect durability. This research explores the correlation between water absorption characteristics (such as by immersion and capillarity) and variables that relate to physical properties and reactivity performance of cement-based composites incorporating QDs from different sources. This study provides an insight into the feasibility of using quarry dust as a sustainable alternative supplementary cementitious material (SCMs) for PC.

4.1 INTRODUCTION AND BACKGROUND

Amid the pressing challenges of climate change and growing environmental concerns, modern construction practices are undergoing a significant shift toward sustainability. Concrete, the dominant worldwide construction material, is drawing increased attention due to its notable carbon emissions, primarily stemming from Ordinary Portland Cement (PC) production, contributing to about 8% of global carbon dioxide emissions.

The call for sustainable construction has driven extensive research on alternative materials like ashes, slags and fine powders. These materials show promise in reducing the environmental impact of concrete production, offering not only a means to cut the carbon footprint but also presenting additional benefits like improved durability, enhanced workability, and reduced resource depletion.

Recent research has extensively explored the effects of supplementary cementitious materials (SCMs) on the durability of concrete. Common SCMs such as fly ash (FA), ground granulated blast slag (GGBS), and silica fume (SF) are known to refine pore structure and reduce water absorption. For instance, FA's pozzolanic reactions generate additional calcium silicate hydrate (CSH) gel, filling voids and reducing permeability [1]. GGBS refines pore structure through secondary reactions during hydration, while SF, with its high specific surface area, effectively fills micro voids in the concrete matrix [2].

Various studies have focused on specific parameters, providing valuable insights into how SCMs affect durability. Studies such as Antoni et al. [3] and San Nicolas et al.[4] have demonstrated that the addition of metakaolin (MK) and rice husk ash (RHA), leads to a notable reduction in surface absorption, water absorption, porosity, and sorptivity and this is also supported by Ramezanianpour and Hooton [5]. There is also evidence of decreased permeability with the inclusion of SCMs in studies by Guneyisi et al. [6] and San Nicolas et.al [4]. However, Nadeem et al [7] have highlighted that while SCMs reduce gas permeability, chloride permeability can increase under elevated temperatures. Chappex and Scrivener [8], [9] conducted accelerated alkali-silica reaction (ASR) tests to understand the effect of MK on ASR, and found that blends

containing MK have lower expansion overtime due to the equal distribution of Si/Ca in CSH.

While the existing research thoroughly documents the macro-level effects of SCMs on concrete durability, it lacks detailed studies correlating these durability enhancements with the mechanism responsible for refining the pore structures, specifically the hydration process and calcium hydroxide consumption. Moreover, the depletion of conventional supplementary cementitious materials (SCM) stocks is accelerating due to the transition from coal-fired power stations for energy production and the increased adoption of the electric arc method in steel production. This shift in energy and manufacturing practices has intensified the demand for alternative materials in the construction industry.

Quarry dust (QD), a fine powder obtained during quarry aggregate crushing, possesses unique properties making it a suitable SCM [10]. Utilizing QD as a partial replacement for PC has been observed to alter the pore structure and chemical composition of hydrated concrete, significantly enhancing its durability [5], [6]. Evaluation of these changes commonly involves parameters such as water absorption, capillarity (sorptivity), and drying shrinkage [2]– [4].

In contrast to extensively used materials like FA, GGBS, and SF, quarry dust remains relatively unexplored [11]. Despite its potential as an SCM, more detailed investigations on the durability of concrete containing QD are needed to promote its use in field applications.

This research aims to address these gaps by examining how quarry dust, under controlled packing conditions, influences hydrate phases and pore structure, thereby impacting crucial durability parameters such as water absorption by immersion, capillarity and shrinkage. The ultimate objective is to determine whether quarry dust can serve as a viable long-term substitute for PC, offering a novel alternative to traditional SCMs in concrete formulations.

4.2 EXPERIMENTAL PROGRAMME AND METHODOLOGY

The experimental programme focuses on selecting the most beneficial PC-QDs mixes by identifying the ideal balance between its highest specific surface area (SSA) and low pore fractions. The findings were used together with results from studies on reactivity

and hydration performance [12] to select the best milling time for each QD. From these findings, and to be consistent across all mixes, QDs milled for 60s were selected. These optimised mixes are used to correlate with water absorption properties and to assess durability performance.

Full details of the methodology can be found in supplementary material [Appendix D].

4.2.1 SPECIFIC SURFACE AREA (SSA)

The specific surface area (SSA) significantly influences the porosity and water absorption properties of materials. In the context of cement composites, materials with higher SSA generally can fill voids more effectively and reduce porosity [16]. A reduction in porosity translates into fewer and smaller capillary pores that hinder water penetration, thus enhancing the composite's durability and resistance to chemical degradation.

In this study, SSA is determined from particle size distribution (PSD) data, using the assumption that the particles are consistently spherical across different materials. The following equation is used to calculate the SSA.

$$SSA = \frac{A_{Total}}{V_{Total} x Density} \qquad \textbf{Equation (4.1)}$$

where,

A_{total} = Total surface area

V_{total} = Total volume

$Density$ = Density of the material (g/cm^3)

4.2.2 PORE AREA FRACTION (SEM-BSE)

The SEM-BSE studies aim to identify the development of hydrates in paste samples. By using a grey thresholding [13] technique, the analysis of the backscattered electron (BSE) images conducted in ImageJ [14] enable the quantification of the area fraction occupied by pores, hydrates, and un-hydrated cement [15]. Further information on the test and its methodology is provided in [12].

4.2.3 MIX PROPERTIES

Some of the relevant properties of the mixes examined in this paper were determined as part of an earlier study by the authors [12] and are summarised in **Table 4.1**.

The mixes were designed to give the optimum packing properties (maximised packing). The mix identified as PC represents the control mix and included cement type CEM I 52.5 as the only binder. Mixes S60, D60 and G60 represent composites made by replacing 40% of the cement with Sandstone, Diorite and Granite QD, respectively. A water/binder ratio of 0.3 was used in all mixes.

Figure 4.1 illustrates the particle size distribution for both the cement and QD60. The mean particle diameter for PC Papar, Tawau and Tarmac are 30.32µm,15.52 µm, 17.34 µm and 14.07 µm respectively.

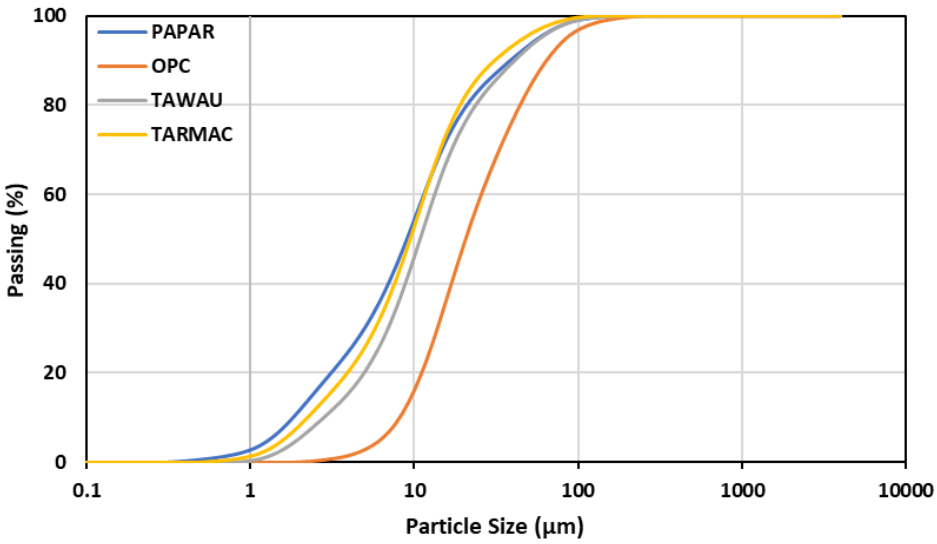

Figure 4.1: Particle size distribution of PC and QDs milled for 60s

Table 4.1: Summary of data for different variables related to physical and reactivity characteristics of cement-based composite.

Mix ID	Portlandite (CH)	Peak Heat of hydration (°C)	Cumulative temperature hour (after 72h) (°C)	Cube compressive strength (MPa)
PC	19.26	73.12	2404	91.2

S60	14.02	55.41	2268	68.3
D60	15.92	50.11	2182	74.8
G60	18.17	57.53	2121	67.5

4.2.4 WATER ABSORPTION BY IMMERSION

Water absorption is another durability indicator. High rates of water absorption are an indication of high porosity, potentially making the materials more susceptible to chemical ingress, or other durability related issues [19].

ASTM C642-06 was used to assess the water absorption of the examined QDs mixes. In this test, the mass of the specimens is measured in four different states: (i) oven dry, (ii) saturated after immersion, (iii) saturated after boiling, and (iv) immersed apparent mass.

4.2.5 WATER ABSORPTION BY CAPILLARITY (SORPTIVITY)

The behaviour of concrete exposed to various harsh conditions largely depends on the permeability of its pore structure. In concrete that is not fully saturated, the rate at which water or different liquids penetrate is primarily influenced by absorption through capillary action [20]. To assess the vulnerability of the examined mixes to water penetration, the method based on ASTM C 1585-04 was used to evaluate the water absorption rates.

In this test, only one surface is exposed to water at ambient temperature, with the remaining surfaces sealed. This reflects the water absorption in structures that only have one side in contact with water. As stipulated in the standard, the initial reading was taken at 60s, followed by a second reading at 5 minutes. As the test progressed, measurements were taken at 10, 20, 30 and 60 minutes. After 1 hour, measurements transitioned to an hourly pattern for up to 6 hours. Post this 6-hour phase, the frequency reduced to daily intervals for the next three days. From the fourth to the seventh day, three readings were taken, each separated by 24hours. The final reading was taken at least 24 hours after the seventh day measurement.

4.2.6 DRYING SHRINKAGE

Drying shrinkage is a critical property that affects long-term performance. Shrinkage cracks increase permeability and as such reduce durability and increase the corrosion likelihood of reinforcing steel [17]. Unrestrained drying shrinkage in cementitious composites causes strains that most often reduce volume but can also lead to swelling. This type of shrinkage is affected by the rate of hydration, temperature, relative humidity, and evaporation rate [18]. External and internal restrains result in shrinkage cracks and can lead to additional curvatures and deflections in structural elements.

Using procedures recommended in ASTM C 596-07, paste specimens of dimensions 40x40x160 mm were cured for 48 hours and then immersed in lime-saturated water for 24 hours. After 72 hours, the specimens were carefully lifted from the water, wiped with a damp cloth, and placed in a length comparator to accurately measure their length. Following this measurement, they were placed in an airy setting to dry, and the changes in length were measured at 7,14,21,28,35,42,49,56, and 63 days.

4.3 RESULTS AND DISCUSSION

4.3.1 SPECIFIC SURFACE AREA (SSA)

Table 4.2 shows that, as expected, the SSA increases with prolonged milling time for all QDs materials. As milling time increases, particles are broken down and further refined, leading to higher surface area. Sandstone displays the most significant rise in SSA, achieving the highest value after 200s of milling. The higher SSA of the milled QDs increases available nucleation sites for the hydration process. This is expected to lead to a denser microstructure, as these particles can react more readily with the calcium hydroxide (CH) released during the hydration of PC, forming secondary CSH gel [22]. Nonetheless, finer particles can coalesce due to electrostatic forces and impact negatively the compaction of the mix.

Table 4.2: SSA of PC and QDs

Specific surface area (SSA) – m^2/kg		
0s	60s	200s

PC	193	-	-
Sandstone (S)	190.5	207.7	399.4
Diorite (D)	188.9	217.2	378.7
Granite (G)	174.7	272.8	372.9

4.3.2 PORE AREA FRACTIONS (SEM-EDX)

Figures 4.2-4.4 show the SEM-BSE images of hydrated paste samples at 28 days for mixes including: 1) un-milled QD (QD0), 2) QD milled for 60s (QD60) and 3) QD milled for 200s (QD200), respectively. The pore area is highlighted in red in the figures, whilst **Table 4.3** summarises the estimated values of pore area fraction.

Table 4.3: Pore area fraction of PC and PC-QDs mixes

	Pore phase area fraction (%)		
	0s	60s	200s
PC	3.1	-	-
Sandstone (S)	5.2	3.5	5.9
Diorite (D)	4.0	5.6	6.0
Granite (G)	6.3	5.9	5.6

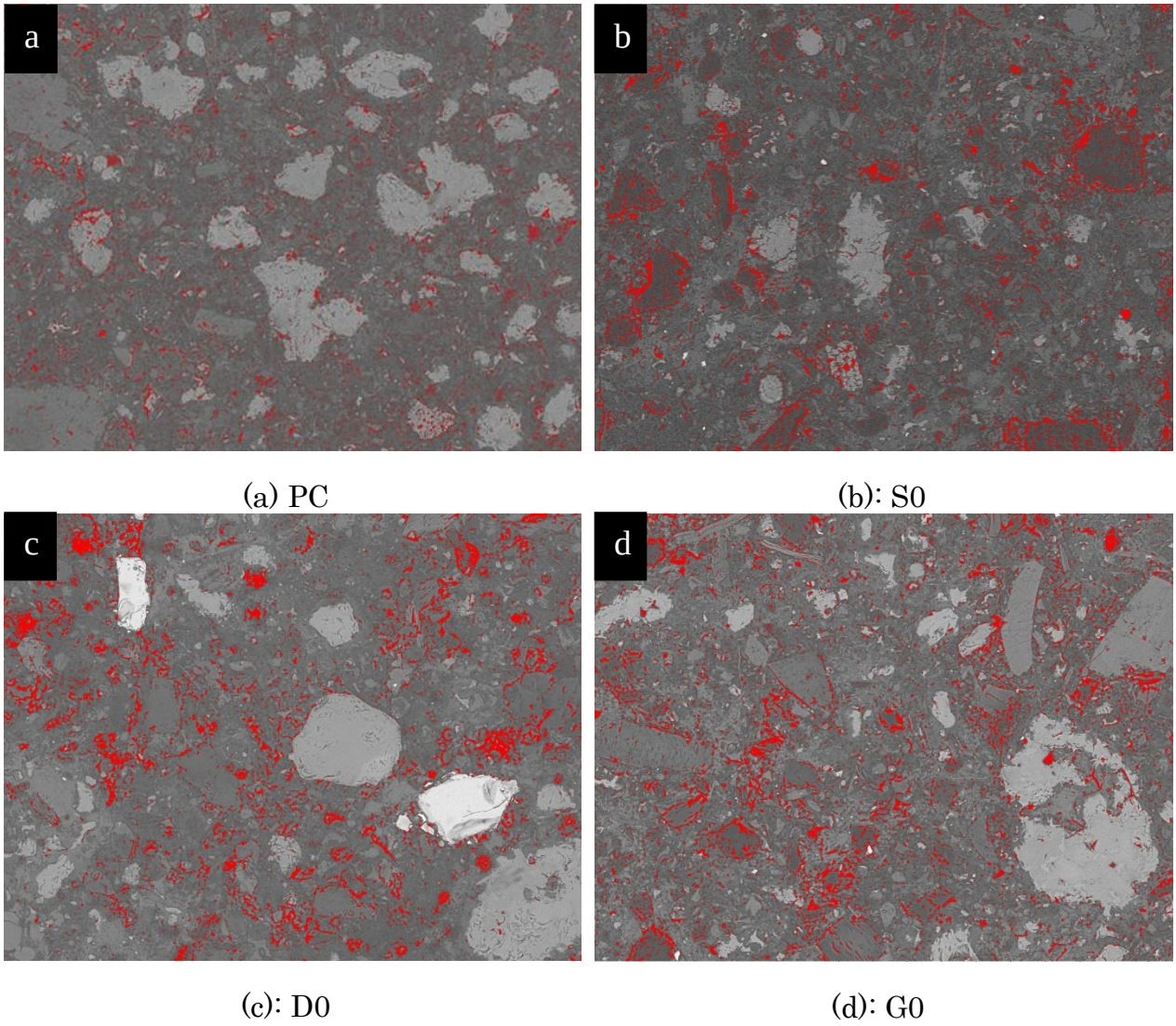

(a) PC (b): S0

(c): D0 (d): G0

Figure 4.2: SEM-BSE images of pore area (in red) at 28 days for un-milled QDs

Despite the fact that un-milled QDs have similar d_{50} to PC (≈ 30 µm), they show higher pore phase area fractions compared to PC. This is most likely due to changes and reductions in hydration reactions in the cementitious system. Previous research by the authors [12] identified monosulfate and monocarbonate in these hydrates conforming the shift in the phases formed. These phases are known to be less dense compared to the calcium silicate hydrates (CSH) gel, and could account for the loss in pore volume [21]. Hence, even if the packing density is similar, the PC dilution effect still reduces the formation of primary CSH, leading to an increase in the overall porosity.

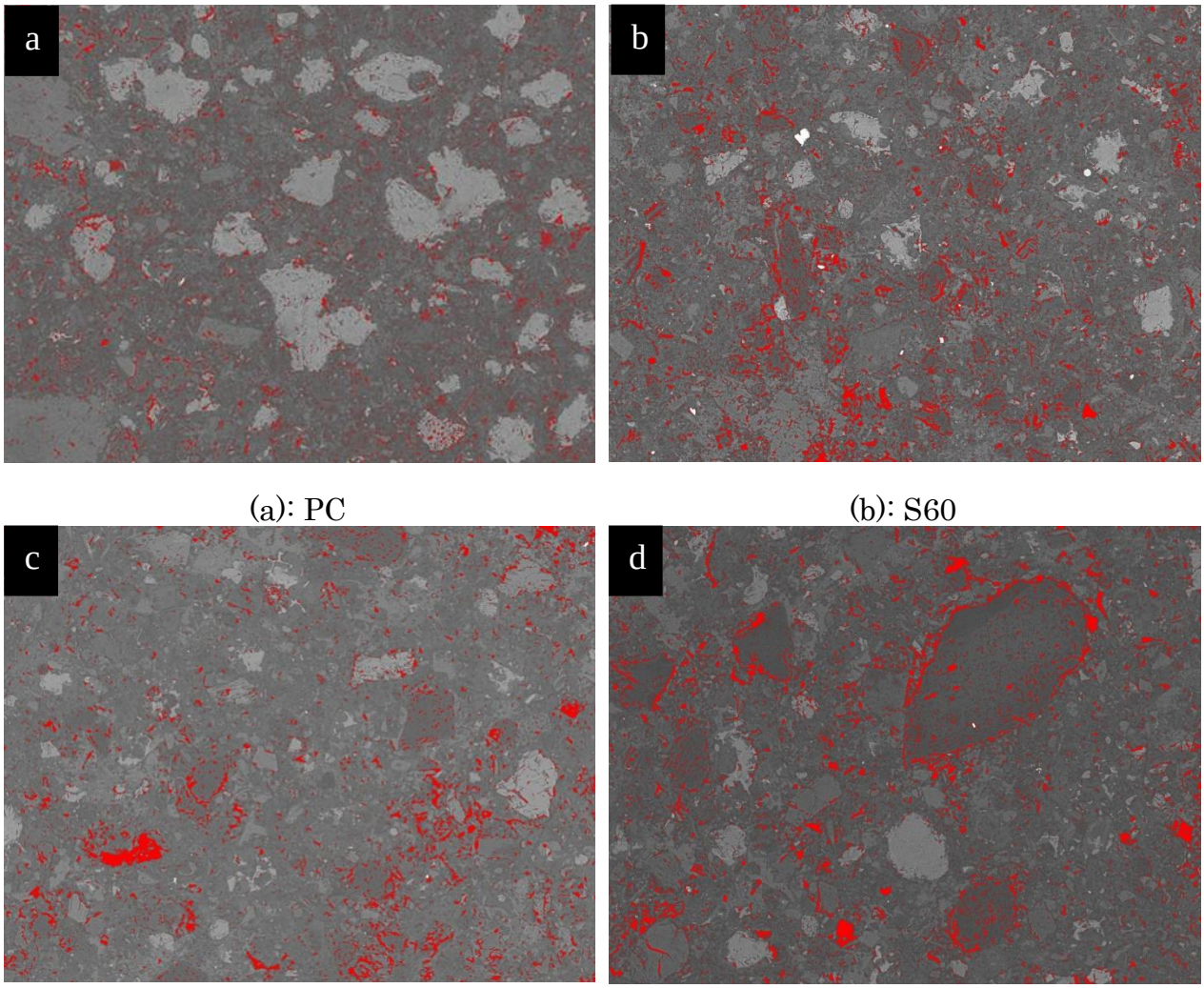

(a): PC (b): S60

(c): D60 (d): G60

Figure 4.3: SEM-BSE images of pore area (in red) at 28 days for QD60

Milling for 60s has varying effects on the performance of the different QDs. The image in **Figure 4.3** shows a notable reduction in the pore phase area fraction of S60. Nonetheless, prolonged milling (200s) of this Sandstone QD seems to offset this benefit, even increasing the pore fraction over that of S0 (**see Figure 4.4 and Table 4.3**), possibly due to coalescence of the dust particles.

D60, on the other hand, shows an increase in porosity over that of D0 and this slight increase continues with milling time (D200). As well as particle coalescence, the increase in milling time may have introduced micro-cracks or altered the Diorite particle morphology in a manner that adversely affected the pores.

Similarly, G60 shows a slight reduction in pore phase area fraction, but not as significant as in S60 and this slight decrease continues with milling time (G200). This is the opposite from Diorite and may be due to the inherent properties of Granite particles. The composition of Granite, largely comprising quartz and feldspar, contributes to its high hardness and mechanical stability, which makes it more resistant to significant particle breakdown during milling. As a result, there is a more controlled reduction in particle size without the excessive formation of micro-cracks or particle agglomeration, which otherwise increase porosity in softer materials such as sandstone and diorite (Stempkowska et al., 2022; Fu et al., 2024).

The angular and rough surface texture of Granite particles contributes to their initially higher porosity. However, this characteristic also limits the extent of porosity increase during milling, as the particles do not readily coalesce or agglomerate (Fu et al., 2024).

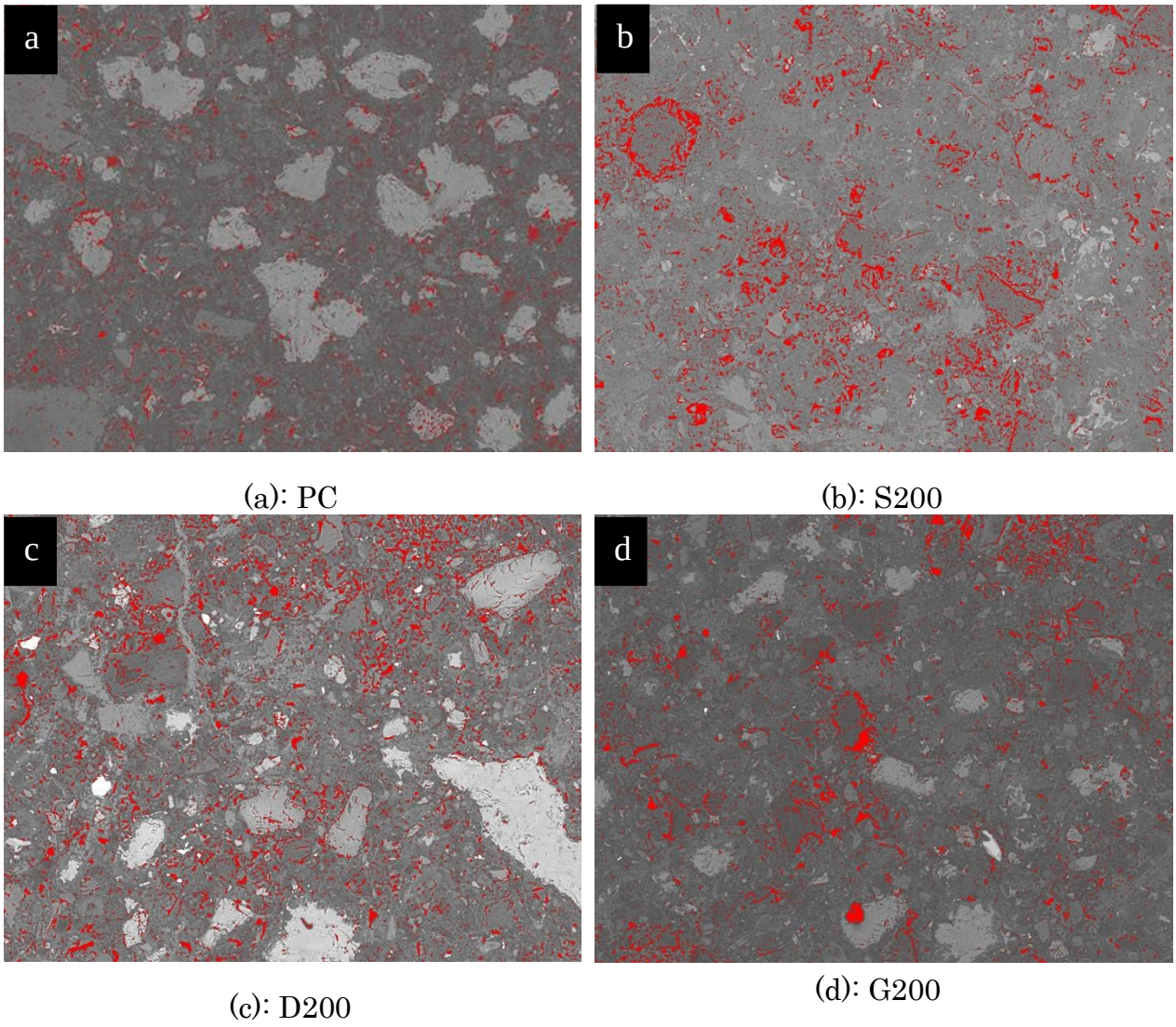

Figure 4.4: SEM-BSE images of pore area (in red) of QDs at 28 days for QD200

4.3.3 WATER ABSORPTION (WA) BY IMMERSION AND VOLUME OF PERMEABLE PORE SPACE (VOIDS)

Water absorption by immersion and volume of permeable pores is shown in **Table 4.4**. PC mixes show the lowest values and act as a reference. Relatively, the blended mixes show an increase in the range of 16-19% for water absorption by immersion and 7-11% in volume of permeable pore space. As the mixes were designed for controlled maximum packing density, the increase in water absorption may be attributed mainly to changes in the chemical reactions of the hydration products. These reactions can lead to the formation of different hydrates or compounds, some

of which can be more porous and have a higher water absorption capacity than the hydration products of cement paste.

The volume permeable pore space in **Table 4.4** was determined following ASTM C642-06, which is a standard test method for determining the density, absorption, and voids in hardened concrete. The key focus here is on the measurement of permeable pore space, which is related to the volume of voids that can be filled with water in a concrete sample.

The procedure for measuring the volume of permeable pores is as follows:

1. Oven Dry Mass (A)

   The specimen is dried in an oven at a temperature of 100 to 110 C until it reaches a constant mass. This ensure that all moisture is removed from the specimen. The mass of the dry specimen is recorded as A.

2. Saturated Mass after Immersion (B)

   The dried specimen is immersed in water for at least 48 hours. This soaking period allows permeable pores to fill with water. After immersion, the surface of the specimen is dried, and the mass is recorded as B.

3. Saturated Mass after Boiling (C)

   After the 48-hour soaking, the specimen is boiled in water for 5 hours. This step ensures that even the finest and least pores are filled with water. Specimen is the allowed to cool in water to room temperature. After cooling, the surface moisture is removed, and the mass is recorded as C

4. Submerged Mass (D)

   The specimen is weighed while fully submerged in water. This submerged mass is recorded as D.

5. Calculation of Volume Permeable Voids (%)

The volume of permeable voids (V) is calculated using the following formula

$$V(\%) = \left(\frac{g_2 - g_1}{g_2} \right) x100$$

Where:

g_1 = Bulk density calculated as, $g_1 = \frac{A}{C - D}$

g_2 = Apparent density calculated as, $g_2 = \frac{A}{A - D}$

Or equivalently

$$V(\%) = \left(\frac{C - A}{C - D} \right) x100$$

Where:

A is the oven-dry mass

C is the saturated mass after boiling

D is the submerged mass

Table 4.4: WA by immersion and Volume of permeable pore space of PC and PC-QDs mixes

Material	Water Absorption by Immersion (%)	Volume of Permeable Pore Space (%)
PC	15.1	26.2
S60	17.5	28.0
D60	18.0	29.0
G60	17.6	28.9

It can be noted from the results shown in **Table 4.4** and **Table 4.1** (previously determined by the authors [12]), that there is a clear relation between water absorption and volume of permeable pores with compressive strength and Peak Heat of Hydration (HoH). By using multiple regression analysis, where WA is the dependent variable and

all the other parameters are the independent variables (see **Figure 4.5**), the following equation was derived:

$$WA = 15.97 - 0.08.(PeakHoH) - 0.03.(CubeStrength) + 0.27.(Voids) \qquad \textbf{Equation (4.2)}$$

Further data are needed to validate this equation.

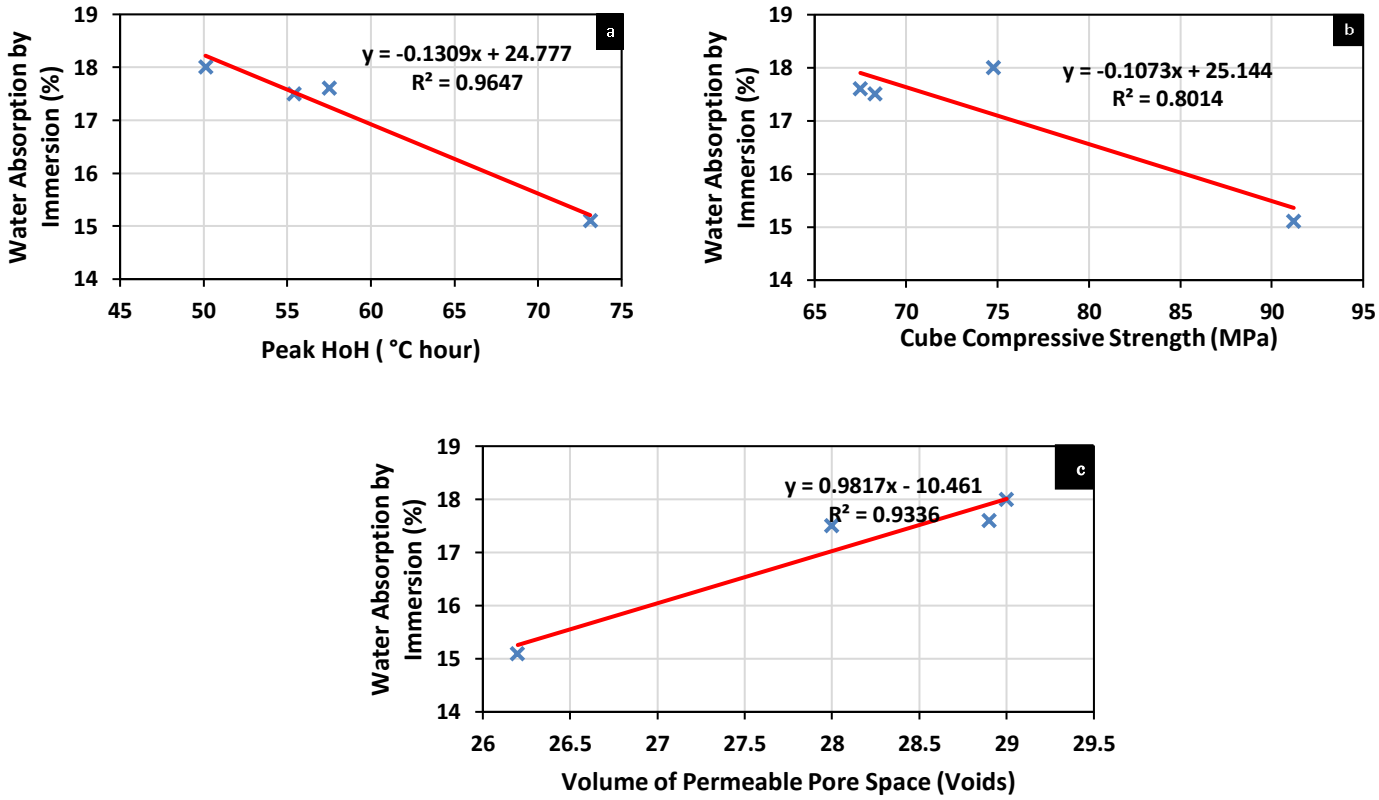

Figure 4.5: Relationship between water absorption by immersion and key parameters

Figure 4.5 illustrates the relationship between water absorption by immersion and three parameters, Peak of Hydration (HoH), Cube Compressive Strength, and Volume of Permeable Pore Space (Voids).

Figure 4.5 (a): A strong negative correlation is observed, indicating that higher HoH, which reflect more hydration, leads to a denser structure with lower water absorption.

Figure 4.5 (b): Similarly, a negative correlation shows that as compressive strength increases, water absorption decreases, suggesting that stronger, denser concretes have less capacity for water intake

Figure 4.5 (c): A positive correlation is evident, where an increase in the volume of permeable voids directly leads to higher water absorption, highlighting the importance of minimizing voids to reduce permeability

4.3.4 WATER ABSORPTION BY CAPILLARITY (SORPTIVITY)

Figure 4.6 shows the variation of water absorbed by capillarity versus the square root of time in seconds for the examined mixes. Water absorption increases rapidly during the first 12 hours and then slows down after 72-hour eventually stabilizing. ASTM C1585-04 determines the "Initial rate of absorption" from the gradient in the range of 35-147√s and the "Secondary rate of absorption" in the range of 320-726√s. These rates are shown in **Table 4.5**. It should be noted that for these values to be valid, the standard specifies that the variation of water absorption with √s should follow a linear relationship with a correlation coefficient greater than 0.98. This was generally observed to be true for all samples, with only the secondary value for PC falling slightly outside this range.

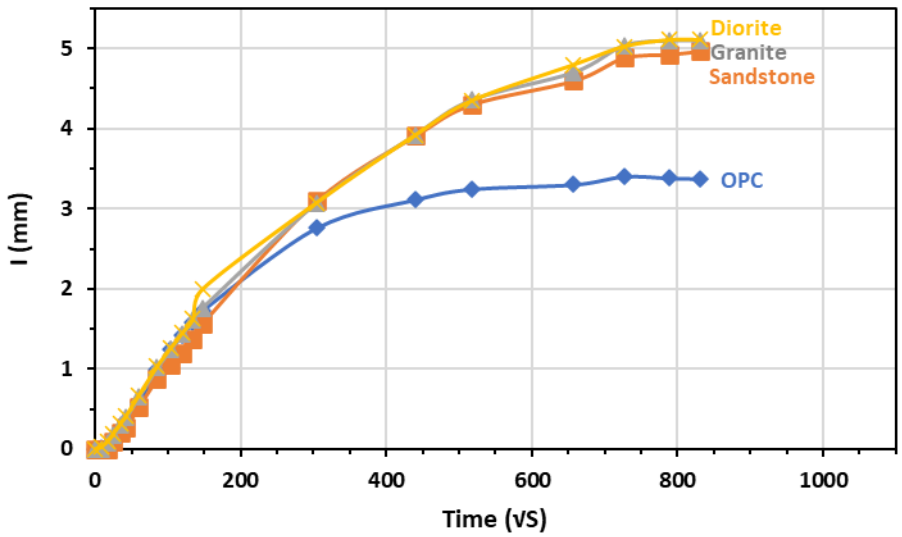

Figure 4.6: Water absorption by capillarity over time of PC-QDs mixes.

Table 4.5: Initial and secondary rates of water absorption for PC and PC-QDs mixes

	Initial rate of absorption		Secondary rate of absorption	
	Slope (mm/√s)	R-value	Slope (mm/√s)	R-value
PC	0.2427	0.9987	0.0432	0.9671
Sandstone	0.2155	0.9972	0.1520	0.9877
Granite	0.2366	0.9987	0.1737	0.9886
Diorite	0.2517	0.9894	0.1801	0.9853

A series of correlations for the rate of capillarity absorption with different parameters was attempted (**Figure 4.7**), and CH and pores area fraction were identified as having the best correlations of R^2= 0.97 and 0.96 respectively (see **Figure 4.7b** and **4.7c**) for the initial rates of water absorption. Only the initial rate of absorption was considered for the mathematical correlation, as it utilizes four data points that maintain a high degree of linearity ($R^2 > 0.98$). The secondary rate of absorption, which consisted of only three data points, was excluded due to insufficient data for establishing a reliable linear relationship.

The results of the quadratic multi-regression analysis led to equation 4.3 for the initial rates and 4.4 for the secondary rates. Further data are needed to validate these equations.

$$IWA = \alpha - \beta(\sum_{i=1}^{3} T_i)^2 - \gamma \sum_{i=1}^{3} T_i.CH + \delta \sum_{i=1}^{3} T_i.\eta$$ **Equation (4.3)**

where:

IWA = Initial rates of Water Absorption

Intercept, α = 0.21

Coefficient for $(\sum_{i=1}^{3} T_i)^2$, β =1.70 x 10^{-8}

Coefficient for $\sum_{i=1}^{3} T_i.CH$, γ =2.67 x 10^{-6}

Coefficient for $\sum_{i=1}^{3} T_i.\eta$, δ =1.57 x 10^{-6}

$\sum_{i=1}^{3} T_i$ =Cumulative temperature for 3 days

CH = Portlandite amount in hydrated cement

η = Pores area fraction

The secondary absorption rates for all systems show a general trend of decreasing as the cumulative temperature hour increases. This can be linked to the hydration process, where longer curing time and higher temperatures encourage the formation of hydration products like calcium silicate hydrates (C-S-H). These products gradually refine the pore structure, reducing permeability.

Systems with higher Portlandite (CH) content tend to exhibit slightly higher secondary absorption rates, possibly due to CH's crystalline nature, which may contribute to larger or more interconnected pores if not fully consumed.

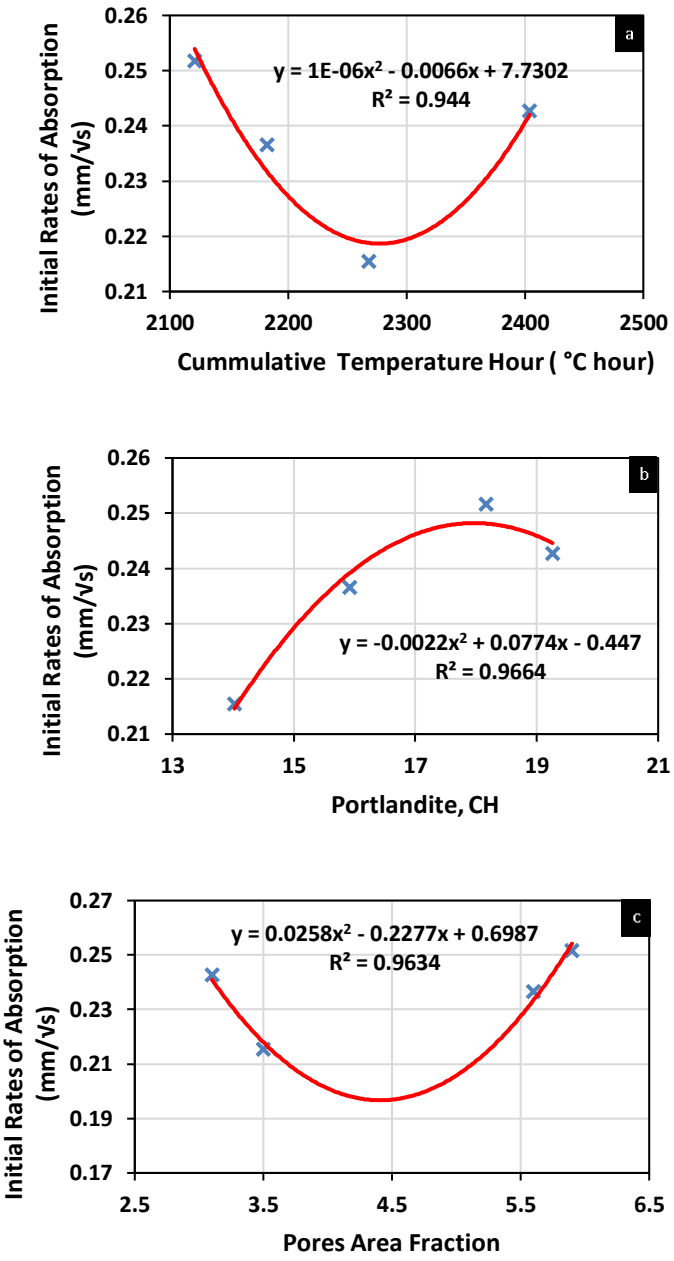

Figure 4.7: Relationship of initial rates of water absorption by capillarity with a) cumulative temperature hour of the semi-adiabatic test, b) portlandite consumption identified by TGA and c) pores area fraction obtained by the SEM-BS

4.3.5 TRANSITION OF CAPILLARITY ACTION TO DIFFUSION

Capillary absorption refers to the movement of water through the small pores and capillaries within the cement due to surface tension of water and the adhesive forces between water and the wall of the capillaries. Cement with higher porosity and with

smaller interconnected pores are more pronounced to this action. The rate and extent of capillary action are a direct effect of the size and connectivity of the pores [23], [24].

On the other hand, diffusion is the movement of water or gas from an area of higher concentration to a lower concentration. The rate of diffusion in cement is influenced by the size, distribution, and connectivity of the pores [24].

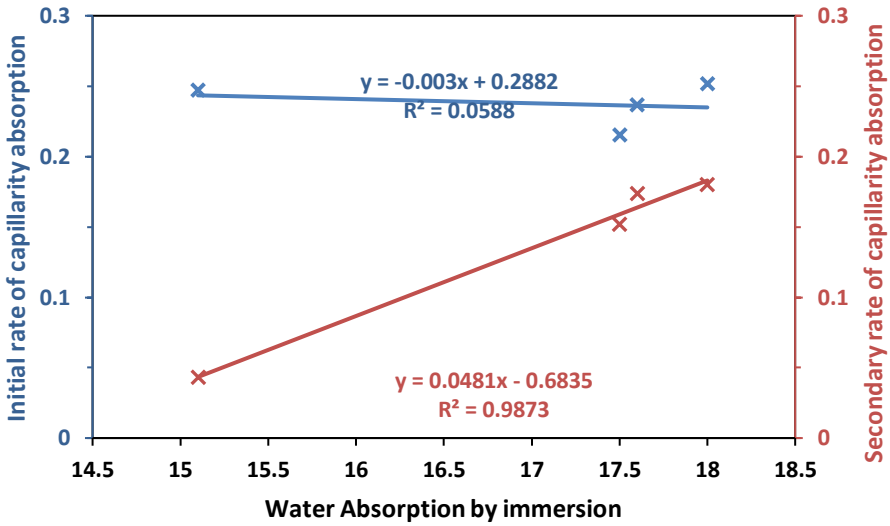

Figure 4.8: Empirical relationship of water absorption by immersion with initial and secondary rate of capillarity absorption

Figure 4.8 presents two distinct trends relating to the capillary absorption of PC-QDs cement when immersed in water. The initial rate of capillary absorption, represented by the nearly horizontal blue line indicates a poor correlation with water absorption by immersion. This suggest that the initial absorption is not controlled by the total volume of pores but rather by the size and distribution of the accessible pores at the surface of the material. The wide variability and low predictability may be due to a diverse pore size distribution.

In contrast, the secondary rate of capillary absorption (orange line) shows a strong correlation. This suggests that once the initial larger pores are saturated, the water absorption is dominated by smaller, more interconnected pores. This implies a more uniform pore structure where the connectivity between pores allows for a consistent diffusion-driven absorption process.

4.3.6 PORES CHARACTERISTIC OF THE PC-QDS CEMENT

Table 4.6 compares the characteristics of pore diameters in different PC-QDs cement. In both pore categories, the PC-QDs mixtures exhibit an increase in both average size and percentage area compared to PC especially for pore diameter larger than 1μm. This suggests that the addition of quarry dust leads to the formation of larger and more frequent pores.

The determination of pore characteristics and frequencies for the sample was conducted through the analysis of Scanning Electron Microscopy (SEM) images using the ImageJ software. This method provided quantitative data on pore sizes and their distribution across the sample surface.

The SEM images were first obtained to capture the microstructural details of the sample. These images were then analyzed using ImageJ. The Grey Threshold method was applied within ImageJ to differentiate the pores from the surrounding material based on pixel intensity. Following this, the "Analyze Particles" function was employed to measure the area of each identified pore.

The frequency of the pores was determined by counting the number of pores in each size category. In the analysis, 4810 pores were identified within the 50nm-1μm range, and 766 pores were identified in the larger pore category (>1μm). This count reflects the frequency of pores in each size range across the analyzed area of the SEM image.

The percentage area (% Area) occupied by the pores in each category was calculated by dividing the total pore area by the total area of the image. This provides a quantitative measure of how much of the material's surface is porous, which is critical for understanding the material's overall porosity and potential performance characteristics.

Table 4.6: Characteristics of pores for PC and PC-QD cement-based composite

Designation	Pore Diameter[25]	Pore Characteristic	PC	S60	D60	G60
Large capillaries	50nm-1μm	Average Size (μm)	0.16	0.19	0.23	0.21

		% Area	1.99	2.04	1.24	1.58
Large capillaries & entrained air	>1μm	Average Size (μm)	2.08	3.13	3.85	3.78
		% Area	1.07	2.99	3.31	3.88

From the information presented in **Table 4.5** and **4.6**, and **Figure 4.8**, it can be seen that capillary absorption rates in cementitious materials are significantly influenced by their pore characteristics. Larger and more numerous pores, as observed in PC-QD cement, result in higher absorption rates compared to PC. The higher percentage of pores area in PC-QD mixes are indicative of a more porous structure compared to PC.

Considering the controlled maximum packing of these mixes, the increased capillary absorption rates in PC-QD can be attributed to differences in hydrate formation. In a previous study by the authors [12], it was found that the incorporation of quarry dust altered the final hydrates from purely CSH (Calcium Silicate Hydrates) and CH (Portlandite) to mixes of CSH, CH, CASH (Calcium Alumina Silicate Hydrates) and AFm phases (Monosulfate and Monocarbonate).

Primary CSH exhibit a denser and less permeable microstructure, while hydrates from the secondary reaction would modify the microstructure and potentially increase porosity.

4.3.7 DRYING SHRINKAGE

The development of drying shrinkage of the examined PC-QDs mixes over a period of 63 days is shown in **Figure 4.9**.

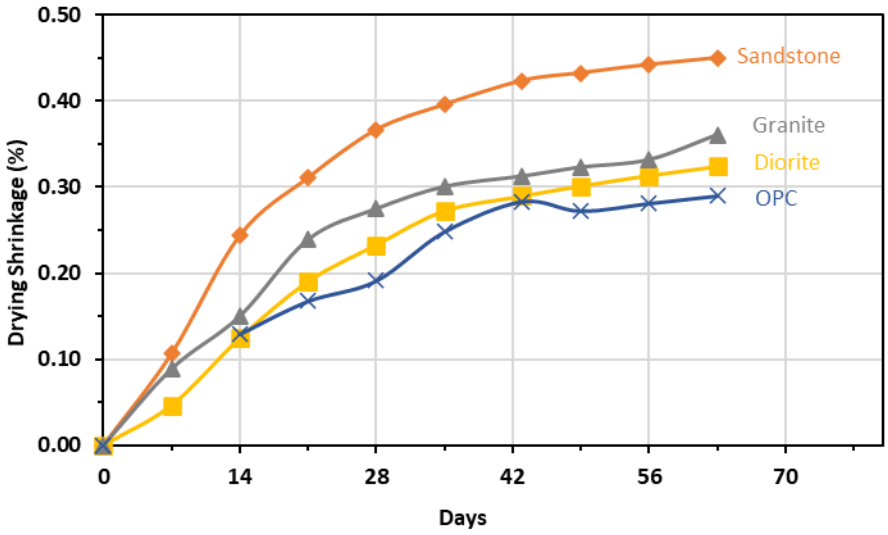

Figure 4.9: Drying shrinkage of PC and PC-QDs mixes

All mixes exhibit a high shrinkage rate during the first 4 weeks of drying, after which shrinkage slows down. S60 demonstrates consistently the highest shrinkage, indicating its susceptibility to moisture loss and contraction, whilst PC exhibits the lowest shrinkage. D60 and G60 have similar shrinkage to PC. The increase in shrinkage rate is consistent with the increase in the volume of large capillaries (see **Table 4.6**) as well as the decrease in initial rate and secondary of absorption (see **Table 4.5**). As shrinkage is driven by surface tension on the capillaries the increase in volume of large capillaries is expected to increase shrinkage. Nonetheless, it is surprising that shrinkage also increases with decreasing rates of absorption. It should be mentioned that these slight decreases in the rates of absorption (from S to G to D) are also surprising from the pore fraction point of view but are consistent with the other absorption characteristics.

4.4 CONCLUSION AND RECOMMENDATIONS

The correlation between water absorption characteristics and variables that relate to physical properties and reactivity performance of cement-based composites

incorporating quarry dusts from different sources was examined in this study. From the discussion presented above, the following conclusions can be drawn.

1. Despite the controlled packing condition of the cement-based composites, PC-QDs mixes (sandstone, granite, and diorite) increase water absorption by around 10% and pore phase area fractions by 20%.
2. Findings reveal general trends where cumulative temperature, and pore area fraction influence water absorption rates, reflecting correlations driven by hydration and microstructural changes. An equation is presented as a preliminary guiding tool to estimate water absorption.
3. All the cement-based mixes exhibit an initial rapid absorption rate, which then decelerates overtime. The capillarity absorption for cementitious mixes with QDs are found to be predictable despite the differences in the nature of the QD. This can be factored into engineering and construction applications, particularly in scenarios where the capillarity behaviour is critical.
4. The rates of water absorption by capillarity are influenced by variables such as pore area fraction, CH consumption, and peak HoH. Equations are found for the Initial and Secondary rates of WA.
5. The initial water absorption in PC-QDs cement is influenced by larger, non-uniformly distributed pores, leading to variable absorption rates. The secondary absorption is governed by smaller, interconnected pores, resulting in a more predictable absorption pattern.
6. The inclusion of QD in cement increases the size and frequency of pores, resulting in a more porous structure and higher capillary absorption rates compared to PC. This change is likely due to the alteration of hydrate composition within the cement matrix, affecting its microstructure and porosity.
7. Shrinkage strains in QD mixes are higher than in the control mix. This appears to be related to the increasing volume of large capillaries.

The addition of QDs to PC significantly alters the pore structure of the material, leading to increased pore size and area. While this can have a slight negative impact on strength and durability, it is a small penalty to pay for a 40% decrease in PC

content in the mix. Understanding these changes and their implications is important for appropriate use and optimization of PC-QD composites in construction and engineering.

This page is intentionally left blank

Chapter 5:Conclusion and recommendation

5.1 CONCLUSIONS

The research aimed to enhance knowledge on the use of milled waste quarry dust (QD) in cementitious mixtures and explore its potential as a filler or supplementary cementitious material (SCMs). The research focused on maximising the amount of QDs in replacing Ordinary Portland Cement (PC) by increasing packing density and its reactivity. Based on the findings from the research, the main conclusions for each phase of study are summarised in this section.

5.1.1 INFLUENCE OF PARTICLE SIZE DISTRIBUTION ON PACKING DENSITY OF BLENDED CEMENT WITH MICROFINES (CHAPTER 2)

- **Evaluation of the 2-Parameter Model**: The conventional 2-parameter model was found to underestimate packing density for microfine particles (finer than 75 μm). This discrepancy is attributed to the model not accounting for the actual particle size distribution (PSD) as the model was developed for discrete particle sizes.
- **Relationship between Packing Density and PSD:** It is found that the packing density is a function of PSD and the volumetric fractions of particles in mixtures.
- **Model modification Incorporating PSD:** The 2-parameter model is modified to include the properties of the actual PSD, by adopting newly defined coefficients of uniformity (Cu) and curvature (Cc), enhancing its accuracy.
- **Particle Interactions:** Due to insensitivity of size ratio to packing density and high standard deviation in PSD, as well as the very small particle sizes in powders, particle interactions (such as loosening and wall effect) are not necessary in the prediction model.
- **Improved Predictive Accuracy:** The modified model significantly improved predictive accuracy, with absolute mean errors reduced to a range of 1.52% to 4.18%.

5.1.2 INFLUENCE OF QD FINENESS ON HYDRATION KINETICS (CHAPTER 3)

This phase of research investigated the role of pre-milled quarry dust (QD) as supplementary cementitious material (SCMs) in cement composites, using tests like semi-adiabatic calorimetry, and scanning electron microscopy. The main findings are:

- **Hydration Kinetics**: It is shown that milling QDs affects the hydration of cement, with varying results based on the milling duration.
- **Enhanced Hydration**: QDs improve early-stage hydration, indicating their role in nucleation processes.
- **Strength Efficiency**: While overall compressive strength in PC-QD mixes is lower than for pure PC mixes, they result in higher strength efficiency per cement weight.
- **Standards Compliance**: Most PC-QD mixes meet the 75% standard for pozzolanic materials, with 60s milled QDs showing the best results.
- **Microstructural Changes**: QDs contribute to the development of new hydrates in the cement matrix, indicating effective alumina utilization.

The study concludes that QDs, particularly milled for 60s to a D_{50} of 10 μm, are effective SCMs offering a sustainable approach to using quarry waste in cementitious materials.

5.1.3 ABSORPTION CHARACTERISTICS AND DRYING SHRINKAGE OF CEMENT-BASED COMPOSITES INCORPORATING QDS (CHAPTER 4)

This phase of research aimed to understand the impact of QDs in controlled packing conditions on its hydrates and pore phase in cement-based mixture and how these impact durability aspects like water absorption and shrinkage. The main findings are:

- **Increased WA:** PC-QD mixes result in a 10% increase in water absorption and a 20% increase in pore phase area fractions.

- **Influencing factors on WA:** WA by immersion is influenced by the heat of hydration, permeable voids, and cube compressive strength, with a specific equation provided for estimation.
- **Capillary Absorption:** Despite differences in QD types, capillary absorption in cementitious mixes is predictable and consistent, crucial for engineering applications.
- **Determinants of Capillary Absorption Rates:** Capillary absorption rates are influenced by pore area fraction, CH consumption, and heat of hydration peak, with distinct equations for initial and secondary rates.
- **Pore distribution impact:** Initial water absorption is influenced by larger, uneven pores, while secondary absorption is more uniform due to smaller, interconnected pores.
- **Shrinkage:** PC-QD mixes exhibit higher shrinkage, likely due to the increased volume of large capillaries.

5.2 RECOMMENDATIONS FOR FUTURE WORK

This section provides recommendations for future work necessary to deepen the knowledge of QDs usage in concrete.

5.2.1 PACKING MODEL.

- It is recommended to validate the application of the coefficient of uniformity (Cu) and curvature (Cc) in the enhanced 2-parameter model for aggregates larger than 75μm.
- The proposed model should be assessed and extended if necessary to include ternary and quaternary mixtures.

5.2.2 QUARRY DUST AS SCMS

- Quantifying the specific amount of each hydrate formed in cement-based composites is crucial. Advanced techniques like XRD-Rietveld and NMR are recommended for this purpose.
- Different method of pre-treatment such as milling and calcination, chemical activation, and controlled curing conditions could be explored to enhance usage of QDs as SCMs.

5.2.3 DURABILITY ASSESSMENT

- Further research with a larger dataset is needed to validate the relationship between water absorption, capillarity with variables shown in this study, especially on HoH peak and CH amount which considered to be novel in this area.
- In addition to water absorption and capillarity, conducting additional tests like freeze-thaw resistance and alkali-silica reaction (ASR) testing will provide valuable insights into the use of QDs in cement-based composite.

Furthermore, it is recommended to incorporate Life Cycle Analysis (LCA) as an essential part of future work for informed decision-making.

This page is intentionally left blank

References

CHAPTER 1
[1] A. Adesina, "Recent advances in the concrete industry to reduce its carbon dioxide emissions," *Environmental Challenges*, vol. 1, p. 100004, Dec. 2020, doi: 10.1016/j.envc.2020.100004.
[2] V. M. John, B. L. Damineli, M. Quattrone, and R. G. Pileggi, "Fillers in cementitious materials — Experience, recent advances and future potential," *Cement and Concrete Research*, vol. 114, pp. 65–78, Dec. 2018, doi: 10.1016/j.cemconres.2017.09.013.
[3] D. K. Panesar and R. Zhang, "Performance comparison of cement replacing materials in concrete: Limestone fillers and supplementary cementing materials – A review," *Construction and Building Materials*, vol. 251, p. 118866, Aug. 2020, doi: 10.1016/j.conbuildmat.2020.118866.
[4] L. E. Burris and M. C. G. Juenger, "Milling as a pretreatment method for increasing the reactivity of natural zeolites for use as supplementary cementitious materials," *Cement and Concrete Composites*, vol. 65, pp. 163–170, Jan. 2016, doi: 10.1016/j.cemconcomp.2015.09.008.
[5] R. Yang *et al.*, "Environmental and economical friendly ultra-high performance-concrete incorporating appropriate quarry-stone powders," *Journal of Cleaner Production*, vol. 260, p. 121112, Jul. 2020, doi: 10.1016/j.jclepro.2020.121112.
[6] Z. Xu, N. Xu, and H. Wang, "Effects of Particle Shapes and Sizes on the Minimum Void Ratios of Sand," *Advances in Civil Engineering*, vol. 2019, pp. 1–12, Apr. 2019, doi: 10.1155/2019/5732656.

CHAPTER 2
[1] T. Proske, S. Hainer, M. Rezvani, and C.-A. Graubner, "Eco-friendly concretes with reduced water and cement contents — Mix design principles and laboratory tests," *Cem. Concr. Res.*, vol. 51, pp. 38–46, Sep. 2013, doi: 10.1016/j.cemconres.2013.04.011.
[2] F. de Larrard, *Concrete mixture proportioning: a scientific approach*. in Modern concrete technology, no. 9. London ; New York: E & FN Spon, 1999.
[3] A. B. Yu, R. P. Zou, and N. Standish, "Modifying the Linear Packing Model for Predicting the Porosity of Nonspherical Particle Mixtures," *Ind. Eng. Chem. Res.*, vol. 35, no. 10, pp. 3730–3741, Jan. 1996, doi: 10.1021/ie950616a.
[4] A. K. H. Kwan and W. W. S. Fung, "Packing density measurement and modelling of fine aggregate and mortar," *Cem. Concr. Compos.*, vol. 31, no. 6, pp. 349–357, Jul. 2009, doi: 10.1016/j.cemconcomp.2009.03.006.
[5] A. K. H. Kwan, K. W. Chan, and V. Wong, "A 3-parameter particle packing model incorporating the wedging effect," *Powder Technol.*, vol. 237, pp. 172–179, Mar. 2013, doi: 10.1016/j.powtec.2013.01.043.
[6] V. Wong and A. K. H. Kwan, "A 3-parameter model for packing density prediction of ternary mixes of spherical particles," *Powder Technol.*, vol. 268, pp. 357–367, Dec. 2014, doi: 10.1016/j.powtec.2014.08.036.

[7] K. W. Chan and A. K. H. Kwan, "Evaluation of particle packing models by comparing with published test results," *Particuology*, vol. 16, pp. 108–115, Oct. 2014, doi: 10.1016/j.partic.2013.11.008.
[8] W. Du, M. Li, Z. Pei, and C. Ma, "Performances of three models in predicting packing densities and optimal mixing fractions of mixtures of micropowders with different sizes," *Powder Technol.*, vol. 397, p. 117095, Jan. 2022, doi: 10.1016/j.powtec.2021.117095.
[9] M. Bala, R. Zentar, and P. Boustingorry, "Parameter analysis of the compressible packing model for Concrete application".
[10] I. Mehdipour and K. H. Khayat, "Understanding the role of particle packing characteristics in rheo-physical properties of cementitious suspensions: A literature review," *Constr. Build. Mater.*, vol. 161, pp. 340–353, Feb. 2018, doi: 10.1016/j.conbuildmat.2017.11.147.
[11] C. C. Furnas, "Grading Aggregates - I. - Mathematical Relations for Beds of Broken Solids of Maximum Density," *Ind. Eng. Chem.*, vol. 23, no. 9, pp. 1052–1058, Sep. 1931, doi: 10.1021/ie50261a017.
[12] T.C Powers, *The Properties of Fresh Concrete*. John Wiley & Sons, New York, 1968.
[13] W.Toufar, E.Klose, and M.born, *Berechnung der Packungsdichte von Korngemischen Aufbereit.-Tech.* 1977.
[14] T. Stovall, F. de Larrard, and M. Buil, "Linear packing density model of grain mixtures," *Powder Technol.*, vol. 48, no. 1, pp. 1–12, Sep. 1986, doi: 10.1016/0032-5910(86)80058-4.
[15] G. Roquier, "The 4-parameter Compressible Packing Model (CPM) for crushed aggregate particles," *Powder Technol.*, vol. 320, pp. 133–142, Oct. 2017, doi: 10.1016/j.powtec.2017.07.028.
[16] Z.-R. Liu, W.-M. Ye, Z. Zhang, Q. Wang, Y.-G. Chen, and Y.-J. Cui, "Particle size ratio and distribution effects on packing behaviour of crushed GMZ bentonite pellets," *Powder Technol.*, vol. 351, pp. 92–101, Jun. 2019, doi: 10.1016/j.powtec.2019.03.038.
[17] Y. Knop and A. Peled, "Sustainable Blended Cements—Influences of Packing Density on Cement Paste Chemical Efficiency," *Materials*, vol. 11, no. 4, p. 625, Apr. 2018, doi: 10.3390/ma11040625.
[18] W. S. Sa, "OBTAINING UNIQUE PARTICLE SIZE DISTRIBUTIONS, THROUGH DYNAMIC CLASSIFICATION APPLIED TO SPIRAL JET MILLS," 2023.
[19] A. K. H. Kwan, V. Wong, and W. W. S. Fung, "A 3-parameter packing density model for angular rock aggregate particles," *Powder Technol.*, vol. 274, pp. 154–162, Apr. 2015, doi: 10.1016/j.powtec.2014.12.054.
[20] S. K. Snehal and B. B. Das, "Pozzolanic reactivity and drying shrinkage characteristics of optimized blended cementitious composites comprising of Nano-Silica particles," *Construction and Building Materials*, vol. 316, p. 125796, Nov. 2021, doi: 10.1016/j.conbuildmat.2021.125796.
[21] M.-H. Zhang and O. E. Gjorv, "Effect of silica fume on cement hydration in low porosity cement pastes," *Cement and Concrete Research*, vol. 21, no. 5, pp. 800-808, 1991, doi: 10.1016/0008-8846(91)90175-H.

[22] K. Terzaghi, R. B. Peck, and G. Mesri, *Soil Mechanics in Engineering Practice*, 3rd ed., New York: John Wiley & Sons, 1996.
[23] R. F. Craig, *Craig's Soil Mechanics*, 7th ed., London: CRC Press, 2004.

CHAPTER 3

[1] X. Jiang, R. Xiao, Y. Bai, B. Huang, and Y. Ma, "Influence of waste glass powder as a supplementary cementitious material (SCM) on physical and mechanical properties of cement paste under high temperatures," *J. Clean. Prod.*, vol. 340, p. 130778, Mar. 2022, doi: 10.1016/j.jclepro.2022.130778.
[2] T. Ramos, A. M. Matos, B. Schmidt, J. Rio, and J. Sousa-Coutinho, "Granitic quarry sludge waste in mortar: Effect on strength and durability," *Constr. Build. Mater.*, vol. 47, pp. 1001–1009, Oct. 2013, doi: 10.1016/j.conbuildmat.2013.05.098.
[3] C. Mitchell, "Production & Process Technology." Goodquarry, mineralsuk,bgs.ac.uk, 2007. [Online]. Available: https://www2.bgs.ac.uk/mineralsuk/download/goodQuarry/good_quarry_production_process.pdf
[4] G. Medina, I. F. Sáez Del Bosque, M. Frías, M. I. Sánchez De Rojas, and C. Medina, "Granite quarry waste as a future eco-efficient supplementary cementitious material (SCM): Scientific and technical considerations," *J. Clean. Prod.*, vol. 148, pp. 467–476, Apr. 2017, doi: 10.1016/j.jclepro.2017.02.048.
[5] D. Ndahirwa, H. Zmamou, H. Lenormand, and N. Leblanc, "The role of supplementary cementitious materials in hydration, durability and shrinkage of cement-based materials, their environmental and economic benefits: A review," *Clean. Mater.*, vol. 5, p. 100123, Sep. 2022, doi: 10.1016/j.clema.2022.100123.
[6] S. Seraj, R. Cano, R. D. Ferron, and M. C. G. Juenger, "The role of particle size on the performance of pumice as a supplementary cementitious material," *Cem. Concr. Compos.*, vol. 80, pp. 135–142, Jul. 2017, doi: 10.1016/j.cemconcomp.2017.03.009.
[7] A. A. Jhatial, I. Nováková, and E. Gjerløw, "A Review on Emerging Cementitious Materials, Reactivity Evaluation and Treatment Methods," *Buildings*, vol. 13, no. 2, p. 526, Feb. 2023, doi: 10.3390/buildings13020526.
[8] Y. Knop and A. Peled, "Packing density modeling of blended cement with limestone having different particle sizes," *Constr. Build. Mater.*, vol. 102, pp. 44–50, Jan. 2016, doi: 10.1016/j.conbuildmat.2015.09.063.
[9] D. C. Chu, J. Kleib, M. Amar, M. Benzerzour, and N.-E. Abriak, "Determination of the degree of hydration of Portland cement using three different approaches: Scanning electron microscopy (SEM-BSE) and Thermogravimetric analysis (TGA)," *Case Stud. Constr. Mater.*, vol. 15, p. e00754, Dec. 2021, doi: 10.1016/j.cscm.2021.e00754.
[10] S. Pradhan, S. Kumar, and S. V. Barai, "Understanding the behavior of recycled aggregate concrete by using thermogravimetric analysis," *Front. Struct. Civ. Eng.*, vol. 14, no. 6, pp. 1561–1572, Dec. 2020, doi: 10.1007/s11709-020-0640-5.
[11] "Pozzolanic Reactivity Test of Supplementary Cementitious Materials," *ACI Mater. J.*, vol. 119, no. 2, Mar. 2022, doi: 10.14359/51734349.
[12] K. L. Scrivener, "Backscattered electron imaging of cementitious microstructures: understanding and quantification," *Cem. Concr. Compos.*, vol. 26, no. 8, pp. 935–945, Nov. 2004, doi: 10.1016/j.cemconcomp.2004.02.029.

[13] C. T. Rueden *et al.*, "ImageJ2: ImageJ for the next generation of scientific image data," *BMC Bioinformatics*, vol. 18, no. 1, p. 529, Dec. 2017, doi: 10.1186/s12859-017-1934-z.

[14] A. Attari, C. McNally, and M. G. Richardson, "A combined SEM–Calorimetric approach for assessing hydration and porosity development in GGBS concrete," *Cem. Concr. Compos.*, vol. 68, pp. 46–56, Apr. 2016, doi: 10.1016/j.cemconcomp.2016.02.001.

[15] L. Li, J. Yang, and X. Shen, "Measuring the hydration product proportion in composite cement paste by using quantitative BSE-EDS image analysis: A comparative study," *Measurement*, vol. 199, p. 111290, Aug. 2022, doi: 10.1016/j.measurement.2022.111290.

[16] X. Xu, Y. Zhao, X. Gu, Z. Zhu, F. Wang, and Z. Zhang, "Effect of Particle Size and Morphology of Siliceous Supplementary Cementitious Material on the Hydration and Autogenous Shrinkage of Blended Cement," *Materials*, vol. 16, no. 4, p. 1638, Feb. 2023, doi: 10.3390/ma16041638.

[17] W. Deboucha, N. Leklou, A. Khelidj, and M. N. Oudjit, "Hydration development of mineral additives blended cement using thermogravimetric analysis (TGA): Methodology of calculating the degree of hydration," *Constr. Build. Mater.*, vol. 146, pp. 687–701, Aug. 2017, doi: 10.1016/j.conbuildmat.2017.04.132.

[18] Y. Cheng, F. Huang, W. Li, R. Liu, G. Li, and J. Wei, "Test research on the effects of mechanochemically activated iron tailings on the compressive strength of concrete," *Constr. Build. Mater.*, vol. 118, pp. 164–170, Aug. 2016, doi: 10.1016/j.conbuildmat.2016.05.020.

[19] L. Wang, F. Guo, Y. Lin, H. Yang, and S. W. Tang, "Comparison between the effects of phosphorous slag and fly ash on the C-S-H structure, long-term hydration heat and volume deformation of cement-based materials," *Constr. Build. Mater.*, vol. 250, p. 118807, Jul. 2020, doi: 10.1016/j.conbuildmat.2020.118807.

[20] "Ettringite formation and the performance of concrete," *Portland Cem. Assoc.*, [Online]. Available: https://www.cement.org/docs/default-source/fc_concrete_technology/is417-ettringite-formation-and-the-performance-of-concrete.pdf?sfvrsn=412%26sfvrsn=412#:~:text=Gypsum%20and%20other%20sulfate%20compounds,form%20ettringite%20at%20early%20ages.

[21] X. Zhu and I. G. Richardson, "Morphology-structural change of C-A-S-H gel in blended cements," *Cem. Concr. Res.*, vol. 168, p. 107156, Jun. 2023, doi: 10.1016/j.cemconres.2023.107156.

[22] T. Tracz and T. Zdeb, "Effect of Hydration and Carbonation Progress on the Porosity and Permeability of Cement Pastes," *Materials*, vol. 12, no. 1, p. 192, Jan. 2019, doi: 10.3390/ma12010192.

CHAPTER 4

[1] M. J. Miah, R. Huaping, S. C. Paul, A. J. Babafemi, and Y. Li, "Long-term strength and durability performance of eco-friendly concrete with supplementary cementitious materials," *Innov. Infrastruct. Solut.*, vol. 8, no. 10, p. 255, Oct. 2023, doi: 10.1007/s41062-023-01225-3.

[2] H. M. Hamada *et al.*, "Effect of silica fume on the properties of sustainable cement concrete," *Journal of Materials Research and Technology*, vol. 24, pp. 8887–8908, May 2023, doi: 10.1016/j.jmrt.2023.05.147.

[3] M. Antoni, J. Rossen, F. Martirena, and K. Scrivener, "Cement substitution by a combination of metakaolin and limestone," *Cement and Concrete Research*, vol. 42, no. 12, pp. 1579–1589, Dec. 2012, doi: 10.1016/j.cemconres.2012.09.006.
[4] R. San Nicolas, M. Cyr, and G. Escadeillas, "Performance-based approach to durability of concrete containing flash-calcined metakaolin as cement replacement," *Construction and Building Materials*, vol. 55, pp. 313–322, Mar. 2014, doi: 10.1016/j.conbuildmat.2014.01.063.
[5] A. M. Ramezanianpour and R. D. Hooton, "A study on hydration, compressive strength, and porosity of Portland-limestone cement mixes containing SCMs," *Cement and Concrete Composites*, vol. 51, pp. 1–13, Aug. 2014, doi: 10.1016/j.cemconcomp.2014.03.006.
[6] E. Güneyisi, M. Gesoğlu, S. Karaoğlu, and K. Mermerdaş, "Strength, permeability and shrinkage cracking of silica fume and metakaolin concretes," *Construction and Building Materials*, vol. 34, pp. 120–130, Sep. 2012, doi: 10.1016/j.conbuildmat.2012.02.017.
[7] A. Nadeem, S. A. Memon, and T. Y. Lo, "Mechanical performance, durability, qualitative and quantitative analysis of microstructure of fly ash and Metakaolin mortar at elevated temperatures," *Construction and Building Materials*, vol. 38, pp. 338–347, Jan. 2013, doi: 10.1016/j.conbuildmat.2012.08.042.
[8] T. Chappex and K. L. Scrivener, "The influence of aluminium on the dissolution of amorphous silica and its relation to alkali silica reaction," *Cement and Concrete Research*, vol. 42, no. 12, pp. 1645–1649, Dec. 2012, doi: 10.1016/j.cemconres.2012.09.009.
[9] T. Chappex and K. Scrivener, "Alkali fixation of C–S–H in blended cement pastes and its relation to alkali silica reaction," *Cement and Concrete Research*, vol. 42, no. 8, pp. 1049–1054, Aug. 2012, doi: 10.1016/j.cemconres.2012.03.010.
[10] Y. Zhao, J. Qiu, J. Xing, and X. Sun, "Recycling of quarry dust for supplementary cementitious materials in low carbon cement," *Construction and Building Materials*, vol. 237, p. 117608, Mar. 2020, doi: 10.1016/j.conbuildmat.2019.117608.
[11] A. Altheeb, "Quarry dust waste-based cementitious composites – A comprehensive review," *Construction and Building Materials*, vol. 350, p. 128817, Oct. 2022, doi: 10.1016/j.conbuildmat.2022.128817.
[12] N. Norbidin, K. Pilakoutas, M. Guadagnini, and B. Nematollahi, "Influence of fineness of quarry dust on hydration kinetics and pozzolanic reactivity in cementitious mixes," p. 35.
[13] A. Attari, C. McNally, and M. G. Richardson, "A combined SEM–Calorimetric approach for assessing hydration and porosity development in GGBS concrete," *Cement and Concrete Composites*, vol. 68, pp. 46–56, Apr. 2016, doi: 10.1016/j.cemconcomp.2016.02.001.
[14] C. T. Rueden *et al.*, "ImageJ2: ImageJ for the next generation of scientific image data," *BMC Bioinformatics*, vol. 18, no. 1, p. 529, Dec. 2017, doi: 10.1186/s12859-017-1934-z.
[15] L. Li, J. Yang, and X. Shen, "Measuring the hydration product proportion in composite cement paste by using quantitative BSE-EDS image analysis: A comparative study," *Measurement*, vol. 199, p. 111290, Aug. 2022, doi: 10.1016/j.measurement.2022.111290.

[16] I. Mehdipour and K. H. Khayat, "Effect of particle-size distribution and specific surface area of different binder systems on packing density and flow characteristics of cement paste," *Cement and Concrete Composites*, vol. 78, pp. 120–131, Apr. 2017, doi: 10.1016/j.cemconcomp.2017.01.005.
[17] W. Zhang, Y. Hama, and S. H. Na, "Drying shrinkage and microstructure characteristics of mortar incorporating ground granulated blast furnace slag and shrinkage reducing admixture," *Construction and Building Materials*, vol. 93, pp. 267–277, Sep. 2015, doi: 10.1016/j.conbuildmat.2015.05.103.
[18] ASTM Standard, "ASTM C 596-07 (Standard Test Method for Drying Shrinkage of Mortar Containing Hydraulic Cement)." ASTM Standard.
[19] "ASTM C 642-06 (Standard Test Method for Density, Absorption, and Voids in Hardened Concrete)."
[20] "ASTM C 1585-04 (Standard Test Method for Measurement of Rate of Absorption of Water by Hydraullic-Cement Concretes)."
[21] B. Lothenbach, G. Le Saout, E. Gallucci, and K. Scrivener, "Influence of limestone on the hydration of Portland cements," *Cement and Concrete Research*, vol. 38, no. 6, pp. 848–860, Jun. 2008, doi: 10.1016/j.cemconres.2008.01.002.
[22] E. John, T. Matschei, and D. Stephan, "Nucleation seeding with calcium silicate hydrate – A review," *Cement and Concrete Research*, vol. 113, pp. 74–85, Nov. 2018, doi: 10.1016/j.cemconres.2018.07.003.
[23] Y. Wang, L. Li, M. An, Y. Sun, Z. Yu, and H. Huang, "Factors Influencing the Capillary Water Absorption Characteristics of Concrete and Their Relationship to Pore Structure," *Applied Sciences*, vol. 12, no. 4, p. 2211, Feb. 2022, doi: 10.3390/app12042211.
[24] S. Dehghanpoor Abyaneh, H. S. Wong, and N. R. Buenfeld, "Computational investigation of capillary absorption in concrete using a three-dimensional mesoscale approach," *Computational Materials Science*, vol. 87, pp. 54–64, May 2014, doi: 10.1016/j.commatsci.2014.01.058.
[25] D. A. Silva, V. M. John, J. L. D. Ribeiro, and H. R. Roman, "Pore size distribution of hydrated cement pastes modified with polymers," *Cement and Concrete Research*, vol. 31, no. 8, pp. 1177–1184, Aug. 2001, doi: 10.1016/S0008-8846(01)00549-X.

This page is intentionally left blank

APPENDIX A

This appendix presents additional information on detail of characterisation testing used in this study.

A.1 METHODOLOGY AND DATA (CHARACTERISATION TESTING)

A.1.1 Milling

(a) Disc used to mill QDs

(b) Causes vibration to break the QDs in finer powder

Figure A.1: Equipment used for milling quarry dust.

Testing procedure:

1. Sample Preparation:

- Quarry dust samples were dried in oven at 110°C for 24 hrs until constant weight.
- Sample was then sieved passing the 75μ aperture. Only samples passing the sieve will be used for the milling process.

2. Loading the quarry dust:

- The quarry dust is placed between the milling disc (**Figure A.1(a)**) to about 150g and loaded onto the mill's feeding hopper as shown in **Figure A.1(b)**

3. Milling process:

- The samples were milled to two different time settings of 60s and 200s.

A.1.2 Particle Size Distribution (PSD)

Figure A.2: Equipment used for PSD

Testing procedure:

1. Sample Preparation and dispersion:

- Quarry dust is dispersed with s dispersing agent using 0.1% of Sodium Hexametaphosphate.
- The sample with agent mixture is stirred to ensure proper dispersion.

2. PSD measurement:

- The steps are followed before introducing the sample into the reservoir.
- Feed ⟶ De-bubble(1^{st}) ⟶ De-bubble(2^{nd}) ⟶ Start circulation ⟶ Set agitation ⟶ Check baseline ⟶ Align system ⟶ Perform blank measurement ⟶ Ensure 100% laser light (red and blue lights emitted).

- Sample introduced slowly into reservoir to achieve a transmittance around 90% on blue light.

3. After completing analysis, data is saved.

Testing results:

HORIBA Laser Scattering Particle Size Distribution Analyzer LA-950

Sample Name	:	Median Size	: 20.59701(μm)
ID#	: 202203141555951	Mean Size	: 30.31944(μm)
Data Name	: PC	Variance	: 831.81(μm²)
Transmittance(R)	: 83.7(%)	Std.Dev.	: 28.8411(μm)
Transmittance(B)	: 81.3(%)	Mode Size	: 16.2400(μm)
Circulation Speed	: 10	Span	: OFF
Agitation Speed	: 10	Geo.Mean Size	: 21.7488(μm)
Ultra Sonic	: 00:30 (2)	Geo.Variance	: 1.3265(μm²)
Form of Distribution	: Manual	Skewness	: 2.7464
Distribution Base	: Volume	Kurtosis	: 14.0121
Material	: Sand	Diameter on Cumulative %	: (1)10.00 (%)- 8.1252(μm)
Source	:		: (2)50.00 (%)- 20.5970(μm)
Lot Number	:		: (3)90.00 (%)- 64.2103(μm)
Test or Assay. Number	:		
Refractive Index (R)	: 1.60-0i in water[RI=1.60(1.600 - 0.000i),Water(1.333)]		
Refractive Index (B)	: 1.60-0i in water[RI=1.60(1.600 - 0.000i),Water(1.333)]		

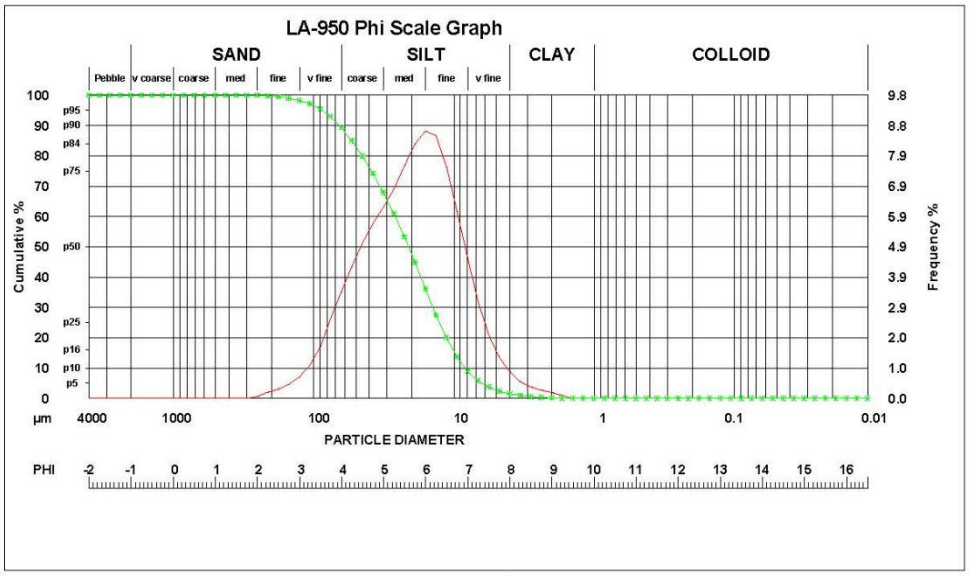

	Diameter	PHI	MILS	Microns	Frequency	Frequency	CUMULATIVE
F PEBBLE	5	-2.00	157.48	4000.00	0.00	0.00	100.00
	6	-1.75	132.42	3363.59	0.00		100.00
	7	-1.50	111.36	2828.43	0.00		100.00
	8	-1.25	93.64	2378.41	0.00		100.00
FINE PEBBLE	10	-1.00	78.74	2000.00	0.00	0.00	100.00
	12	-0.75	66.21	1681.79	0.00		100.00
	14	-0.50	55.68	1414.21	0.00		100.00
	16	-0.25	46.82	1189.21	0.00		100.00
V CRS SAND	18	0.00	39.37	1000.00	0.00	0.00	100.00
	20	0.25	33.11	840.90	0.00		100.00
	25	0.50	27.84	707.11	0.00		100.00
	30	0.75	23.41	594.60	0.00		100.00
CRS SAND	35	1.00	19.69	500.00	0.00	0.00	100.00
	40	1.25	16.55	420.45	0.00		100.00
	45	1.50	13.92	353.55	0.00		100.00
	50	1.75	11.70	297.30	0.00		100.00
MED SAND	60	2.00	9.84	250.00	0.05	0.05	99.95
	70	2.25	8.28	210.22	0.20		99.75
	80	2.50	6.96	176.78	0.30		99.46
	100	2.75	5.85	148.65	0.46		99.00
FINE SAND	120	3.00	4.92	125.00	0.70	1.66	98.30
	140	3.25	4.14	105.11	1.07		97.23
	170	3.50	3.48	88.39	1.69		95.54
	200	3.75	2.93	74.33	2.64		92.90
V FINE SAND	230	4.00	2.46	62.50	3.51	8.90	89.39
	270	4.25	2.07	52.56	4.34		85.06
	325	4.50	1.74	44.19	5.12		79.94
	400	4.75	1.46	37.16	5.76		74.18
CRS SILT	450	5.00	1.23	31.25	6.29	21.51	67.88
	500	5.25	1.03	26.28	6.89		60.99
	635	5.50	0.87	22.10	7.67		53.32
		5.75	0.73	18.58	8.38		44.94
MED SILT		6.00	0.62	15.63	8.82	31.76	36.12
		6.25	0.52	13.14	8.67		27.45
		6.50	0.43	11.05	7.62		19.83
		6.75	0.37	9.29	6.16		13.67
FINE SILT		7.00	0.31	7.81	4.64	27.09	9.03
		7.25	0.26	6.57	3.20		5.83
		7.50	0.22	5.52	2.10		3.73
		7.75	0.18	4.65	1.37		2.36
V FINE SILT		8.00	0.15	3.91	0.89	7.56	1.47
		8.25	0.13	3.28	0.55		0.93
		8.50	0.11	2.76	0.38		0.55

	Diameter	PHI	MILS	Microns	Frequency	Frequency	CUMULATIVE
	8.75	0.09	2.32	0.27			0.28
	9.00	0.08	1.95	0.19			0.09
	9.25	0.06	1.64	0.09			0.00
	9.50	0.05	1.38	0.00			0.00
	9.75	0.05	1.16	0.00			0.00
CLAY	10.00	0.04	0.98	0.00	1.47		0.00
	10.25	0.03	0.82	0.00			0.00
	10.50	0.03	0.69	0.00			0.00
	10.75	0.02	0.58	0.00			0.00
	11.00	0.02	0.49	0.00			0.00
	11.25	0.02	0.41	0.00			0.00
	11.50	0.01	0.35	0.00			0.00
	11.75	0.01	0.29	0.00			0.00
	12.00	0.01	0.24	0.00			0.00
	12.25	0.01	0.21	0.00			0.00
	12.50	0.01	0.17	0.00			0.00
	12.75	0.01	0.15	0.00			0.00
	13.00	0.00	0.12	0.00			0.00
	13.25	0.00	0.10	0.00			0.00
	13.50	0.00	0.09	0.00			0.00
	13.75	0.00	0.07	0.00			0.00
	14.00	0.00	0.06	0.00			0.00
	14.25	0.00	0.05	0.00			0.00
	14.50	0.00	0.04	0.00			0.00
	14.75	0.00	0.04	0.00			0.00
	15.00	0.00	0.03	0.00			0.00
	15.25	0.00	0.03	0.00			0.00
	15.50	0.00	0.02	0.00			0.00
	15.75	0.00	0.02	0.00			0.00
	16.00	0.00	0.02	0.00			0.00
	16.25	0.00	0.01	0.00			0.00
COLLOID	16.50	0.00	0.01	0.00	0.00		0.00

1 / 1

Figure A.3: PSD for PC

HORIBA Laser Scattering Particle Size Distribution Analyzer LA-950

Sample Name	:	Median Size	: 21.62322(μm)
ID#	: 202103111157640	Mean Size	: 32.62286(μm)
Data Name	: passing 75micron	Variance	: 879.80(μm²)
Transmittance(R)	: 78.5(%)	Std.Dev.	: 29.6614(μm)
Transmittance(B)	: 70.6(%)	Mode Size	: 54.9296(μm)
Circulation Speed	: 10	Span	: OFF
Agitation Speed	: 10	Geo.Mean Size	: 20.3860(μm)
Ultra Sonic	: 00:30 (2)	Geo.Variance	: 1.6296(μm²)
Form of Distribution	: Manual	Skewness	: 1.3938
Distribution Base	: Volume	Kurtosis	: 5.1903
Material	: Sand	Diameter on Cumulative %	: (1)10.00 (%)- 4.8808(μm)
Source	:		: (2)50.00 (%)- 21.6232(μm)
Lot Number	:		: (3)90.00 (%)- 74.4102(μm)
Test or Assay. Number	:		
Refractive Index (R)	: 1.60-0i in water[RI=1.60(1.600 - 0.000i),Water(1.333)]		
Refractive Index (B)	: 1.60-0i in water[RI=1.60(1.600 - 0.000i),Water(1.333)]		

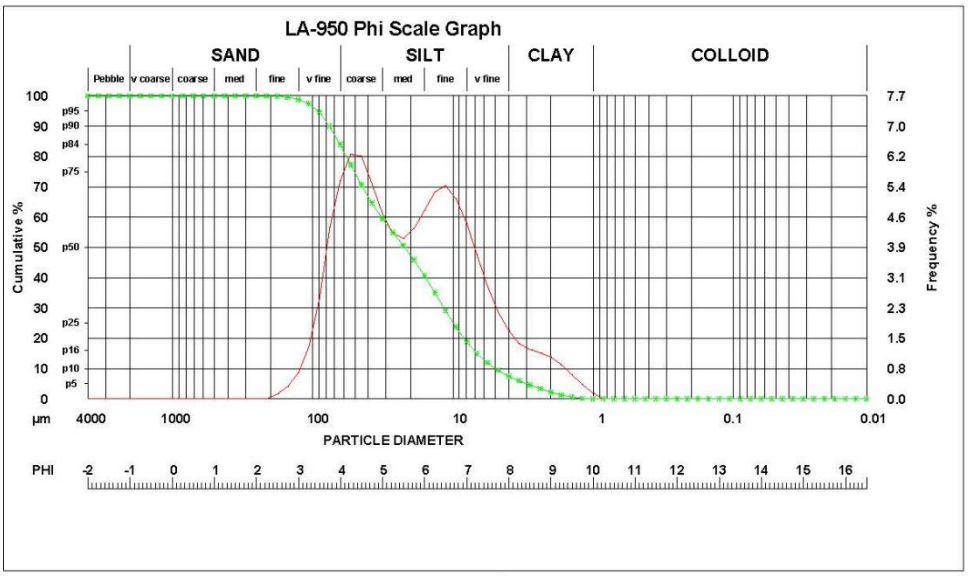

	Diameter	PHI	MILS	Microns	Frequency	Frequency	CUMULATIVE
F PEBBLE	5	-2.00	157.48	4000.00	0.00	0.00	100.00
	6	-1.75	132.42	3363.59	0.00		100.00
	7	-1.50	111.36	2828.43	0.00		100.00
	8	-1.25	93.64	2378.41	0.00		100.00
FINE PEBBLE	10	-1.00	78.74	2000.00	0.00	0.00	100.00
	12	-0.75	66.21	1681.79	0.00		100.00
	14	-0.50	55.68	1414.21	0.00		100.00
	16	-0.25	46.82	1189.21	0.00		100.00
V CRS SAND	18	0.00	39.37	1000.00	0.00	0.00	100.00
	20	0.25	33.11	840.90	0.00		100.00
	25	0.50	27.84	707.11	0.00		100.00
	30	0.75	23.41	594.60	0.00		100.00
CRS SAND	35	1.00	19.69	500.00	0.00	0.00	100.00
	40	1.25	16.55	420.45	0.00		100.00
	45	1.50	13.92	353.55	0.00		100.00
	50	1.75	11.70	297.30	0.00		100.00
MED SAND	60	2.00	9.84	250.00	0.00	0.00	100.00
	70	2.25	8.28	210.22	0.00		100.00
	80	2.50	6.96	176.78	0.12		99.88
	100	2.75	5.85	148.65	0.34		99.54
FINE SAND	120	3.00	4.92	125.00	0.71	1.17	98.83
	140	3.25	4.14	105.11	1.41		97.42
	170	3.50	3.48	88.39	2.74		94.68
	200	3.75	2.93	74.33	4.72		89.96
V FINE SAND	230	4.00	2.46	62.50	6.00	14.87	83.96
	270	4.25	2.07	52.56	6.72		77.24
	325	4.50	1.74	44.19	6.68		70.56
	400	4.75	1.46	37.16	5.92		64.63
CRS SILT	450	5.00	1.23	31.25	5.10	24.43	59.53
	500	5.25	1.03	26.28	4.56		54.98
	635	5.50	0.87	22.10	4.41		50.57
		5.75	0.73	18.58	4.68		45.89
MED SILT		6.00	0.62	15.63	5.18	18.83	40.71
		6.25	0.52	13.14	5.69		35.02
		6.50	0.43	11.05	5.87		29.15
		6.75	0.37	9.29	5.51		23.65
FINE SILT		7.00	0.31	7.81	4.84	21.90	18.81
		7.25	0.26	6.57	3.95		14.86
		7.50	0.22	5.52	3.08		11.77
		7.75	0.18	4.65	2.39		9.38
V FINE SILT		8.00	0.15	3.91	1.89	11.31	7.49
		8.25	0.13	3.28	1.52		5.97
		8.50	0.11	2.76	1.36		4.61

	Diameter	PHI	MILS	Microns	Frequency	Frequency	CUMULATIVE
	8.75	0.09	2.32	1.27		3.34	
	9.00	0.08	1.95	1.16		2.18	
	9.25	0.06	1.64	0.95		1.24	
	9.50	0.05	1.38	0.67		0.56	
	9.75	0.05	1.16	0.40		0.16	
CLAY	10.00	0.04	0.98	0.16	7.49	0.00	
	10.25	0.03	0.82	0.00		0.00	
	10.50	0.03	0.69	0.00		0.00	
	10.75	0.02	0.58	0.00		0.00	
	11.00	0.02	0.49	0.00		0.00	
	11.25	0.02	0.41	0.00		0.00	
	11.50	0.01	0.35	0.00		0.00	
	11.75	0.01	0.29	0.00		0.00	
	12.00	0.01	0.24	0.00		0.00	
	12.25	0.01	0.21	0.00		0.00	
	12.50	0.01	0.17	0.00		0.00	
	12.75	0.01	0.15	0.00		0.00	
	13.00	0.00	0.12	0.00		0.00	
	13.25	0.00	0.10	0.00		0.00	
	13.50	0.00	0.09	0.00		0.00	
	13.75	0.00	0.07	0.00		0.00	
	14.00	0.00	0.06	0.00		0.00	
	14.25	0.00	0.05	0.00		0.00	
	14.50	0.00	0.04	0.00		0.00	
	14.75	0.00	0.04	0.00		0.00	
	15.00	0.00	0.03	0.00		0.00	
	15.25	0.00	0.03	0.00		0.00	
	15.50	0.00	0.02	0.00		0.00	
	15.75	0.00	0.02	0.00		0.00	
	16.00	0.00	0.02	0.00		0.00	
	16.25	0.00	0.01	0.00		0.00	
COLLOID	16.50	0.00	0.01	0.00	0.00	0.00	

1 / 1

Figure A.4: PSD for S0

HORIBA Laser Scattering Particle Size Distribution Analyzer LA-950

Sample Name	:	Median Size	: 9.02577(µm)
ID#	: 202103111211643	Mean Size	: 15.52184(µm)
Data Name	: 60s	Variance	: 396.00(µm²)
Transmittance(R)	: 80.5(%)	Std.Dev.	: 19.8997(µm)
Transmittance(B)	: 70.6(%)	Mode Size	: 10.7969(µm)
Circulation Speed	: 10	Span	: OFF
Agitation Speed	: 10	Geo.Mean Size	: 8.4990(µm)
Ultra Sonic	: 00:30 (2)	Geo.Variance	: 1.7400(µm²)
Form of Distribution	: Manual	Skewness	: 2.9879
Distribution Base	: Volume	Kurtosis	: 14.5960
Material	: Sand	Diameter on Cumulative %	: (1)10.00 (%)- 1.8178(µm)
Source	:		: (2)50.00 (%)- 9.0258(µm)
Lot Number	:		: (3)90.00 (%)- 38.5744(µm)
Test or Assay. Number	:		
Refractive Index (R)	: 1.60-0i in water[RI=1.60(1.600 - 0.000i),Water(1.333)]		
Refractive Index (B)	: 1.60-0i in water[RI=1.60(1.600 - 0.000i),Water(1.333)]		

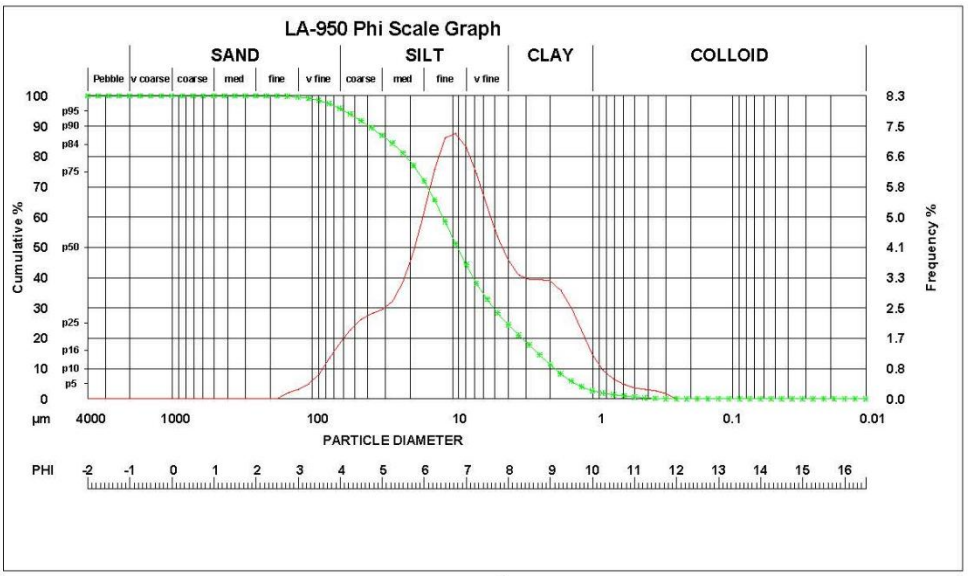

	Diameter	PHI	MILS	Microns	Frequency	Frequency	CUMULATIVE
F PEBBLE	5	-2.00	157.48	4000.00	0.00	0.00	100.00
	6	-1.75	132.42	3363.59	0.00		100.00
	7	-1.50	111.36	2828.43	0.00		100.00
	8	-1.25	93.64	2378.41	0.00		100.00
FINE PEBBLE	10	-1.00	78.74	2000.00	0.00	0.00	100.00
	12	-0.75	66.21	1681.79	0.00		100.00
	14	-0.50	55.68	1414.21	0.00		100.00
	16	-0.25	46.82	1189.21	0.00		100.00
V CRS SAND	18	0.00	39.37	1000.00	0.00	0.00	100.00
	20	0.25	33.11	840.90	0.00		100.00
	25	0.50	27.84	707.11	0.00		100.00
	30	0.75	23.41	594.60	0.00		100.00
CRS SAND	35	1.00	19.69	500.00	0.00	0.00	100.00
	40	1.25	16.55	420.45	0.00		100.00
	45	1.50	13.92	353.55	0.00		100.00
	50	1.75	11.70	297.30	0.00		100.00
MED SAND	60	2.00	9.84	250.00	0.00	0.00	100.00
	70	2.25	8.28	210.22	0.00		100.00
	80	2.50	6.96	176.78	0.00		100.00
	100	2.75	5.85	148.65	0.16		99.84
FINE SAND	120	3.00	4.92	125.00	0.25	0.41	99.59
	140	3.25	4.14	105.11	0.40		99.20
	170	3.50	3.48	88.39	0.67		98.53
	200	3.75	2.93	74.33	1.12		97.42
V FINE SAND	230	4.00	2.46	62.50	1.52	3.70	95.89
	270	4.25	2.07	52.56	1.89		94.00
	325	4.50	1.74	44.19	2.18		91.82
	400	4.75	1.46	37.16	2.34		89.49
CRS SILT	450	5.00	1.23	31.25	2.45	8.86	87.04
	500	5.25	1.03	26.28	2.68		84.36
	635	5.50	0.87	22.10	3.22		81.14
		5.75	0.73	18.58	4.05		77.10
MED SILT		6.00	0.62	15.63	5.12	15.06	71.97
		6.25	0.52	13.14	6.30		65.67
		6.50	0.43	11.05	7.18		59.49
		6.75	0.37	9.29	7.29		51.20
FINE SILT		7.00	0.31	7.81	6.93	27.70	44.27
		7.25	0.26	6.57	6.19		38.07
		7.50	0.22	5.52	5.28		32.80
		7.75	0.18	4.65	4.46		28.34
V FINE SILT		8.00	0.15	3.91	3.83	19.77	24.50
		8.25	0.13	3.28	3.41		21.09
		8.50	0.11	2.76	3.28		17.81

	Diameter	PHI	MILS	Microns	Frequency	Frequency	CUMULATIVE
	8.75	0.09	2.32	3.28			14.53
	9.00	0.08	1.95	3.25			11.28
	9.25	0.06	1.64	2.99			8.29
	9.50	0.05	1.38	2.50			5.79
	9.75	0.05	1.16	1.88			3.91
CLAY	10.00	0.04	0.98	1.23	21.82		2.68
	10.25	0.03	0.82	0.80			1.88
	10.50	0.03	0.69	0.55			1.33
	10.75	0.02	0.58	0.40			0.94
	11.00	0.02	0.49	0.31			0.63
	11.25	0.02	0.41	0.26			0.37
	11.50	0.01	0.35	0.22			0.15
	11.75	0.01	0.29	0.15			0.00
	12.00	0.01	0.24	0.00			0.00
	12.25	0.01	0.21	0.00			0.00
	12.50	0.01	0.17	0.00			0.00
	12.75	0.01	0.15	0.00			0.00
	13.00	0.00	0.12	0.00			0.00
	13.25	0.00	0.10	0.00			0.00
	13.50	0.00	0.09	0.00			0.00
	13.75	0.00	0.07	0.00			0.00
	14.00	0.00	0.06	0.00			0.00
	14.25	0.00	0.05	0.00			0.00
	14.50	0.00	0.04	0.00			0.00
	14.75	0.00	0.04	0.00			0.00
	15.00	0.00	0.03	0.00			0.00
	15.25	0.00	0.03	0.00			0.00
	15.50	0.00	0.02	0.00			0.00
	15.75	0.00	0.02	0.00			0.00
	16.00	0.00	0.02	0.00			0.00
	16.25	0.00	0.01	0.00			0.00
COLLOID	16.50	0.00	0.01	0.00	2.68		0.00

1 / 1

Figure A.5: PSD for S60

HORIBA Laser Scattering Particle Size Distribution Analyzer LA-950

Sample Name	:	Median Size	: 7.79576(μm)
ID#	: 202103111229646	Mean Size	: 10.42115(μm)
Data Name	: 200s	Variance	: 116.46(μm²)
Transmittance(R)	: 78.1(%)	Std.Dev.	: 10.7919(μm)
Transmittance(B)	: 67.8(%)	Mode Size	: 10.8205(μm)
Circulation Speed	: 10	Span	: OFF
Agitation Speed	: 10	Geo.Mean Size	: 6.5140(μm)
Ultra Sonic	: 00:30 (2)	Geo.Variance	: 1.6076(μm²)
Form of Distribution	: Manual	Skewness	: 2.8744
Distribution Base	: Volume	Kurtosis	: 15.6154
Material	: Sand	Diameter on Cumulative %	: (1)10.00 (%)- 1.4932(μm)
Source	:		: (2)50.00 (%)- 7.7958(μm)
Lot Number	:		: (3)90.00 (%)- 21.5219(μm)
Test or Assay. Number	:		
Refractive Index (R)	: 1.60-0i in water[RI=1.60(1.600 - 0.000i),Water(1.333)]		
Refractive Index (B)	: 1.60-0i in water[RI=1.60(1.600 - 0.000i),Water(1.333)]		

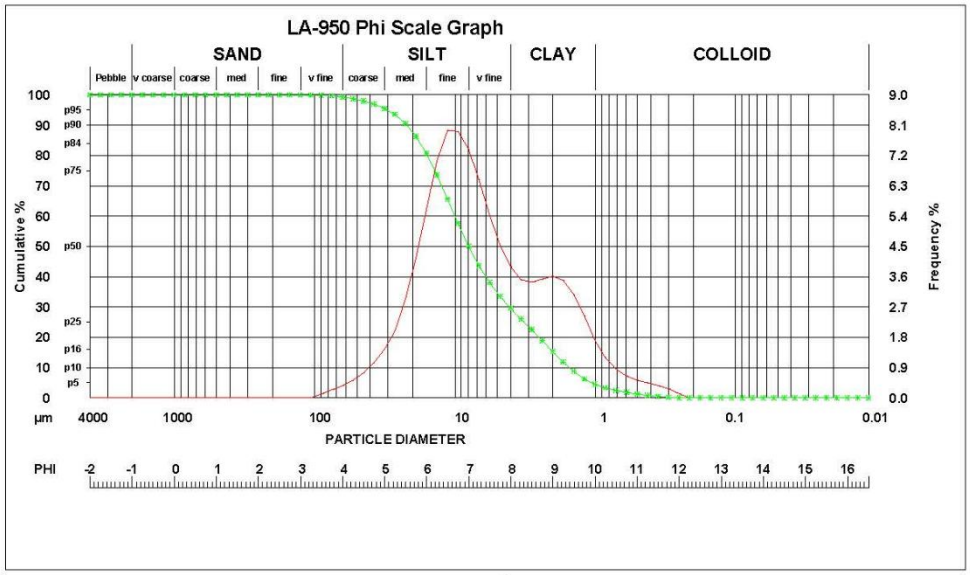

	Diameter	PHI	MILS	Microns	Diameter Frequency	Diameter Frequency	CUMULATIVE
F PEBBLE	5	-2.00	157.48	4000.00	0.00	0.00	100.00
	6	-1.75	132.42	3363.59	0.00		100.00
	7	-1.50	111.36	2828.43	0.00		100.00
	8	-1.25	93.64	2378.41	0.00		100.00
FINE PEBBLE	10	-1.00	78.74	2000.00	0.00	0.00	100.00
	12	-0.75	66.21	1681.79	0.00		100.00
	14	-0.50	55.68	1414.21	0.00		100.00
	16	-0.25	46.82	1189.21	0.00		100.00
V CRS SAND	18	0.00	39.37	1000.00	0.00	0.00	100.00
	20	0.25	33.11	840.90	0.00		100.00
	25	0.50	27.84	707.11	0.00		100.00
	30	0.75	23.41	594.60	0.00		100.00
CRS SAND	35	1.00	19.69	500.00	0.00	0.00	100.00
	40	1.25	16.55	420.45	0.00		100.00
	45	1.50	13.92	353.55	0.00		100.00
	50	1.75	11.70	297.30	0.00		100.00
MED SAND	60	2.00	9.84	250.00	0.00	0.00	100.00
	70	2.25	8.28	210.22	0.00		100.00
	80	2.50	6.96	176.78	0.00		100.00
	100	2.75	5.85	148.65	0.00		100.00
FINE SAND	120	3.00	4.92	125.00	0.00	0.00	100.00
	140	3.25	4.14	105.11	0.00		100.00
	170	3.50	3.48	88.39	0.12		99.88
	200	3.75	2.93	74.33	0.23		99.65
V FINE SAND	230	4.00	2.46	62.50	0.36	0.71	99.29
	270	4.25	2.07	52.56	0.52		98.78
	325	4.50	1.74	44.19	0.74		98.03
	400	4.75	1.46	37.16	1.05		96.98
CRS SILT	450	5.00	1.23	31.25	1.44	3.75	95.54
	500	5.25	1.03	26.28	2.00		93.54
	635	5.50	0.87	22.10	2.97		90.57
		5.75	0.73	18.58	4.21		86.36
MED SILT		6.00	0.62	15.63	5.67	14.85	80.69
		6.25	0.52	13.14	7.11		73.58
		6.50	0.43	11.05	8.03		65.55
		6.75	0.37	9.29	8.00		57.55
FINE SILT		7.00	0.31	7.81	7.46	30.60	50.09
		7.25	0.26	6.57	6.54		43.55
		7.50	0.22	5.52	5.48		38.06
		7.75	0.18	4.65	4.59		33.49
V FINE SILT		8.00	0.15	3.91	3.94	20.55	29.54
		8.25	0.13	3.28	3.54		26.00
		8.50	0.11	2.76	3.47		22.53

	Diameter	PHI	MILS	Microns	Diameter Frequency	Diameter Frequency	CUMULATIVE
	8.75	0.09	2.32	3.56			18.97
	9.00	0.08	1.95	3.65			15.32
	9.25	0.06	1.64	3.52			11.80
	9.50	0.05	1.38	3.10			8.70
	9.75	0.05	1.16	2.47			6.24
CLAY	10.00	0.04	0.98	1.73	25.04		4.51
	10.25	0.03	0.82	1.20			3.30
	10.50	0.03	0.69	0.87			2.43
	10.75	0.02	0.58	0.66			1.77
	11.00	0.02	0.49	0.53			1.24
	11.25	0.02	0.41	0.45			0.78
	11.50	0.01	0.35	0.38			0.41
	11.75	0.01	0.29	0.28			0.13
	12.00	0.01	0.24	0.13			0.00
	12.25	0.01	0.21	0.00			0.00
	12.50	0.01	0.17	0.00			0.00
	12.75	0.01	0.15	0.00			0.00
	13.00	0.00	0.12	0.00			0.00
	13.25	0.00	0.10	0.00			0.00
	13.50	0.00	0.09	0.00			0.00
	13.75	0.00	0.07	0.00			0.00
	14.00	0.00	0.06	0.00			0.00
	14.25	0.00	0.05	0.00			0.00
	14.50	0.00	0.04	0.00			0.00
	14.75	0.00	0.04	0.00			0.00
	15.00	0.00	0.03	0.00			0.00
	15.25	0.00	0.03	0.00			0.00
	15.50	0.00	0.02	0.00			0.00
	15.75	0.00	0.02	0.00			0.00
	16.00	0.00	0.02	0.00			0.00
	16.25	0.00	0.01	0.00			0.00
COLLOID	16.50	0.00	0.01	0.00	4.51		0.00

1 / 1

Figure A.6: PSD for S200

HORIBA Laser Scattering Particle Size Distribution Analyzer LA-950

Sample Name	:	Median Size	: 9.45550(μm)
ID#	: 202101221255603	Mean Size	: 14.07450(μm)
Data Name	: 60s	Variance	: 245.93(μm²)
Transmittance(R)	: 76.6(%)	Std.Dev.	: 15.6822(μm)
Transmittance(B)	: 65.8(%)	Mode Size	: 10.8103(μm)
Circulation Speed	: 10	Span	: OFF
Agitation Speed	: 10	Geo.Mean Size	: 8.8758(μm)
Ultra Sonic	: 00:30 (2)	Geo.Variance	: 1.5226(μm²)
Form of Distribution	: Manual	Skewness	: 2.8693
Distribution Base	: Volume	Kurtosis	: 13.6607
Material	: Sand	Diameter on Cumulative %	: (1)10.00 (%)- 2.2214(μm)
Source	:		: (2)50.00 (%)- 9.4555(μm)
Lot Number	:		: (3)90.00 (%)- 30.9626(μm)
Test or Assay. Number	:		
Refractive Index (R)	: 1.60-0i in water[RI=1.60(1.600 - 0.000i),Water(1.333)]		
Refractive Index (B)	: 1.60-0i in water[RI=1.60(1.600 - 0.000i),Water(1.333)]		

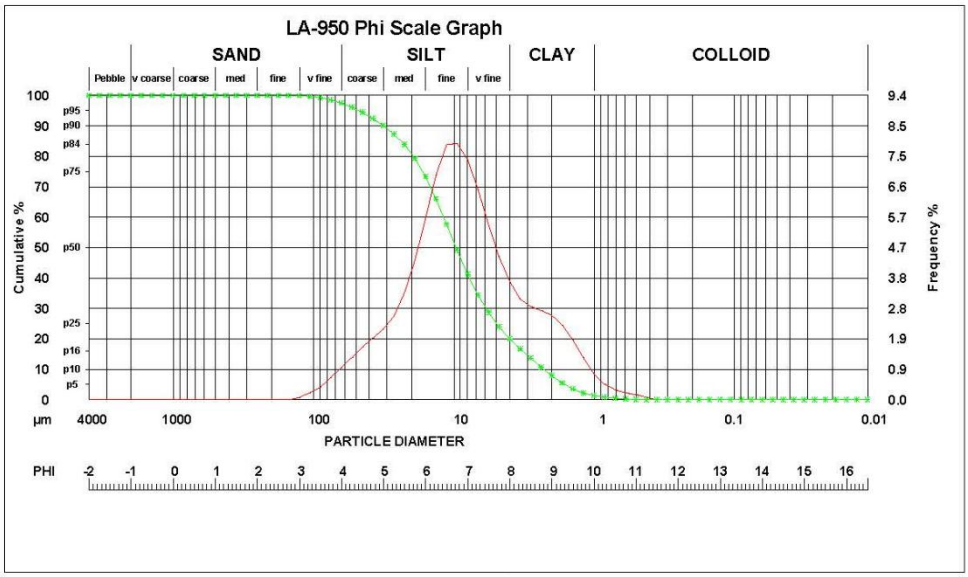

	Diameter	PHI	MILS	Microns	Frequency	Frequency	CUMULATIVE
F PEBBLE	5	-2.00	157.48	4000.00	0.00	0.00	100.00
	6	-1.75	132.42	3363.59	0.00		100.00
	7	-1.50	111.36	2828.43	0.00		100.00
	8	-1.25	93.84	2378.41	0.00		100.00
FINE PEBBLE	10	-1.00	78.74	2000.00	0.00	0.00	100.00
	12	-0.75	66.21	1681.79	0.00		100.00
	14	-0.50	55.68	1414.21	0.00		100.00
	16	-0.25	46.82	1189.21	0.00		100.00
V CRS SAND	18	0.00	39.37	1000.00	0.00	0.00	100.00
	20	0.25	33.11	840.90	0.00		100.00
	25	0.50	27.84	707.11	0.00		100.00
	30	0.75	23.41	594.60	0.00		100.00
CRS SAND	35	1.00	19.69	500.00	0.00	0.00	100.00
	40	1.25	16.55	420.45	0.00		100.00
	45	1.50	13.92	353.55	0.00		100.00
	50	1.75	11.70	297.30	0.00		100.00
MED SAND	60	2.00	9.84	250.00	0.00	0.00	100.00
	70	2.25	8.28	210.22	0.00		100.00
	80	2.50	6.96	176.78	0.00		100.00
	100	2.75	5.85	148.65	0.00		100.00
FINE SAND	120	3.00	4.92	125.00	0.06	0.06	99.94
	140	3.25	4.14	105.11	0.22		99.72
	170	3.50	3.48	88.39	0.40		99.31
	200	3.75	2.93	74.33	0.72		98.59
V FINE SAND	230	4.00	2.46	62.50	1.04	2.38	97.56
	270	4.25	2.07	52.56	1.38		96.18
	325	4.50	1.74	44.19	1.72		94.46
	400	4.75	1.46	37.16	2.02		92.44
CRS SILT	450	5.00	1.23	31.25	2.31	7.43	90.13
	500	5.25	1.03	26.28	2.73		87.40
	635	5.50	0.87	22.10	3.51		83.89
		5.75	0.73	18.58	4.59		79.29
MED SILT		6.00	0.62	15.63	5.95	16.78	73.35
		6.25	0.52	13.14	7.37		65.97
		6.50	0.43	11.05	8.39		57.59
		6.75	0.37	9.29	8.43		49.16
FINE SILT		7.00	0.31	7.81	7.90	32.08	41.27
		7.25	0.26	6.57	6.91		34.36
		7.50	0.22	5.52	5.73		28.63
		7.75	0.18	4.65	4.70		23.93
V FINE SILT		8.00	0.15	3.91	3.89	21.23	20.04
		8.25	0.13	3.28	3.31		16.73
		8.50	0.11	2.76	3.06		13.67

	Diameter	PHI	MILS	Microns	Frequency	Frequency	CUMULATIVE
	8.75	0.09	2.32	2.93			10.73
	9.00	0.08	1.95	2.78			7.95
	9.25	0.06	1.64	2.45			5.50
	9.50	0.05	1.38	1.95			3.55
	9.75	0.05	1.16	1.39			2.16
CLAY	10.00	0.04	0.98	0.85	18.73		1.31
	10.25	0.03	0.82	0.52			0.79
	10.50	0.03	0.69	0.33			0.46
	10.75	0.02	0.58	0.22			0.24
	11.00	0.02	0.49	0.16			0.07
	11.25	0.02	0.41	0.07			0.00
	11.50	0.01	0.35	0.00			0.00
	11.75	0.01	0.29	0.00			0.00
	12.00	0.01	0.24	0.00			0.00
	12.25	0.01	0.21	0.00			0.00
	12.50	0.01	0.17	0.00			0.00
	12.75	0.01	0.15	0.00			0.00
	13.00	0.00	0.12	0.00			0.00
	13.25	0.00	0.10	0.00			0.00
	13.50	0.00	0.09	0.00			0.00
	13.75	0.00	0.07	0.00			0.00
	14.00	0.00	0.06	0.00			0.00
	14.25	0.00	0.05	0.00			0.00
	14.50	0.00	0.04	0.00			0.00
	14.75	0.00	0.04	0.00			0.00
	15.00	0.00	0.03	0.00			0.00
	15.25	0.00	0.03	0.00			0.00
	15.50	0.00	0.02	0.00			0.00
	15.75	0.00	0.02	0.00			0.00
	16.00	0.00	0.02	0.00			0.00
	16.25	0.00	0.01	0.00			0.00
COLLOID	16.50	0.00	0.01	0.00	1.31		0.00

Figure A.7: PSD for D60

HORIBA Laser Scattering Particle Size Distribution Analyzer LA-950

Sample Name	:	Median Size	: 7.37715(μm)
ID#	: 202102231131613	Mean Size	: 10.44108(μm)
Data Name	: 200s	Variance	: 131.01(μm²)
Transmittance(R)	: 80.6(%)	Std.Dev.	: 11.4460(μm)
Transmittance(B)	: 70.4(%)	Mode Size	: 10.8054(μm)
Circulation Speed	: 10	Span	: OFF
Agitation Speed	: 10	Geo.Mean Size	: 6.3790(μm)
Ultra Sonic	: 00:30 (2)	Geo.Variance	: 1.6065(μm²)
Form of Distribution	: Manual	Skewness	: 2.9016
Distribution Base	: Volume	Kurtosis	: 14.9735
Material	: Sand	Diameter on Cumulative %	: (1)10.00 (%)- 1.4931(μm)
Source	:		: (2)50.00 (%)- 7.3771(μm)
Lot Number	:		: (3)90.00 (%)- 22.0426(μm)
Test or Assay. Number	:		
Refractive Index (R)	: 1.60-0i in water[RI=1.60(1.600 - 0.000i),Water(1.333)]		
Refractive Index (B)	: 1.60-0i in water[RI=1.60(1.600 - 0.000i),Water(1.333)]		

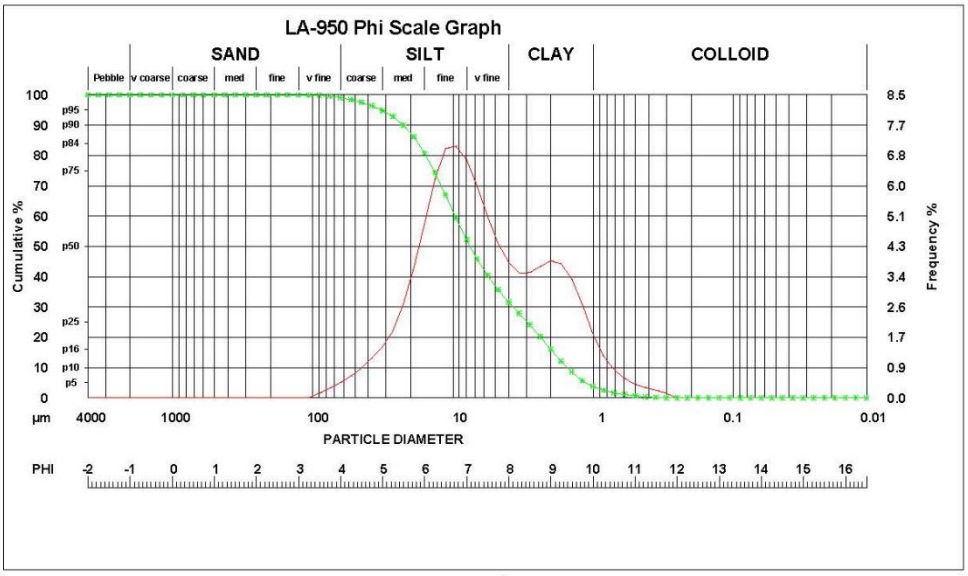

	Diameter	PHI	MILS	Microns	Diameter Frequency	Diameter Frequency	CUMULATIVE
F PEBBLE	5	-2.00	157.48	4000.00	0.00	0.00	100.00
	6	-1.75	132.42	3363.59	0.00		100.00
	7	-1.50	111.36	2828.43	0.00		100.00
	8	-1.25	93.64	2378.41	0.00		100.00
FINE PEBBLE	10	-1.00	78.74	2000.00	0.00	0.00	100.00
	12	-0.75	66.21	1681.79	0.00		100.00
	14	-0.50	55.68	1414.21	0.00		100.00
	16	-0.25	46.82	1189.21	0.00		100.00
V CRS SAND	18	0.00	39.37	1000.00	0.00	0.00	100.00
	20	0.25	33.11	840.90	0.00		100.00
	25	0.50	27.84	707.11	0.00		100.00
	30	0.75	23.41	594.60	0.00		100.00
CRS SAND	35	1.00	19.69	500.00	0.00	0.00	100.00
	40	1.25	16.55	420.45	0.00		100.00
	45	1.50	13.92	353.55	0.00		100.00
	50	1.75	11.70	297.30	0.00		100.00
MED SAND	60	2.00	9.84	250.00	0.00	0.00	100.00
	70	2.25	8.28	210.22	0.00		100.00
	80	2.50	6.96	176.78	0.00		100.00
	100	2.75	5.85	148.65	0.00		100.00
FINE SAND	120	3.00	4.92	125.00	0.00	0.00	100.00
	140	3.25	4.14	105.11	0.00		100.00
	170	3.50	3.48	88.39	0.14		99.86
	200	3.75	2.93	74.33	0.29		99.57
V FINE SAND	230	4.00	2.46	62.50	0.45	0.88	99.12
	270	4.25	2.07	52.56	0.64		98.48
	325	4.50	1.74	44.19	0.89		97.59
	400	4.75	1.46	37.16	1.19		96.40
CRS SILT	450	5.00	1.23	31.25	1.52	4.25	94.88
	500	5.25	1.03	26.28	2.00		92.88
	635	5.50	0.87	22.10	2.83		90.05
		5.75	0.73	18.58	3.92		86.13
MED SILT		6.00	0.62	15.63	5.23	13.97	80.91
		6.25	0.52	13.14	6.56		74.34
		6.50	0.43	11.05	7.48		66.86
		6.75	0.37	9.29	7.55		59.31
FINE SILT		7.00	0.31	7.81	7.14	28.73	52.17
		7.25	0.26	6.57	6.36		45.81
		7.50	0.22	5.52	5.43		40.38
		7.75	0.18	4.65	4.65		35.73
V FINE SILT		8.00	0.15	3.91	4.07	20.51	31.66
		8.25	0.13	3.28	3.75		27.90
		8.50	0.11	2.76	3.76		24.14

	Diameter	PHI	MILS	Microns	Diameter Frequency	Diameter Frequency	CUMULATIVE
	8.75	0.09	2.32	3.93			20.21
	9.00	0.08	1.95	4.11			16.10
	9.25	0.06	1.64	4.03			12.07
	9.50	0.05	1.38	3.56			8.51
	9.75	0.05	1.16	2.81			5.70
CLAY	10.00	0.04	0.98	1.92	27.87		3.78
	10.25	0.03	0.82	1.27			2.51
	10.50	0.03	0.69	0.85			1.66
	10.75	0.02	0.58	0.58			1.08
	11.00	0.02	0.49	0.41			0.67
	11.25	0.02	0.41	0.31			0.37
	11.50	0.01	0.35	0.23			0.14
	11.75	0.01	0.29	0.14			0.00
	12.00	0.01	0.24	0.00			0.00
	12.25	0.01	0.21	0.00			0.00
	12.50	0.01	0.17	0.00			0.00
	12.75	0.01	0.15	0.00			0.00
	13.00	0.00	0.12	0.00			0.00
	13.25	0.00	0.10	0.00			0.00
	13.50	0.00	0.09	0.00			0.00
	13.75	0.00	0.07	0.00			0.00
	14.00	0.00	0.06	0.00			0.00
	14.25	0.00	0.05	0.00			0.00
	14.50	0.00	0.04	0.00			0.00
	14.75	0.00	0.04	0.00			0.00
	15.00	0.00	0.03	0.00			0.00
	15.25	0.00	0.03	0.00			0.00
	15.50	0.00	0.02	0.00			0.00
	15.75	0.00	0.02	0.00			0.00
	16.00	0.00	0.02	0.00			0.00
	16.25	0.00	0.01	0.00			0.00
COLLOID	16.50	0.00	0.01	0.00	3.78		0.00

1 / 1

Figure A.8: PSD for D200

HORIBA Laser Scattering Particle Size Distribution Analyzer LA-950

Sample Name	:	Median Size	: 18.16599(µm)
ID#	: 202103111433647	Mean Size	: 29.92839(µm)
Data Name	: passing 75micron	Variance	: 812.98(µm²)
Transmittance(R)	: 75.6(%)	Std.Dev.	: 28.5128(µm)
Transmittance(B)	: 71.3(%)	Mode Size	: 12.3793(µm)
Circulation Speed	: 10	Span	: OFF
Agitation Speed	: 10	Geo.Mean Size	: 19.6803(µm)
Ultra Sonic	: 00:30 (2)	Geo.Variance	: 1.4713(µm²)
Form of Distribution	: Manual	Skewness	: 1.7763
Distribution Base	: Volume	Kurtosis	: 6.7530
Material	: Sand	Diameter on Cumulative %	: (1)10.00 (%)- 6.1405(µm)
Source	:		: (2)50.00 (%)- 18.1660(µm)
Lot Number	:		: (3)90.00 (%)- 70.1690(µm)
Test or Assay. Number	:		
Refractive Index (R)	: 1.60-0i in water[RI=1.60(1.600 - 0.000i),Water(1.333)]		
Refractive Index (B)	: 1.60-0i in water[RI=1.60(1.600 - 0.000i),Water(1.333)]		

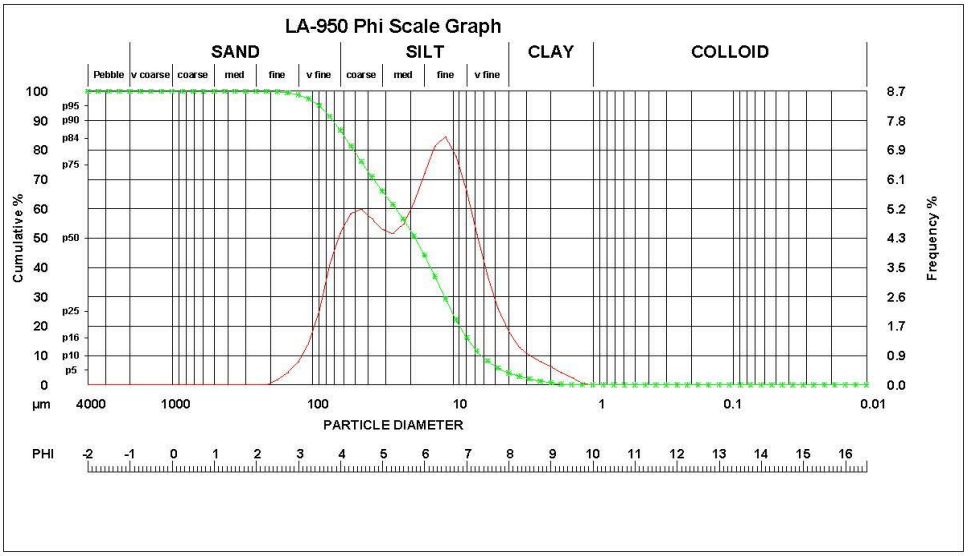

	Diameter	PHI	MILS	Microns	Frequency	Diameter Frequency	CUMULATIVE
F PEBBLE	5	-2.00	157.48	4000.00	0.00	0.00	100.00
	6	-1.75	132.42	3363.59	0.00		100.00
	7	-1.50	111.36	2828.43	0.00		100.00
	8	-1.25	93.64	2378.41	0.00		100.00
FINE PEBBLE	10	-1.00	78.74	2000.00	0.00	0.00	100.00
	12	-0.75	66.21	1681.79	0.00		100.00
	14	-0.50	55.68	1414.21	0.00		100.00
	16	-0.25	46.82	1189.21	0.00		100.00
V CRS SAND	18	0.00	39.37	1000.00	0.00	0.00	100.00
	20	0.25	33.11	840.90	0.00		100.00
	25	0.50	27.84	707.11	0.00		100.00
	30	0.75	23.41	594.60	0.00		100.00
CRS SAND	35	1.00	19.69	500.00	0.00	0.00	100.00
	40	1.25	16.55	420.45	0.00		100.00
	45	1.50	13.92	353.55	0.00		100.00
	50	1.75	11.70	297.30	0.00		100.00
MED SAND	60	2.00	9.84	250.00	0.00	0.00	100.00
	70	2.25	8.28	210.22	0.00		100.00
	80	2.50	6.96	176.78	0.15		99.85
	100	2.75	5.85	148.65	0.37		99.48
FINE SAND	120	3.00	4.92	125.00	0.71	1.23	98.77
	140	3.25	4.14	105.11	1.28		97.49
	170	3.50	3.48	88.39	2.29		95.20
	200	3.75	2.93	74.33	3.73		91.47
V FINE SAND	230	4.00	2.46	62.50	4.69	12.00	86.78
	270	4.25	2.07	52.56	5.29		81.48
	325	4.50	1.74	44.19	5.44		76.04
	400	4.75	1.46	37.16	5.15		70.89
CRS SILT	450	5.00	1.23	31.25	4.81	20.69	66.08
	500	5.25	1.03	26.28	4.69		61.39
	635	5.50	0.87	22.10	4.97		56.43
		5.75	0.73	18.58	5.64		50.79
MED SILT		6.00	0.62	15.63	6.54	21.83	44.25
		6.25	0.52	13.14	7.39		36.86
		6.50	0.43	11.05	7.68		29.18
		6.75	0.37	9.29	7.09		22.09
FINE SILT		7.00	0.31	7.81	6.01	28.18	16.08
		7.25	0.26	6.57	4.65		11.43
		7.50	0.22	5.52	3.35		8.08
		7.75	0.18	4.65	2.37		5.71
V FINE SILT		8.00	0.15	3.91	1.67	12.04	4.04
		8.25	0.13	3.28	1.16		2.88
		8.50	0.11	2.76	0.91		1.96

	Diameter	PHI	MILS	Microns	Frequency	Diameter Frequency	CUMULATIVE
	8.75	0.09	2.32		0.74		1.23
	9.00	0.08	1.95		0.57		0.66
	9.25	0.06	1.64		0.39		0.27
	9.50	0.05	1.38		0.23		0.05
	9.75	0.05	1.16		0.05		0.00
CLAY	10.00	0.04	0.98		0.00	4.04	0.00
	10.25	0.03	0.82		0.00		0.00
	10.50	0.03	0.69		0.00		0.00
	10.75	0.02	0.58		0.00		0.00
	11.00	0.02	0.49		0.00		0.00
	11.25	0.02	0.41		0.00		0.00
	11.50	0.01	0.35		0.00		0.00
	11.75	0.01	0.29		0.00		0.00
	12.00	0.01	0.24		0.00		0.00
	12.25	0.01	0.21		0.00		0.00
	12.50	0.01	0.17		0.00		0.00
	12.75	0.01	0.15		0.00		0.00
	13.00	0.00	0.12		0.00		0.00
	13.25	0.00	0.10		0.00		0.00
	13.50	0.00	0.09		0.00		0.00
	13.75	0.00	0.07		0.00		0.00
	14.00	0.00	0.06		0.00		0.00
	14.25	0.00	0.05		0.00		0.00
	14.50	0.00	0.04		0.00		0.00
	14.75	0.00	0.04		0.00		0.00
	15.00	0.00	0.03		0.00		0.00
	15.25	0.00	0.03		0.00		0.00
	15.50	0.00	0.02		0.00		0.00
	15.75	0.00	0.02		0.00		0.00
	16.00	0.00	0.02		0.00		0.00
	16.25	0.00	0.01		0.00		0.00
COLLOID	16.50	0.00	0.01		0.00	0.00	0.00

1 / 1

Figure A.9: PSD for G0

HORIBA Laser Scattering Particle Size Distribution Analyzer LA-950

Sample Name	:	Median Size	: 10.86526(μm)
ID#	: 202103111441649	Mean Size	: 17.33612(μm)
Data Name	: 60s	Variance	: 392.58(μm²)
Transmittance(R)	: 72.9(%)	Std.Dev.	: 19.8138(μm)
Transmittance(B)	: 64.8(%)	Mode Size	: 10.8324(μm)
Circulation Speed	: 10	Span	: OFF
Agitation Speed	: 10	Geo.Mean Size	: 10.8022(μm)
Ultra Sonic	: 00:30 (2)	Geo.Variance	: 1.5187(μm²)
Form of Distribution	: Manual	Skewness	: 2.8435
Distribution Base	: Volume	Kurtosis	: 13.6478
Material	: Sand	Diameter on Cumulative %	: (1)10.00 (%)- 2.7968(μm)
Source	:		: (2)50.00 (%)- 10.8653(μm)
Lot Number	:		: (3)90.00 (%)- 40.9878(μm)
Test or Assay. Number	:		
Refractive Index (R)	: 1.60-0i in water[RI=1.60(1.600 - 0.000i),Water(1.333)]		
Refractive Index (B)	: 1.60-0i in water[RI=1.60(1.600 - 0.000i),Water(1.333)]		

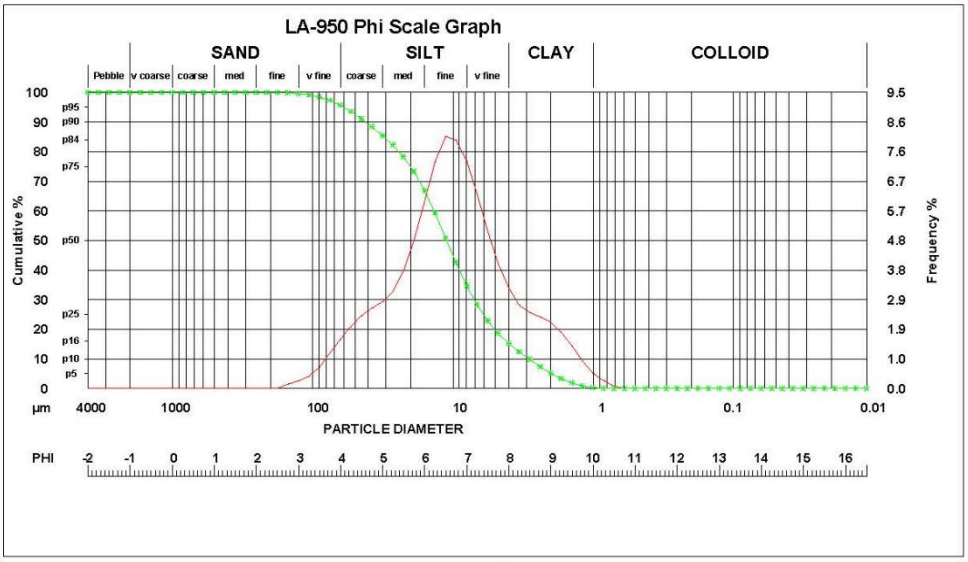

	Diameter	PHI	MILS	Microns	Diameter Frequency	Diameter Frequency	CUMULATIVE
F PEBBLE	5	-2.00	157.48	4000.00	0.00	0.00	100.00
	6	-1.75	132.42	3363.59	0.00		100.00
	7	-1.50	111.36	2828.43	0.00		100.00
	8	-1.25	93.64	2378.41	0.00		100.00
FINE PEBBLE	10	-1.00	78.74	2000.00	0.00	0.00	100.00
	12	-0.75	66.21	1681.79	0.00		100.00
	14	-0.50	55.68	1414.21	0.00		100.00
	16	-0.25	46.82	1189.21	0.00		100.00
V CRS SAND	18	0.00	39.37	1000.00	0.00	0.00	100.00
	20	0.25	33.11	840.90	0.00		100.00
	25	0.50	27.84	707.11	0.00		100.00
	30	0.75	23.41	594.60	0.00		100.00
CRS SAND	35	1.00	19.69	500.00	0.00	0.00	100.00
	40	1.25	16.55	420.45	0.00		100.00
	45	1.50	13.92	353.55	0.00		100.00
	50	1.75	11.70	297.30	0.00		100.00
MED SAND	60	2.00	9.84	250.00	0.00	0.00	100.00
	70	2.25	8.28	210.22	0.00		100.00
	80	2.50	6.96	176.78	0.00		100.00
	100	2.75	5.85	148.65	0.14		99.86
FINE SAND	120	3.00	4.92	125.00	0.25	0.39	99.61
	140	3.25	4.14	105.11	0.40		99.21
	170	3.50	3.48	88.39	0.70		98.51
	200	3.75	2.93	74.33	1.19		97.32
V FINE SAND	230	4.00	2.46	62.50	1.64	3.93	95.68
	270	4.25	2.07	52.56	2.08		93.61
	325	4.50	1.74	44.19	2.45		91.16
	400	4.75	1.46	37.16	2.71		88.45
CRS SILT	450	5.00	1.23	31.25	2.92	10.16	85.53
	500	5.25	1.03	26.28	3.26		82.26
	635	5.50	0.87	22.10	3.97		78.29
		5.75	0.73	18.58	5.00		73.28
MED SILT		6.00	0.62	15.63	6.30	18.54	66.98
		6.25	0.52	13.14	7.64		59.34
		6.50	0.43	11.05	8.51		50.83
		6.75	0.37	9.29	8.40		42.43
FINE SILT		7.00	0.31	7.81	7.70	32.26	34.73
		7.25	0.26	6.57	6.57		28.16
		7.50	0.22	5.52	5.30		22.86
		7.75	0.18	4.65	4.23		18.63
V FINE SILT		8.00	0.15	3.91	3.42	19.52	15.21
		8.25	0.13	3.28	2.82		12.39
		8.50	0.11	2.76	2.57		9.82
		8.75	0.09	2.32	2.42		7.40
		9.00	0.08	1.95	2.25		5.15
		9.25	0.06	1.64	1.91		3.25
		9.50	0.05	1.38	1.44		1.81
		9.75	0.05	1.16	0.95		0.86
CLAY		10.00	0.04	0.98	0.51	14.86	0.35
		10.25	0.03	0.82	0.27		0.08
		10.50	0.03	0.69	0.08		0.00
		10.75	0.02	0.58	0.00		0.00
		11.00	0.02	0.49	0.00		0.00
		11.25	0.02	0.41	0.00		0.00
		11.50	0.01	0.35	0.00		0.00
		11.75	0.01	0.29	0.00		0.00
		12.00	0.01	0.24	0.00		0.00
		12.25	0.01	0.21	0.00		0.00
		12.50	0.01	0.17	0.00		0.00
		12.75	0.01	0.15	0.00		0.00
		13.00	0.00	0.12	0.00		0.00
		13.25	0.00	0.10	0.00		0.00
		13.50	0.00	0.09	0.00		0.00
		13.75	0.00	0.07	0.00		0.00
		14.00	0.00	0.06	0.00		0.00
		14.25	0.00	0.05	0.00		0.00
		14.50	0.00	0.04	0.00		0.00
		14.75	0.00	0.04	0.00		0.00
		15.00	0.00	0.03	0.00		0.00
		15.25	0.00	0.03	0.00		0.00
		15.50	0.00	0.02	0.00		0.00
		15.75	0.00	0.02	0.00		0.00
		16.00	0.00	0.02	0.00		0.00
		16.25	0.00	0.01	0.00		0.00
COLLOID		16.50	0.00	0.01	0.00	0.35	0.00

1 / 1

Figure A10: PSD for G60

HORIBA Laser Scattering Particle Size Distribution Analyzer LA-950

Sample Name	:	Median Size	: 8.64733(µm)
ID#	: 202103111446650	Mean Size	: 11.53803(µm)
Data Name	: 200s	Variance	: 135.87(µm²)
Transmittance(R)	: 71.9(%)	Std.Dev.	: 11.6563(µm)
Transmittance(B)	: 61.7(%)	Mode Size	: 10.8275(µm)
Circulation Speed	: 10	Span	: OFF
Agitation Speed	: 10	Geo.Mean Size	: 7.4380(µm)
Ultra Sonic	: 00:30 (2)	Geo.Variance	: 1.5507(µm²)
Form of Distribution	: Manual	Skewness	: 2.7557
Distribution Base	: Volume	Kurtosis	: 13.9806
Material	: Sand	Diameter on Cumulative %	: (1)10.00 (%)- 1.7702(µm)
Source	:		: (2)50.00 (%)- 8.6473(µm)
Lot Number	:		: (3)90.00 (%)- 23.6543(µm)
Test or Assay. Number	:		
Refractive Index (R)	: 1.60-0i in water[RI=1.60(1.600 - 0.000i),Water(1.333)]		
Refractive Index (B)	: 1.60-0i in water[RI=1.60(1.600 - 0.000i),Water(1.333)]		

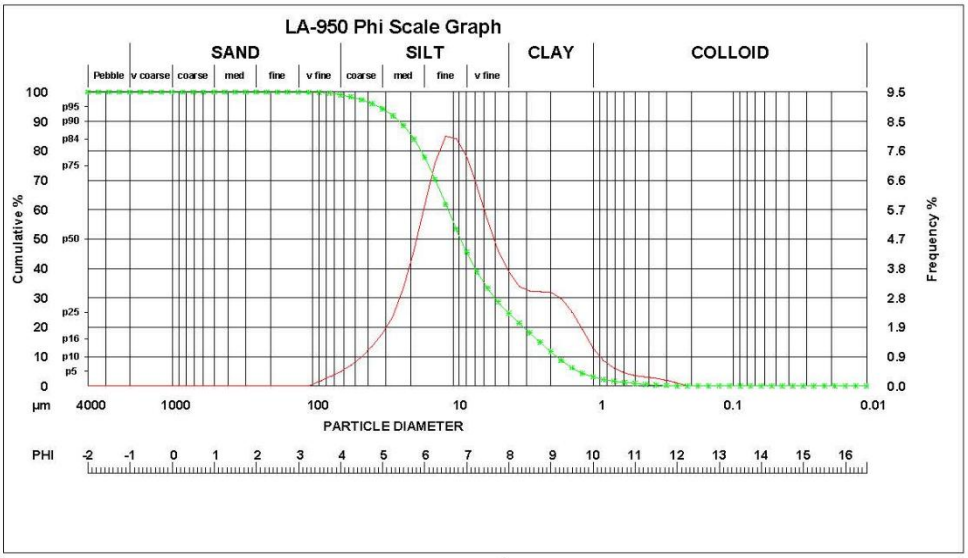

	Diameter	PHI	MILS	Microns	Frequency	Frequency	CUMULATIVE
F PEBBLE	5	-2.00	157.48	4000.00	0.00	0.00	100.00
	6	-1.75	132.42	3363.59	0.00		100.00
	7	-1.50	111.36	2828.43	0.00		100.00
	8	-1.25	93.64	2378.41	0.00		100.00
FINE PEBBLE	10	-1.00	78.74	2000.00	0.00	0.00	100.00
	12	-0.75	66.21	1681.79	0.00		100.00
	14	-0.50	55.68	1414.21	0.00		100.00
	16	-0.25	46.82	1189.21	0.00		100.00
V CRS SAND	18	0.00	39.37	1000.00	0.00	0.00	100.00
	20	0.25	33.11	840.90	0.00		100.00
	25	0.50	27.84	707.11	0.00		100.00
	30	0.75	23.41	594.60	0.00		100.00
CRS SAND	35	1.00	19.69	500.00	0.00	0.00	100.00
	40	1.25	16.55	420.45	0.00		100.00
	45	1.50	13.92	353.55	0.00		100.00
	50	1.75	11.70	297.30	0.00		100.00
MED SAND	60	2.00	9.84	250.00	0.00	0.00	100.00
	70	2.25	8.28	210.22	0.00		100.00
	80	2.50	6.96	176.78	0.00		100.00
	100	2.75	5.85	148.65	0.00		100.00
FINE SAND	120	3.00	4.92	125.00	0.00	0.00	100.00
	140	3.25	4.14	105.11	0.00		100.00
	170	3.50	3.48	88.39	0.15		99.85
	200	3.75	2.93	74.33	0.31		99.54
V FINE SAND	230	4.00	2.46	62.50	0.48	0.94	99.06
	270	4.25	2.07	52.56	0.69		98.37
	325	4.50	1.74	44.19	0.98		97.39
	400	4.75	1.46	37.16	1.34		96.05
CRS SILT	450	5.00	1.23	31.25	1.77	4.78	94.28
	500	5.25	1.03	26.28	2.36		91.92
	635	5.50	0.87	22.10	3.36		88.57
		5.75	0.73	18.58	4.63		83.94
MED SILT		6.00	0.62	15.63	6.11	16.46	77.83
		6.25	0.52	13.14	7.58		70.25
		6.50	0.43	11.05	8.50		61.75
		6.75	0.37	9.29	8.42		53.33
FINE SILT		7.00	0.31	7.81	7.79	32.29	45.54
		7.25	0.26	6.57	6.75		38.79
		7.50	0.22	5.52	5.59		33.20
		7.75	0.18	4.65	4.61		28.60
V FINE SILT		8.00	0.15	3.91	3.87	20.82	24.72
		8.25	0.13	3.28	3.38		21.35
		8.50	0.11	2.76	3.22		18.12
		8.75	0.09	2.32	3.21		14.91
		9.00	0.08	1.95	3.18		11.73
		9.25	0.06	1.64	2.96		8.77
		9.50	0.05	1.38	2.51		6.26
		9.75	0.05	1.16	1.92		4.35
CLAY		10.00	0.04	0.98	1.28	21.65	3.07
		10.25	0.03	0.82	0.85		2.22
		10.50	0.03	0.69	0.59		1.63
		10.75	0.02	0.58	0.44		1.19
		11.00	0.02	0.49	0.35		0.84
		11.25	0.02	0.41	0.30		0.54
		11.50	0.01	0.35	0.25		0.29
		11.75	0.01	0.29	0.19		0.10
		12.00	0.01	0.24	0.10		0.00
		12.25	0.01	0.21	0.00		0.00
		12.50	0.01	0.17	0.00		0.00
		12.75	0.01	0.15	0.00		0.00
		13.00	0.00	0.12	0.00		0.00
		13.25	0.00	0.10	0.00		0.00
		13.50	0.00	0.09	0.00		0.00
		13.75	0.00	0.07	0.00		0.00
		14.00	0.00	0.06	0.00		0.00
		14.25	0.00	0.05	0.00		0.00
		14.50	0.00	0.04	0.00		0.00
		14.75	0.00	0.04	0.00		0.00
		15.00	0.00	0.03	0.00		0.00
		15.25	0.00	0.03	0.00		0.00
		15.50	0.00	0.02	0.00		0.00
		15.75	0.00	0.02	0.00		0.00
		16.00	0.00	0.02	0.00		0.00
		16.25	0.00	0.01	0.00		0.00
COLLOID		16.50	0.00	0.01	0.00	3.07	0.00

1 / 1

Figure A11: PSD for G200

A.1.3 X-ray fluorescence (XRF)

(a) Crucible and base plate use for fuse bead preparation

(b) 10g flux mixed with 1g of QD sample

(c) Le Neo Fluxer

Figure A.12: Equipment used for the fuse bead preparation.

Testing procedure (fuse bead synthesis):

Claisse LeNeo Fluxer is used for the preparation.

1. Approximately 10g of flux and up to 1 g of the QD sample is weighted using a 4-decimal place balance (this is necessary for use in the Zetium machine)

2. The flux and QD sample is thoroughly mixed to ensure removal of any agglomerates (**Figure A.12(b)**)

3. Mount the casting dish into the grey base plate of the LeNeo (see **Figure A.12(c)**) and hold the upper lever fully up and insert the crucible (filled with flux+ QD).

4. Once the correct program (Disk-WROXI LeNEO 40mm1') was selected, the 'Start' button is pressed.

5. Checked that the crucible and casting disc are correctly mounted, and the main door closed and pressed 'Confirm'.

6. The furnace proceeded to make the fused bead typically about 22minutes for the standard WROXI program.

7. At the end of the process, once the platinum ware cooled down, the upper black lever was pressed up to remove the crucible and the casting dish to retrieve the fused bead.

8. Fused bead was stored in a cool and dry place for analysis in the Zetium machine.

Figure A.13: PANalytical Zetium for XRF analysis

Testing procedure for XRF analysis:

PANalytical Zetium is used for the analysis.

1. The following testing flow were used for this analysis.
2. Place sample cup ⟶ Open sample changer ⟶ Delete existing programme ⟶ Select sample position ⟶ Verify position ⟶ Set type to routine ⟶ Select application ⟶ Enter sample ID ⟶ Set number of repeats ⟶ Set priority ⟶ Match archive to application ⟶ Calibration and processing parameters ⟶ Tick 'with cup' ⟶ Edit flux/final weights ⟶ Add and measure.
3. After completing analysis, data can be retrieved from PC.

A.1.4 X-ray Diffraction (XRD)

Figure A.14: Bruker D2 Phaser for XRD

This page is intentionally left blank

APPENDIX B

Chapter 2: Influence of particle size distribution on packing density of blended cement with quarry fines having different particle sizes.

This appendix presents additional information on detail of method of testing and experimental data for chapter 2.

B.1 METHODOLOGY AND DATA (CHAPTER 2)

B.1.1 Initial Packing Density

(a) Mechanical mixer used for mixing (b) Resulting paste to be poured into cylindrical mould.

Figure B.1: Equipment used to determine the initial packing density

Testing procedure:

1. The amount of water, Ordinary Portland cement (PC), quarry dust (QDs), and superplasticizer (SP) were measured, and each material are placed in its own container.

2. PC and QDs were dry mixed for a duration of 2 minutes to ensure homogeneity.
3. All water is poured into the mixing bowl.
4. Half of the cementitious powder (PC + QDs) and SP were introduced into the mixing bowl, followed by running the mixer on a low setting for 3 minutes.
5. The remaining cementitious powder (PC + QDs) and SP are split into two equal parts. Each part is gradually added into the mixing bowl, with the mixer running on low setting for 3 minutes each addition.
6. The resulting paste is moved to a cylindrical mould, filling at three layers with 25 tamping each. Any excess is scrapped off with a straight edge and the weight of the paste in mould is weighed and recorded.
7. The process from step (3)-(6) is repeated with different amount of quarry dust in the mixture and finally the packing density is identified.

This page is intentionally left blank

APPENDIX C

Chapter 3: Influence of milling as a pre-treatment of quarry dust for use in cementitious mixes.

This appendix presents additional information on detail of testing and results for chapter 3.

C.1 METHODOLOGY AND DATA (CHAPTER 3)

C.1.1 Heat of hydration (Semi-adiabatic)

The measurement method involves placing a freshly mixed sample of PC-QDs into the calorimeter and monitoring the temperature of the specimens for 72 hours as shown in **Figure C.1a**. These semi-adiabatic calorimeters rely on some form of insulation around the sample to prevent heat loss. For each testing batch, 3 samples were run at the same time.

(a) Semi-adiabatic calorimeter

(b) Cells of calorimeter

Figure C.1: Set-up of the testing equipment to determine the HoH.

Testing procedure:

1. **Preparation of PC-QDs mix:** A fresh mix of PC and QDs was prepared to the required proportions.
2. **Immediate transfer to calorimeter:** After mixing, the fresh PC-QDs sample was immediately transferred into the calorimeter to begin temperature measurement. (Thermocouple is inserted into the mixed paste at this point)
3. **Temperature monitoring:** The temperature of the specimen was monitored continuously for 72 hours (recorded to the data-logger) within the calorimeter, allowing for thorough observation of temperature changes.

Multiple tests: For each batch of tests, three samples were run simultaneously (see **Figure C.1b**)

C.1.3 Cube Compressive strength

The cube compressive strength is a widely recognized method that helps determine the strength of concrete, and thereby its suitability for specific construction applications. In term of pozzolanic reactivity, its strength directly relates to the formation of CSH. Researchers has reported pozzolanicity based on the strength activity index (SAI).

The SAI is calculated as the percentage ratio of the compressive strength of the sample to the compressive strength of the reference (pure PC). The SAI must be at least 75% at 7 days or 28 days to be considered as having pozzolanic activity according to ASTM C618.

(a) 20mm cubes

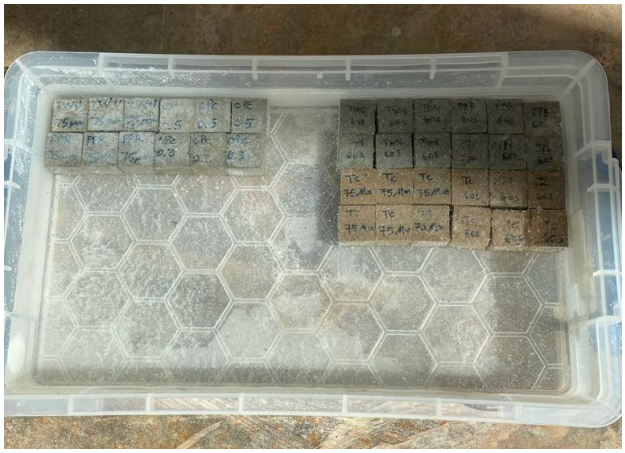

(b) Samples cured for 7 and 28 days.

Figure C.13: Cube compressive testing

Testing procedure:

1. **Sample preparation:**

- Concrete cubes of 20mm incorporating QDs were prepared in accordance with the mix design (**Figure C.13(a)**)
- Samples were cured for 7 and 28 days, depending on the testing date (**Figure C.13(b)**)

2. **Cube Crushing:**

    - The cured sample is placed centrally on the machine's plate and loaded gradually applied until the cube failed. The maximum load at failure was recorded (figure C.13 c-h)

(c) Shimadzu 2000kN machine

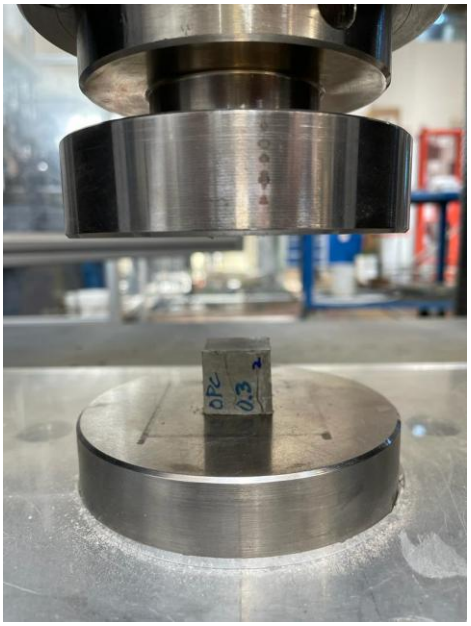

(d) Cube placed on the centre of platen.

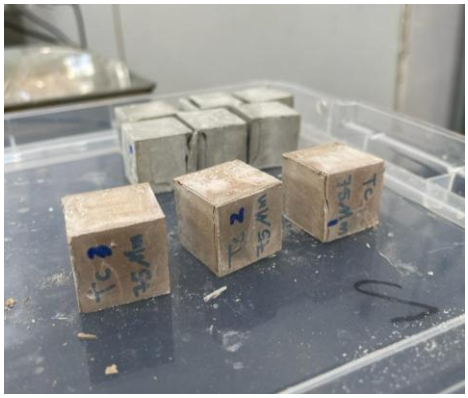

(e) Crushed G0 cube samples

(f) Crushed S0 cube samples

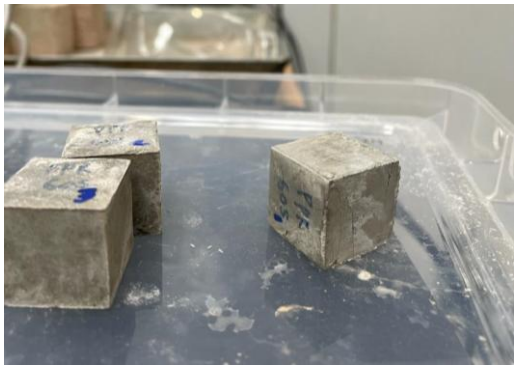

(g) Crushed S60 cube samples

(h) Crushed D0 and PC cube samples

Figure C.13: Cube compressive testing

C.1.4 Scanning electron microscopy (SEM-EDX)

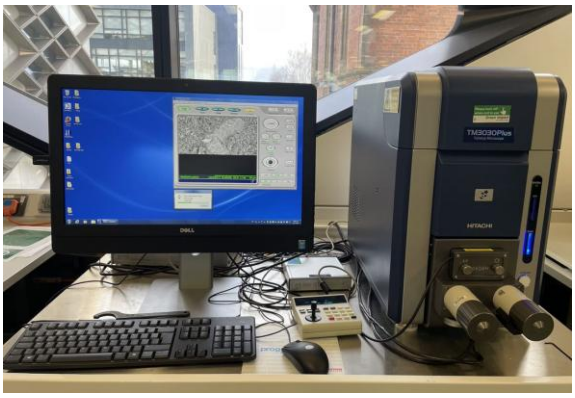

(a) Tabletop SEM (Hitachi TM3030Plus)

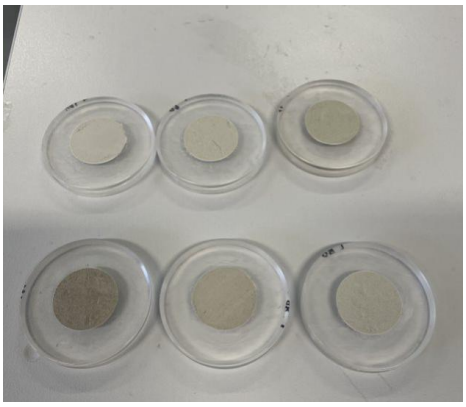

(b) Sample preparation for powder material

(c) Arresting hydration in acetone solution

(d) Arresting hydration in acetone solution

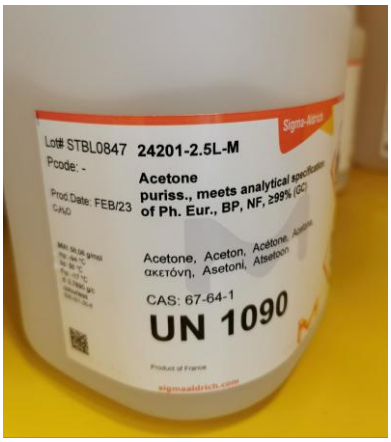

(e) Acetone used for stopping hydration

(f): Image of filter, conical flask, and vacuum pump

Figure C.14: Equipment used for SEM-EDS analysis.

Testing procedure for arresting hydration:

i. Samples were crushed using a percussion mortar to attain a size of 6mm x 6mm x 6mm, which is suitable size for SEM analysis.

ii. The crushed sample was mixed with 25ml of acetone in a beaker for 10 minutes.

iii. The arresting process commenced by placing the sample in a conical flask. The flask was fitted with a filter paper to separate the liquid from the solid components. To expedite the separation process, the conical flask was attached to a vacuum pump, which extracted the liquid from the flask.

iv. After the initial acetone was removed, an additional 25ml of fresh acetone was mixed with the sample. This mixture was transferred to a plastic container, which was then closed and sealed using parafilm for 1 day.

v. After 1 day, the mixture of sample and acetone was placed in the filter attached to the conical flask for approximately 10 minutes for drying to ensure all the liquid was pumped out.

vi. The sample was placed in a plastic bag and stored in a desiccator.

Testing procedure for SEM-EDS:

1. Sample Preparation:

- The sample was polished using XXXX to achieve a smooth surface.
- Sample was thoroughly cleaned to eliminate any residual polishing compounds.

2. Mounting the sample:

- The sample was securely mounted onto an SEM stub using conductive adhesive to ensure stability and proper orientation.

3. Loading sample:

- The prepared sample was carefully loaded into the SEM chamber. The orientation and position were adjusted to target the areas of interest for the EDS analysis.

4. SEM imaging:

- High-resolution images were captured to analyse the microstructure and surface characteristics.

5. EDS analysis:

- EDS (Energy Dispersive X-ray Spectroscopy) was conducted to identify and quantify the elemental composition of the sample.

6. Data interpretation:

- The SEM images and EDS spectra were analysed to understand the material's microstructural properties and elemental composition.
- The results were compiled and interpreted in the context of the material's characteristics and the study's objectives.

Testing results:

Appendix C

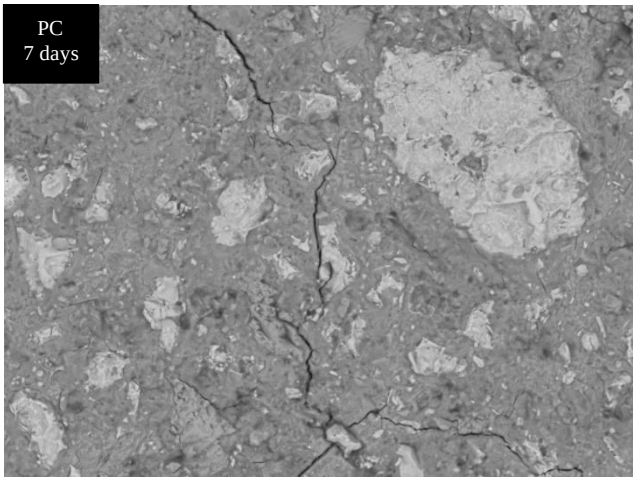

SEM-BSE image

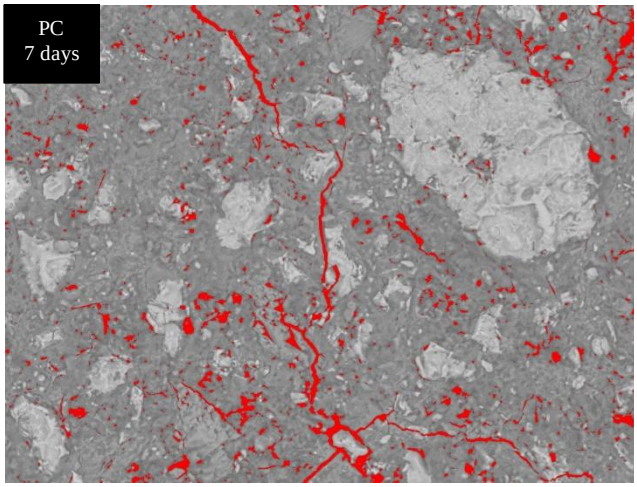

Pores

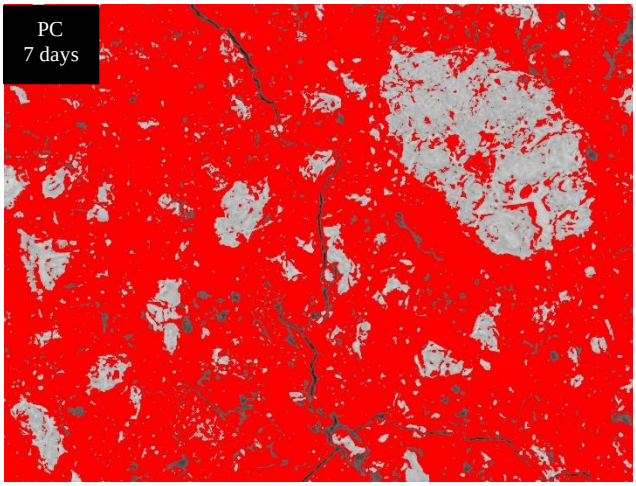

Hydrates

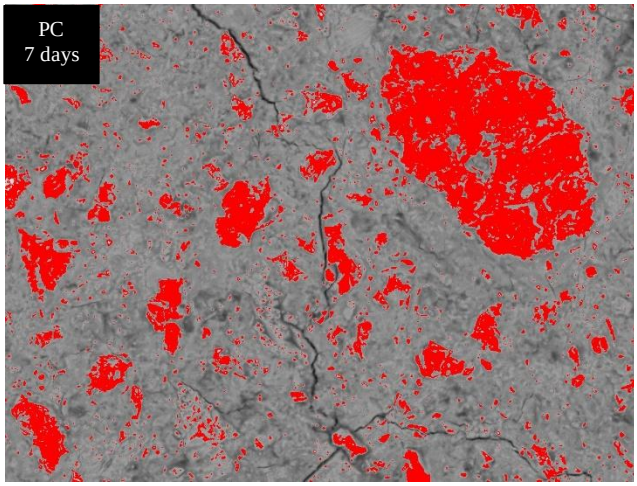

Un-hydrated cement

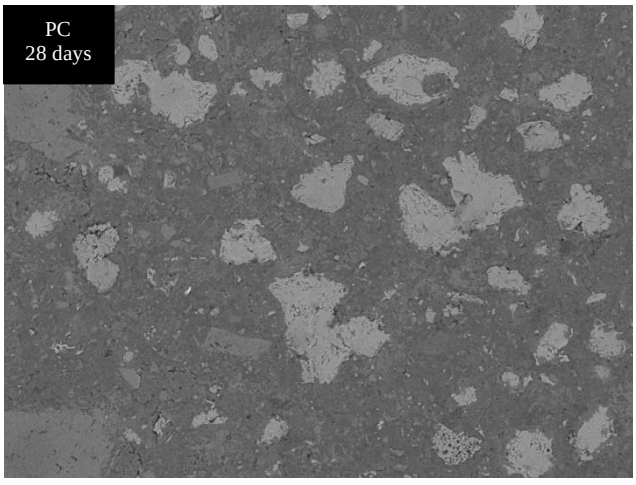

SEM-BSE image

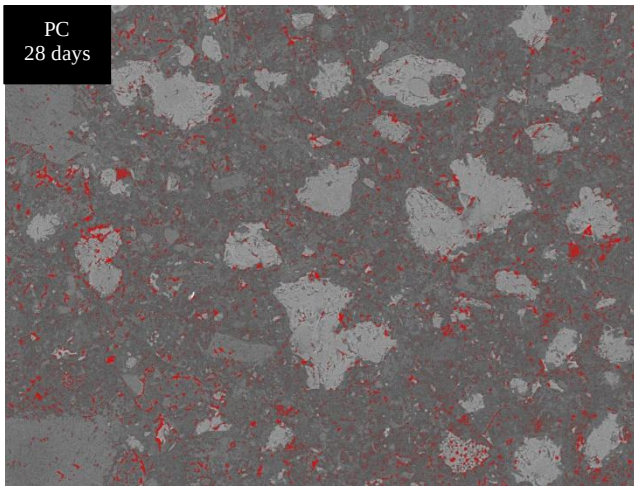

Pores

Appendix C

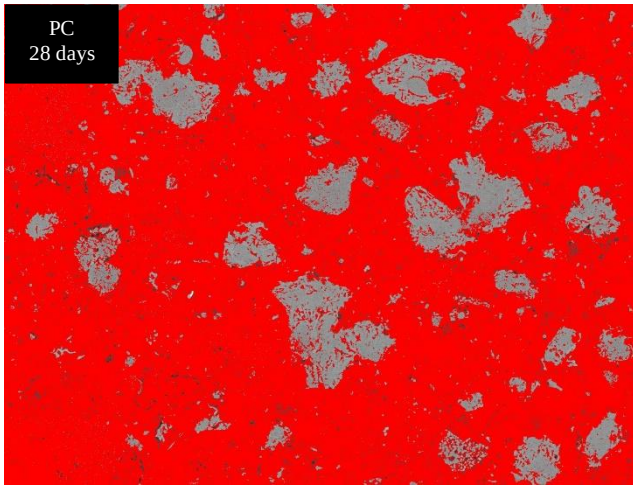

Hydrates

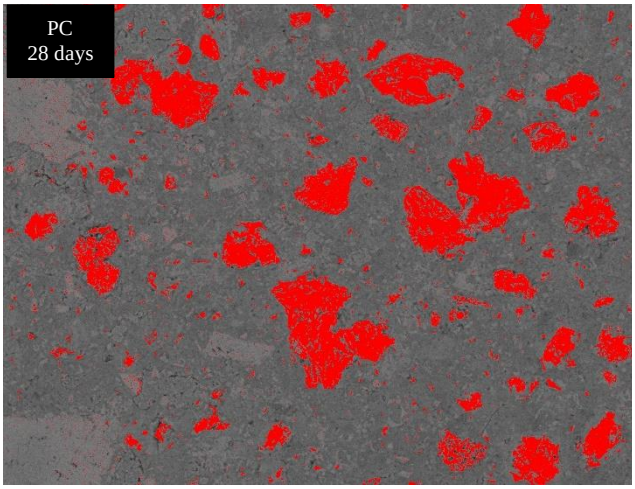

Un-hydrated cement

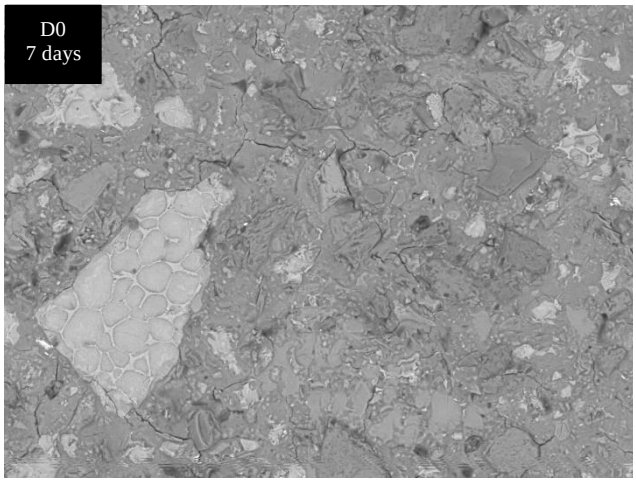

SEM-BSE image

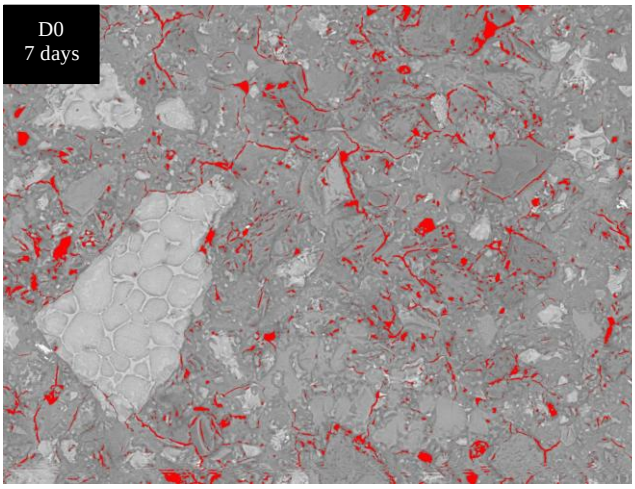

Pores

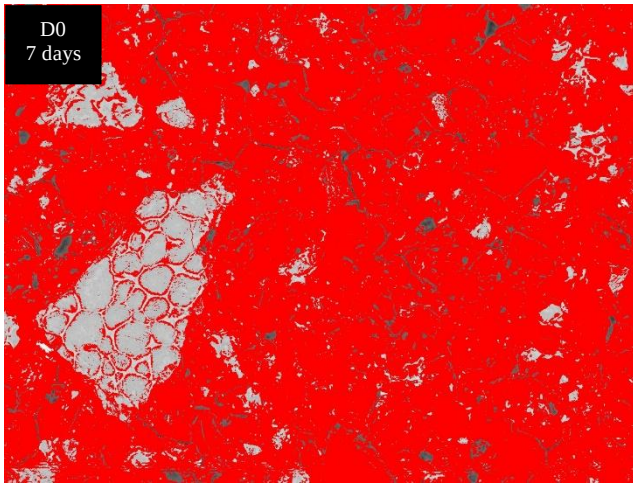

Hydrates

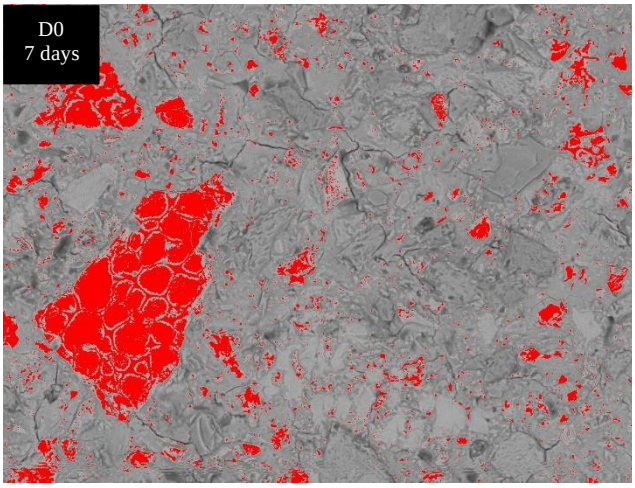

Un-hydrated cement

Appendix C

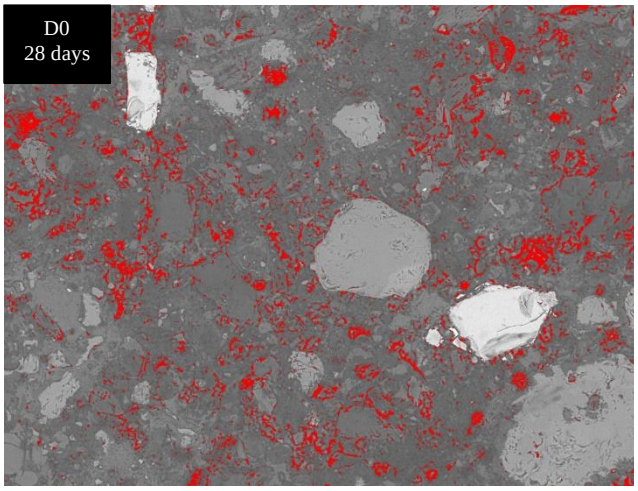

Pores

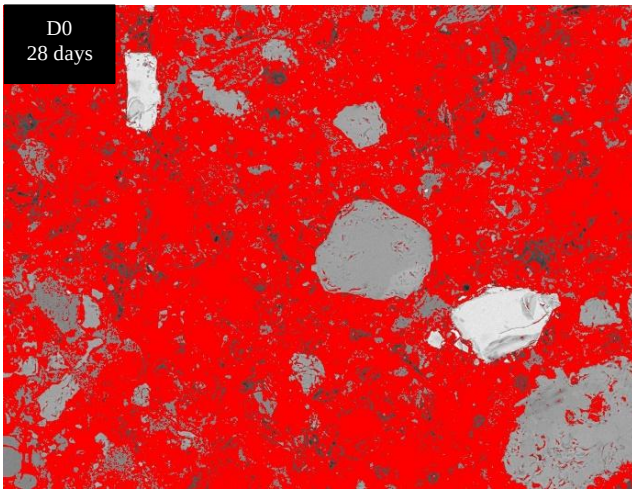

CSH

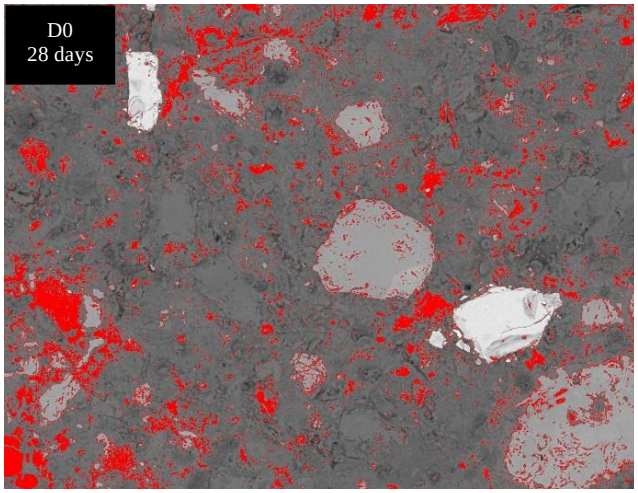

CH

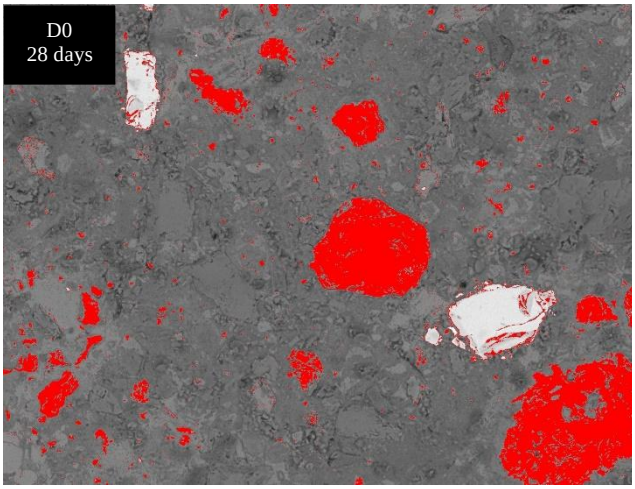

Un-hydrated cement

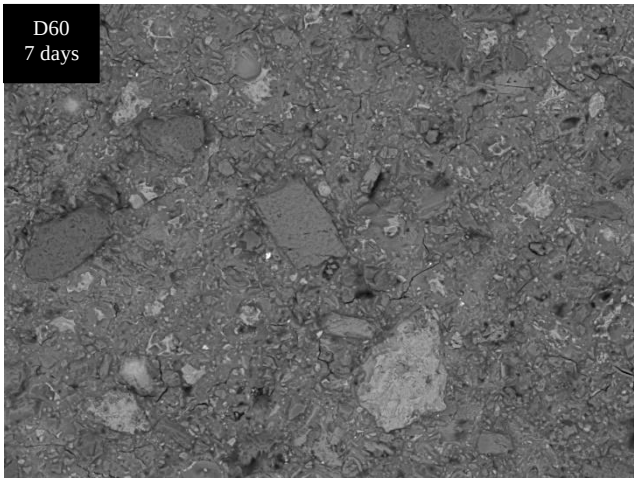

SEM-BSE

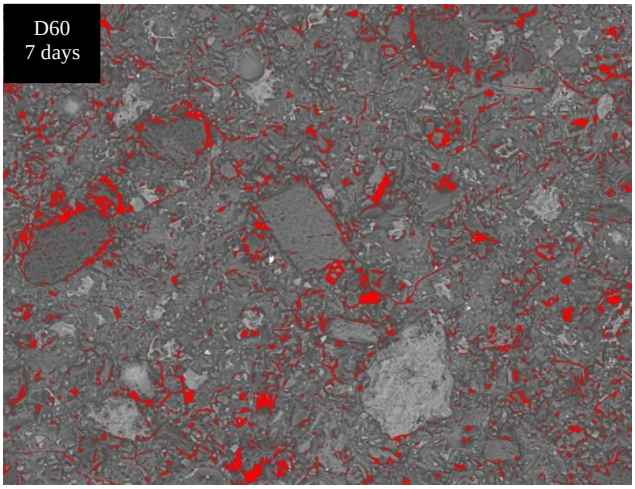

Pores

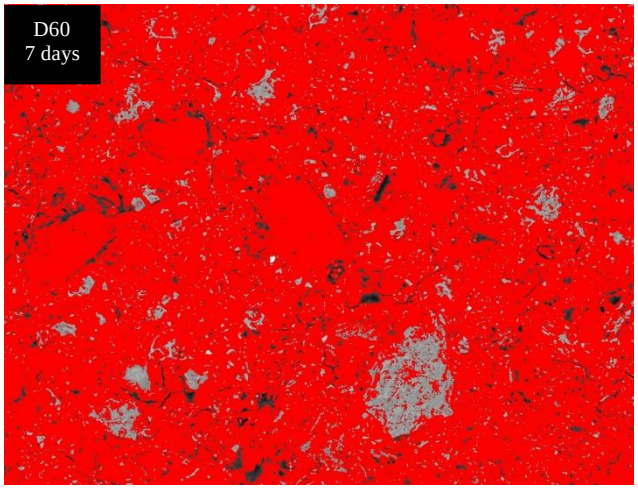

Hydrates

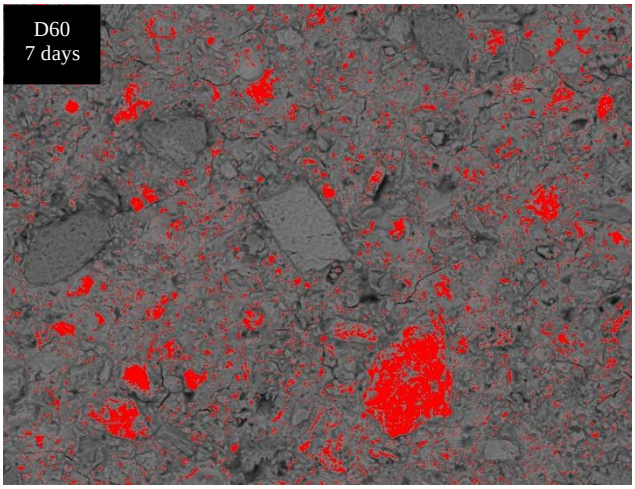

Un-hydrated cement

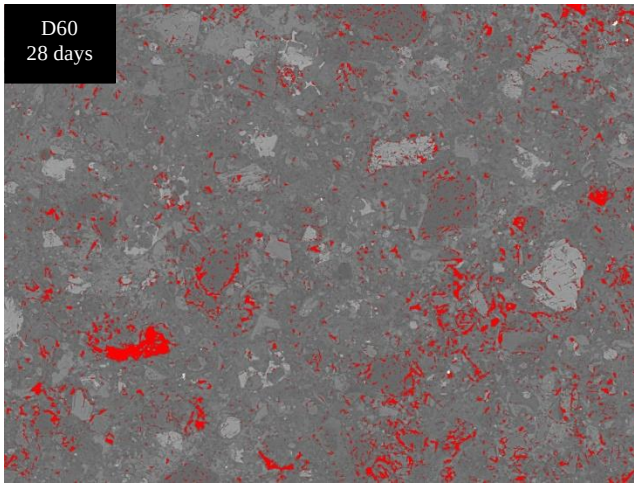

Pores

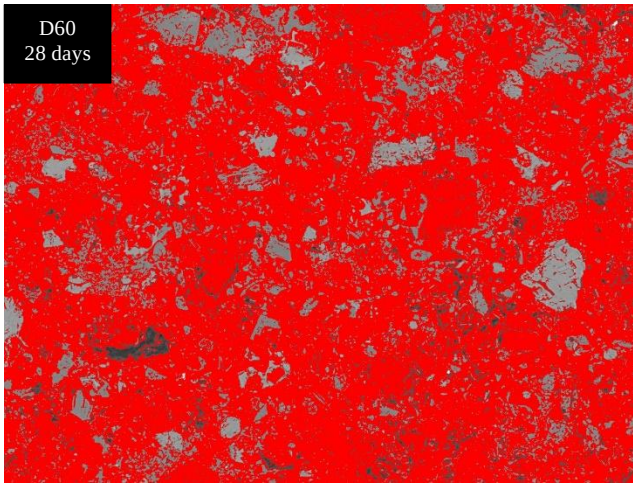

CSH

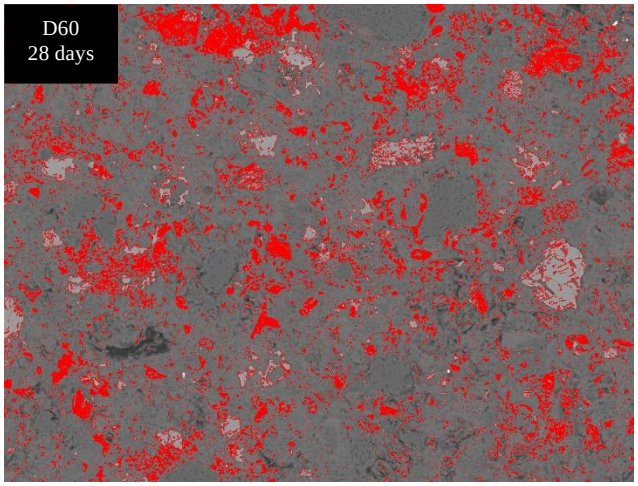

CH

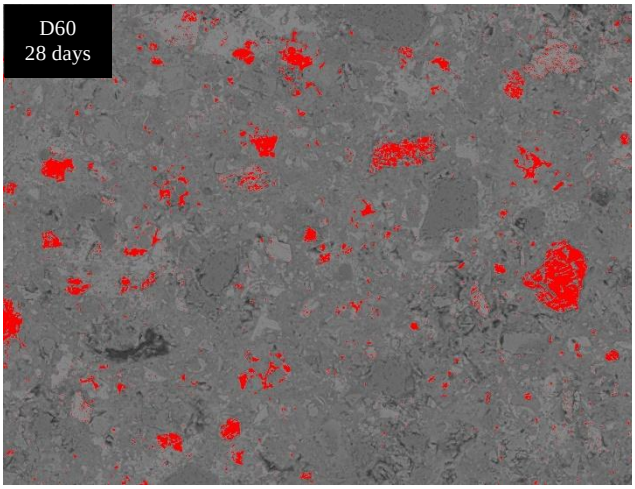

Un-hydrated cement

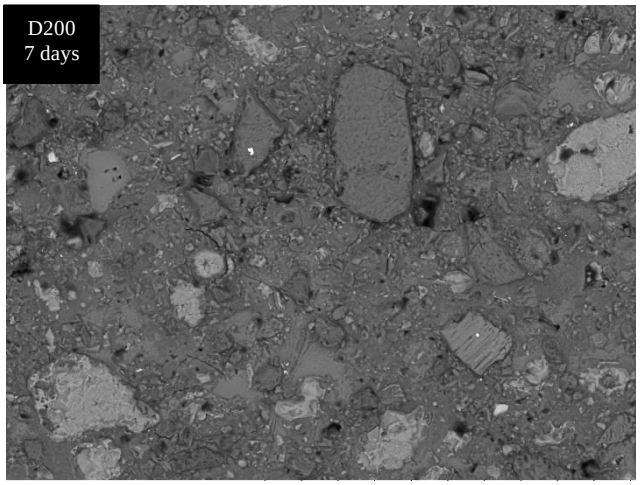

SEM-BSE image

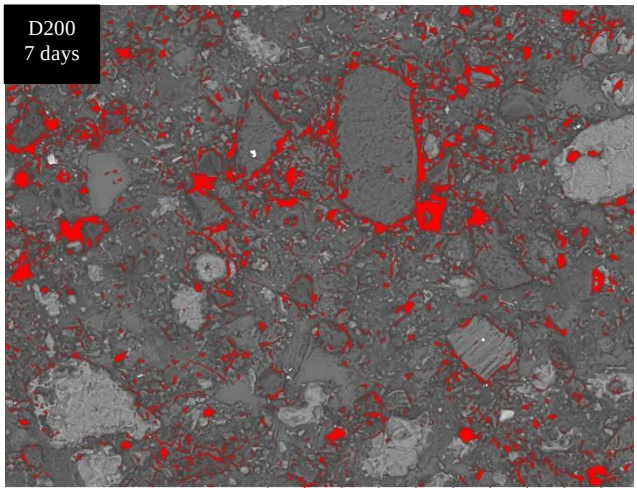

Pores

Appendix C

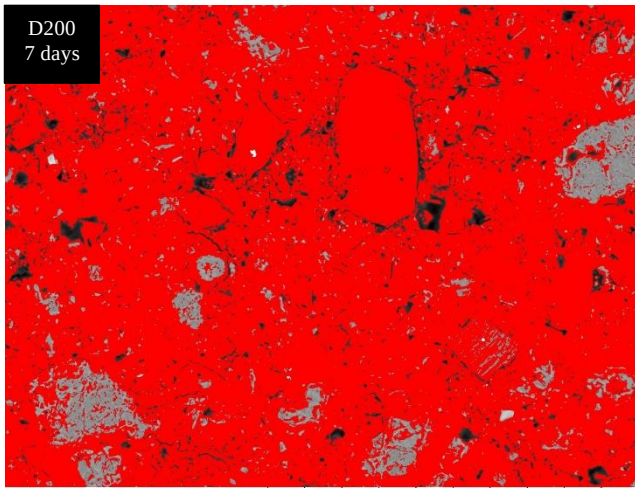

Hydrates

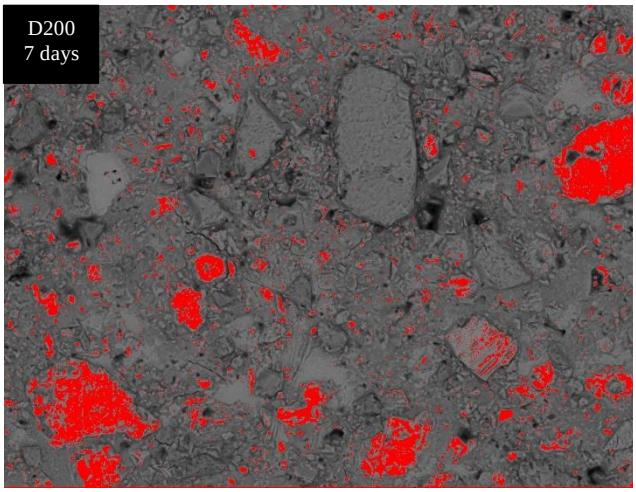

Un-hydrated cement

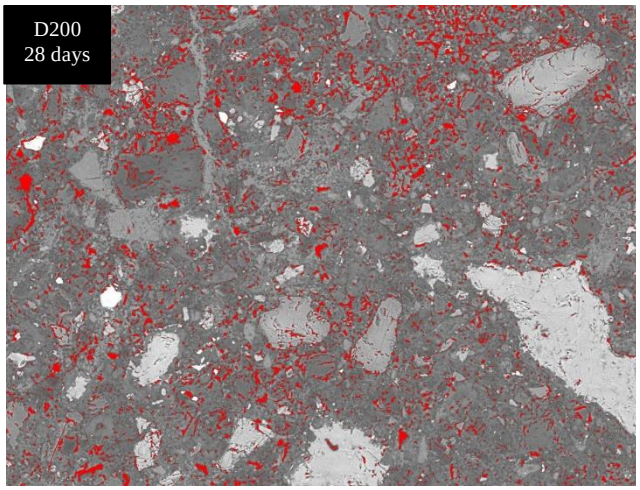

Pores

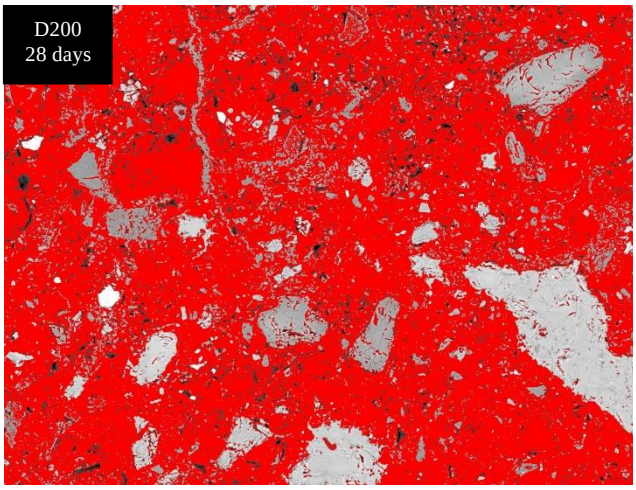

CSH

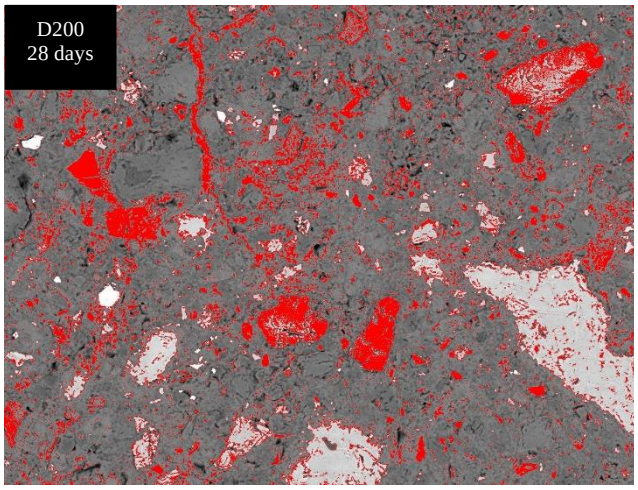

CH

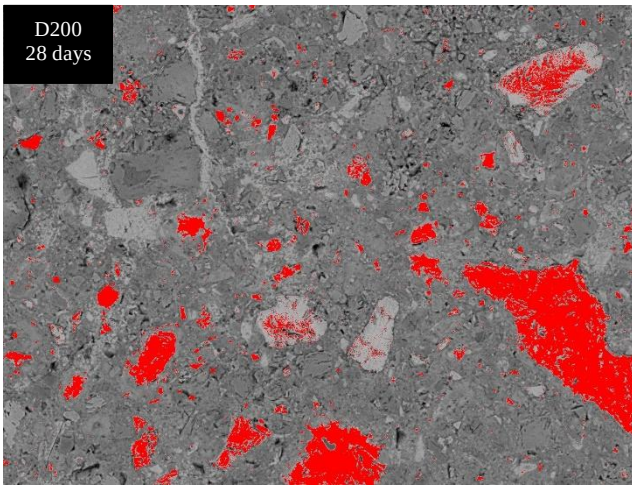

Un-hydrated cement

Appendix C

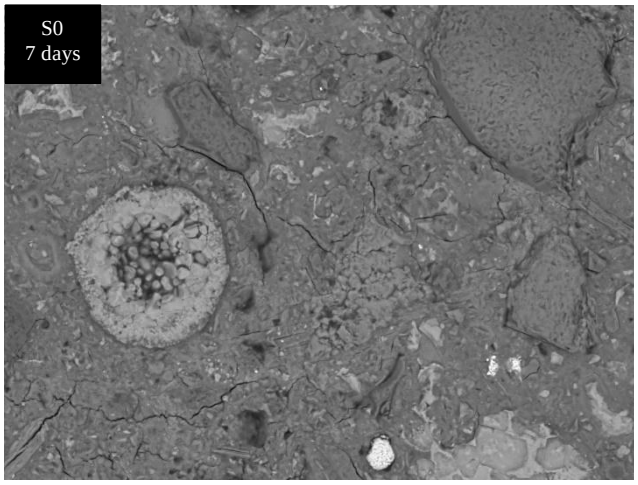

SEM-BSE image

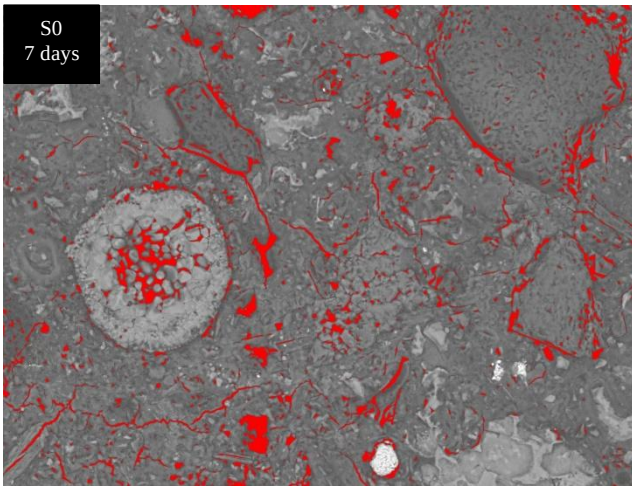

Pores

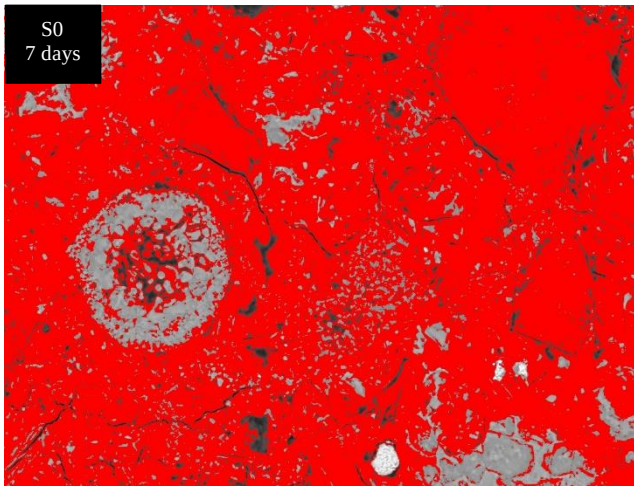

Hydrates

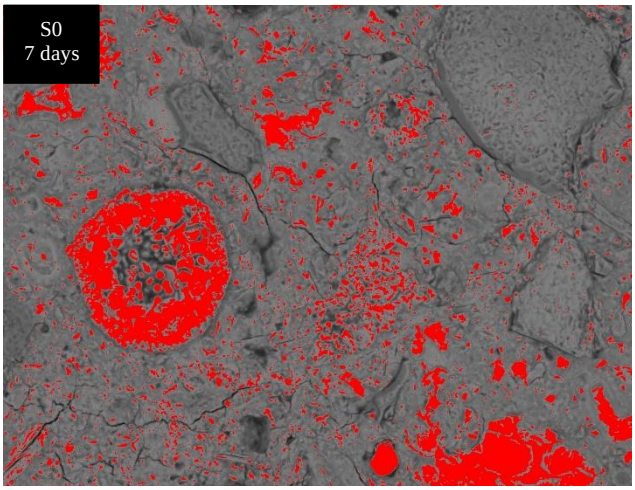

Un-hydrated cement

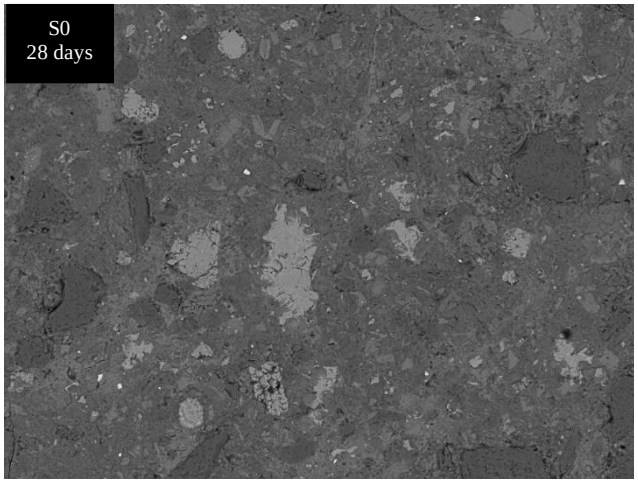

SEM-BSE

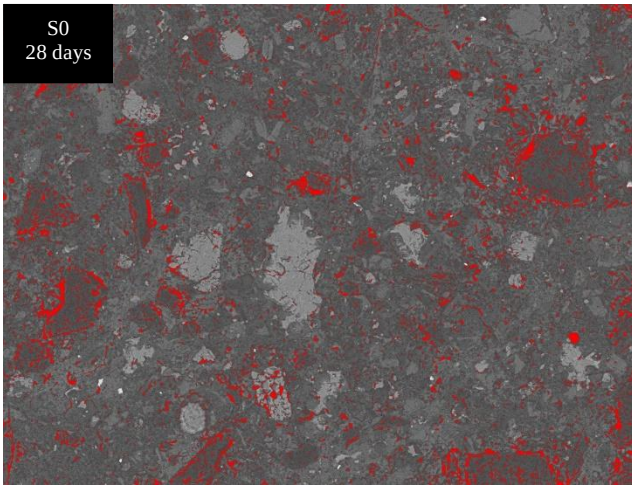

Pores

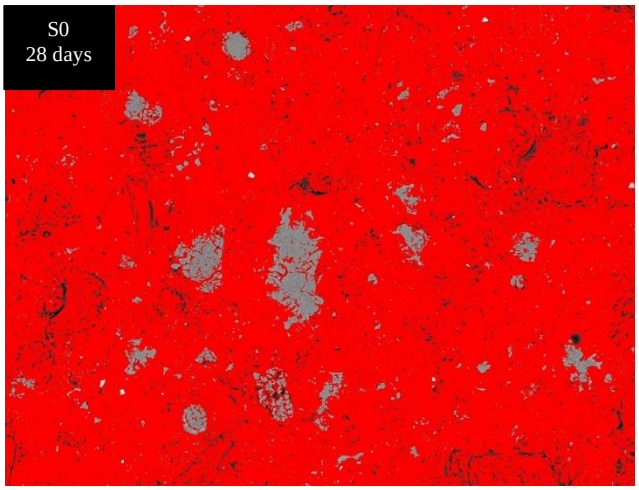

Hydrates

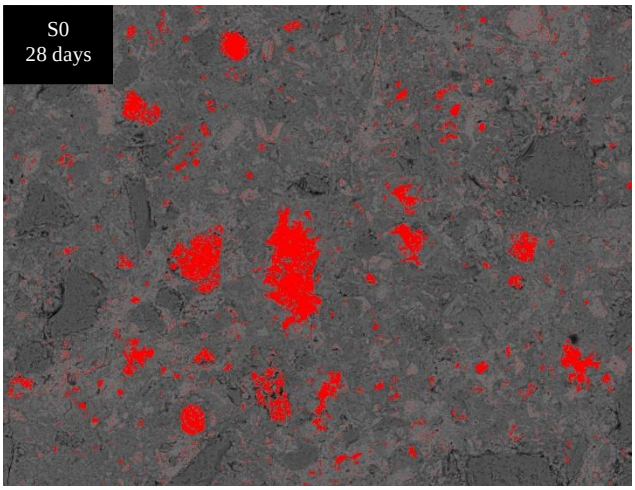

Un-hydrated cement

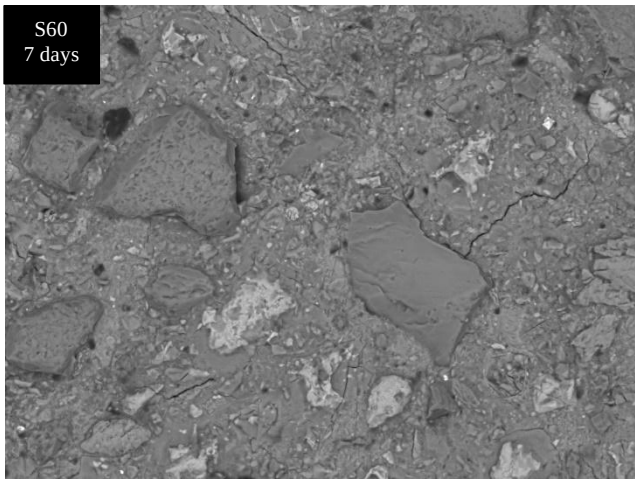

SEM-BSE

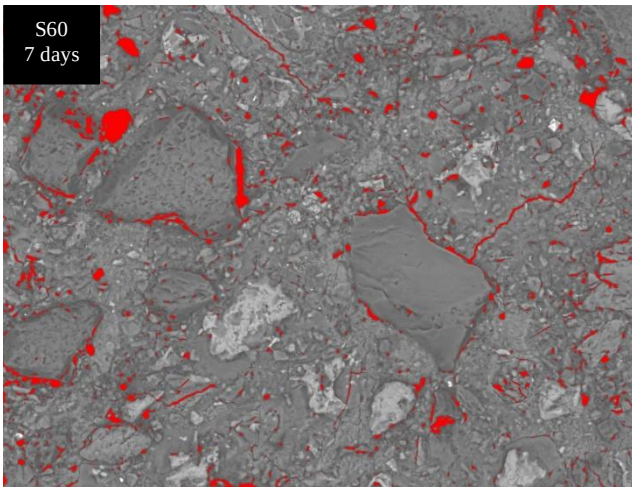

Pores

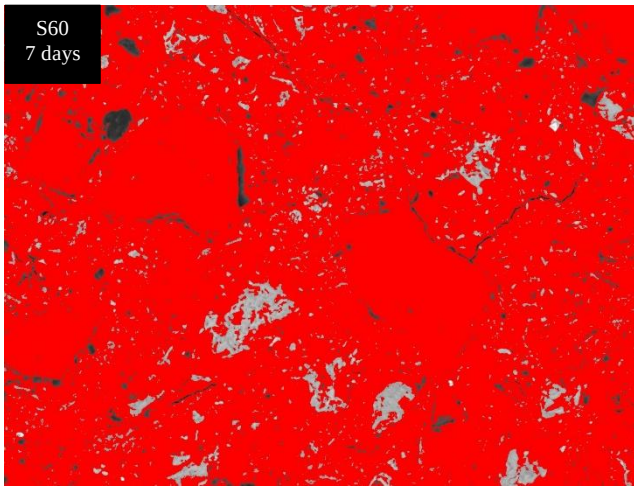

Hydrates

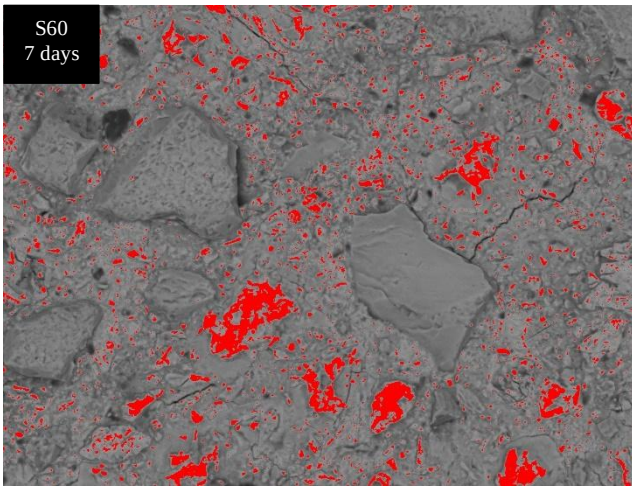

Un-hydrated cement

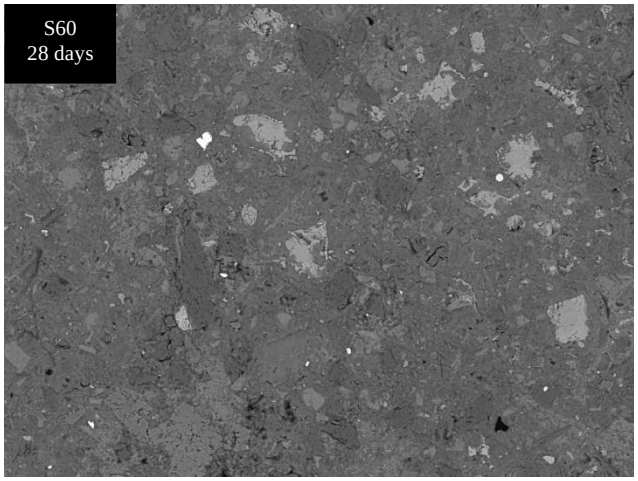

SEM-BSE

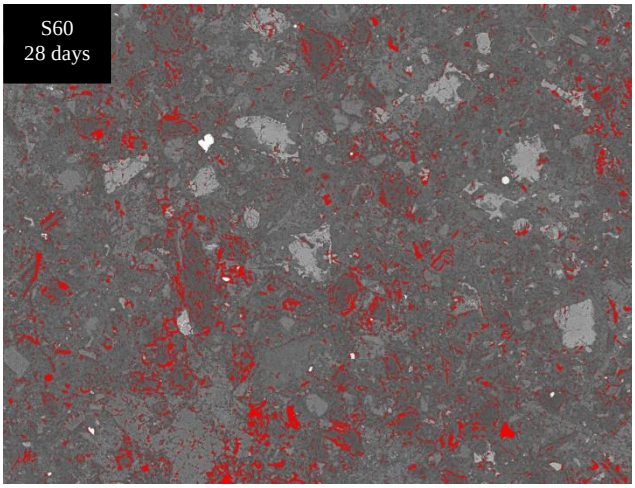

Pores

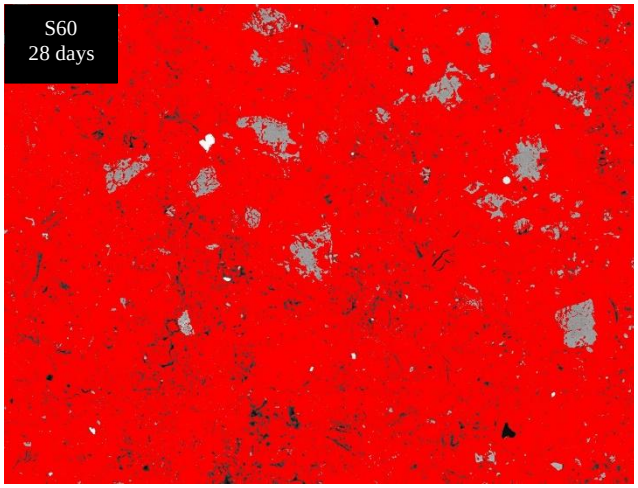

CH

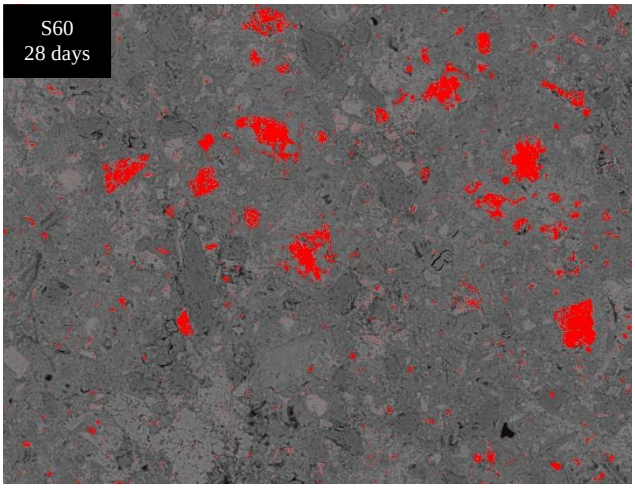

Un-hydrated cement

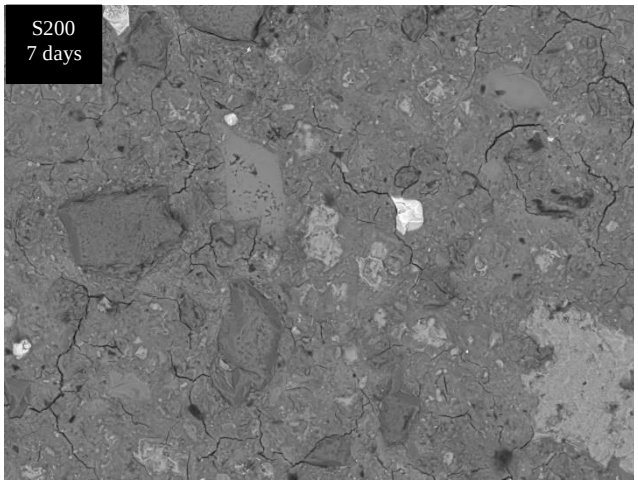

SEM-BSE image

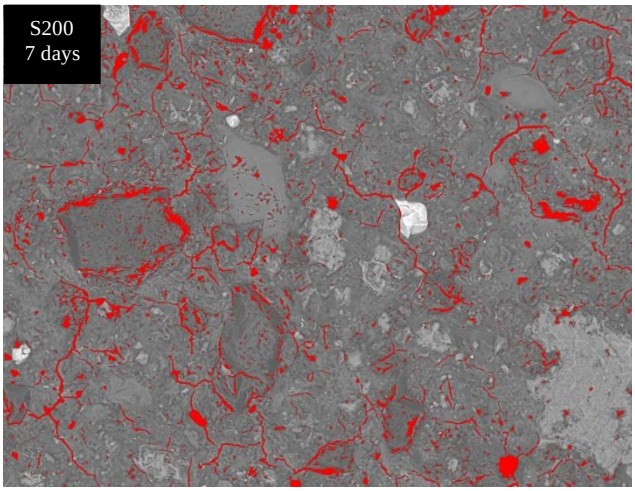

Pores

S200
7 days

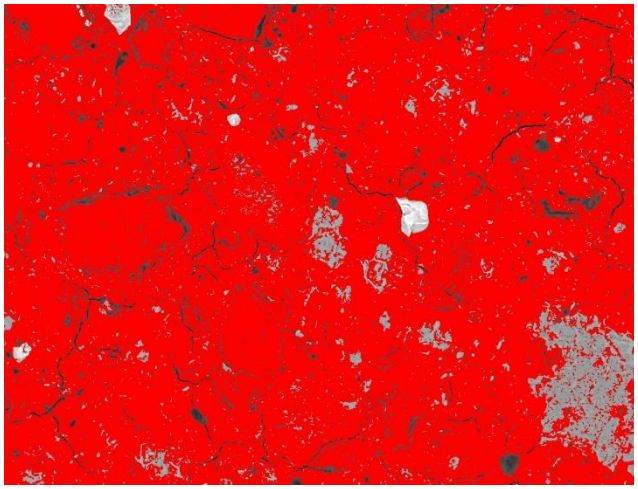

Hydrates

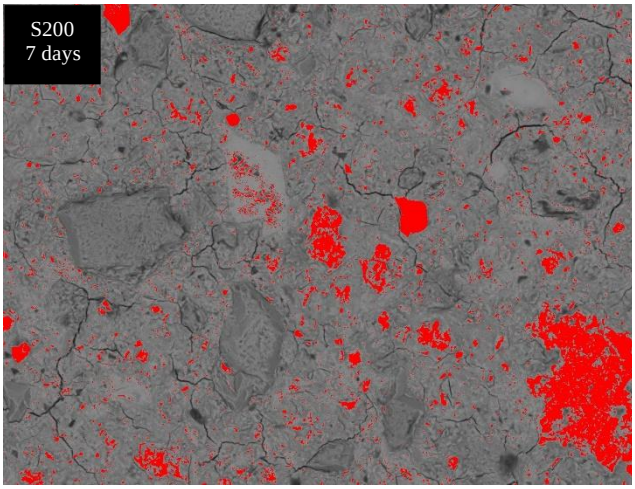

Un-hydrated cement

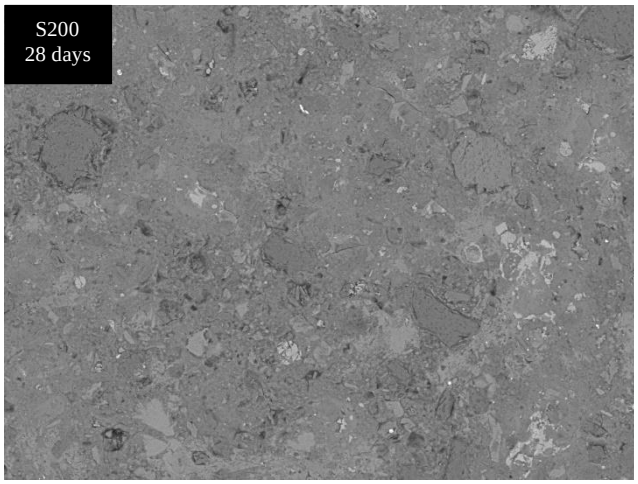

SEM-BSE

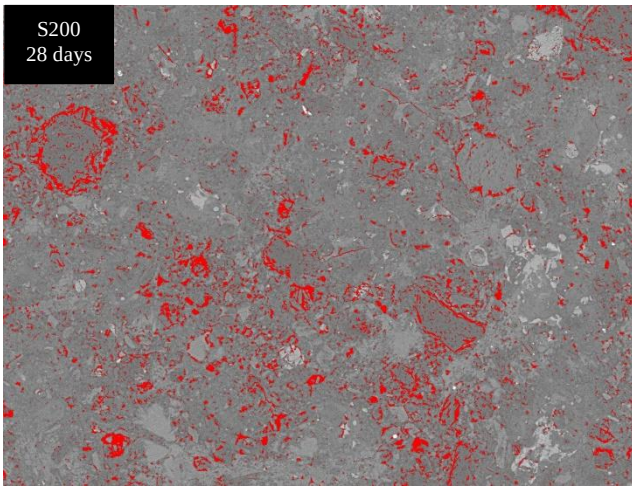

Pores

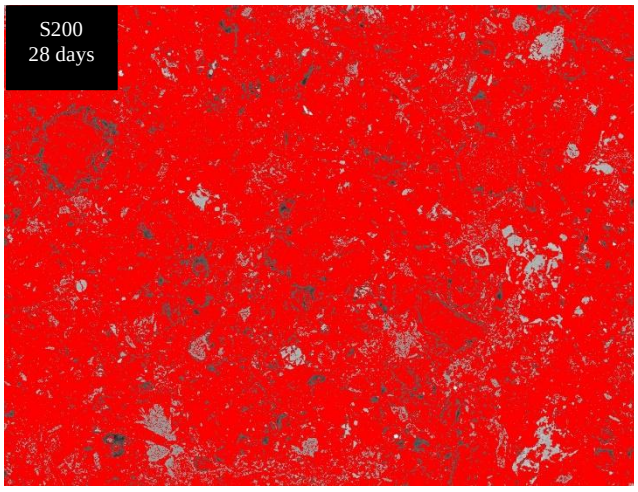

Hydrates

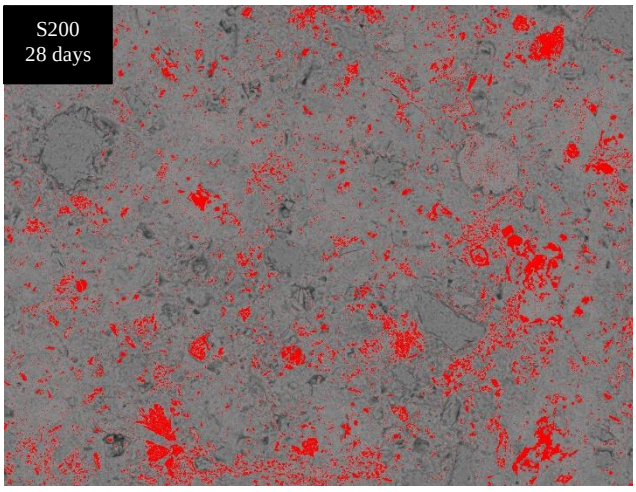

Un-hydrated cement

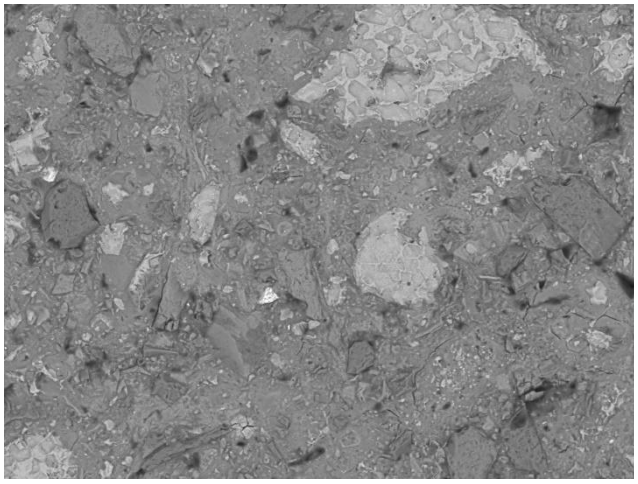

SEM-BSE image

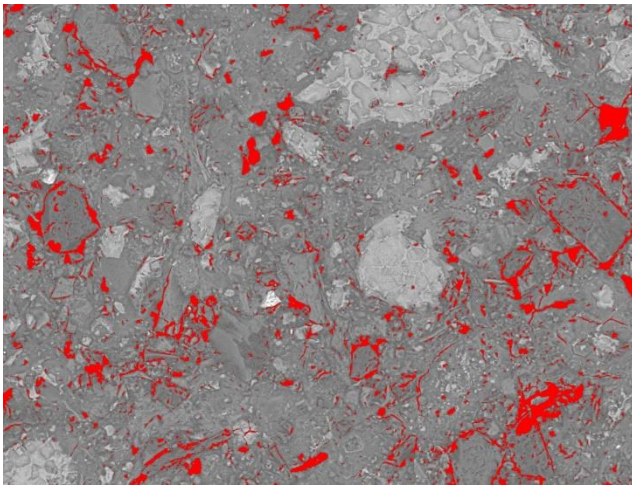

Pores

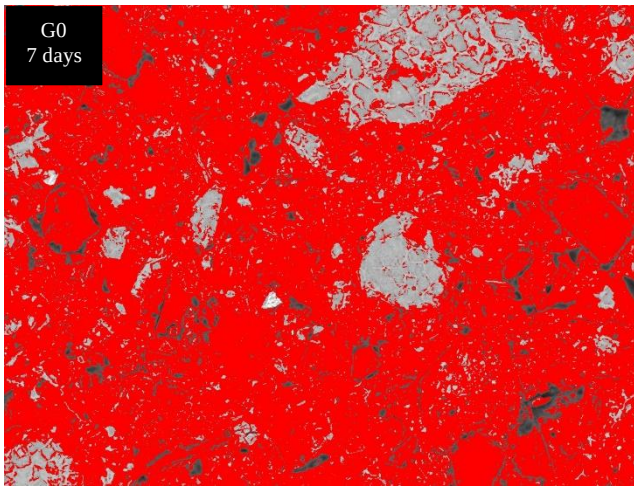

Hydrates

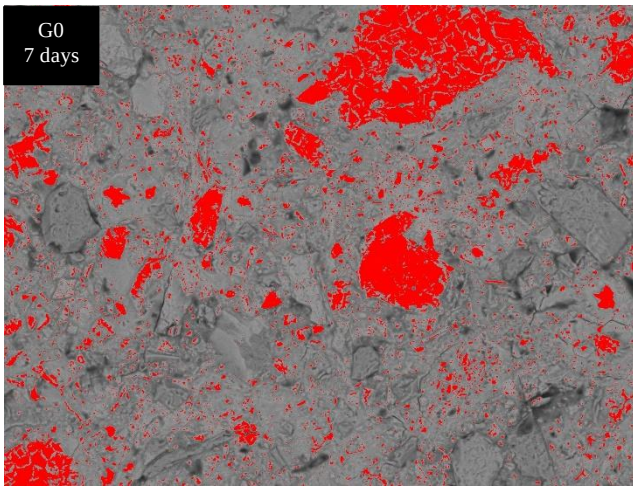

Un-hydrated cement

Appendix C

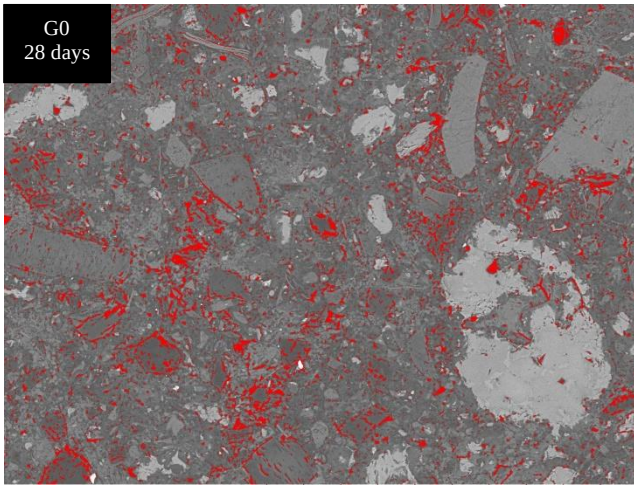

Pores

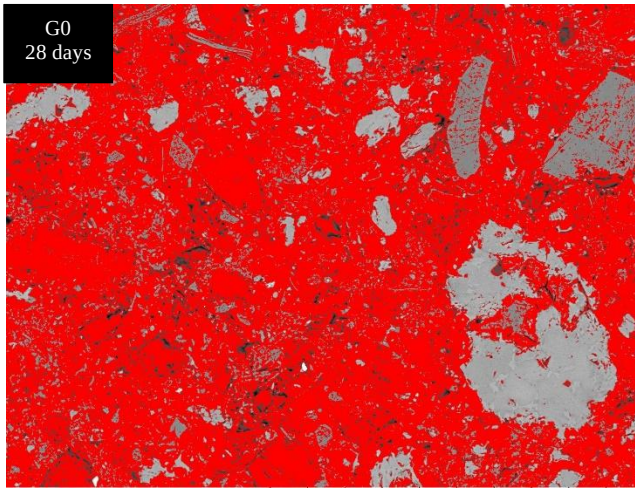

CSH

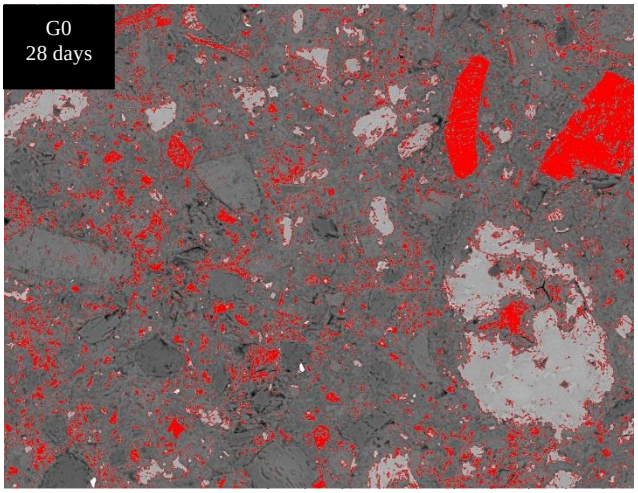

CH

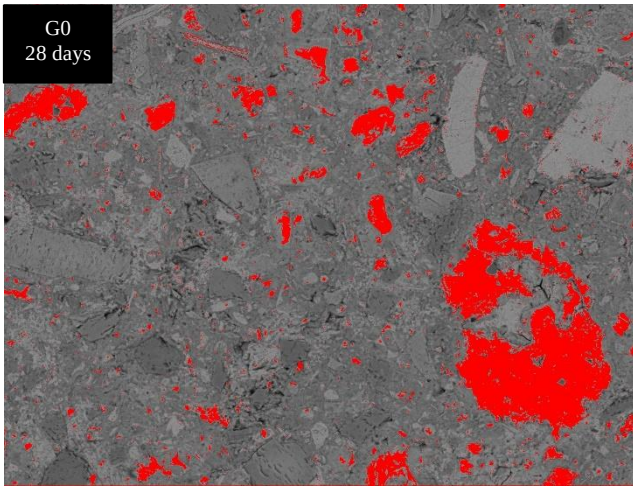

Un-hydrated cement

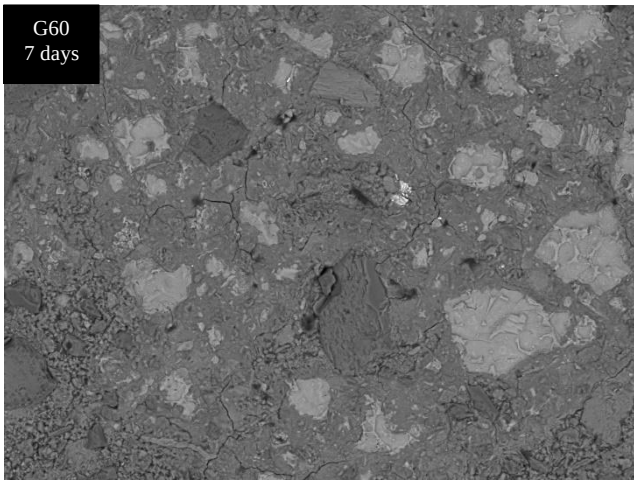

SEM-BSE image

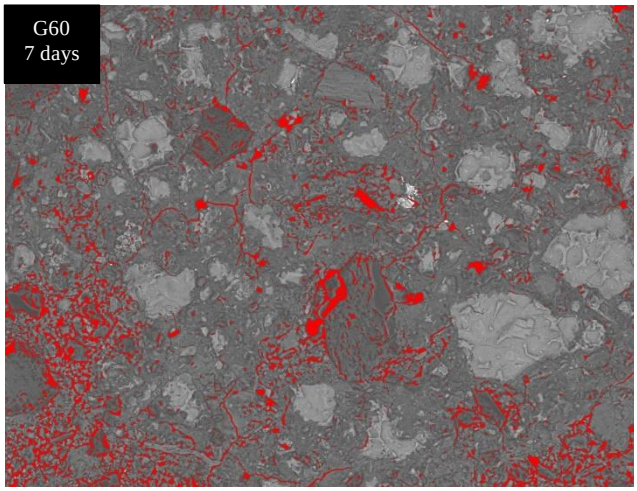

Pores

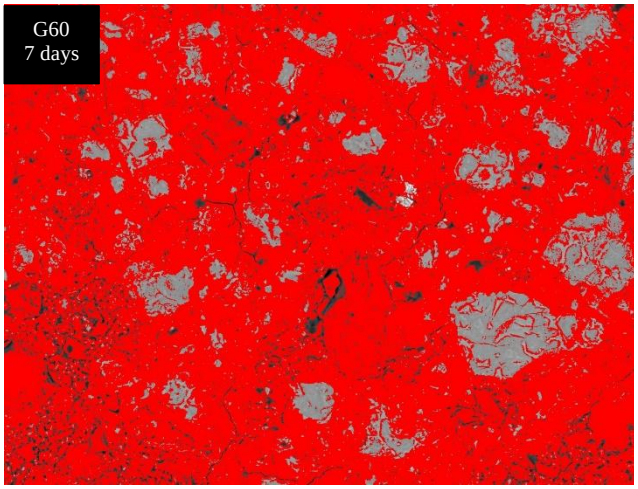

Hydrates

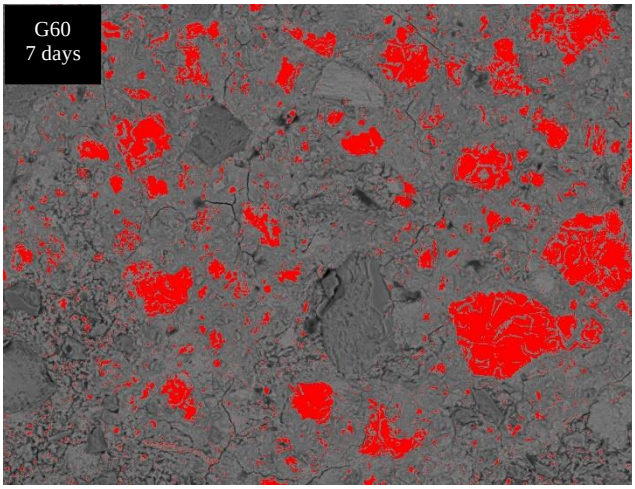

Un-hydrated cement

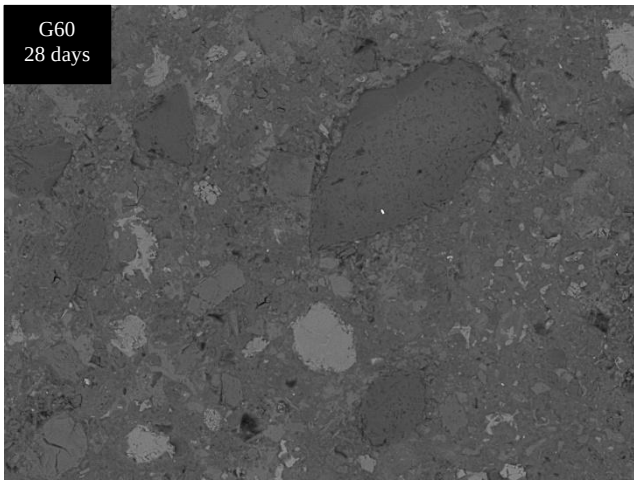

SEM-BSE

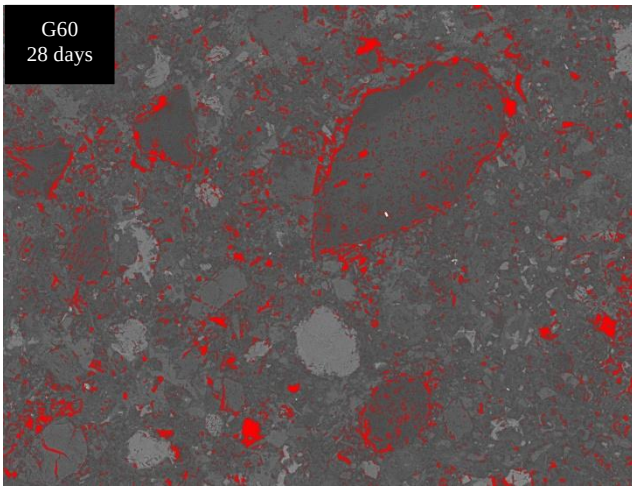

Pores

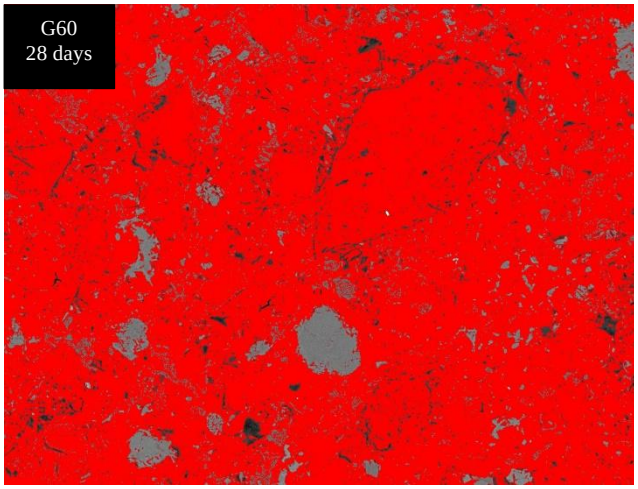

Hydrates

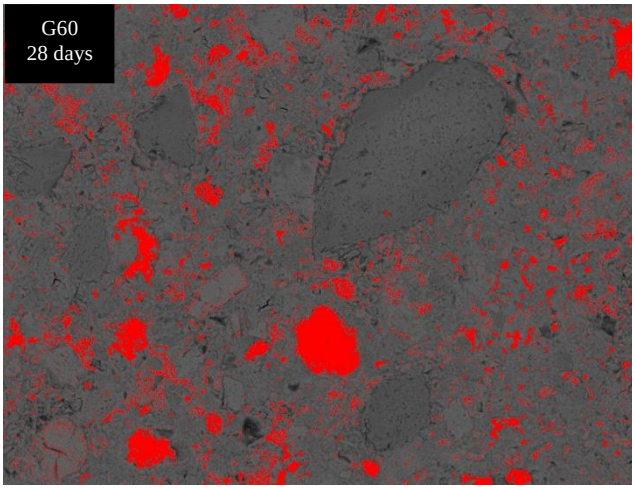

Un-hydrated cement

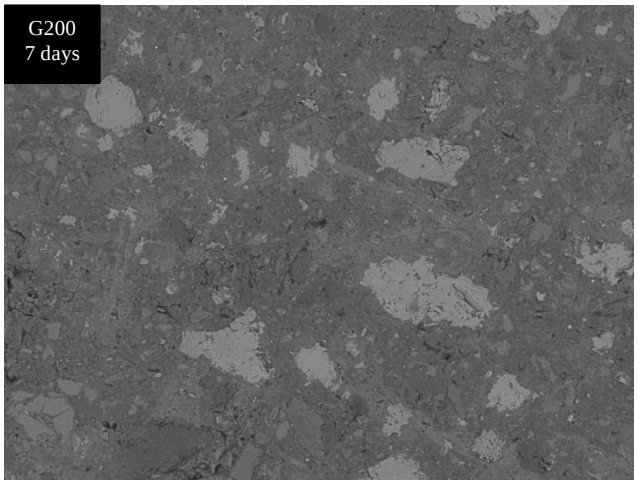

SEM-BSE image

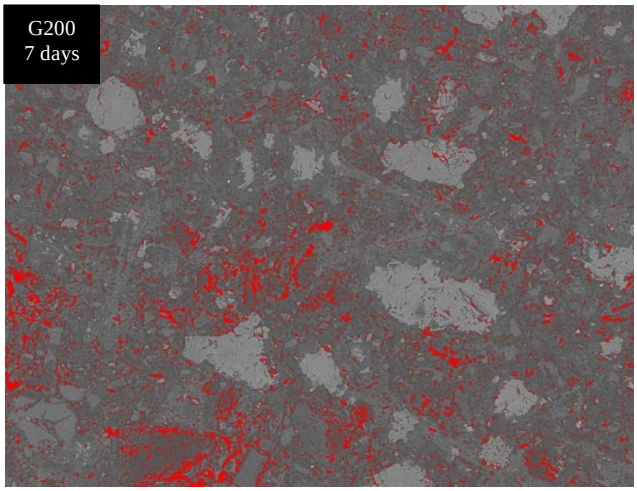

Pores

Appendix C

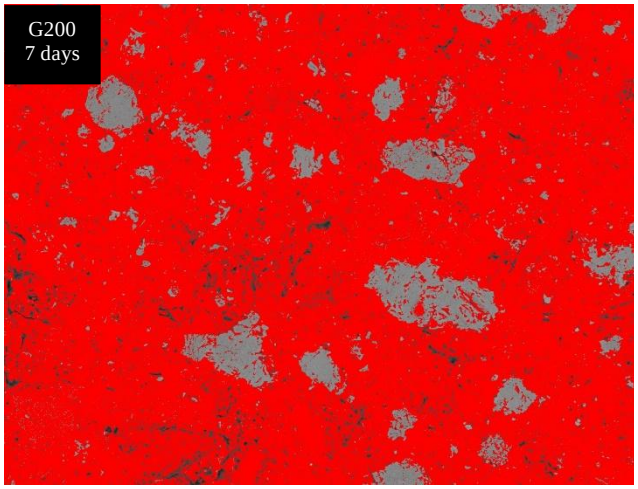

Hydrates

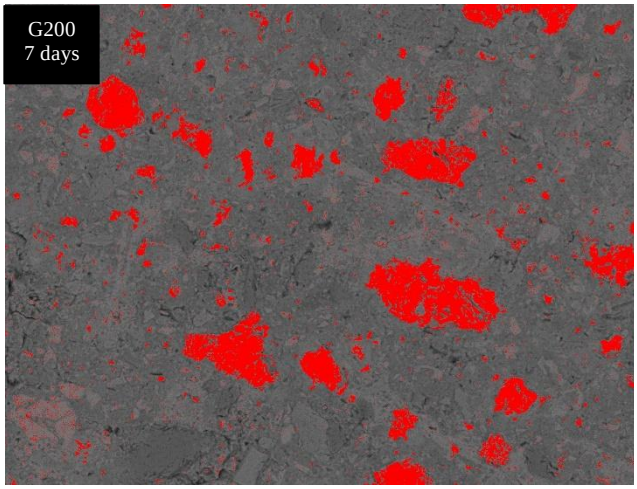

Un-hydrated cement

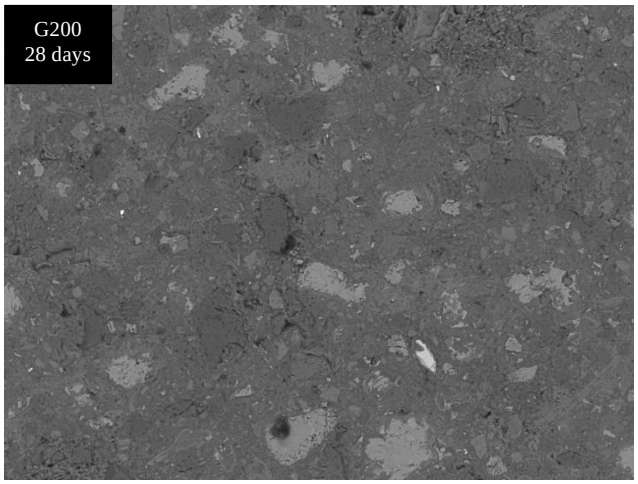

Pores

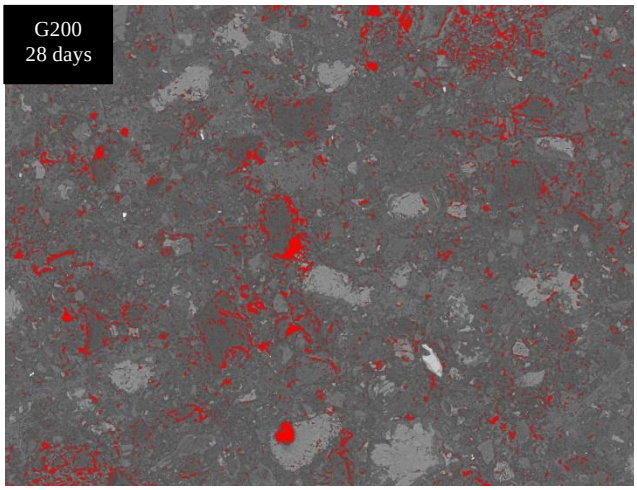

CSH

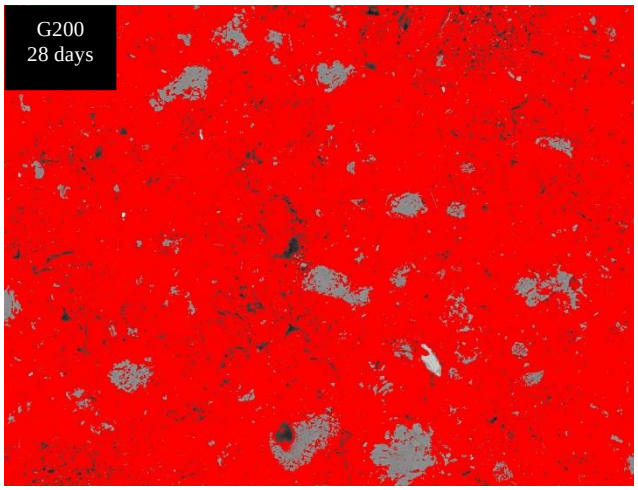

CH

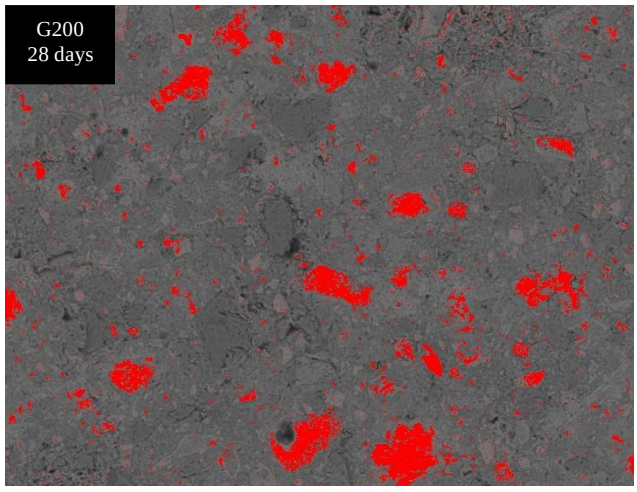

Un-hydrated cement

Table C.1 : Atomic ratio for PC (7days)

	Calcium	Silicon	Aluminium	Sulfur	Al/Ca	Si/Ca	S/Ca	Ca/Si	Al/Si
1	67.1	18.18	6.03	1.72	0.09	0.27	0.03	3.69	0.33
2	60.9	18.3	5.91	2.94	0.10	0.30	0.05	3.33	0.32
3	68.07	19.83	3.7	2.02	0.05	0.29	0.03	3.43	0.19
4	62.59	23.15	3.93	4.35	0.06	0.37	0.07	2.70	0.17
5	61.58	18.21	6.58	2.41	0.11	0.30	0.04	3.38	0.36
6	60.22	20.32	6.41	2.87	0.11	0.34	0.05	2.96	0.32
7	62.16	21	5.29	3.18	0.09	0.34	0.05	2.96	0.25
8	69.93	17.34	4.14	2.64	0.06	0.25	0.04	4.03	0.24
9	61.82	18.56	7.63	3.65	0.12	0.30	0.06	3.33	0.41
10	59.57	20.73	5.5	3.71	0.09	0.35	0.06	2.87	0.27
11	62.04	18.42	5.62	3.74	0.09	0.30	0.06	3.37	0.31
12	57.18	20.44	7.78	4.27	0.14	0.36	0.07	2.80	0.38
13	63.81	22.94	6.19	1.25	0.10	0.36	0.02	2.78	0.27
14	61.68	19.49	5.34	2.43	0.09	0.32	0.04	3.16	0.27
15	65.19	20.52	6.53	2.18	0.10	0.31	0.03	3.18	0.32
16	56	19.9	6.23	2.82	0.11	0.36	0.05	2.81	0.31
17	58.48	23.88	5.7	1.6	0.10	0.41	0.03	2.45	0.24
18	65.93	18.67	4.91	2.28	0.07	0.28	0.03	3.53	0.26
19	59.14	18.49	7.14	3.44	0.12	0.31	0.06	3.20	0.39
20	59.66	18.49	6.36	1.63	0.11	0.31	0.03	3.23	0.34
21	66.07	17.64	6.35	2.19	0.10	0.27	0.03	3.75	0.36
22	66.05	17.57	5.79	2.31	0.09	0.27	0.03	3.76	0.33
23	57.16	20.23	6.28	3.85	0.11	0.35	0.07	2.83	0.31
24	58.99	19.93	7.13	5.23	0.12	0.34	0.09	2.96	0.36
25	65.04	18.73	5.82	3.07	0.09	0.29	0.05	3.47	0.31
26	63.99	17.82	4.68	3.98	0.07	0.28	0.06	3.59	0.26
27	62.41	22.59	5.65	2.27	0.09	0.36	0.04	2.76	0.25
28	63.6	20.63	4.84	1.49	0.08	0.32	0.02	3.08	0.23
29	60.76	21.63	5.72	2.9	0.09	0.36	0.05	2.81	0.26
30	64.64	17.14	5.52	3.75	0.09	0.27	0.06	3.77	0.32
31	62.53	20.29	6.97	3.38	0.11	0.32	0.05	3.08	0.34
32	66.82	18.45	4.01	2.61	0.06	0.28	0.04	3.62	0.22
33	60.85	23.63	5.75	2.39	0.09	0.39	0.04	2.58	0.24
34	57.01	19.98	6.32	3.87	0.11	0.35	0.07	2.85	0.32
35	61.48	18.95	6.91	4.52	0.11	0.31	0.07	3.24	0.36
36	65.25	18.23	5.34	3.1	0.08	0.28	0.05	3.58	0.29
37	64	17.8	4.7	4.05	0.07	0.28	0.06	3.60	0.26
38	53.8	23.98	7.12	3.65	0.13	0.45	0.07	2.24	0.30
39	65.08	20.03	4.78	1.23	0.07	0.31	0.02	3.25	0.24
40	60.87	21.94	5.33	2.89	0.09	0.36	0.05	2.77	0.24
41	63.62	19.72	6.53	3.42	0.10	0.31	0.05	3.23	0.33
42	68	18.9	3.71	2.2	0.05	0.28	0.03	3.60	0.20
43	63.68	23.7	4.99	1.05	0.08	0.37	0.02	2.69	0.21

44	68.24	17.89	5.11	3.31	0.07	0.26	0.05	3.81	0.29
45	62.04	23.62	6.21	2.52	0.10	0.38	0.04	2.63	0.26
46	67.32	19.77	5.41	2.65	0.08	0.29	0.04	3.41	0.27
47	60.93	16.44	4.08	2.67	0.07	0.27	0.04	3.71	0.25
48	55.6	21.26	6.66	2.79	0.12	0.38	0.05	2.62	0.31
49	55.64	20.57	9.52	3.99	0.17	0.37	0.07	2.70	0.46
50	66.16	18.44	6.26	3.07	0.09	0.28	0.05	3.59	0.34
51	64.64	18.43	6.97	2.16	0.11	0.29	0.03	3.51	0.38
52	60.54	18.58	7.91	3.77	0.13	0.31	0.06	3.26	0.43
53	62.4	19.09	7.65	3.31	0.12	0.31	0.05	3.27	0.40
54	68.03	19.58	7.69	2.44	0.11	0.29	0.04	3.47	0.39
55	60.99	18.16	5.92	4.08	0.10	0.30	0.07	3.36	0.33
56	65.49	20.38	5.73	2.21	0.09	0.31	0.03	3.21	0.28
57	60.94	20.28	5.27	2.35	0.09	0.33	0.04	3.00	0.26
58	63.07	19.9	4.32	3.15	0.07	0.32	0.05	3.17	0.22
59	60.11	20.9	5.96	3.72	0.10	0.35	0.06	2.88	0.29
60	66.53	21.72	6	4.47	0.09	0.33	0.07	3.06	0.28
61	57.16	17.96	10.53	1.38	0.18	0.31	0.02	3.18	0.59
62	58.02	24.21	5.18	4.61	0.09	0.42	0.08	2.40	0.21

Table C.2 : Atomic ratio for S0 (7days)

	Calcium	Silicon	Aluminium	Sulfur	Al/Ca	Si/Ca	S/Ca	Ca/Si	Al/Si
1	42.12	37.84	3.27	2.12	0.08	0.90	0.05	1.11	0.09
2	51.27	22.04	8.52	2.94	0.17	0.43	0.06	2.33	0.39
3	54.21	26.44	6.72	2.11	0.12	0.49	0.04	2.05	0.25
4	5.22	88.1	2.35	0.29	0.45	16.88	0.06	0.06	0.03
5	69.49	19.27	3.33	1.51	0.05	0.28	0.02	3.61	0.17
6	58.41	28.1	7.04	0.73	0.12	0.48	0.01	2.08	0.25
7	55.04	20.88	7.34	3.74	0.13	0.38	0.07	2.64	0.35
8	56.74	18.85	6.84	1.36	0.12	0.33	0.02	3.01	0.36
9	40.44	30.65	8.6	2.11	0.21	0.76	0.05	1.32	0.28
10	56.36	20.6	7.93	1.55	0.14	0.37	0.03	2.74	0.38
11	54.36	25.44	7.36	4.04	0.14	0.47	0.07	2.14	0.29
12	63.16	20.16	6.16	1.3	0.10	0.32	0.02	3.13	0.31
13	59.56	15.12	11.09	0.66	0.19	0.25	0.01	3.94	0.73
14	68.09	14.96	2.16	1.14	0.03	0.22	0.02	4.55	0.14
15	57.58	17.04	6.3	1.38	0.11	0.30	0.02	3.38	0.37
16	57.86	19.51	6.73	2.35	0.12	0.34	0.04	2.97	0.34
17	2.26	96.76	0	0.35	0.00	42.81	0.15	0.02	0.00
18	11.53	74.52	2.72	1.12	0.24	6.46	0.10	0.15	0.04
19	63.98	15.92	11.19	0.57	0.17	0.25	0.01	4.02	0.70
20	33.2	48.1	5.88	1.51	0.18	1.45	0.05	0.69	0.12
21	42.27	28.14	11.82	2.31	0.28	0.67	0.05	1.50	0.42
22	48.59	24.17	8.74	2.62	0.18	0.50	0.05	2.01	0.36
23	54.17	16.81	13.41	2.16	0.25	0.31	0.04	3.22	0.80
24	66.98	28.05	2.33	0.86	0.03	0.42	0.01	2.39	0.08
25	67.69	23.33	4.67	1.04	0.07	0.34	0.02	2.90	0.20
26	22.59	15.06	5.82	30.95	0.26	0.67	1.37	1.50	0.39
27	64.25	19.5	7.74	0.33	0.12	0.30	0.01	3.29	0.40
28	63.95	20.27	6.08	0.98	0.10	0.32	0.02	3.15	0.30
29	81.23	7.7	1.96	1.69	0.02	0.09	0.02	10.55	0.25
30	48.69	33.5	6.17	1.03	0.13	0.69	0.02	1.45	0.18
31	54.13	18.69	7.87	4.37	0.15	0.35	0.08	2.90	0.42
32	59.06	20.7	6.67	1.11	0.11	0.35	0.02	2.85	0.32
33	82.95	13.07	0.94	0.17	0.01	0.16	0.00	6.35	0.07
34	63.85	19.32	3.64	1.31	0.06	0.30	0.02	3.30	0.19
35	68.33	17.43	3.57	1.93	0.05	0.26	0.03	3.92	0.20
36	57.2	21.01	6.49	2.23	0.11	0.37	0.04	2.72	0.31
37	41.81	34.59	6.94	1.63	0.17	0.83	0.04	1.21	0.20
38	61.59	22.82	5.64	0.88	0.09	0.37	0.01	2.70	0.25
39	42.11	28.64	12.99	2.89	0.31	0.68	0.07	1.47	0.45
40	36.75	43.83	4.76	2.32	0.13	1.19	0.06	0.84	0.11
41	58.11	24.4	5.02	2.55	0.09	0.42	0.04	2.38	0.21
42	53.3	25.91	7.83	1.89	0.15	0.49	0.04	2.06	0.30
43	59.46	18.46	10.65	2.58	0.18	0.31	0.04	3.22	0.58

44	54.74	40.34	1.45	0.52	0.03	0.74	0.01	1.36	0.04
45	62.65	18.73	10.06	0.93	0.16	0.30	0.01	3.34	0.54
46	51.94	18.5	7.78	3.89	0.15	0.36	0.07	2.81	0.42
47	49.05	26.72	5.87	2.74	0.12	0.54	0.06	1.84	0.22
48	50.33	29.08	7.08	2.05	0.14	0.58	0.04	1.73	0.24
49	56.13	21.58	7.64	2.44	0.14	0.38	0.04	2.60	0.35
50	6.51	31.44	21.19	0.93	3.25	4.83	0.14	0.21	0.67
51	4.08	31.7	20.41	3.99	5.00	7.77	0.98	0.13	0.64
52	44.34	25.33	6.78	2.79	0.15	0.57	0.06	1.75	0.27
53	42.56	44.11	3.81	2.22	0.09	1.04	0.05	0.96	0.09
54	7.02	84.93	2.72	1.17	0.39	12.10	0.17	0.08	0.03
55	59.26	19.21	5.45	0.67	0.09	0.32	0.01	3.08	0.28
56	61.24	16.82	5.87	2.99	0.10	0.27	0.05	3.64	0.35
57	53.65	23.57	6.56	2.05	0.12	0.44	0.04	2.28	0.28
58	57.52	20.77	7.39	2.35	0.13	0.36	0.04	2.77	0.36
59	67.19	19.56	5.19	0.33	0.08	0.29	0.00	3.44	0.27
60	30.93	34.3	12.32	1.51	0.40	1.11	0.05	0.90	0.36
61	21.98	42.7	15.68	1.49	0.71	1.94	0.07	0.51	0.37
62	33.67	34.69	11.98	2.46	0.36	1.03	0.07	0.97	0.35

Table C.3 : Atomic ratio for S60 (7days)

	Calcium	Silicon	Aluminium	Sulfur	Al/Ca	Si/Ca	S/Ca	Ca/Si	Al/Si
1	48.41	40.82	4.23	2.24	0.09	0.84	0.05	1.19	0.10
2	47.4	30.56	8.69	3.83	0.18	0.64	0.08	1.55	0.28
3	64.49	17.23	6.94	2.71	0.11	0.27	0.04	3.74	0.40
4	5.17	91.81	0.86	0.79	0.17	17.76	0.15	0.06	0.01
5	59.98	26.76	6.07	1.96	0.10	0.45	0.03	2.24	0.23
6	44.83	30.28	11.18	0.93	0.25	0.68	0.02	1.48	0.37
7	64	18.67	7.02	2.17	0.11	0.29	0.03	3.43	0.38
8	59.77	19.06	8.3	2.1	0.14	0.32	0.04	3.14	0.44
9	56.18	23.72	7.41	2.03	0.13	0.42	0.04	2.37	0.31
10	65.19	19.54	6.53	1.53	0.10	0.30	0.02	3.34	0.33
11	55.67	26.02	7.42	2.9	0.13	0.47	0.05	2.14	0.29
12	60.54	27.62	4.7	2.49	0.08	0.46	0.04	2.19	0.17
13	59.77	25.22	6.02	2.94	0.10	0.42	0.05	2.37	0.24
14	54.34	35.16	5.33	2.12	0.10	0.65	0.04	1.55	0.15
15	53.8	17.7	11.25	4.04	0.21	0.33	0.08	3.04	0.64
16	20.95	31.86	15.37	1.35	0.73	1.52	0.06	0.66	0.48
17	27.68	56.21	5.17	3.57	0.19	2.03	0.13	0.49	0.09
18	2.85	96.71	0	0.04	0.00	33.93	0.01	0.03	0.00
19	44.22	35.59	8.85	3.26	0.20	0.80	0.07	1.24	0.25
20	62.17	16.6	11.63	2.52	0.19	0.27	0.04	3.75	0.70
21	64.56	25.86	3.24	0.87	0.05	0.40	0.01	2.50	0.13
22	53.7	27.78	7.11	3.87	0.13	0.52	0.07	1.93	0.26
23	36.66	29.64	12.21	2.62	0.33	0.81	0.07	1.24	0.41
24	50.25	32.1	7.39	3.3	0.15	0.64	0.07	1.57	0.23
25	45.42	36.95	7.79	2.49	0.17	0.81	0.05	1.23	0.21
26	55.28	25.43	6.63	3.31	0.12	0.46	0.06	2.17	0.26
27	65.27	25.02	3.56	1.94	0.05	0.38	0.03	2.61	0.14
28	49.46	22.68	8.57	3.71	0.17	0.46	0.08	2.18	0.38
29	53.87	26.87	9.98	2.33	0.19	0.50	0.04	2.00	0.37
30	54.18	22.45	9.23	3.33	0.17	0.41	0.06	2.41	0.41
31	54.34	20.05	9.96	3.81	0.18	0.37	0.07	2.71	0.50
32	29.89	6.95	6.63	0.53	0.22	0.23	0.02	4.30	0.95
33	13.46	83.6	1.29	0.6	0.10	6.21	0.04	0.16	0.02
34	61.88	18.94	8.62	2.52	0.14	0.31	0.04	3.27	0.46
35	52.71	24.01	9.85	2.38	0.19	0.46	0.05	2.20	0.41
36	52.35	27.59	5.77	4.31	0.11	0.53	0.08	1.90	0.21
37	24.72	41.99	14.63	1.56	0.59	1.70	0.06	0.59	0.35
38	71.76	11.28	6.98	3.17	0.10	0.16	0.04	6.36	0.62
39	44.51	34.27	8.52	2.92	0.19	0.77	0.07	1.30	0.25
40	57.04	24.15	9	3.48	0.16	0.42	0.06	2.36	0.37
41	4.85	91.14	1.15	1.02	0.24	18.79	0.21	0.05	0.01
42	55.51	21.81	8.45	2.86	0.15	0.39	0.05	2.55	0.39
43	53.53	25.62	11.09	2.86	0.21	0.48	0.05	2.09	0.43

44	62.12	20.31	8.18	1.26	0.13	0.33	0.02	3.06	0.40
45	42.92	39.89	7.42	2.87	0.17	0.93	0.07	1.08	0.19
46	12.29	81.6	3.33	0.37	0.27	6.64	0.03	0.15	0.04
47	59.02	21.26	9.57	0.98	0.16	0.36	0.02	2.78	0.45
48	52.81	29.96	7.32	2.4	0.14	0.57	0.05	1.76	0.24
49	54.14	23.43	10.17	1.94	0.19	0.43	0.04	2.31	0.43
50	46.63	27.49	13.77	2.54	0.30	0.59	0.05	1.70	0.50
51	62.79	21.1	9.19	0.57	0.15	0.34	0.01	2.98	0.44
52	31.86	55.47	4.24	1.32	0.13	1.74	0.04	0.57	0.08
53	23.95	67.59	2.93	1.83	0.12	2.82	0.08	0.35	0.04
54	65.91	22.68	4.15	0.97	0.06	0.34	0.01	2.91	0.18
55	38.54	54.99	2.71	1.44	0.07	1.43	0.04	0.70	0.05
56	41.3	41.75	6.92	1.94	0.17	1.01	0.05	0.99	0.17
57	11.72	52.61	16.25	1.25	1.39	4.49	0.11	0.22	0.31
58	50.61	27.14	6.73	3.28	0.13	0.54	0.06	1.86	0.25
59	57.63	30.67	5.79	1.84	0.10	0.53	0.03	1.88	0.19
60	59.29	25.92	5.67	2.52	0.10	0.44	0.04	2.29	0.22
61	49.29	29.42	8.08	3.33	0.16	0.60	0.07	1.68	0.27
62	67.62	23.43	6.57	0	0.10	0.35	0.00	2.89	0.28

Table C.4: Atomic ratio for S200 (7days)

	Calcium	Silicon	Aluminium	Sulfur	Al/Ca	Si/Ca	S/Ca	Ca/Si	Al/Si
1	19.74	41.28	19.45	0.77	0.99	2.09	0.04	0.48	0.47
2	30.86	20.41	11.58	2.71	0.38	0.66	0.09	1.51	0.57
3	26.33	60.18	3.32	0.44	0.13	2.29	0.02	0.44	0.06
4	15.69	67.88	5.07	1.63	0.32	4.33	0.10	0.23	0.07
5	40.22	31.74	10.26	1.71	0.26	0.79	0.04	1.27	0.32
6	55.83	21.66	6.83	2.25	0.12	0.39	0.04	2.58	0.32
7	41.31	26.5	8.53	1.63	0.21	0.64	0.04	1.56	0.32
8	45.45	25.05	6.64	2.12	0.15	0.55	0.05	1.81	0.27
9	42.07	23.53	6.96	2.2	0.17	0.56	0.05	1.79	0.30
10	65.11	14.45	5	1.03	0.08	0.22	0.02	4.51	0.35
11	39.58	33.07	5.48	2.19	0.14	0.84	0.06	1.20	0.17
12	53.54	16.99	5.9	3.84	0.11	0.32	0.07	3.15	0.35
13	81.27	8.32	1.79	0.74	0.02	0.10	0.01	9.77	0.22
14	57.59	19.52	7.48	2.09	0.13	0.34	0.04	2.95	0.38
15	56.4	23.6	7.29	2.05	0.13	0.42	0.04	2.39	0.31
16	49.52	22.4	8.33	1.79	0.17	0.45	0.04	2.21	0.37
17	48.5	16.21	5.77	7.84	0.12	0.33	0.16	2.99	0.36
18	53.97	21.95	8.26	1.74	0.15	0.41	0.03	2.46	0.38
19	48.24	24.09	6.8	1.65	0.14	0.50	0.03	2.00	0.28
20	52.9	26.21	6.56	1.98	0.12	0.50	0.04	2.02	0.25
21	19.37	45.17	15.56	0.9	0.80	2.33	0.05	0.43	0.34
22	1.96	95.84	0.37	0.48	0.19	48.90	0.24	0.02	0.00
23	22.33	47.5	7.88	1.72	0.35	2.13	0.08	0.47	0.17
24	69.34	15.14	2.34	0.49	0.03	0.22	0.01	4.58	0.15
25	60.57	17.2	8.85	0.46	0.15	0.28	0.01	3.52	0.51
26	31.38	29.88	5.55	1.4	0.18	0.95	0.04	1.05	0.19
27	50.21	23.71	7.9	2.23	0.16	0.47	0.04	2.12	0.33
28	51.69	16.84	5.08	1.61	0.10	0.33	0.03	3.07	0.30
29	42.72	22.56	8.35	2.67	0.20	0.53	0.06	1.89	0.37
30	40.34	27.13	9.06	2.09	0.22	0.67	0.05	1.49	0.33
31	59.7	21.94	5.76	1.83	0.10	0.37	0.03	2.72	0.26
32	37.81	30.92	10.44	1.01	0.28	0.82	0.03	1.22	0.34
33	61.8	15.79	8.01	0.89	0.13	0.26	0.01	3.91	0.51
34	58.48	20.85	7.66	1.06	0.13	0.36	0.02	2.80	0.37
35	47.27	24.05	7.72	1.49	0.16	0.51	0.03	1.97	0.32
36	35.06	25.62	8.7	2.69	0.25	0.73	0.08	1.37	0.34
37	3.89	92.04	1.06	0.51	0.27	23.66	0.13	0.04	0.01
38	39.07	31.52	10.54	1.22	0.27	0.81	0.03	1.24	0.33
39	57.93	17.59	6.64	5.48	0.11	0.30	0.09	3.29	0.38
40	44.69	23.84	7.95	2.32	0.18	0.53	0.05	1.87	0.33
41	35.54	29.25	10.81	1.58	0.30	0.82	0.04	1.22	0.37
42	2.18	96.04	0.67	0.06	0.31	44.06	0.03	0.02	0.01
43	45.2	24.4	8.22	2.09	0.18	0.54	0.05	1.85	0.34
44	6.46	89.82	0.95	0	0.15	13.90	0.00	0.07	0.01

45	31.66	36.68	11.43	1.17	0.36	1.16	0.04	0.86	0.31
46	41.3	2.23	7.14	1.57	0.17	0.05	0.04	18.52	3.20
47	50.52	25.75	10.89	1.07	0.22	0.51	0.02	1.96	0.42
48	39.36	30.84	5.42	2.04	0.14	0.78	0.05	1.28	0.18
49	60.32	12.7	5.29	1.24	0.09	0.21	0.02	4.75	0.42
50	52.32	19.22	8.66	1.54	0.17	0.37	0.03	2.72	0.45
51	15.43	73.09	3.01	0.63	0.20	4.74	0.04	0.21	0.04
52	60.05	19.59	7.19	1.68	0.12	0.33	0.03	3.07	0.37
53	23.66	59.07	5.42	0.62	0.23	2.50	0.03	0.40	0.09
54	55.89	25.28	5.2	2.12	0.09	0.45	0.04	2.21	0.21
55	60.28	25.16	5.42	1.2	0.09	0.42	0.02	2.40	0.22
56	64.46	24.29	5.3	1.01	0.08	0.38	0.02	2.65	0.22
57	58.41	25.27	6.03	1.44	0.10	0.43	0.02	2.31	0.24
58	52.97	16.77	5.95	1.03	0.11	0.32	0.02	3.16	0.35
59	43.17	36.68	6.66	1.62	0.15	0.85	0.04	1.18	0.18
60	24.15	55.82	6.27	1.54	0.26	2.31	0.06	0.43	0.11
61	46.56	21.46	8.24	1.32	0.18	0.46	0.03	2.17	0.38
62	54.15	20.18	7.99	2.18	0.15	0.37	0.04	2.68	0.40

Table C.5: Atomic ratio for D0 (7days)

	Calcium	Silicon	Aluminium	Sulfur	Al/Ca	Si/Ca	S/Ca	Ca/Si	Al/Si
1	52.86	29.06	7.95	2.04	0.15	0.55	0.04	1.82	0.27
2	58.39	21.36	7.96	1.34	0.14	0.37	0.02	2.73	0.37
3	56.94	24.66	7.18	2.37	0.13	0.43	0.04	2.31	0.29
4	61.11	24.89	5.19	1.34	0.08	0.41	0.02	2.46	0.21
5	66.11	17.37	6.41	2.15	0.10	0.26	0.03	3.81	0.37
6	48.24	31.06	9.31	2.27	0.19	0.64	0.05	1.55	0.30
7	64.82	17.35	5.66	1.88	0.09	0.27	0.03	3.74	0.33
8	61.15	22.57	7.75	1.43	0.13	0.37	0.02	2.71	0.34
9	31.43	41.61	19.62	0.38	0.62	1.32	0.01	0.76	0.47
10	52.02	26.82	8.31	2.51	0.16	0.52	0.05	1.94	0.31
11	59.67	22.46	6.4	2.17	0.11	0.38	0.04	2.66	0.28
12	17.1	75.49	2.67	1.5	0.16	4.41	0.09	0.23	0.04
13	59.76	23.43	7.02	2.58	0.12	0.39	0.04	2.55	0.30
14	44.62	33.35	9.88	2.36	0.22	0.75	0.05	1.34	0.30
15	44.47	30.45	13.06	1.34	0.29	0.68	0.03	1.46	0.43
16	61.61	21.51	7.37	2.32	0.12	0.35	0.04	2.86	0.34
17	58.6	25.28	8.32	2.17	0.14	0.43	0.04	2.32	0.33
18	58.21	26.38	7.84	1.53	0.13	0.45	0.03	2.21	0.30
19	49.41	28.39	12.75	2.02	0.26	0.57	0.04	1.74	0.45
20	53.32	28.49	9.03	2.13	0.17	0.53	0.04	1.87	0.32
21	60.63	24.24	6.62	2.52	0.11	0.40	0.04	2.50	0.27
22	43.43	23.24	11.96	2.13	0.28	0.54	0.05	1.87	0.51
23	38.57	31.94	13.57	1.75	0.35	0.83	0.05	1.21	0.42
24	25.5	46.82	19.95	0.63	0.78	1.84	0.02	0.54	0.43
25	52.24	38.7	3	1.55	0.06	0.74	0.03	1.35	0.08
26	55.81	21.3	8.58	2.75	0.15	0.38	0.05	2.62	0.40
27	39.47	32.83	11.24	2.15	0.28	0.83	0.05	1.20	0.34
28	59.75	25.57	5.5	1.15	0.09	0.43	0.02	2.34	0.22
29	26.56	46.37	17.79	0.46	0.67	1.75	0.02	0.57	0.38
30	62.77	20.59	7.97	2.62	0.13	0.33	0.04	3.05	0.39
31	54.48	24.84	7.43	2.53	0.14	0.46	0.05	2.19	0.30
32	53.55	25.84	8.28	2.48	0.15	0.48	0.05	2.07	0.32
33	54.13	23.68	8.93	2.23	0.16	0.44	0.04	2.29	0.38
34	43.03	27.72	7.32	2.69	0.17	0.64	0.06	1.55	0.26
35	50.77	27.77	6.41	1.89	0.13	0.55	0.04	1.83	0.23
36	19.3	59.86	9.68	1.24	0.50	3.10	0.06	0.32	0.16
37	57.13	23.54	7.7	1.46	0.13	0.41	0.03	2.43	0.33
38	43.91	29.11	8.54	2.55	0.19	0.66	0.06	1.51	0.29
39	29.24	61.37	3.73	1.33	0.13	2.10	0.05	0.48	0.06
40	41.47	43.13	5.67	2.43	0.14	1.04	0.06	0.96	0.13
41	28.38	40.22	15.19	1.15	0.54	1.42	0.04	0.71	0.38
42	31.63	37.89	18.84	1.54	0.60	1.20	0.05	0.83	0.50
43	60.37	24.71	6.18	1.24	0.10	0.41	0.02	2.44	0.25
44	52.23	24.59	8.94	1.59	0.17	0.47	0.03	2.12	0.36

45	53.98	25.6	8.11	1.3	0.15	0.47	0.02	2.11	0.32
46	48.03	30.8	8.25	2.21	0.17	0.64	0.05	1.56	0.27
47	45.35	30.12	11.23	2.72	0.25	0.66	0.06	1.51	0.37
48	33.81	40.09	12.19	2.5	0.36	1.19	0.07	0.84	0.30
49	23.09	66.43	3.49	0.98	0.15	2.88	0.04	0.35	0.05
50	48	29.02	8.34	1.64	0.17	0.60	0.03	1.65	0.29
51	39.11	38.58	10.06	1.39	0.26	0.99	0.04	1.01	0.26
52	39.15	32.94	11.96	1.89	0.31	0.84	0.05	1.19	0.36
53	72.1	12.68	4.47	1.51	0.06	0.18	0.02	5.69	0.35
54	55.36	24.06	7.23	2.35	0.13	0.43	0.04	2.30	0.30
55	35.19	44.27	10.02	1.08	0.28	1.26	0.03	0.79	0.23
56	59.55	14.85	8.4	2.25	0.14	0.25	0.04	4.01	0.57
57	47.22	30.45	9.62	1.99	0.20	0.64	0.04	1.55	0.32
58	52.47	31.96	5.62	1.07	0.11	0.61	0.02	1.64	0.18
59	60.88	20.37	6.42	2.01	0.11	0.33	0.03	2.99	0.32
60	51.5	26.26	7.91	2.68	0.15	0.51	0.05	1.96	0.30
61	55.79	25.24	6.1	1.43	0.11	0.45	0.03	2.21	0.24
62	40.42	34.38	11.51	1.96	0.28	0.85	0.05	1.18	0.33

Table C.6: Atomic ratio for D60 (7days)

	Calcium	Silicon	Aluminium	Sulfur	Al/Ca	Si/Ca	S/Ca	Ca/Si	Al/Si
1	47.04	28.41	11.66	2.15	0.25	0.60	0.05	1.66	0.41
2	13.79	81.33	2.46	0.85	0.18	5.90	0.06	0.17	0.03
3	45.26	33.11	10.69	2.57	0.24	0.73	0.06	1.37	0.32
4	43.21	33.17	12.01	2.93	0.28	0.77	0.07	1.30	0.36
5	51.04	33.05	5.68	3.97	0.11	0.65	0.08	1.54	0.17
6	45.75	24.88	12.14	2.09	0.27	0.54	0.05	1.84	0.49
7	48.05	27.39	12.61	2.78	0.26	0.57	0.06	1.75	0.46
8	41.46	34.57	12.73	2.27	0.31	0.83	0.05	1.20	0.37
9	36.49	36.29	15.49	1.73	0.42	0.99	0.05	1.01	0.43
10	51.5	28.48	10.82	2.66	0.21	0.55	0.05	1.81	0.38
11	55.47	24.31	8.45	2.05	0.15	0.44	0.04	2.28	0.35
12	23.61	44.46	19.7	1.61	0.83	1.88	0.07	0.53	0.44
13	38.08	32.42	14.01	2.67	0.37	0.85	0.07	1.17	0.43
14	12.03	52.42	21.06	0.76	1.75	4.36	0.06	0.23	0.40
15	57.83	23.96	8.82	2.58	0.15	0.41	0.04	2.41	0.37
16	54.46	29.94	7.47	2.55	0.14	0.55	0.05	1.82	0.25
17	53.82	23.51	10.15	3.45	0.19	0.44	0.06	2.29	0.43
18	52.76	28.03	9.55	3.31	0.18	0.53	0.06	1.88	0.34
19	37.86	34.86	13.69	2.89	0.36	0.92	0.08	1.09	0.39
20	47.48	28.52	11.44	4.06	0.24	0.60	0.09	1.66	0.40
21	39.93	35.11	15.69	1.12	0.39	0.88	0.03	1.14	0.45
22	51.59	29.08	9.37	1.3	0.18	0.56	0.03	1.77	0.32
23	47.64	29.04	11.43	2.26	0.24	0.61	0.05	1.64	0.39
24	62.4	25.58	4.61	2.09	0.07	0.41	0.03	2.44	0.18
25	49.99	29.56	9.22	3.41	0.18	0.59	0.07	1.69	0.31
26	47.41	30.79	14.17	2.55	0.30	0.65	0.05	1.54	0.46
27	56.84	24.42	8.42	2.35	0.15	0.43	0.04	2.33	0.34
28	59.37	25.38	6.65	2.56	0.11	0.43	0.04	2.34	0.26
29	50.25	29.98	8.4	2.9	0.17	0.60	0.06	1.68	0.28
30	41.22	35.39	10.83	3.53	0.26	0.86	0.09	1.16	0.31
31	53.64	26.92	8.08	3.27	0.15	0.50	0.06	1.99	0.30
32	38.97	33.79	17.53	1.41	0.45	0.87	0.04	1.15	0.52
33	48.17	28.72	11.67	1.96	0.24	0.60	0.04	1.68	0.41
34	50.58	29.05	9.63	1.88	0.19	0.57	0.04	1.74	0.33
35	58.19	25.79	8.8	1.18	0.15	0.44	0.02	2.26	0.34
36	23.59	59.88	8.05	1.64	0.34	2.54	0.07	0.39	0.13
37	43.15	36.61	9.84	1.39	0.23	0.85	0.03	1.18	0.27
38	52.56	26.86	9.99	3.32	0.19	0.51	0.06	1.96	0.37
39	50.61	38.81	4.71	2.15	0.09	0.77	0.04	1.30	0.12
40	61.89	20.21	8.27	2.63	0.13	0.33	0.04	3.06	0.41
41	45.95	34.3	10.27	2.97	0.22	0.75	0.06	1.34	0.30
42	57.9	25.23	7.48	2.55	0.13	0.44	0.04	2.29	0.30
43	60.6	22.34	6.88	1.93	0.11	0.37	0.03	2.71	0.31

44	17.88	67.9	7.37	1.5	0.41	3.80	0.08	0.26	0.11
45	50.72	25.89	10.74	3.75	0.21	0.51	0.07	1.96	0.41
46	49.9	29.63	10.47	1.75	0.21	0.59	0.04	1.68	0.35
47	43.9	32.29	10.06	2.1	0.23	0.74	0.05	1.36	0.31
48	58.39	23.56	8.41	2.24	0.14	0.40	0.04	2.48	0.36
49	53.96	26.4	8.66	2.48	0.16	0.49	0.05	2.04	0.33
50	39.6	35.44	16.12	2.43	0.41	0.89	0.06	1.12	0.45
51	55.51	22.58	9.8	2.82	0.18	0.41	0.05	2.46	0.43
52	32.31	45.05	11.17	1.27	0.35	1.39	0.04	0.72	0.25
53	54.13	28.48	6.97	3	0.13	0.53	0.06	1.90	0.24
54	56.21	24.8	8.65	2.49	0.15	0.44	0.04	2.27	0.35
55	53.46	27.05	7.22	3.23	0.14	0.51	0.06	1.98	0.27
56	45.91	33.99	8.36	2.64	0.18	0.74	0.06	1.35	0.25
57	49.3	30.27	9.82	2.97	0.20	0.61	0.06	1.63	0.32
58	51.95	21.17	11.62	2.78	0.22	0.41	0.05	2.45	0.55
59	42.92	30.59	14	3.52	0.33	0.71	0.08	1.40	0.46
60	60.26	25.05	7.17	1.1	0.12	0.42	0.02	2.41	0.29
61	40.17	35.51	14.03	2.49	0.35	0.88	0.06	1.13	0.40
62	35.88	36.56	13.9	2.57	0.39	1.02	0.07	0.98	0.38

Table C.7: Atomic ratio for D200 (7days)

	Calcium	Silicon	Aluminium	Sulfur	Al/Ca	Si/Ca	S/Ca	Ca/Si	Al/Si
1	39.99	30.47	13.48	1.83	0.34	0.76	0.05	1.31	0.44
2	54.85	24.62	6.98	1.35	0.13	0.45	0.02	2.23	0.28
3	61.73	21.46	6.9	1.55	0.11	0.35	0.03	2.88	0.32
4	31.63	31.58	5.43	1.63	0.17	1.00	0.05	1.00	0.17
5	54.28	23.51	7.17	4	0.13	0.43	0.07	2.31	0.30
6	52.72	28.59	7.1	1.76	0.13	0.54	0.03	1.84	0.25
7	23.75	42.88	13.98	1.7	0.59	1.81	0.07	0.55	0.33
8	45.12	40.09	6.12	2.53	0.14	0.89	0.06	1.13	0.15
9	42.42	31.46	13.75	1.81	0.32	0.74	0.04	1.35	0.44
10	55.53	28.02	7.44	1.48	0.13	0.50	0.03	1.98	0.27
11	46.15	32.32	8.72	2.14	0.19	0.70	0.05	1.43	0.27
12	59.39	21.85	6.83	1.65	0.12	0.37	0.03	2.72	0.31
13	74.39	13.65	4.83	1.09	0.06	0.18	0.01	5.45	0.35
14	59.6	26.63	6.47	1.05	0.11	0.45	0.02	2.24	0.24
15	34.98	45.48	8.26	2.06	0.24	1.30	0.06	0.77	0.18
16	38.8	33.38	12.11	2.8	0.31	0.86	0.07	1.16	0.36
17	43.48	37.83	9.09	2.09	0.21	0.87	0.05	1.15	0.24
18	38.36	38.56	9.69	2.55	0.25	1.01	0.07	0.99	0.25
19	56.61	25	5.49	0.93	0.10	0.44	0.02	2.26	0.22
20	27.3	41.21	18.67	2.11	0.68	1.51	0.08	0.66	0.45
21	64.36	21.49	5.09	1.06	0.08	0.33	0.02	2.99	0.24
22	49.94	25.83	9.35	2.4	0.19	0.52	0.05	1.93	0.36
23	51.5	25.51	7.57	1.63	0.15	0.50	0.03	2.02	0.30
24	39.7	33.08	10.57	1.82	0.27	0.83	0.05	1.20	0.32
25	38.15	32.61	12.57	2.03	0.33	0.85	0.05	1.17	0.39
26	49.05	29.69	8.28	2.05	0.17	0.61	0.04	1.65	0.28
27	45.1	28.6	12.47	3.19	0.28	0.63	0.07	1.58	0.44
28	47.82	27.86	976	2.42	20.41	0.58	0.05	1.72	35.03
29	48.93	22.97	9.33	2.38	0.19	0.47	0.05	2.13	0.41
30	58.58	20.9	6.76	2.4	0.12	0.36	0.04	2.80	0.32
31	72.87	13.01	5.83	0.85	0.08	0.18	0.01	5.60	0.45
32	33.03	33.81	19.02	1.06	0.58	1.02	0.03	0.98	0.56
33	37.29	33.41	12.98	3.21	0.35	0.90	0.09	1.12	0.39
34	7.6	55.84	18.03	0.08	2.37	7.35	0.01	0.14	0.32
35	45.89	28.31	10.49	3.16	0.23	0.62	0.07	1.62	0.37
36	13.93	50.89	16.05	0.4	1.15	3.65	0.03	0.27	0.32
37	54.61	28.47	6.89	1.16	0.13	0.52	0.02	1.92	0.24
38	42.38	39.42	6.38	2.67	0.15	0.93	0.06	1.08	0.16
39	27.75	56.27	5.13	1.63	0.18	2.03	0.06	0.49	0.09
40	52.42	26.79	7.49	2.04	0.14	0.51	0.04	1.96	0.28
41	78.79	12.02	3.37	0.51	0.04	0.15	0.01	6.55	0.28
42	42.5	33.46	9.68	4.72	0.23	0.79	0.11	1.27	0.29
43	26.89	46.9	12.34	1.53	0.46	1.74	0.06	0.57	0.26
44	41.79	36.84	8.46	1.58	0.20	0.88	0.04	1.13	0.23

45	8.31	57.9	15.23	0.21	1.83	6.97	0.03	0.14	0.26
46	38.4	34.35	16.09	1.99	0.42	0.89	0.05	1.12	0.47
47	54.61	23.89	9	1.69	0.16	0.44	0.03	2.29	0.38
48	62.49	24.46	6.03	1.04	0.10	0.39	0.02	2.55	0.25
49	53.58	25.68	10.91	2.38	0.20	0.48	0.04	2.09	0.42
50	50.79	27.3	7.88	2.37	0.16	0.54	0.05	1.86	0.29
51	42.5	29.32	13.54	2.16	0.32	0.69	0.05	1.45	0.46
52	48.51	32.17	8.7	2.05	0.18	0.66	0.04	1.51	0.27
53	51.23	25.17	9.59	3.4	0.19	0.49	0.07	2.04	0.38
54	45.51	32.5	9.02	1.95	0.20	0.71	0.04	1.40	0.28
55	47.67	39.07	4	1.8	0.08	0.82	0.04	1.22	0.10
56	51.6	20.26	8.22	2.66	0.16	0.39	0.05	2.55	0.41
57	46.02	28.82	9.68	2.95	0.21	0.63	0.06	1.60	0.34
58	54.24	29.62	6.12	1.16	0.11	0.55	0.02	1.83	0.21
59	52.87	23.23	8.05	1.35	0.15	0.44	0.03	2.28	0.35
60	58.03	23.23	8.97	1.22	0.15	0.40	0.02	2.50	0.39
61	46.43	30.53	9.02	3.15	0.19	0.66	0.07	1.52	0.30
62	41.17	33.48	14.21	2.02	0.35	0.81	0.05	1.23	0.42

Table C.8: Atomic ratio for G0 (7days)

	Calcium	Silicon	Aluminium	Sulfur	Al/Ca	Si/Ca	S/Ca	Ca/Si	Al/Si
1	51.08	24.77	10.93	1.96	0.21	0.48	0.04	2.06	0.44
2	36.32	51.4	3.53	1.79	0.10	1.42	0.05	0.71	0.07
3	53.66	24.02	8.35	2.97	0.16	0.45	0.06	2.23	0.35
4	40.57	34.79	11.59	1.88	0.29	0.86	0.05	1.17	0.33
5	18.92	56.19	11.23	0.87	0.59	2.97	0.05	0.34	0.20
6	57.41	22.46	8.62	2.52	0.15	0.39	0.04	2.56	0.38
7	35.18	49.63	6.63	1.96	0.19	1.41	0.06	0.71	0.13
8	60.22	25.07	7.26	2.48	0.12	0.42	0.04	2.40	0.29
9	32.08	58.43	4.13	1.27	0.13	1.82	0.04	0.55	0.07
10	52.17	24.5	6.52	2.37	0.12	0.47	0.05	2.13	0.27
11	42.22	33.3	11.07	1.81	0.26	0.79	0.04	1.27	0.33
12	55.78	25.46	6.67	2.84	0.12	0.46	0.05	2.19	0.26
13	45.32	25.86	11.42	2.1	0.25	0.57	0.05	1.75	0.44
14	51.44	28.37	8.68	1.97	0.17	0.55	0.04	1.81	0.31
15	88.54	5.33	1.59	0.33	0.02	0.06	0.00	16.61	0.30
16	36.11	32.88	12.9	1.25	0.36	0.91	0.03	1.10	0.39
17	25.67	46.64	13.57	0.63	0.53	1.82	0.02	0.55	0.29
18	58.03	22.03	7.22	2.3	0.12	0.38	0.04	2.63	0.33
19	48.05	24.59	8.78	2.79	0.18	0.51	0.06	1.95	0.36
20	56.39	24.44	7	2.54	0.12	0.43	0.05	2.31	0.29
21	56.21	20.65	6.88	2	0.12	0.37	0.04	2.72	0.33
22	61.45	21.5	7.16	2.26	0.12	0.35	0.04	2.86	0.33
23	55.27	24.9	8.43	2.68	0.15	0.45	0.05	2.22	0.34
24	57.39	27.02	6.67	1.85	0.12	0.47	0.03	2.12	0.25
25	55.65	19.69	12.3	2.59	0.22	0.35	0.05	2.83	0.62
26	47.16	36.63	7.02	2	0.15	0.78	0.04	1.29	0.19
27	49.33	11.11	4.06	1.67	0.08	0.23	0.03	4.44	0.37
28	52.09	22.26	12.28	1.56	0.24	0.43	0.03	2.34	0.55
29	60.08	25.28	5.83	1.84	0.10	0.42	0.03	2.38	0.23
30	53.75	25.09	8.01	2.24	0.15	0.47	0.04	2.14	0.32
31	71.03	19.95	3.76	0.96	0.05	0.28	0.01	3.56	0.19
32	55.11	24.5	7.9	2.91	0.14	0.44	0.05	2.25	0.32
33	57.14	23.92	7.83	1.75	0.14	0.42	0.03	2.39	0.33
34	50.25	16.12	13.87	0.67	0.28	0.32	0.01	3.12	0.86
35	53.98	26.49	8.98	2.82	0.17	0.49	0.05	2.04	0.34
36	53.29	27.19	7.17	1.51	0.13	0.51	0.03	1.96	0.26
37	63.56	19.37	9.29	0.36	0.15	0.30	0.01	3.28	0.48
38	57.54	21.29	10.54	3	0.18	0.37	0.05	2.70	0.50
39	57.44	21.95	10.01	2.62	0.17	0.38	0.05	2.62	0.46
40	61.6	21.68	6.46	1.96	0.10	0.35	0.03	2.84	0.30
41	43.75	32.96	11.88	3.29	0.27	0.75	0.08	1.33	0.36
42	63.8	22.17	4.95	0.95	0.08	0.35	0.01	2.88	0.22

43	57.6	23.82	7.74	1.81	0.13	0.41	0.03	2.42	0.32
44	55.04	26.58	5.77	2.9	0.10	0.48	0.05	2.07	0.22
45	60.66	21.16	7.85	3.14	0.13	0.35	0.05	2.87	0.37
46	54.48	23.97	8.77	1.71	0.16	0.44	0.03	2.27	0.37
47	52.23	17.2	10.1	1.22	0.19	0.33	0.02	3.04	0.59
48	44.12	36	8.56	1.56	0.19	0.82	0.04	1.23	0.24
49	9.51	84.52	1.66	1.6	0.17	8.89	0.17	0.11	0.02
50	54.05	26.63	6.61	1.77	0.12	0.49	0.03	2.03	0.25
51	58.98	25.12	5.57	1.79	0.09	0.43	0.03	2.35	0.22
52	63.46	23.15	5.03	1.54	0.08	0.36	0.02	2.74	0.22
53	66.74	17.32	6.79	2.29	0.10	0.26	0.03	3.85	0.39
54	71.57	15.32	5.35	1.68	0.07	0.21	0.02	4.67	0.35
55	62.01	18.09	8.79	1.88	0.14	0.29	0.03	3.43	0.49
56	7.75	57.92	19.13	1	2.47	7.47	0.13	0.13	0.33
57	61.11	23.42	6.63	2.2	0.11	0.38	0.04	2.61	0.28
58	37.59	37.04	9.77	1.64	0.26	0.99	0.04	1.01	0.26
59	41.22	29.59	10.58	3.06	0.26	0.72	0.07	1.39	0.36
60	23.78	44.68	14.17	1.48	0.60	1.88	0.06	0.53	0.32
61	57.22	24.61	7.34	2.33	0.13	0.43	0.04	2.33	0.30
62	26.97	42.53	12.48	1.82	0.46	1.58	0.07	0.63	0.29

Table C.9: Atomic ratio for G60 (7days)

	Calcium	Silicon	Aluminium	Sulfur	Al/Ca	Si/Ca	S/Ca	Ca/Si	Al/Si
1	49.38	28.19	7.19	1.07	0.15	0.57	0.02	1.75	0.26
2	22.79	67.53	2.09	0.85	0.09	2.96	0.04	0.34	0.03
3	11.27	83.77	1.24	0.17	0.11	7.43	0.02	0.13	0.01
4	51.67	25.92	6.95	1.73	0.13	0.50	0.03	1.99	0.27
5	29.77	39.27	11.88	1.15	0.40	1.32	0.04	0.76	0.30
6	47.2	24.68	9.87	1.28	0.21	0.52	0.03	1.91	0.40
7	48.6	31.05	5.92	0.7	0.12	0.64	0.01	1.57	0.19
8	50.34	25.4	8.21	1.72	0.16	0.50	0.03	1.98	0.32
9	55.54	24.38	6.03	1.44	0.11	0.44	0.03	2.28	0.25
10	49.43	24.32	8.47	2.13	0.17	0.49	0.04	2.03	0.35
11	51.64	22.3	6.9	2.06	0.13	0.43	0.04	2.32	0.31
12	61.16	22.52	6.88	0.61	0.11	0.37	0.01	2.72	0.31
13	50.56	22.6	9.16	2.14	0.18	0.45	0.04	2.24	0.41
14	54.43	22.81	6.32	1.78	0.12	0.42	0.03	2.39	0.28
15	41.78	25.37	10.92	1.04	0.26	0.61	0.02	1.65	0.43
16	54.02	19.99	10.16	1.37	0.19	0.37	0.03	2.70	0.51
17	52.68	27.98	6.96	0.99	0.13	0.53	0.02	1.88	0.25
18	46.12	23.52	9.96	1.78	0.22	0.51	0.04	1.96	0.42
19	49.48	24.06	8.13	1.02	0.16	0.49	0.02	2.06	0.34
20	16.83	48.59	14.22	0.45	0.84	2.89	0.03	0.35	0.29
21	49.36	25.36	6.56	1.6	0.13	0.51	0.03	1.95	0.26
22	51.76	23.7	7.59	1.26	0.15	0.46	0.02	2.18	0.32
23	39.34	31.7	7.53	1.54	0.19	0.81	0.04	1.24	0.24
24	54.42	22.79	7.56	1.18	0.14	0.42	0.02	2.39	0.33
25	49.6	29.05	5.28	1.43	0.11	0.59	0.03	1.71	0.18
26	46.3	25.24	8.42	1.93	0.18	0.55	0.04	1.83	0.33
27	75.03	11.38	2.83	0.32	0.04	0.15	0.00	6.59	0.25
28	38.83	32.19	7.75	0.98	0.20	0.83	0.03	1.21	0.24
29	39.99	27.31	10.44	1.44	0.26	0.68	0.04	1.46	0.38
30	48.26	11.29	5.72	0.44	0.12	0.23	0.01	4.27	0.51
31	38.04	29.77	9.38	1.81	0.25	0.78	0.05	1.28	0.32
32	14.4	50.6	19.18	0.29	1.33	3.51	0.02	0.28	0.38
33	46.87	26.37	9.27	1.22	0.20	0.56	0.03	1.78	0.35
34	21.31	45	13.85	0.98	0.65	2.11	0.05	0.47	0.31
35	33.93	36.65	11.4	1.23	0.34	1.08	0.04	0.93	0.31
36	51.25	27.45	6.56	1.09	0.13	0.54	0.02	1.87	0.24
37	50.2	25.6	6.78	0.65	0.14	0.51	0.01	1.96	0.26
38	55.17	20.05	7.79	1.16	0.14	0.36	0.02	2.75	0.39
39	60.95	20.41	5.23	0.69	0.09	0.33	0.01	2.99	0.26
40	24.19	41.2	16.68	0.45	0.69	1.70	0.02	0.59	0.40
41	15.68	50.55	20.71	0.22	1.32	3.22	0.01	0.31	0.41
42	34.7	37.36	9.24	0.21	0.27	1.08	0.01	0.93	0.25
43	37.9	28.19	7.98	0.23	0.21	0.74	0.01	1.34	0.28
44	49.11	23.51	8.4	1.15	0.17	0.48	0.02	2.09	0.36

45	50.9	24.84	7.48	1.46	0.15	0.49	0.03	2.05	0.30
46	44.71	28.49	9.45	0.66	0.21	0.64	0.01	1.57	0.33
47	43.84	28.03	9.33	0.9	0.21	0.64	0.02	1.56	0.33
48	49.86	24.06	8.33	0.84	0.17	0.48	0.02	2.07	0.35
49	27.3	40.43	16.73	0.95	0.61	1.48	0.03	0.68	0.41
50	53.59	23.79	5.87	1.52	0.11	0.44	0.03	2.25	0.25
51	54.48	26.89	5.82	1.26	0.11	0.49	0.02	2.03	0.22
52	51.62	23.9	9.83	0.69	0.19	0.46	0.01	2.16	0.41
53	40.19	31.2	8.28	1.03	0.21	0.78	0.03	1.29	0.27
54	45	23.71	11.26	1.4	0.25	0.53	0.03	1.90	0.47
55	46.47	29.13	7.32	1.98	0.16	0.63	0.04	1.60	0.25
56	50.12	24.78	7.11	2.09	0.14	0.49	0.04	2.02	0.29
57	49.9	24.73	7.73	1.39	0.15	0.50	0.03	2.02	0.31
58	60.54	21.6	5.73	1.67	0.09	0.36	0.03	2.80	0.27
59	28.68	45.22	6.51	1.15	0.23	1.58	0.04	0.63	0.14
60	46.71	27.43	8.65	1.33	0.19	0.59	0.03	1.70	0.32
61	46.48	12.84	6.75	0.53	0.15	0.28	0.01	3.62	0.53
62	58.42	24.71	4.17	1.03	0.07	0.42	0.02	2.36	0.17

Table C.10: Atomic ratio for PC (28days)

	Calcium	Silicon	Aluminium	Sulfur	Al/Ca	Si/Ca	S/Ca	Ca/Si	Al/Si
1	65.72	13.46	3.56	2.13	0.05	0.20	0.03	4.88	0.26
2	65.59	18.42	6.82	1.07	0.10	0.28	0.02	3.56	0.37
3	73.31	15.47	4.94	1.52	0.07	0.21	0.02	4.74	0.32
4	71.19	19.1	4.13	1.88	0.06	0.27	0.03	3.73	0.22
5	64.63	17.95	5.9	1.94	0.09	0.28	0.03	3.60	0.33
6	64.53	22.03	5.16	2.5	0.08	0.34	0.04	2.93	0.23
7	78.79	12.36	1.21	0.73	0.02	0.16	0.01	6.37	0.10
8	67.63	17.7	4.48	2.45	0.07	0.26	0.04	3.82	0.25
9	69.45	20.65	4.2	1.34	0.06	0.30	0.02	3.36	0.20
10	67.72	19.28	5.02	1.58	0.07	0.28	0.02	3.51	0.26
11	69.5	19.02	3.46	1.53	0.05	0.27	0.02	3.65	0.18
12	69.39	19.18	3.5	1.84	0.05	0.28	0.03	3.62	0.18
13	63.61	21.22	6.52	2.11	0.10	0.33	0.03	3.00	0.31
14	63.47	18.93	4.91	2.9	0.08	0.30	0.05	3.35	0.26
15	67.46	18.2	5.04	1.78	0.07	0.27	0.03	3.71	0.28
16	66.34	20.2	6.22	1.62	0.09	0.30	0.02	3.28	0.31
17	67.64	19.71	4.44	1.42	0.07	0.29	0.02	3.43	0.23
18	60.11	22.12	7.36	1.69	0.12	0.37	0.03	2.72	0.33
19	60.52	19.21	6.61	3.01	0.11	0.32	0.05	3.15	0.34
20	66.21	16.78	5.61	2.24	0.08	0.25	0.03	3.95	0.33
21	66.16	22.86	3.41	1.59	0.05	0.35	0.02	2.89	0.15
22	64.88	21.68	5.01	2.69	0.08	0.33	0.04	2.99	0.23
23	65.59	20.94	5.16	1.61	0.08	0.32	0.02	3.13	0.25
24	65.89	22.17	5.09	2.37	0.08	0.34	0.04	2.97	0.23
25	67.45	17.72	4.36	2.73	0.06	0.26	0.04	3.81	0.25
26	64.9	21.01	4.91	1.62	0.08	0.32	0.02	3.09	0.23
27	61.94	17.82	5.73	3.09	0.09	0.29	0.05	3.48	0.32
28	64.55	17.98	5.57	2.85	0.09	0.28	0.04	3.59	0.31
29	66.58	19.18	4.29	2.64	0.06	0.29	0.04	3.47	0.22
30	82.26	8.05	2.65	1.87	0.03	0.10	0.02	10.22	0.33
31	67.82	18.32	5.62	2.34	0.08	0.27	0.03	3.70	0.31
32	67.57	18.33	5.59	1.66	0.08	0.27	0.02	3.69	0.30
33	66.11	20.92	3.97	1.19	0.06	0.32	0.02	3.16	0.19
34	65.65	19.03	4.43	2.66	0.07	0.29	0.04	3.45	0.23
35	70.04	16	5.17	2.21	0.07	0.23	0.03	4.38	0.32
36	70.07	14.86	3.68	1.35	0.05	0.21	0.02	4.72	0.25
37	68.98	20.18	3.48	1.78	0.05	0.29	0.03	3.42	0.17
38	66.66	17.21	3.28	2.65	0.05	0.26	0.04	3.87	0.19
39	58.76	19.97	5.66	2.91	0.10	0.34	0.05	2.94	0.28
40	71.68	15.68	3.74	1.42	0.05	0.22	0.02	4.57	0.24
41	66.57	17.4	5.01	1.85	0.08	0.26	0.03	3.83	0.29
42	66.87	19.19	5.74	2.09	0.09	0.29	0.03	3.48	0.30
43	72.84	18.76	2.96	1.33	0.04	0.26	0.02	3.88	0.16
44	62.09	19.35	4.92	2.54	0.08	0.31	0.04	3.21	0.25

45	65.05	16.45	4.72	2.05	0.07	0.25	0.03	3.95	0.29
46	63.83	20.24	3.53	1.88	0.06	0.32	0.03	3.15	0.17
47	68.91	16.79	4.73	1.23	0.07	0.24	0.02	4.10	0.28
48	69.91	19.62	4.75	0.89	0.07	0.28	0.01	3.56	0.24
49	67.72	19.16	5.17	1.62	0.08	0.28	0.02	3.53	0.27
50	63.93	19.58	5.25	1.36	0.08	0.31	0.02	3.27	0.27
51	71.99	16.32	4.9	1.32	0.07	0.23	0.02	4.41	0.30
52	64.57	18.02	6.08	2.22	0.09	0.28	0.03	3.58	0.34
53	67.28	17.48	6.65	1.3	0.10	0.26	0.02	3.85	0.38
54	64.01	18.28	5.61	2.39	0.09	0.29	0.04	3.50	0.31
55	62.47	19.76	5.73	1.98	0.09	0.32	0.03	3.16	0.29
56	65.13	19.86	4.55	2.83	0.07	0.30	0.04	3.28	0.23
57	68.93	20.96	3.61	1.9	0.05	0.30	0.03	3.29	0.17

Table C.11: Atomic ratio for S0 (28days)

	Calcium	Silicon	Aluminium	Sulfur	Al/Ca	Si/Ca	S/Ca	Ca/Si	Al/Si
1	43.81	39.67	6.87	2.55	0.16	0.91	0.06	1.10	0.17
2	55.96	28.73	7.16	2.27	0.13	0.51	0.04	1.95	0.25
3	50.57	32.26	5.68	1.83	0.11	0.64	0.04	1.57	0.18
4	51.41	32.15	7.91	2.51	0.15	0.63	0.05	1.60	0.25
5	58.41	25.02	7.61	1.61	0.13	0.43	0.03	2.33	0.30
6	67.3	18.93	6.43	2.62	0.10	0.28	0.04	3.56	0.34
7	55.65	29.77	6.59	1.96	0.12	0.53	0.04	1.87	0.22
8	52.88	30.01	6.95	2.3	0.13	0.57	0.04	1.76	0.23
9	53.73	29.63	8.69	2.9	0.16	0.55	0.05	1.81	0.29
10	54.87	26.71	7.67	1.76	0.14	0.49	0.03	2.05	0.29
11	45.26	42.57	5.94	2.05	0.13	0.94	0.05	1.06	0.14
12	53.14	30.44	8.34	2.4	0.16	0.57	0.05	1.75	0.27
13	47.88	40.17	6.36	0.97	0.13	0.84	0.02	1.19	0.16
14	47.98	36.94	6.82	2.13	0.14	0.77	0.04	1.30	0.18
15	53.36	28.98	9.43	1.11	0.18	0.54	0.02	1.84	0.33
16	51.46	29.53	7.86	1.6	0.15	0.57	0.03	1.74	0.27
17	30.29	57.93	4.74	2.15	0.16	1.91	0.07	0.52	0.08
18	35.34	50.26	4.66	3.01	0.13	1.42	0.09	0.70	0.09
19	35.68	53.91	6.05	0.68	0.17	1.51	0.02	0.66	0.11
20	58.04	30.31	4.92	1.39	0.08	0.52	0.02	1.91	0.16
21	61.33	21.19	8.38	0.76	0.14	0.35	0.01	2.89	0.40
22	49.16	31.16	8.52	1.78	0.17	0.63	0.04	1.58	0.27
23	59.36	27.51	7.09	1.25	0.12	0.46	0.02	2.16	0.26
24	56.41	26.81	8.46	2.66	0.15	0.48	0.05	2.10	0.32
25	52.14	35.87	5.91	2.33	0.11	0.69	0.04	1.45	0.16
26	59.22	26.52	6.76	0.99	0.11	0.45	0.02	2.23	0.25
27	55.13	29.28	6.16	0.95	0.11	0.53	0.02	1.88	0.21
28	56.51	30.58	5.56	1.74	0.10	0.54	0.03	1.85	0.18
29	56.27	25.84	6.94	2.01	0.12	0.46	0.04	2.18	0.27
30	53.26	27.29	7.71	1.88	0.14	0.51	0.04	1.95	0.28
31	41.7	41.26	7.49	1.21	0.18	0.99	0.03	1.01	0.18
32	42.22	44.36	4.66	1.52	0.11	1.05	0.04	0.95	0.11
33	57.33	26.25	5.02	1.12	0.09	0.46	0.02	2.18	0.19
34	54.21	23.53	7.13	2.18	0.13	0.43	0.04	2.30	0.30
35	56.43	28.47	7.49	1.57	0.13	0.50	0.03	1.98	0.26
36	41.04	40.22	7.12	1.97	0.17	0.98	0.05	1.02	0.18
37	30.79	48.65	8.32	1.46	0.27	1.58	0.05	0.63	0.17
38	44.28	30.02	11.4	2.27	0.26	0.68	0.05	1.48	0.38
39	50.83	36.95	5.68	1.56	0.11	0.73	0.03	1.38	0.15
40	38.53	36.13	9.74	2.73	0.25	0.94	0.07	1.07	0.27
41	34.74	58.21	3.12	0.85	0.09	1.68	0.02	0.60	0.05
42	49.99	37.11	5.3	1.45	0.11	0.74	0.03	1.35	0.14
43	34.07	56.04	3.86	1.46	0.11	1.64	0.04	0.61	0.07
44	32.49	38.86	15.11	1.1	0.47	1.20	0.03	0.84	0.39

45	34.16	55.68	4.99	0.87	0.15	1.63	0.03	0.61	0.09
46	45.6	32.99	9.28	1.74	0.20	0.72	0.04	1.38	0.28
47	34.08	53.69	3.7	1.41	0.11	1.58	0.04	0.63	0.07
48	32.43	56.33	4.74	2.06	0.15	1.74	0.06	0.58	0.08
49	52.51	34.79	6.73	1.29	0.13	0.66	0.02	1.51	0.19
50	16.07	78.82	2.16	0.68	0.13	4.90	0.04	0.20	0.03
51	43.62	41.38	6.58	2.51	0.15	0.95	0.06	1.05	0.16
52	59.29	26.21	7.09	2.34	0.12	0.44	0.04	2.26	0.27
53	62.4	22.87	7.65	1.43	0.12	0.37	0.02	2.73	0.33
54	44.28	29.88	9.75	3.32	0.22	0.67	0.07	1.48	0.33
55	53.32	34.6	4.55	1.71	0.09	0.65	0.03	1.54	0.13
56	57.26	25.6	661	1.64	11.54	0.45	0.03	2.24	25.82
57	55.07	28.7	7.14	2	0.13	0.52	0.04	1.92	0.25
58	52.7	31.28	6.89	3.17	0.13	0.59	0.06	1.68	0.22
59	51.96	33.43	4.95	2.47	0.10	0.64	0.05	1.55	0.15
60	47.7	40.95	4.97	2.29	0.10	0.86	0.05	1.16	0.12
61	47	27.04	10.62	2.42	0.23	0.58	0.05	1.74	0.39
62	54.92	27.84	7.03	2.51	0.13	0.51	0.05	1.97	0.25

Table C.12: Atomic ratio for S60 (28days)

	Calcium	Silicon	Aluminium	Sulfur	Al/Ca	Si/Ca	S/Ca	Ca/Si	Al/Si
1	54.98	27.78	9.19	1.81	0.17	0.51	0.03	1.98	0.33
2	38.63	37.23	12.16	1.77	0.31	0.96	0.05	1.04	0.33
3	52.29	35.19	5.53	2.01	0.11	0.67	0.04	1.49	0.16
4	58.38	29.7	5.82	1.65	0.10	0.51	0.03	1.97	0.20
5	58.58	24.98	7.78	1.18	0.13	0.43	0.02	2.35	0.31
6	49	31.89	8.41	2.23	0.17	0.65	0.05	1.54	0.26
7	52.59	27.33	8.2	2.29	0.16	0.52	0.04	1.92	0.30
8	51.16	33.5	5.74	1.56	0.11	0.65	0.03	1.53	0.17
9	61.35	23.67	6.38	2.14	0.10	0.39	0.03	2.59	0.27
10	60.03	26.89	6.33	1.42	0.11	0.45	0.02	2.23	0.24
11	52.02	25.17	10.13	1.56	0.19	0.48	0.03	2.07	0.40
12	50.85	33.02	6.65	1.85	0.13	0.65	0.04	1.54	0.20
13	49.97	33.78	6.26	2.5	0.13	0.68	0.05	1.48	0.19
14	31.07	51.18	7.98	1.57	0.26	1.65	0.05	0.61	0.16
15	57.48	24.8	6.36	2.16	0.11	0.43	0.04	2.32	0.26
16	50.72	28.65	8.78	3.02	0.17	0.56	0.06	1.77	0.31
17	62.33	23.99	6.03	1.47	0.10	0.38	0.02	2.60	0.25
18	54.34	26.11	8.12	3.07	0.15	0.48	0.06	2.08	0.31
19	29.32	54.45	5.77	1.28	0.20	1.86	0.04	0.54	0.11
20	52.74	31.35	6.37	2.12	0.12	0.59	0.04	1.68	0.20
21	52.76	28.63	8.52	2.13	0.16	0.54	0.04	1.84	0.30
22	65.2	23.99	4.58	1.11	0.07	0.37	0.02	2.72	0.19
23	63.36	23.08	5.54	2.39	0.09	0.36	0.04	2.75	0.24
24	59.46	25.28	6.67	1.91	0.11	0.43	0.03	2.35	0.26
25	49.93	36.3	6.39	2.91	0.13	0.73	0.06	1.38	0.18
26	56.67	29.07	6.35	2.1	0.11	0.51	0.04	1.95	0.22
27	55.65	28.74	6.72	2.01	0.12	0.52	0.04	1.94	0.23
28	45.88	33.51	6.86	1.81	0.15	0.73	0.04	1.37	0.20
29	54.43	31.29	5.66	1.79	0.10	0.57	0.03	1.74	0.18
30	50.7	32.88	7.22	2.69	0.14	0.65	0.05	1.54	0.22
31	55.56	26.53	6.04	1.43	0.11	0.48	0.03	2.09	0.23
32	42.89	33.16	11.63	1.49	0.27	0.77	0.03	1.29	0.35
33	59.74	23.78	6.98	1.16	0.12	0.40	0.02	2.51	0.29
34	56.65	27.57	5.7	1.71	0.10	0.49	0.03	2.05	0.21
35	53.36	22.06	5.86	8.03	0.11	0.41	0.15	2.42	0.27
36	57.86	25.7	6.26	2.27	0.11	0.44	0.04	2.25	0.24
37	14.99	77.3	2.62	1.79	0.17	5.16	0.12	0.19	0.03
38	57.37	28.46	7.75	1.7	0.14	0.50	0.03	2.02	0.27
39	59.04	26.03	7.07	2.83	0.12	0.44	0.05	2.27	0.27
40	55.4	29.27	7.12	1.88	0.13	0.53	0.03	1.89	0.24
41	54.84	31.61	5.71	1.58	0.10	0.58	0.03	1.73	0.18
42	57.21	26.85	6.47	2.4	0.11	0.47	0.04	2.13	0.24
43	47.58	39.2	4.95	1.94	0.10	0.82	0.04	1.21	0.13
44	51.72	28.56	7.53	1.75	0.15	0.55	0.03	1.81	0.26

45	53.33	32.16	7.24	1.31	0.14	0.60	0.02	1.66	0.23
46	62.47	24.07	5.98	1.54	0.10	0.39	0.02	2.60	0.25
47	40.68	47.52	4.93	2.96	0.12	1.17	0.07	0.86	0.10
48	63.6	27.15	4.09	1.97	0.06	0.43	0.03	2.34	0.15
49	47.13	35.62	6.34	1.66	0.13	0.76	0.04	1.32	0.18
50	54.25	29.97	7.56	1.66	0.14	0.55	0.03	1.81	0.25
51	40.46	50.76	3.58	1.42	0.09	1.25	0.04	0.80	0.07
52	60.34	25.79	5.66	1.77	0.09	0.43	0.03	2.34	0.22
53	57.47	25.81	5.73	1.97	0.10	0.45	0.03	2.23	0.22
54	44.18	21.37	9	2.86	0.20	0.48	0.06	2.07	0.42
55	41.35	47.3	4.94	2.31	0.12	1.14	0.06	0.87	0.10

Table C.13: Atomic ratio for S200 (28days)

	Calcium	Silicon	Aluminium	Sulfur	Al/Ca	Si/Ca	S/Ca	Ca/Si	Al/Si
1	46.25	30.11	8.01	3.08	0.17	0.65	0.07	1.54	0.27
2	59.27	23.76	7.05	1.29	0.12	0.40	0.02	2.49	0.30
3	52.27	28.69	8.68	1.53	0.17	0.55	0.03	1.82	0.30
4	56	25.84	7.49	2.41	0.13	0.46	0.04	2.17	0.29
5	59.97	23.74	7.14	1.62	0.12	0.40	0.03	2.53	0.30
6	55.5	29.62	8.31	1.94	0.15	0.53	0.03	1.87	0.28
7	60.78	26.38	4.48	1.48	0.07	0.43	0.02	2.30	0.17
8	57.17	26.49	7.35	3.03	0.13	0.46	0.05	2.16	0.28
9	54.24	27.5	8.37	1.78	0.15	0.51	0.03	1.97	0.30
10	61.33	24.92	5.92	2.09	0.10	0.41	0.03	2.46	0.24
11	47.84	34.02	9.37	1.46	0.20	0.71	0.03	1.41	0.28
12	61.81	22.29	6.93	1.87	0.11	0.36	0.03	2.77	0.31
13	47.99	30.07	9.07	1.69	0.19	0.63	0.04	1.60	0.30
14	53.02	24.87	10.71	3.6	0.20	0.47	0.07	2.13	0.43
15	60.89	24.53	4.79	1.36	0.08	0.40	0.02	2.48	0.20
16	48.56	32.76	9.28	1.47	0.19	0.67	0.03	1.48	0.28
17	31.27	53.35	7.13	1.79	0.23	1.71	0.06	0.59	0.13
18	60.53	21.12	7.54	3.32	0.12	0.35	0.05	2.87	0.36
19	38.23	37.93	11.02	1.27	0.29	0.99	0.03	1.01	0.29
20	46.11	38.39	6.59	2.08	0.14	0.83	0.05	1.20	0.17
21	58.06	25.15	7.74	1.64	0.13	0.43	0.03	2.31	0.31
22	57.1	24.72	6.82	2.26	0.12	0.43	0.04	2.31	0.28
23	55.21	24.74	8.39	2.65	0.15	0.45	0.05	2.23	0.34
24	48.85	31.6	10.24	2.68	0.21	0.65	0.05	1.55	0.32
25	53.61	26.08	8.19	1.82	0.15	0.49	0.03	2.06	0.31
26	46.7	37.79	6.59	1.72	0.14	0.81	0.04	1.24	0.17
27	55.14	27.27	7.65	1.77	0.14	0.49	0.03	2.02	0.28
28	58.89	24.1	6.78	2.49	0.12	0.41	0.04	2.44	0.28
29	53.21	27.13	9.23	1.85	0.17	0.51	0.03	1.96	0.34
30	42.73	37.72	7.51	2.19	0.18	0.88	0.05	1.13	0.20
31	55.51	25.76	7.89	2.6	0.14	0.46	0.05	2.15	0.31
32	56.94	29.08	5.16	2.1	0.09	0.51	0.04	1.96	0.18
33	54.59	27.3	6.58	2.64	0.12	0.50	0.05	2.00	0.24
34	51.6	28.32	10.06	3.4	0.19	0.55	0.07	1.82	0.36
35	51.43	28.23	9.3	2.15	0.18	0.55	0.04	1.82	0.33
36	48.85	30.6	10.46	2.31	0.21	0.63	0.05	1.60	0.34
37	57.54	22.64	6.86	2.13	0.12	0.39	0.04	2.54	0.30
38	40.2	46.35	6.02	1.42	0.15	1.15	0.04	0.87	0.13
39	24.26	59.26	7.46	1.37	0.31	2.44	0.06	0.41	0.13
40	55.67	26.95	5.53	1	0.10	0.48	0.02	2.07	0.21
41	50.57	32.71	7.45	1.89	0.15	0.65	0.04	1.55	0.23
42	31.98	39.7	12.82	1.98	0.40	1.24	0.06	0.81	0.32
43	62.67	27.44	3.56	1.41	0.06	0.44	0.02	2.28	0.13

44	58.8	25.84	8.36	2.77	0.14	0.44	0.05	2.28	0.32
45	42.49	33.12	10.01	2.5	0.24	0.78	0.06	1.28	0.30
46	42.76	40.83	6.78	2.13	0.16	0.95	0.05	1.05	0.17
47	53.72	24.38	8.54	3.41	0.16	0.45	0.06	2.20	0.35
48	57.11	25.49	6.92	2.13	0.12	0.45	0.04	2.24	0.27
49	57.32	25.51	6.38	3.21	0.11	0.45	0.06	2.25	0.25
50	52.29	27.14	8.8	2.36	0.17	0.52	0.05	1.93	0.32
51	56.01	26.25	8.46	1.62	0.15	0.47	0.03	2.13	0.32
52	44.16	40.38	7.22	2.25	0.16	0.91	0.05	1.09	0.18
53	60.43	24.85	5.03	1.95	0.08	0.41	0.03	2.43	0.20
54	49.92	28.62	10.19	2.28	0.20	0.57	0.05	1.74	0.36
55	47.53	32.2	7.23	1.88	0.15	0.68	0.04	1.48	0.22
56	44.01	36.23	8.03	2.59	0.18	0.82	0.06	1.21	0.22
57	60.29	21.36	6.3	1.87	0.10	0.35	0.03	2.82	0.29
58	55.56	29.75	5.15	2.01	0.09	0.54	0.04	1.87	0.17
59	57.42	25.23	6.36	2.51	0.11	0.44	0.04	2.28	0.25
60	55.46	27.92	6.1	2.53	0.11	0.50	0.05	1.99	0.22

Table C.14: Atomic ratio for D0 (28days)

	Calcium	Silicon	Aluminium	Sulfur	Al/Ca	Si/Ca	S/Ca	Ca/Si	Al/Si
1	33.8	34.17	10.19	1.07	0.30	1.01	0.03	0.99	0.30
2	43.41	16.79	7.68	1.83	0.18	0.39	0.04	2.59	0.46
3	58.43	20.15	3.83	0.99	0.07	0.34	0.02	2.90	0.19
4	63	20.25	4.64	1.31	0.07	0.32	0.02	3.11	0.23
5	50.57	24.52	7.26	0.8	0.14	0.48	0.02	2.06	0.30
6	47.26	25.62	8.34	1.94	0.18	0.54	0.04	1.84	0.33
7	43.78	28.76	6.55	1.71	0.15	0.66	0.04	1.52	0.23
8	29.28	39.93	5.72	0.77	0.20	1.36	0.03	0.73	0.14
9	43.58	26.72	5.75	1.85	0.13	0.61	0.04	1.63	0.22
10	26.83	12.9	3.35	0.46	0.12	0.48	0.02	2.08	0.26
11	63.79	22.74	5.34	1.13	0.08	0.36	0.02	2.81	0.23
12	54.28	20.68	6.53	1.46	0.12	0.38	0.03	2.62	0.32
13	58.86	22.21	6.45	1.32	0.11	0.38	0.02	2.65	0.29
14	28.12	36.42	14.06	1.71	0.50	1.30	0.06	0.77	0.39
15	46.63	29.16	8.05	2.41	0.17	0.63	0.05	1.60	0.28
16	56.83	21.64	5.13	1.21	0.09	0.38	0.02	2.63	0.24
17	40.09	28.83	12.5	2.14	0.31	0.72	0.05	1.39	0.43
18	50.24	19.85	7.59	2.89	0.15	0.40	0.06	2.53	0.38
19	59.75	4.32	1.52	0.34	0.03	0.07	0.01	13.83	0.35
20	49.67	22.76	7.18	1.77	0.14	0.46	0.04	2.18	0.32
21	38.37	34.37	13.51	1.4	0.35	0.90	0.04	1.12	0.39
22	19.14	49.2	21.65	0.26	1.13	2.57	0.01	0.39	0.44
23	60.05	15.8	8.21	0.87	0.14	0.26	0.01	3.80	0.52
24	55.55	21.52	7	1.88	0.13	0.39	0.03	2.58	0.33
25	33.56	33.5	14.23	0.94	0.42	1.00	0.03	1.00	0.42
26	56.56	8.09	2.93	0.44	0.05	0.14	0.01	6.99	0.36
27	65.75	21.48	5.28	1.61	0.08	0.33	0.02	3.06	0.25
28	47.74	27.15	8.63	0.46	0.18	0.57	0.01	1.76	0.32
29	53.51	25.48	10.01	1.06	0.19	0.48	0.02	2.10	0.39
30	51.92	20.03	6.02	1.12	0.12	0.39	0.02	2.59	0.30
31	49.02	17.86	4.65	0.55	0.09	0.36	0.01	2.74	0.26
32	47.8	21.36	5.91	1.49	0.12	0.45	0.03	2.24	0.28
33	46.54	26.9	7.56	1.59	0.16	0.58	0.03	1.73	0.28
34	54.93	21.29	6.69	1.34	0.12	0.39	0.02	2.58	0.31
35	48.06	24.38	6.01	1.3	0.13	0.51	0.03	1.97	0.25
36	14.91	48.41	27.24	0.27	1.83	3.25	0.02	0.31	0.56
37	65.39	17.2	5.14	1.33	0.08	0.26	0.02	3.80	0.30
38	46.7	27.43	7.83	1.56	0.17	0.59	0.03	1.70	0.29
39	40.94	28.08	10.06	1.26	0.25	0.69	0.03	1.46	0.36
40	58.79	21.01	6.96	2.04	0.12	0.36	0.03	2.80	0.33
41	44.04	24.78	4.43	1.83	0.10	0.56	0.04	1.78	0.18
42	58.14	22.53	4.08	0.91	0.07	0.39	0.02	2.58	0.18
43	49.73	26.62	6.69	1.23	0.13	0.54	0.02	1.87	0.25
44	39.73	33.88	11.13	1.12	0.28	0.85	0.03	1.17	0.33

45	47.28	28.25	4.47	1.19	0.09	0.60	0.03	1.67	0.16
46	49.58	20.96	9.94	0.54	0.20	0.42	0.01	2.37	0.47
47	33.02	36.07	8.44	1.27	0.26	1.09	0.04	0.92	0.23
48	46.34	27.37	10.32	2.08	0.22	0.59	0.04	1.69	0.38
49	50.09	20.08	7.42	2.18	0.15	0.40	0.04	2.49	0.37
50	55.2	20.46	5.34	2.15	0.10	0.37	0.04	2.70	0.26
51	46.89	22.11	6.77	2.35	0.14	0.47	0.05	2.12	0.31
52	49.86	19.22	7.33	1.5	0.15	0.39	0.03	2.59	0.38
53	52.66	25.25	7.46	1.2	0.14	0.48	0.02	2.09	0.30
54	33.79	33.66	19.13	0.5	0.57	1.00	0.01	1.00	0.57
55	48.85	25.71	5.65	1.44	0.12	0.53	0.03	1.90	0.22
56	32.12	32.68	13.41	1.03	0.42	1.02	0.03	0.98	0.41
57	35.53	29.84	9.31	1.36	0.26	0.84	0.04	1.19	0.31
58	43.74	25.34	9.35	1.24	0.21	0.58	0.03	1.73	0.37
59	53.12	24.83	5	1.28	0.09	0.47	0.02	2.14	0.20
60	31.65	40.47	4.14	1.56	0.13	1.28	0.05	0.78	0.10
61	45.27	27.78	7.85	1.24	0.17	0.61	0.03	1.63	0.28
62	37.14	12.3	6.4	1.05	0.17	0.33	0.03	3.02	0.52

Table C.15: Atomic ratio for D60 (28days)

	Calcium	Silicon	Aluminium	Sulfur	Al/Ca	Si/Ca	S/Ca	Ca/Si	Al/Si
1	61.71	25.73	6	1.54	0.10	0.42	0.02	2.40	0.23
2	51.92	30.37	7.3	1.92	0.14	0.58	0.04	1.71	0.24
3	64.97	18.09	3.47	2.43	0.05	0.28	0.04	3.59	0.19
4	61.38	23.07	7.22	1.94	0.12	0.38	0.03	2.66	0.31
5	41.95	48.26	3.9	1.45	0.09	1.15	0.03	0.87	0.08
6	52.73	24.8	8.87	1.95	0.17	0.47	0.04	2.13	0.36
7	27.94	38.55	3.33	0.77	0.12	1.38	0.03	0.72	0.09
8	50.67	28.9	9.5	1.43	0.19	0.57	0.03	1.75	0.33
9	54.1	23.71	7.29	1.82	0.13	0.44	0.03	2.28	0.31
10	56.09	23.01	8.15	2.4	0.15	0.41	0.04	2.44	0.35
11	58.94	25.28	6.56	0.95	0.11	0.43	0.02	2.33	0.26
12	57.2	26.06	6.63	1.75	0.12	0.46	0.03	2.19	0.25
13	59.39	25.32	6.94	1.64	0.12	0.43	0.03	2.35	0.27
14	56.99	23.92	7.47	1.93	0.13	0.42	0.03	2.38	0.31
15	58.64	24.19	5.93	2.45	0.10	0.41	0.04	2.42	0.25
16	65	18.06	7.97	1.85	0.12	0.28	0.03	3.60	0.44
17	28.98	62.29	3.48	1.38	0.12	2.15	0.05	0.47	0.06
18	50.11	30.91	6.85	1.55	0.14	0.62	0.03	1.62	0.22
19	62.36	24.84	5.43	1.55	0.09	0.40	0.02	2.51	0.22
20	47.36	31.59	7.08	2.14	0.15	0.67	0.05	1.50	0.22
21	60.56	30.12	3.41	1.05	0.06	0.50	0.02	2.01	0.11
22	53.39	26.73	7.74	1.76	0.14	0.50	0.03	2.00	0.29
23	59.3	22.97	7.52	1.73	0.13	0.39	0.03	2.58	0.33
24	53.97	24.38	7.36	2.45	0.14	0.45	0.05	2.21	0.30
25	52.24	26.66	9.83	2.57	0.19	0.51	0.05	1.96	0.37
26	50.1	30.99	8.43	1.81	0.17	0.62	0.04	1.62	0.27
27	51.17	29.98	9.4	1.61	0.18	0.59	0.03	1.71	0.31
28	57.75	24.97	8.77	2.09	0.15	0.43	0.04	2.31	0.35
29	49.04	29.91	9.36	2.42	0.19	0.61	0.05	1.64	0.31
30	59.16	25.79	5.78	2.26	0.10	0.44	0.04	2.29	0.22
31	48.83	38.28	5.26	1.63	0.11	0.78	0.03	1.28	0.14
32	58.58	21.67	10.26	1.52	0.18	0.37	0.03	2.70	0.47
33	55.88	26.47	8.26	2.08	0.15	0.47	0.04	2.11	0.31
34	29.78	45.53	11.12	1.53	0.37	1.53	0.05	0.65	0.24
35	41.72	34.29	13.67	1.59	0.33	0.82	0.04	1.22	0.40
36	60.34	22.26	5.37	2.97	0.09	0.37	0.05	2.71	0.24
37	51.54	27.088	12	1.73	0.23	0.53	0.03	1.90	0.44
38	49.27	23.83	8.59	2.29	0.17	0.48	0.05	2.07	0.36
39	53.2	30.43	5.95	2.6	0.11	0.57	0.05	1.75	0.20
40	47.25	29.46	10.56	2.05	0.22	0.62	0.04	1.60	0.36
41	17.48	50.35	16.76	0.46	0.96	2.88	0.03	0.35	0.33
42	60.82	23.78	6.61	1.42	0.11	0.39	0.02	2.56	0.28
43	64.93	20.02	5.77	2.36	0.09	0.31	0.04	3.24	0.29
44	63.33	19.35	7.81	1.82	0.12	0.31	0.03	3.27	0.40

45	66.47	18.87	6.04	1.21	0.09	0.28	0.02	3.52	0.32
46	48.05	31.56	10.87	1.13	0.23	0.66	0.02	1.52	0.34
47	49.98	29.41	7.96	2.52	0.16	0.59	0.05	1.70	0.27
48	57.52	21.59	6.23	2.78	0.11	0.38	0.05	2.66	0.29
49	52.77	27.38	9.58	0.96	0.18	0.52	0.02	1.93	0.35
50	63.26	21.89	6.32	1.87	0.10	0.35	0.03	2.89	0.29
51	64.81	21.49	5.43	0.4	0.08	0.33	0.01	3.02	0.25
52	52.76	26.9	10.66	1.55	0.20	0.51	0.03	1.96	0.40
53	57.55	25.31	7.65	1.53	0.13	0.44	0.03	2.27	0.30
54	53.35	28.31	8.32	2.35	0.16	0.53	0.04	1.88	0.29
55	51.43	27.22	8.4	2.84	0.16	0.53	0.06	1.89	0.31
56	57.51	25.23	8.81	1.91	0.15	0.44	0.03	2.28	0.35
57	56.81	25	8.74	1.58	0.15	0.44	0.03	2.27	0.35
58	57.56	25.93	6.61	2.27	0.11	0.45	0.04	2.22	0.25
59	54.42	32.13	4.97	1.86	0.09	0.59	0.03	1.69	0.15
60	9.51	89.4	0.63	0.25	0.07	9.40	0.03	0.11	0.01
61	38.37	38.04	11.51	1.1	0.30	0.99	0.03	1.01	0.30
62	42.64	33.38	8.64	1.2	0.20	0.78	0.03	1.28	0.26

Table C.16: Atomic ratio for D200 (28days)

	Calcium	Silicon	Aluminium	Sulfur	Al/Ca	Si/Ca	S/Ca	Ca/Si	Al/Si
1	65.74	30.78	1.75	0	0.03	0.47	0.00	2.14	0.06
2	55.48	25.88	8.43	1.85	0.15	0.47	0.03	2.14	0.33
3	47.9	20	19.18	0	0.40	0.42	0.00	2.40	0.96
4	51.65	30.04	7.87	2.19	0.15	0.58	0.04	1.72	0.26
5	50.36	35.62	5.82	1.17	0.12	0.71	0.02	1.41	0.16
6	56.3	28.14	8.38	1.73	0.15	0.50	0.03	2.00	0.30
7	57.48	26.1	7.96	0.91	0.14	0.45	0.02	2.20	0.30
8	60.59	23.29	8.59	2.4	0.14	0.38	0.04	2.60	0.37
9	60.63	21.2	8.6	0.9	0.14	0.35	0.01	2.86	0.41
10	41.12	38.29	8.82	1.61	0.21	0.93	0.04	1.07	0.23
11	50.1	36.95	5.6	1.96	0.11	0.74	0.04	1.36	0.15
12	58.64	25.79	8.37	1.59	0.14	0.44	0.03	2.27	0.32
13	58.4	23.56	8.62	1.38	0.15	0.40	0.02	2.48	0.37
14	55.48	27.87	9.11	1.77	0.16	0.50	0.03	1.99	0.33
15	6.85	84.04	5.07	1.69	0.74	12.27	0.25	0.08	0.06
16	41.3	34.11	10.85	2.46	0.26	0.83	0.06	1.21	0.32
17	59.65	23.38	8.13	0.42	0.14	0.39	0.01	2.55	0.35
18	59.96	19.9	10	2.18	0.17	0.33	0.04	3.01	0.50
19	53.04	26.97	7.71	0.84	0.15	0.51	0.02	1.97	0.29
20	62.53	23.65	6.93	1.63	0.11	0.38	0.03	2.64	0.29
21	65.92	25.32	5.66	0.95	0.09	0.38	0.01	2.60	0.22
22	44.33	37.14	10.51	2.51	0.24	0.84	0.06	1.19	0.28
23	65.19	20.16	5.53	1.69	0.08	0.31	0.03	3.23	0.27
24	63.24	21.14	8.01	1.51	0.13	0.33	0.02	2.99	0.38
25	93.27	2.24	0.73	1.01	0.01	0.02	0.01	41.64	0.33
26	59.89	24.16	5.84	1.11	0.10	0.40	0.02	2.48	0.24
27	59.23	25.73	4.6	0.57	0.08	0.43	0.01	2.30	0.18
28	66.03	17.75	6.73	0.86	0.10	0.27	0.01	3.72	0.38
29	26.54	45.24	18.15	1.69	0.68	1.70	0.06	0.59	0.40
30	35.22	37.28	20.68	0.22	0.59	1.06	0.01	0.94	0.55
31	65.74	23.13	4.11	1.15	0.06	0.35	0.02	2.84	0.18
32	55.55	30.77	5.95	1.89	0.11	0.55	0.03	1.81	0.19
33	52.71	29	9.62	1.73	0.18	0.55	0.03	1.82	0.33
34	18.7	45.56	22.77	0.91	1.22	2.44	0.05	0.41	0.50
35	51.59	34.09	8.13	1.28	0.16	0.66	0.02	1.51	0.24
36	49.1	29.33	13.02	0.84	0.27	0.60	0.02	1.67	0.44
37	42.55	28.88	15.32	1.77	0.36	0.68	0.04	1.47	0.53
38	1.99	50.58	2.66	0	1.34	25.42	0.00	0.04	0.05
39	46.63	31.03	9.09	1.62	0.19	0.67	0.03	1.50	0.29
40	36.92	36.41	11.22	2.28	0.30	0.99	0.06	1.01	0.31
41	52.93	30.39	9.42	0.63	0.18	0.57	0.01	1.74	0.31
42	16.41	49.28	21.18	0.27	1.29	3.00	0.02	0.33	0.43
43	55.37	25.1	9.5	1.95	0.17	0.45	0.04	2.21	0.38
44	59.55	28.62	4.5	2.53	0.08	0.48	0.04	2.08	0.16

45	39.15	39.26	10.18	1.63	0.26	1.00	0.04	1.00	0.26
46	43.59	31.19	7.64	0.87	0.18	0.72	0.02	1.40	0.24
47	57.45	26.76	6.72	0.73	0.12	0.47	0.01	2.15	0.25
48	48.89	31.74	8.85	0.76	0.18	0.65	0.02	1.54	0.28
49	54.62	27.48	9.83	1.61	0.18	0.50	0.03	1.99	0.36
50	50.58	33.78	7	1.95	0.14	0.67	0.04	1.50	0.21
51	54.6	29.59	8.01	1.03	0.15	0.54	0.02	1.85	0.27
52	65.99	19.94	6.62	0.5	0.10	0.30	0.01	3.31	0.33
53	53.61	27.7	7.87	1.03	0.15	0.52	0.02	1.94	0.28
54	38.57	37.39	12.54	1.37	0.33	0.97	0.04	1.03	0.34
55	43.51	32.5	14.02	2.32	0.32	0.75	0.05	1.34	0.43
56	21.33	42.33	4.72	0.29	0.22	1.98	0.01	0.50	0.11
57	50.78	32.47	7.53	1.81	0.15	0.64	0.04	1.56	0.23
58	47.8	32.35	8.09	2.4	0.17	0.68	0.05	1.48	0.25
59	52.71	29.59	8.15	1.66	0.15	0.56	0.03	1.78	0.28
60	56.49	23.96	8.51	1.38	0.15	0.42	0.02	2.36	0.36
61	54.89	26.32	10.99	1.47	0.20	0.48	0.03	2.09	0.42
62	51.7	29.68	7.73	2.62	0.15	0.57	0.05	1.74	0.26

Table C.17: Atomic ratio for G0 (28days)

	Calcium	Silicon	Aluminium	Sulfur	Al/Ca	Si/Ca	S/Ca	Ca/Si	Al/Si
1	58.73	21.72	5.93	1.78	0.10	0.37	0.03	2.70	0.27
2	56.02	19.09	9.56	1.11	0.17	0.34	0.02	2.93	0.50
3	56.3	29.88	6.41	1.29	0.11	0.53	0.02	1.88	0.21
4	53.66	19.76	11.23	0.86	0.21	0.37	0.02	2.72	0.57
5	60.32	20.24	7.2	2.73	0.12	0.34	0.05	2.98	0.36
6	53.16	29.13	6.35	2.25	0.12	0.55	0.04	1.82	0.22
7	33.09	37.29	13.29	0.99	0.40	1.13	0.03	0.89	0.36
8	50.78	31.99	9.85	2.2	0.19	0.63	0.04	1.59	0.31
9	48.18	36.62	6.64	2.06	0.14	0.76	0.04	1.32	0.18
10	46.12	30.44	8.68	2.23	0.19	0.66	0.05	1.52	0.29
11	51.16	29.64	8.02	2.12	0.16	0.58	0.04	1.73	0.27
12	32.12	31.07	12.84	1.72	0.40	0.97	0.05	1.03	0.41
13	58.84	20.81	7.6	2.22	0.13	0.35	0.04	2.83	0.37
14	58.46	26.6	7.73	2.03	0.13	0.46	0.03	2.20	0.29
15	43.96	29.79	8.56	1.84	0.19	0.68	0.04	1.48	0.29
16	62.46	17.42	9.76	2.69	0.16	0.28	0.04	3.59	0.56
17	40.65	39.07	10.2	2.12	0.25	0.96	0.05	1.04	0.26
18	6.19	58.02	16.75	0.09	2.71	9.37	0.01	0.11	0.29
19	52.87	25.02	8.85	4.55	0.17	0.47	0.09	2.11	0.35
20	42.99	33.91	12.48	1.64	0.29	0.79	0.04	1.27	0.37
21	48.33	37.9	6.72	1.5	0.14	0.78	0.03	1.28	0.18
22	51.41	27.63	11.18	1.31	0.22	0.54	0.03	1.86	0.40
23	35.69	34.45	13.15	2.53	0.37	0.97	0.07	1.04	0.38
24	42.2	40.9	6.96	2.93	0.16	0.97	0.07	1.03	0.17
25	62.91	13.69	5.55	1.1	0.09	0.22	0.02	4.60	0.41
26	54.01	30.61	6.52	1.94	0.12	0.57	0.04	1.76	0.21
27	61.43	20.63	8	1.58	0.13	0.34	0.03	2.98	0.39
28	40.54	27.75	13.13	2.15	0.32	0.68	0.05	1.46	0.47
29	29.87	43.76	11.2	2.2	0.37	1.47	0.07	0.68	0.26
30	32.79	33.18	12.46	1.69	0.38	1.01	0.05	0.99	0.38
31	39.27	33.75	11.49	1.65	0.29	0.86	0.04	1.16	0.34
32	38.71	36.93	12.08	1.18	0.31	0.95	0.03	1.05	0.33
33	57.07	26.6	8.26	1.9	0.14	0.47	0.03	2.15	0.31
34	37.68	34.07	12.01	1.77	0.32	0.90	0.05	1.11	0.35
35	42.18	38.82	6.63	3.06	0.16	0.92	0.07	1.09	0.17
36	56	27.55	4.15	1.8	0.07	0.49	0.03	2.03	0.15
37	49.26	28.14	8.35	1.97	0.17	0.57	0.04	1.75	0.30
38	63.28	21.51	5.14	2.01	0.08	0.34	0.03	2.94	0.24
39	58.03	22.78	7.04	2.31	0.12	0.39	0.04	2.55	0.31
40	54.22	22.59	6.48	2.24	0.12	0.42	0.04	2.40	0.29
41	51.63	27.17	7.82	1.73	0.15	0.53	0.03	1.90	0.29
42	45.52	31.32	11.13	2.04	0.24	0.69	0.04	1.45	0.36
43	64.85	19.78	5.89	2.15	0.09	0.31	0.03	3.28	0.30
44	62.28	19.61	6.29	2.23	0.10	0.31	0.04	3.18	0.32

45	82.88	9.2	2.04	0.68	0.02	0.11	0.01	9.01	0.22
46	27.19	43.23	13.39	1.18	0.49	1.59	0.04	0.63	0.31
47	44.27	34.58	10.24	1.12	0.23	0.78	0.03	1.28	0.30
48	46.76	34.46	8.04	2.23	0.17	0.74	0.05	1.36	0.23
49	59.42	19.65	7.77	1.69	0.13	0.33	0.03	3.02	0.40
50	51.86	26.53	7.39	1.5	0.14	0.51	0.03	1.95	0.28
51	56.51	26.16	7.82	1.62	0.14	0.46	0.03	2.16	0.30
52	51.63	30	6.91	2.43	0.13	0.58	0.05	1.72	0.23
53	48.1	31.72	9.65	2.1	0.20	0.66	0.04	1.52	0.30
54	64.52	19.9	7.4	1.2	0.11	0.31	0.02	3.24	0.37
55	60.79	24.55	6.26	1.29	0.10	0.40	0.02	2.48	0.25
56	61.1	24.02	5.14	1.18	0.08	0.39	0.02	2.54	0.21
57	63.68	22.2	5.51	1.87	0.09	0.35	0.03	2.87	0.25
58	41.31	33.61	12.01	1.4	0.29	0.81	0.03	1.23	0.36
59	57.5	23.28	7.75	2.03	0.13	0.40	0.04	2.47	0.33
60	48.23	34.94	7.38	1.12	0.15	0.72	0.02	1.38	0.21
61	57.71	24.76	7.1	1.98	0.12	0.43	0.03	2.33	0.29
62	58.61	23.72	6.77	1.69	0.12	0.40	0.03	2.47	0.29

Table C.18: Atomic ratio for G60 (28days)

	Calcium	Silicon	Aluminium	Sulfur	Al/Ca	Si/Ca	S/Ca	Ca/Si	Al/Si
1	53.04	27.16	8.88	0.9	0.17	0.51	0.02	1.95	0.33
2	28.13	43.04	13.29	1.35	0.47	1.53	0.05	0.65	0.31
3	49.22	30.46	8.89	2.16	0.18	0.62	0.04	1.62	0.29
4	55.87	24.99	8.45	1.87	0.15	0.45	0.03	2.24	0.34
5	57.1	24.12	7.58	2.39	0.13	0.42	0.04	2.37	0.31
6	48.42	26.11	8.7	2.41	0.18	0.54	0.05	1.85	0.33
7	54.69	31.32	4.95	1.63	0.09	0.57	0.03	1.75	0.16
8	59.17	21.43	7.59	1.33	0.13	0.36	0.02	2.76	0.35
9	52.8	24.57	9.93	1.71	0.19	0.47	0.03	2.15	0.40
10	51.24	25.7	10.28	2.07	0.20	0.50	0.04	1.99	0.40
11	50.35	20.97	9.4	2.81	0.19	0.42	0.06	2.40	0.45
12	53.01	29.96	7.34	2.2	0.14	0.57	0.04	1.77	0.24
13	62.16	19.18	9.19	1.11	0.15	0.31	0.02	3.24	0.48
14	41.77	44.9	4.43	1.48	0.11	1.07	0.04	0.93	0.10
15	52.8	25.97	7.95	1.61	0.15	0.49	0.03	2.03	0.31
16	57.15	20.89	6.91	1.35	0.12	0.37	0.02	2.74	0.33
17	60.37	27.08	4.45	1.57	0.07	0.45	0.03	2.23	0.16
18	57.55	25.87	6.75	0.85	0.12	0.45	0.01	2.22	0.26
19	49.82	25.47	10.38	1.52	0.21	0.51	0.03	1.96	0.41
20	54.66	25.12	8.36	1.65	0.15	0.46	0.03	2.18	0.33
21	49.3	27.54	9.39	1.76	0.19	0.56	0.04	1.79	0.34
22	61.52	21.82	5.23	1.91	0.09	0.35	0.03	2.82	0.24
23	66.25	18.43	5.1	2.04	0.08	0.28	0.03	3.59	0.28
24	57.93	22.33	8.09	2.7	0.14	0.39	0.05	2.59	0.36
25	51.68	31.99	5.75	1.98	0.11	0.62	0.04	1.62	0.18
26	42.78	37.47	9.39	1.33	0.22	0.88	0.03	1.14	0.25
27	60.16	33.31	3.39	0.56	0.06	0.55	0.01	1.81	0.10
28	53.27	28.05	6.67	1.74	0.13	0.53	0.03	1.90	0.24
29	59.62	25.16	7.03	1.28	0.12	0.42	0.02	2.37	0.28
30	35.3	50.81	5.93	1.42	0.17	1.44	0.04	0.69	0.12
31	54.66	32.87	3.93	1.7	0.07	0.60	0.03	1.66	0.12
32	39.67	35.01	9.59	2.09	0.24	0.88	0.05	1.13	0.27
33	1.79	96.52	0.34	0.19	0.19	53.92	0.11	0.02	0.00
34	43.39	41.3	4.56	2.36	0.11	0.95	0.05	1.05	0.11
35	56.68	25.14	5.4	1.82	0.10	0.44	0.03	2.25	0.21
36	36.07	37.98	10.82	2.31	0.30	1.05	0.06	0.95	0.28
37	59.28	23.41	7.75	1.27	0.13	0.39	0.02	2.53	0.33
38	45.43	38.88	6.36	2.68	0.14	0.86	0.06	1.17	0.16
39	53.86	25.47	7.2	1.57	0.13	0.47	0.03	2.11	0.28
40	58.44	24.3	5.82	2.5	0.10	0.42	0.04	2.40	0.24
41	49.58	28.44	8.97	1.65	0.18	0.57	0.03	1.74	0.32
42	58.18	25.46	7.52	1.22	0.13	0.44	0.02	2.29	0.30
43	58.96	24.4	8.49	1.6	0.14	0.41	0.03	2.42	0.35

44	41.64	42.75	6.67	2.29	0.16	1.03	0.05	0.97	0.16
45	51.42	29.74	6.61	2.04	0.13	0.58	0.04	1.73	0.22
46	52.97	25.69	7.79	2.77	0.15	0.48	0.05	2.06	0.30
47	53.65	26.27	8.35	3.97	0.16	0.49	0.07	2.04	0.32
48	48.68	31.93	9.01	2.5	0.19	0.66	0.05	1.52	0.28
49	35.36	53.72	3.73	1.78	0.11	1.52	0.05	0.66	0.07
50	56.06	24.89	8.1	1.17	0.14	0.44	0.02	2.25	0.33
51	56.03	24.79	5.18	1.65	0.09	0.44	0.03	2.26	0.21
52	34.07	28.45	12.65	1.87	0.37	0.84	0.05	1.20	0.44
53	58.66	22.54	5.55	2.29	0.09	0.38	0.04	2.60	0.25
54	48.89	24.09	10.48	2.31	0.21	0.49	0.05	2.03	0.44
55	57.04	29.55	6.42	0.69	0.11	0.52	0.01	1.93	0.22
56	40.24	31.05	12.67	2.27	0.31	0.77	0.06	1.30	0.41
57	63.68	20.06	6.24	1.46	0.10	0.32	0.02	3.17	0.31
58	45.97	27.92	11.52	1.98	0.25	0.61	0.04	1.65	0.41
59	57.11	23.13	9.06	1.41	0.16	0.41	0.02	2.47	0.39
60	45.7	26.46	10.19	3.02	0.22	0.58	0.07	1.73	0.39

Table C.19: Atomic ratio for G200 (28days)

	Calcium	Silicon	Aluminium	Sulfur	Al/Ca	Si/Ca	S/Ca	Ca/Si	Al/Si
1	44.76	38.53	6.72	1.15	0.15	0.86	0.03	1.16	0.17
2	48.18	31.45	7.17	1.62	0.15	0.65	0.03	1.53	0.23
3	63.4	22.17	4.69	1.04	0.07	0.35	0.02	2.86	0.21
4	60.82	27.16	5.02	1.47	0.08	0.45	0.02	2.24	0.18
5	54.64	25.43	8.68	1.36	0.16	0.47	0.02	2.15	0.34
6	50.57	30.78	9.34	2.73	0.18	0.61	0.05	1.64	0.30
7	48.4	27.59	7.21	1.45	0.15	0.57	0.03	1.75	0.26
8	56.11	23.43	7.9	1.31	0.14	0.42	0.02	2.39	0.34
9	60.97	27.98	4.36	0.49	0.07	0.46	0.01	2.18	0.16
10	67.8	23.43	2.25	0.48	0.03	0.35	0.01	2.89	0.10
11	58.84	24.22	7.94	1.3	0.13	0.41	0.02	2.43	0.33
12	57.51	21.32	8.12	2.7	0.14	0.37	0.05	2.70	0.38
13	51.71	24.79	9.87	1.13	0.19	0.48	0.02	2.09	0.40
14	57.26	22.22	6.81	1.88	0.12	0.39	0.03	2.58	0.31
15	52.54	30.42	6.64	3.58	0.13	0.58	0.07	1.73	0.22
16	55.11	25.15	7.13	2.09	0.13	0.46	0.04	2.19	0.28
17	25.31	57.65	5.57	0.63	0.22	2.28	0.02	0.44	0.10
18	51.33	28.73	9.4	0.7	0.18	0.56	0.01	1.79	0.33
19	40.94	35.2	11.02	0.91	0.27	0.86	0.02	1.16	0.31
20	61.01	20.02	7.68	1.62	0.13	0.33	0.03	3.05	0.38
21	54.66	25.68	6.79	2.02	0.12	0.47	0.04	2.13	0.26
22	55.08	24.26	7.23	2.47	0.13	0.44	0.04	2.27	0.30
23	55.95	24.15	7.42	1.31	0.13	0.43	0.02	2.32	0.31
24	46.57	29.95	8.88	1.8	0.19	0.64	0.04	1.55	0.30
25	30.05	38.47	12.64	1.57	0.42	1.28	0.05	0.78	0.33
26	43.96	29.05	10.75	2.6	0.24	0.66	0.06	1.51	0.37
27	46.15	29.5	8.94	1.78	0.19	0.64	0.04	1.56	0.30
28	50.73	28.49	8.03	2.04	0.16	0.56	0.04	1.78	0.28
29	32.72	40.19	9.99	1.19	0.31	1.23	0.04	0.81	0.25
30	48.58	28.04	9.13	2.99	0.19	0.58	0.06	1.73	0.33
31	36.06	36.54	9.74	1.23	0.27	1.01	0.03	0.99	0.27
32	50.88	27.1	9.33	1.9	0.18	0.53	0.04	1.88	0.34
33	45.43	27.47	11.28	2.33	0.25	0.60	0.05	1.65	0.41
34	43.78	29.92	10.89	1.93	0.25	0.68	0.04	1.46	0.36
35	36.14	42.41	6.21	1.73	0.17	1.17	0.05	0.85	0.15
36	55.52	26.92	7.88	1.5	0.14	0.48	0.03	2.06	0.29
37	51.76	26.62	7.23	2.13	0.14	0.51	0.04	1.94	0.27
38	55.6	25.11	7.33	2.11	0.13	0.45	0.04	2.21	0.29
39	48.27	35.88	6.26	2.05	0.13	0.74	0.04	1.35	0.17
40	38.87	41.09	8.57	1.2	0.22	1.06	0.03	0.95	0.21
41	39.7	34.04	10.77	2.31	0.27	0.86	0.06	1.17	0.32
42	49.1	25.04	7.66	1.72	0.16	0.51	0.04	1.96	0.31
43	53.69	24.47	8	1.67	0.15	0.46	0.03	2.19	0.33
44	44.65	29.44	10.04	1.48	0.22	0.66	0.03	1.52	0.34

45	51.83	30.82	7.12	2.48	0.14	0.59	0.05	1.68	0.23
46	52.05	23.59	8.22	1.51	0.16	0.45	0.03	2.21	0.35
47	63.47	23.18	6.65	0.86	0.10	0.37	0.01	2.74	0.29
48	57.79	24.95	6.19	2.61	0.11	0.43	0.05	2.32	0.25
49	53.13	30.82	6.22	1.77	0.12	0.58	0.03	1.72	0.20
50	51.09	27.97	8.52	1.62	0.17	0.55	0.03	1.83	0.30
51	56.96	26.1	7.76	2.3	0.14	0.46	0.04	2.18	0.30

This page is intentionally left blank

APPENDIX D

Chapter 4: Absorption characteristics and drying shrinkage of cement-based composites incorporating QDs

This appendix presents additional information on detail of testing and results for chapter 4.

D.1 METHODOLOGY AND DATA (CHAPTER 4)

D.1.1 Drying shrinkage

(a) Length comparator reading

(b): Curing in lime saturated water

Figure D.1: Work involved for the drying shrinkage test.

Testing procedure:

Testing was performed based on ASTM C596-07

1. Materials Preparation:

- A cement paste mix was prepared using 60% of PC and 40% of QDs (milled after 60s).
- The cement, QDs, SP and water were of the correct proportions.

2. Mould preparation:

- A mould size of 40 x 40 x 160mm prism was used.
- The mould was cleaned, and a release agent was applied.

3. Sample preparation:

- The cement paste was placed into the mould, compacted to ensure it filled the mould completely and to remove any air bubbles.
- Surface was finished smoothly.
- Moulded were covered with plastic sheets for 48 hours at a temperature of 23 ±2C.

4. Demoulding and initial measurement:

- After the initial curing, specimens were removed from the mould and were immersed in lime saturated water for 24hours.
- After 24hours, specimens were removed from the lime saturated water and wiped with damp cloth and immediately the length of the specimens was measured using a length comparator device as shown in figure D.1(a). This was the initial length measurement.

5. Air dry and subsequent measurement:

- Samples were air dried, and after each subsequent 7 days, the length of the specimen was measured again using the same comparator device until it reaches 63 days.

6. Calculation:

- The drying shrinkage was calculated as the differences between the initial and final lengths, expressed as a percentage of the initial length.

D.2.1 Density, absorption, and voids in hardened cement

(a) Oven dry samples

(b) Samples in oven

(c) Samples cooled in desiccator.

(d) Samples immersed in water for 48hrs

(e) Samples boiled for 5hrs.

Figure D.2: Work involved for the density, absorption, and voids test.

Testing procedure:

Testing was performed based on ASTM C642-06

1. Sample Preparation:

- A prism of 40 x 40x160mm were used for this test.
- The sample is a representative of the selected mix of 60% PC and 40% QDs

2. Oven dry mass:

- The initial prism mass was determined and were air dried in an oven at a temperature of 100 to 110°C for 24 hours. See figure D.2(a) and D.2(b).
- After reaching a constant weight, samples were removed from the oven and was allowed to cool in a desiccator as shown in figure D.2(c) to a temperature of 20 to 25°C.
- The mass was then determined, and this value is designated as A.

3. Saturated mass after immersion:

- The dried samples were then immersed in water at approximately 21°C for 48 hours (figure D.2(d)).
- Specimen were surfaced dried by removing surface moisture with a towel, and the mass was determined. This value was designated as B.

4. Saturated mass after boiling:

- The specimen was placed in a water bath, covered with tap water, and boiled for 5 hours (see figure D.2(e)).
- It was allowed to cool by natural loss heat for 24hours to a final temperature of 20 to 25°C.
- Moisture was removed with a towel, and the mass of the specimen was determined. This value was designated as C.

5. Immersed apparent mass:

- After immersion and boiling, the specimen was suspended by a wire and the apparent mass in water was determined. This apparent mass was designated D.

D.3.1 Absorption (Sorptivity) of water

(a) Sample conditioned in environmental chamber.

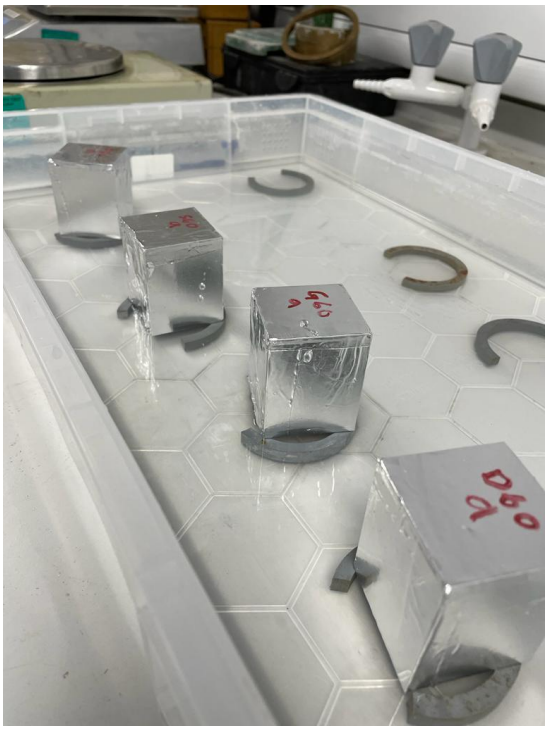

(b) Procedure of the water absorption.

Figure D.3: Work included in the water absorption by capillarity test.

Testing procedure:

Testing was performed based on ASTM C1585-04

1. Test specimen:

- The test specimens used for this test is of 50 x 40mm cube.
- The sample is a representative of the selected mix of 60% PC and 40% QDs

2. Sample conditioning:

- Test specimens were placed in the environmental chamber (figure D.3(a)) at a temperature of 50 ± 2°C and relative humidity (RH) of 80 ± 3% for 3 days.

- After the 3 days, each specimen was placed inside a sealable plastic. The plastic was stored at 23 ± 2°C for at least 15 days before the start of the adsorption procedure.

3. Procedure:

- Specimens was removed from the plastic storage, and the mass of the conditioned specimen was recorded to the nearest 0.01g before the side surfaces were sealed.
- Four measurements of the surface to be exposed to water were measured. The measurements were measured to the nearest 0.1mm and the average was calculated to the nearest 0.1mm.
- The side surface of each specimen was sealed with a sealing tape as shown in figure D.3(b)

4. Absorption procedure:

- The mass of the sealed specimens was measured to the nearest 0.01g and recorded as the initial mass for water absorption calculation.
- A support device is placed at the bottom of the container and filled with tap water to a level of 3mm above the top of the support device for the duration of the test.
- The timing device was started, and the test surface of the specimen was immediately placed on the support device (see figure D.3()). The time and date of initial contact with water were recorded.
- The mass was recorded at the time intervals as shown in table D.1.

Table D.1

Times and tolerances for the measurement schedule

Time	60s	5 min	10 min	20 min	30 min	60min	Every hour up to 6h	Once a day up to 3 days	Day 4 to 7, 3 measurements 24 h apart	Day 7 to 9, 1 measurement
Tolerance	2s	10s	2min	2min	2min	2min	5min	2h	2h	2h

- For each mass determination, the test specimen was removed from the container and any surface water was blotted off with a dampened paper towel.
- The specimen was inverted so that the wet surface did not come in contact with the balance pan, and within 15s of removal, the mass was measured to the nearest 0.01g.
- The specimen was immediately replaced on the support device, and the timing was started.